CATIONIC RHODIUM COMPLEXES WITH CHELATING PHOSPHINE AND PHOSPHINE ALKENE LIGANDS. APPLICATION IN DEHYDROGENATION AND DEHYDROCOUPLING REACTIONS.

Romaeo Dallanegra

A thesis submitted in partial fulfilment of the requirements for the degree of Doctor of Philosophy at the University of Oxford.

Linacre College April 2011

The work presented in this thesis was carried out between October 2007 and April 2011 under the supervision of Professor Andrew S. Weller. All of the work is my own unless otherwise stated and has not been submitted previously for any other degree at this, or any other, university.

Romaeo Dallanegra

April 2011

To the group:

“Becky gave me an amazing catalyst for free, unfortunately it wasn’t rhodium NBD…”

Contents

Acknowledgements vi
Abbreviations viii
Abstract x
1 Introduction 1
1.1 Reactive transition metal species 1
1.1.1 Low coordinate complexes 1
1.1.2 Weak stabilising interactions 1
1.1.3 σ-complexes 5
1.2 Phosphine ligands 8
1.2.1 Introduction 8
1.2.2 Hemilabile phosphine ligands 10
1.3 Dehydrogenation and dehydrocoupling 14
1.3.1 Alkane dehydrogenation 14
1.3.2 Intramolecular alkyl phosphine dehydrogenation 15
1.3.2.1 Phosphine-alkene ligands in catalysis 23
1.3.3 Dehydropolymerisation of silanes 27
1.3.4 Dehydrogenation and dehydrocoupling of amine-boranes 28
1.3.4.1 Introduction 28
1.3.4.2 Early examples 29
1.3.4.3 Catalytic systems 32
1.3.4.4 Amine-borane σ-complexes and ..... their role in dehydrocoupling processes 34
1.4 References 55
2 Phosphine-alkene complexes of DPEphos and XANTphos 61
2.1 Introduction 61
2.1.1 Hydrosilylation of alkenes 62
2.2 Results and discussion 64
2.2.1 Synthesis of complexes [Rh(POP){PCyp$_2$(η^2-C$_5$H$_7$)}][BAr$^F_4$] **(1/ 2)** 64
2.2.2 Reactivity of **1** and **2** with H_2 68
2.2.3 Reactivity of **1** and **2** with silanes 82
2.2.4 Reactivity of **1** with amine-boranes 84
2.2.5 Dehydrogenation of cyclopentylthioether ligands 85
2.3 Conclusions and future work 94
2.4 References 95
3 Dehydrocoupling of amine-boranes ..... with the {RhPR$_2$(η^2-C$_5$H$_7$)}$^+$ fragment 97
3.1 Introduction 97

3.2 Results and discussion 98
3.2.1 Reactivity of **i-9** with amine-boranes 98
3.2.2 Amine-borane dehydrocoupling catalysis with **i-9** 107
3.2.3 Reactivity of **i-9** with $H_3B{\cdot}NMe_2BH_2{\cdot}NMe_2H$ 110
3.2.4 Reactivity of **i-9** with $[H_2B{\cdot}NMeH]_3$ 119
3.2.5 A view to a mechanism for the dehydrocoupling of ..... $H_3B{\cdot}NMe_2H$ and $H_3B{\cdot}NMeH_2$ with **i-9** 124
3.3 Conclusions 127
3.4 References 128
4 Dehydrocoupling of amine-boranes ..... with the {Rh(diphosphine)}$^+$ fragment 129
4.1 Introduction 129
4.2 Results and discussion 130
4.2.1 Cationic Rh(I) diphosphine $H_3B{\cdot}NMe_3$ complexes 130
4.2.2 Reactivity of **11**, **12**, **25** and **26** in ..... the catalytic dehydrocoupling of $H_3B{\cdot}NMe_2H$ 141
4.2.3 Role of $H_2B{=}NMe_2$ in $H_3B{\cdot}NMe_2H$ dehydrocoupling 152
4.2.4 Role of $H_3B{\cdot}NMe_2BH_2{\cdot}NMe_2H$ in $H_3B{\cdot}NMe_2H$ dehydrocoupling . 154
4.2.5 Proposed mechanism for $H_3B{\cdot}NMe_2H$ dehydrocoupling ..... using **12**, **25** and **26** 157
4.2.6 Reactivity of **12**, **25** and **26** in ..... the catalytic dehydrocoupling of $H_3B{\cdot}NMeH_2$ 161
4.3 Conclusions 164
4.4 Future Work 165
4.5 References 166
5 Experimental 168
5.1 General 168
5.2 Nuclear Magnetic Resonance spectroscopy 168
5.3 Mass spectrometry 169
5.4 X-ray crystallography 169
5.5 Starting materials 169
5.6 Synthesis of new complexes 170
5.7 Dehydrocoupling methodology 193
5.7.1 $H_3B{\cdot}NMe_2H$ dehydrocoupling experiments ..... for dehydrocoupling plots 193
5.7.2 $H_3B{\cdot}NMeH_2$ polymerisation 194
5.8 References 195
5.9 Crystallographic data 196
5.10 Publications 199

Acknowledgements

Firstly I would like to thank my supervisor Prof. Andrew S. Weller for giving me the fantastic opportunity to undertake my D. Phil at the University of Oxford, an experience that I never thought I would be privileged to encounter and one that I will never forget. His sound guidance, wisdom and unfaltering support and belief in my ability have been truly appreciated.

During the course of my D. Phil I have had the great privilege to work with a number of valued colleagues and friends all of whom have contributed in some part whether big or small to the output of work that you find written in this thesis and without whom this body of work really would not have been at all possible:

To my long serving, chilli cracker eating, bike loving, white wine/ rosé spritzer drinking and sarcasm deficient kiwi PDRA Dr. Adrian B. Chaplin I owe a great deal. In the past three and a half years Adrian has taught me everything I know in the lab and is an epitome to the statement that chemistry really is "as easy as a-b-c, 1-2-3". When the complexes weren't crystallising, when the structures weren't solving and oligomer was just being… well… oligomer, Adrian always had a solution and time to spare to give advice even when already overwhelmed with several other reactions, projects, papers, part II's, secret romances and cycle races. I honestly do not think I have been in the company of a bigger perfectionist in everything from C-C agostics to fondue (no salad) – my International Chemistry Superstar. Cheers chief.

To my fellow D. Phil students in the Weller Lab- Tom (Dr. Thomas M. Douglas), Bex (Rebekah J. Pawley), Loz (Laura J. Sewell) and Indy (Indrek Pernik) I say a massive thank you. Working in S10 would definitely not have been as fun without you guys for your incessant support, friendship and of course the casual "loving" abuse. Specifically, Tom thanks for the tuition, showing me how organometallic chemistry was done in the early days and for my nickname (DL) which I don't think I'll ever escape; Bex for being the best older lab sister you could ever want, the many ESI-MS-athons, feeding me home cooked haut cuisine on so many

occasions I can't recall and of course finally taking Sam off my hands; Loz for always being there to offer a hug, Heat news, some hand cream and reassure me that I smell nice when the chemistry was misbehaving as well as being a key part of air sensitive Team A-B. Indy, all I need say is "Speedos". My heart-warming thanks also goes to Dr. Rachel "Pernod and coke" Hiney and Dr. Miguel "He could play right back for Luton Town" A. M. Huertos.

To the part II's; Sévérine, Nell, Rach, Ash, Woolfy, Seb, Georgie, Will, Hevz and in particular my own two protégées Jen (Jennifer Tsim) and CJ (Charlotte J. Stevens). Having been daunted by the prospect of supervising (problem solving) final year undergraduates through the final year of their degree you guys made it so much easier with your enthusiastic, supportive, bright and bubbly outlook and overall willingness to learn, it has been a sheer pleasure to be part of your development. From "braun" complexes and "peaky" NMR spectra to Freddie Mercury and things that should *never* be put in a Schlenk, so many great memories, both in and outside the lab/ UC, sober and distinctly less so!

To all the support staff in the CRL, specifically Dr. Nick H. Rees for the master class in NMR spectroscopy and the introduction to "disco" music during my time in the department, Robin Procter for his Mass Spec wizardry, Dr. Amber L. Thompson for X-ray crystallography and Alan Roper for the outrageously biased Oxford United F.C. chat.

Thanks to my wider field of friends in the CRL over the years, to everyone at Linacre College (specifically Erica J. Lacey) and the ICHS squad- you know who you are. If I also didn't give senior scientist Samuel E. M. Keegan a special mention for, amongst over things, all the free chocolate I do not think I would be forgiven.

I have also had the honour of collaborating with several groups – thanks to Ben Pilgrim and Prof. Timothy J. Donohoe, Alasdair P. M. Robertson and Prof. Ian Manners and especially Dr. Gilles Alcaraz and Prof. Sylviane Sabo-Etienne for hosting my 3 week *stage* in Toulouse.

Finally I'd like to say a big big thank you to my parents for their unwavering care, encouragement, belief and love.

Abbreviations

3c-2e	3-centre-2-electron
4c-4e	4-centre-4-electron
AB	Ammonia-borane
Ar	Aryl
atm	atmospheres
avg.	average
$[BAr^F_4]^-$	$[B\{3,5\text{-}C_6H_3(CF_3)_2\}_4]^-$
BINAP	2,2'-bis(diphenylphosphino)-1,1'-binaphthyl
calc.	calculated
cat.	catalyst
Cp	Cyclopentadienyl
Cyp	Cyclopentyl
COD	1,5-Cyclooctadiene
COE	Cyclooctene
DFT	Density Functional Theory
DLS	Dynamic Light Scattering
DMAB	Dimethylamineborane
DME	Dimethoxyether
DMSO	Dimethylsulphoxide
DPEphos	Bis(2-diphenylphosphinophenyl)ether
dppb	1,4-Bis(diphenylphosphino)butane
dppe	1,2-Bis(diphenylphosphino)ethane
dppm	1,1-Bis(diphenylphosphino)methane
dpp_{pent}	1,5-Bis(diphenylphosphino)pentane
dpp_{prop}	1,3-Bis(diphenylphosphino)propane
ESI-MS	Electrospray Ionisation Mass Spectrometry
fac	facial
fwhm	full width at half maximum

GPC	Gel Permeation Chromatography
K_{eq}	Equilibrium constant
M	mol dm^{-3}
mer	meridional
Mes	mesityl
MMAB	Monomethylamineborane
M_w	Molecular weight
m/z	mass to charge ratio
nacnac	β-diiminate
NBA	Natural bite angle
NBD	Norbornadiene
NHC	*N*-heterocyclic carbene
NMR	Nuclear Magnetic Resonance
PAL	Phosphine-alkene ligands
PDI	Polydispersity index
POP'	Bis(2-diphenylphosphinoethyl)ether
RDS	Rate determining step
RT	Room temperature
$t_{½}$	half life
TBAF	*Tetra-n*-butylammonium fluoride
tbe	*tert*-butylethylene
TEM	Transmission Electron Microscopy
THF	Tetrahydrofuran
TOF	Turnover frequency
TMAB	Trimethylamineborane
TRISPHAT	$[P(O_2C_6Cl_4)]^{3-}$
$tropp^{Ph}$	dibenzo-tropylidenyldiphenylphosphane
XAFS	X-ray Absorption fine structure
XANTphos	4,5-Bis(diphenylphosphino)-9,9-dimethylxanthene

Abstract

A series of cationic Rh(I) diphosphine and phosphine-alkene complexes have been isolated and fully characterised. The reactivity of these species towards hydrogenation, dehydrogenation and dehydrocoupling reactions has been investigated.

The use of potentially hemilabile ligands DPEphos and XANTphos in the intramolecular dehydrogenation chemistry of tricyclopentylphosphine is reported. The comparison in reactivity of these isolated diphosphine phosphine-alkene complexes towards hydrogenation and with acetonitrile is discussed along with their ability to dehydrocouple secondary silane, Ph_2SiH_2, and amine-borane $H_3B{\cdot}NMe_2H$. The acceptorless dehydrogenation of a tethered cyclopentane with cationic Rh(I) diphosphine complexes has also been extended to include thioethers.

Isolated cationic Rh(I) phosphine-alkene complexes with labile fluorobenzene ligands are found to act as a source of the reactive 12-electron $[Rh\{PR_2(\eta^2\text{-}C_5H_7)\}]^+$ (R = cyclopentyl (Cyp)/ ^{i}Pr) fragment in solution and can coordinate two amine-borane ligands (either $H_3B{\cdot}NMe_3$, $H_3B{\cdot}NMe_2H$ or $H_3B{\cdot}NMeH_2$) in a novel and unique bis-σ-binding mode. The catalytic activity of some of these isolated complexes in the dehydrocoupling of $H_3B{\cdot}NMe_2H$ and $H_3B{\cdot}NMeH_2$ has been determined. With a view to further understanding the mechanism of catalytic transition metal assisted amine-borane dehydrogenation and dehydrocoupling, known B-N intermediates $H_3B{\cdot}NMe_2BH_2{\cdot}NMe_2H$ and $[H_2B{\cdot}NMeH]_3$ were also coordinated to the $[Rh\{PCyp_2(\eta^2\text{-}C_5H_7)\}]^+$ fragment and investigated with regard to their role in the catalytic cycle.

Structure activity relationships determined from stoichiometric reactions of cationic Rh(I) diphosphine fluorobenzene complexes with amine-boranes enabled the design of a highly efficient homogeneous catalyst capable of dehydrogenating $H_3B{\cdot}NMe_2H$ to $[H_2BNMe_2]_2$ at 0.2

mol% loading in 30 minutes at 298 K. Rapid dehydrogenation and dehydrocoupling of $H_3B{\cdot}NMeH_2$ to form high molecular weight poly(*N*-methylaminoborane) with a low PDI has also been achieved. Investigations using model aminoborane $H_2B{=}N^iPr_2$ and intermediate B-N species $H_3B{\cdot}NMe_2BH_2{\cdot}NMe_2H$ and $[H_2B{\cdot}NMeH]_3$ has helped establish an overall mechanistic rationale for this process.

1 INTRODUCTION

1.1 Reactive transition metal species

1.1.1 Low coordinate complexes

Low coordinate transition metal complexes have long been implicated in the catalytic cycles of many homogeneous processes.[1] Their highly reactive and transient nature, however, has repeatedly hampered their definitive characterisation. Therefore efforts to understand how these, often *in situ* generated, species interact with substrate molecules and catalytically turnover remains key to the development of efficient catalysts. Their formation commonly involves the dissociation of a ligand from the metal coordination sphere to create a vacant coordination site.[2] Genuine examples of crystallographically characterised low coordinate group 9 complexes, although known, are rare (Figure 1.1).[3,4,5,6]

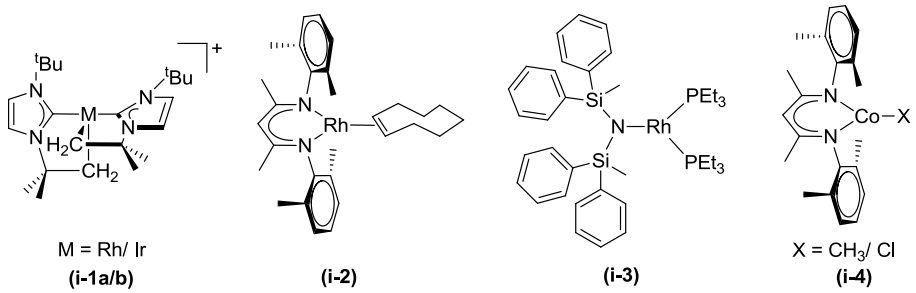
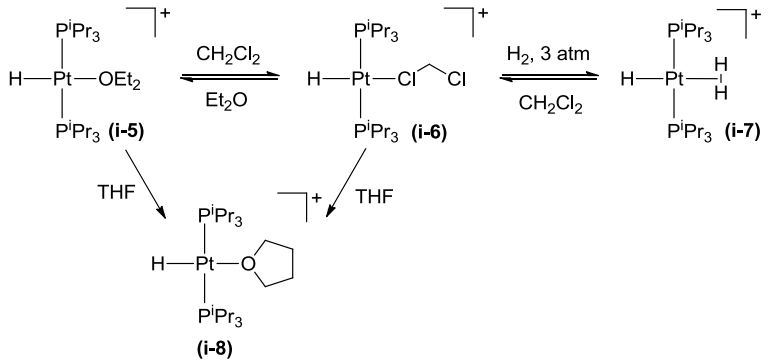


Figure 1.1 Examples of crystallographically characterised group 9 low coordinate complexes. Anion not shown.

1.1.2 Weak stabilising interactions

Solvent, counteranion and agostic interactions can often play an important role by stabilising low coordinate metal centres through coordination to a vacant site.[7] In a catalytic sense it is important however that the strength of these interactions is not strong enough to prevent dissociation and therefore subsequent reactivity with substrates.

Polar solvents are ubiquitous in organometallic chemistry as a result of their high dielectric constants which allow them to solubilise transition metal complexes unlike non-polar solvents (*e.g.* alkanes) which often suffer in this regard.[8] DMSO, THF, pyridine and MeCN are known to be strongly coordinating polar solvents, whereas polar CH_2Cl_2, $(CH_3)_2CO$ and Et_2O coordinate much more weakly (Scheme 1.1).[7] A coordination in each case occurs *via* the donation of a lone pair of electrons of an electronegative atom (*e.g.* O, S, N, Cl) into a vacant metal *d* orbital.

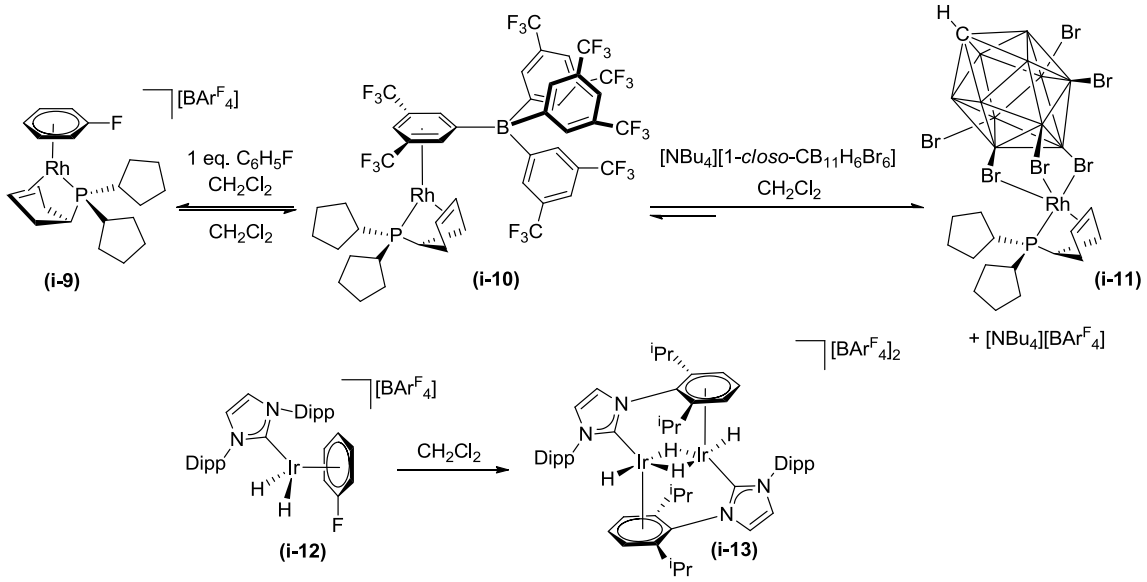


Scheme 1.1 Use of Et_2O and CH_2Cl_2 as weakly coordinating ligands. $[BAr^F_4]^-$ anions not shown.

The first fully characterised example of dichloromethane coordination to a transition metal complex was reported by Kubas *et al.* in 1996 (Scheme 1.1).[9] Addition of CH_2Cl_2 to $[Pt(P^iPr_3)_2(H)(OEt_2)][BAr^F_4]$ **(i-5)**, itself an example of the weak coordination of a diethylether ligand, results in the formation of $[Pt(P^iPr_3)_2(H)(CH_2Cl_2)][BAr^F_4]$ **(i-6)**. The weak nature of the Pt-Cl bond of **i-6** is illustrated by the fact that under a hydrogen atmosphere $[Pt(P^iPr_3)_2(H)(\eta^2\text{-}H_2)][BAr^F_4]$ **(i-7)** is the preferred product. Addition of THF to **i-5** or **i-6** yields the equivalent THF complex, $[Pt(P^iPr_3)_2(H)(THF)][BAr^F_4]$ **(i-8)**, showing that THF is a more strongly coordinating ligand than both Et_2O and CH_2Cl_2. Numerous examples of cationic group 9 complexes containing weak solvent interactions are now known.[10]

Arene solvents have also been shown to coordinate to transition metal complexes in a variety of coordination modes (η^2, η^4 and η^6), however they frequently form strong bonds which are not

easily displaced.[7] Recent work with group 9 metals however has highlighted that with the introduction of electron withdrawing groups on the aryl ring (e.g. C_6H_5F, 1,2-$C_6H_4F_2$), this interaction can be sufficiently reduced so as to act as a labile ligand suitable for stabilising low coordinate fragments (Scheme 1.2).[11,12,13]



Scheme 1.2 Weakly coordinating properties of C_6H_5F, [BAr$^F_4$]$^-$ and [1-*closo*-$CB_{11}H_6Br_6$]$^-$.

Complex **i-10** shows that in CH_2Cl_2, coordination of a weakly coordinating anion, [BAr$^F_4$]$^-$, is preferred over CH_2Cl_2.[14] Addition of 1 equivalent of C_6H_5F establishes an equilibrium between **i-9** and **i-10** whilst addition of [NBu$_4$][1-*closo*-$CB_{11}H_6Br_6$] establishes an equilibrium between complexes of the two weakly coordinating anions **i-10** and **i-11**. Aldridge and co-workers have recently shown that an arene bridged dimer **(i-13)** is formed when [Ir(IPr)(H)$_2$(η^6-C_6H_5F)][BAr$^F_4$] **(i-12)** (IPr = *N,N'*-bis(2,6-diisopropylphenyl)imidazol-2-ylidene) is dissolved in CH_2Cl_2.[13] Weakly coordinating anions also play an important role in stabilising reactive cationic intermediates.[15] Their weakly coordinating character is derived from the negative charge of the anion being delocalised over the whole fragment giving a Lewis acidic (non-nucleophilic) core. Carboranes and borate based anions such as [BAr$^F_4$]$^-$ represent two prominent classes in this field.[8,16,17]

Metal centres can also be stabilised by weak C-H bond interactions. The term "agostic interaction" was defined by Brookhart and Green in the 1980s as an attractive interaction between a metal and a proximal C-H bond of a ligand already coordinated to the metal centre,[18] differing from longer electrostatic anagostic metal-C-H "hydrogen bond" interactions and intermolecular σ-alkane interactions.[19] Since the first example of an agostic bond reported by Trofimenko in 1968,[20] agostic interactions have been shown to stabilise a host of low coordinate transition metal complexes through intramolecular α-, β-, or γ- C-H interactions, the nomenclature indicating the position from the metal centre (*e.g.* Figure 1.2).[21,22]

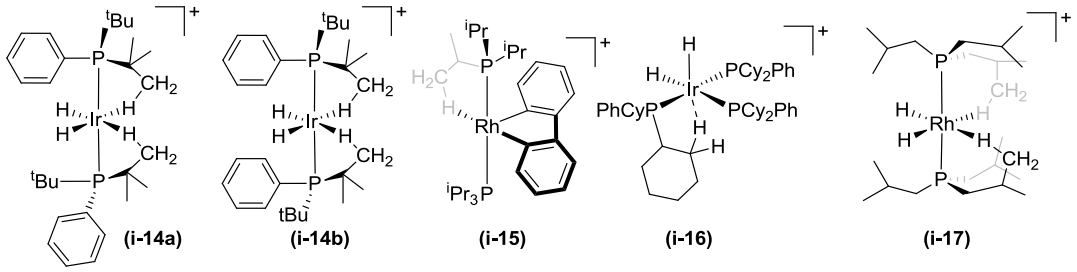
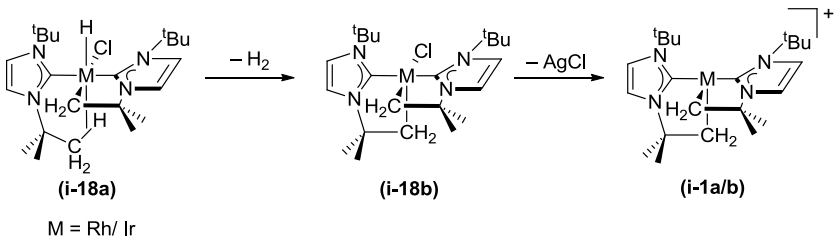


Figure 1.2 Examples of crystallographically characterised agostic complexes. Anions not shown.[23,24,25,26]

Short M-H distances (1.8 Å – 2.3 Å) and small M-C-H angles (90 - 140°) are characteristic of an agostic interaction, while the CH resonance is observed at lower frequency with a reduced CH coupling constant compared to the free ligand by NMR spectroscopy.[19] Despite the implication of agostic complexes in many C-H activation processes, crystallographic data for both the agostic intermediate and the activated product are limited to two examples by Nolan[3] (2005, Scheme 1.3) and Weller (2009)[27]. Nolan described the formation of ^{t}Bu-NHC Rh and Ir complexes which contain both a ^{t}Bu agostic **(i-18a/b)** and a cyclometallated ^{t}Bu interaction **(i-1a/b)** (Scheme 1.3). Weller's example is discussed later in Scheme 1.21.



Scheme 1.3 Nolan's structures of both an agostic complex and its C-H activated product.

1.1.3 σ-complexes

The coordination of substrates to transition metal centres *via* σ-bonding interactions are thought to be the first step in the catalytic cycle of many reactions prior to formal oxidative addition.[28] Characterisation of complexes of this type, therefore, represents a key effort to push forward the generation of efficient transition metal catalysts for use in synthetically challenging reactions. Examples of σ-complexes involving X-H bonds, where X = H, B, C, P, Si and Sn,[29] and C-C σ-complexes are known.[30,31]Dihydrogen σ-complexes are the simplest type of σ-interaction as they, by nature, can only involve the two electrons available in the σ-bond between the two hydrogen atoms in a 3c-2e bond with the metal centre. The σ-bond is made up of both the donation of these two electrons from the hydrogen σ-orbitals into a transition metal *d* orbital and the backdonation of electron density from the metal centre into σ* orbitals of the hydrogen atoms (Figure 1.3).[32]

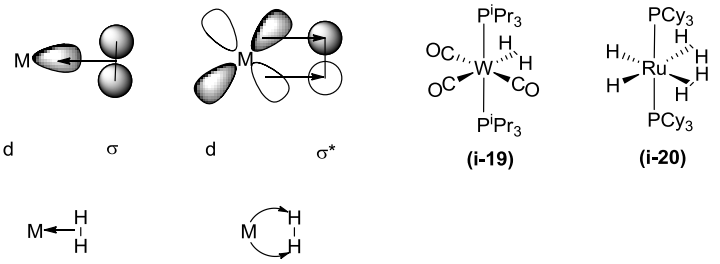
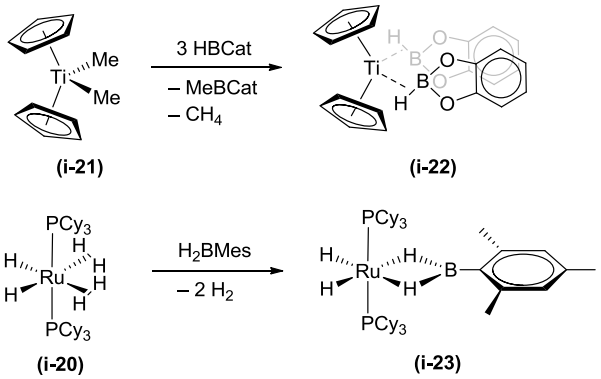


Figure 1.3 A metal-dihydrogen σ-bond. The first example of a dihydrogen complex by Kubas **(i-19)** and the first example of a bis-dihydrogen complex by Sabo-Etienne **(i-20)**.

The result of the backdonation into the hydrogen antibonding orbitals is to weaken the H-H bond which is identified by its lengthening from that observed in free dihydrogen (0.74 Å). Elongation of the H-H bond can be sustained up to approximately 1.5 Å after which the bond breaks forming a dihydride complex, the product of formal oxidative addition.[29] The first dihydrogen complex, $W(CO)_3(P^iPr_3)_2(\eta^2\text{-}H_2)$ **(i-19)** was prepared and characterised by Kubas in 1984 from the addition of hydrogen to $W(CO)_3(P^iPr_3)_2$,[33] however there now exist examples of dihydrogen complexes for the majority of the transition metals, significantly with regard to this work for Ir and Rh and, as of 2011, Co.[34,35] Bis-σ-dihydrogen complexes are rare.[36] The first

crystallographically characterised example $Ru(PCy_3)_2(H)_2(\eta^2\text{-}H_2)_2$ **(i-20)** (Figure 1.3), was reported by the group of Sabo-Etienne in 2000.[37] Characterisation of dihydrogen complexes is inherently difficult. Kubas initially identified **i-19** by compiling evidence from irregular ν_{WH} stretching frequencies in the IR spectrum and a significant *J*(HD) value (33.5 Hz) for the coordinated η^2-HD ligand in the ^{1}H NMR spectrum obtained from the addition of HD to **i-19** to form the equivalent complex $W(CO)_3(P^iPr_3)_2(\eta^2\text{-}HD)$.[33] Today a combination of X-ray and neutron crystallography and NMR T_1 spin relaxation measurements are the most useful methods for confirming the coordination of a dihydrogen ligand (T_1 ~ 20 ms) over a dihydride (T_1 ~ 200 ms).[29]

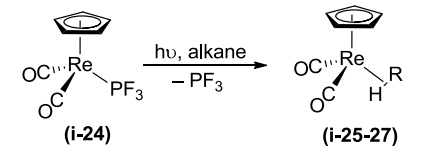
Borane reagents play a large role in transition metal-mediated organic functionalisation but until relatively recently little has been understood as to their interaction with the metal. The first example of a structurally characterised σ-borane complex was reported by Hartwig in 1996.[38] The bis-σ-borane complex $TiCp_2(HBcat)_2$ **(i-22)** (HBcat = catecholborane) (Scheme 1.4) was identified as an 18 electron complex with the HBcat ligands acting as 2 electron donors. Remarkably, the geometry about the boron atom was found to be non-planar, a result of backdonation of electron density from the metal into the low lying p orbital on boron. (This concept is discussed further with amine-boranes in Figure 1.9). Hartwig *et al.* have since reported a range of bis-σ-borane complexes for Ti, Nb, Mn, Re using pinacol-, catechol- and dialkylboranes in an area which remains current.[39]



Scheme 1.4 The first example of a transition metal bis-σ-borane complex by Hartwig **(i-22)** and the first example of mono-σ-borane coordination by Sabo-Etienne **(i-23)**.

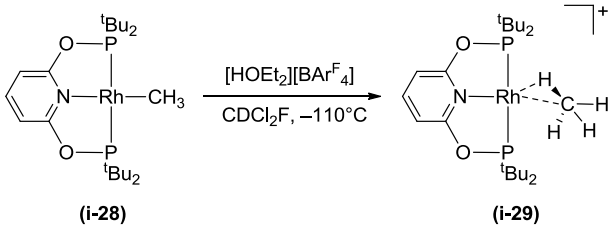
In 2007 Sabo-Etienne and co-workers published the first example of mono-σ-borane coordination using H_2BMes (Mes = mesityl).[40] Addition of H_2BMes to low coordinate bis-σ dihydrogen complex $[Ru(PCy_3)_2(H)_2(\eta^2\text{-}H_2)]$ **(i-20)** quantitatively forms $[Ru(PCy_3)_2(H)_2(\eta^2\text{-}H_2BMes)]$ **(i-23)** with the concomitant release of two equivalents of hydrogen (Scheme 1.4). Two geminal σ-B-H bonds coordinate to Ru forming a 4c-4e bond. Stradiotto *et al.* have since characterised a related cationic Ru mono-σ-borane complex.[41]

In comparison to the other varieties of σ-complex, intermolecular σ-alkane complexes remain elusive. The inert nature of the non-polar C-H bond which has weak σ-donor character and additionally significant steric hindrance of the alkyl moiety gives rise to poor transition metal coordination capability.[21,42] The first reported evidence for transition metal σ-alkane complexes was reported by Perutz and co-workers in 1975 who characterised $Cr(CO)_5(CH_4)$ and $Fe(CO)_4(CH_4)$ by UV-spectroscopy upon the photolysis of $Cr(CO)_6$ and $Fe(CO)_5$ respectively in a methane matrix at 12 K.[43] Time resolved infrared spectroscopy (TRIR) of similar metal alkane carbonyl complexes has provided additional evidence as has been discussed in independent studies by von Gustorf[44] and more recently George *et. al.*[45] NMR spectroscopic data of complexes with general formula $ReCp(CO)_2(alkane)$ **(i-25-27)** have been obtained by Ball and co-workers from the photolysis of, for example, $ReCp(CO)_2(PF_3)$ **(i-24)** in alkane solvent at low temperature (Scheme 1.5).[46]



Scheme 1.5 Formation of Re alkane complexes **i-25-27**.

Two crystal structures of transition metal alkane complexes have been reported although they have been subject to debate as to whether they are definitively *true* σ-complexes; heptane coordinated to an Fe(II) porphyrin complex[47] and methylcyclohexane coordinated to a tris-aryl oxide U(III) complex.[48] Both are found to be unstable in solution. In 2009 a σ-methane complex was fully characterised by NMR spectroscopy for the first time by Brookhart (Scheme 1.6),[42] although only at −110 °C in Freon solvent (free and bound hydrogen atoms are still found to be exchanging). Above this temperature the complex is unstable (methane dissociation $t_{½}$ = 83 minutes (−87 °C)).



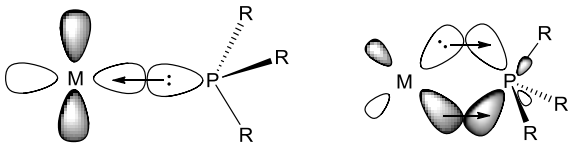
Scheme 1.6 Protonation of **i-28** by $[H(OEt_2)_2][B\{3,5\text{-}C_6H_3(CF_3)_2\}_4]$ to form **i-29**, the first example of a fully characterised σ-methane complex. PONOP = 2,6-$(^tBu_2PO)_2C_5H_3N$. $[BAr^F{}_4]^-$ anion not shown.

1.2 Phosphine ligands

1.2.1 Introduction

Tertiary phosphines (PR_3) represent an important class of ligand in organometallic chemistry as their ability to stabilise complexes can be easily tuned by careful variation of the electronic and steric properties of the R groups.[7] Phosphines can act as both σ-donor and π-acceptor ligands. The available lone pair on the phosphorus atom donates into an empty metal *d* orbital forming a

σ-bond, whilst π-backdonation from the metal occurs into the σ* orbital of the P-R bond and the phosphorus dπ component (Figure 1.4). More electronegative R groups result in a lowering in energy of the P-R σ* orbital making it more accessible to backbonding from the metal. PF_3 has similar π-acceptor character to CO, whilst at the other end of the spectrum, PMe_3 is a relatively weak π-acceptor.



Ligands in order of π-accepting character:

$PMe_3 \approx P(NR_2)_3 < PAr_3 < P(OMe)_3 < P(OAr)_3 < PCl_3 < CO \approx PF_3$

Figure 1.4 The strength of phosphine coordination to transition metals can be greatly influenced by the nature of the R groups of the phosphine.

The electronic effects of changing the R group were first quantified by Tolman who observed a change in the CO stretching frequency of complexes with the general formula $Ni(CO)_3(PR_3)$.[49] Increased σ-donation from the phosphine results in more electron density at the metal centre and subsequently on the CO ligands *via* backdonation from the metal, leading to a decrease in ν(CO). The steric bulk of a phosphine was later quantified by Tolman by taking a space filling model of the phosphine with the metal at the vertex and measuring the angle made between the outermost atoms on the substituents and the metal at a fixed M-P distance (θ, in Figure 1.5).

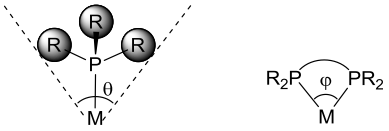


Figure 1.5 The Tolman cone angle (θ) and bite angle (φ) of a diphosphine.

Unsymmetrical phosphines and diphosphines have since been found to be better represented using averaged half angles of the substituents and chelated backbone respectively.[50] The P-M-P angle made upon coordination of chelating diphosphine ligands is known as the bite angle (φ in Figure 1.5). Altering the R substituents and the length and the nature of the backbone has been

shown to have a profound effect in catalysis with subtle changes resulting in remarkably different catalytic activities.[51] The semi-quantitative measurement of pocket angle has been derived to assess the steric hinderance at the metal active site caused by the diphosphine bite angle and R substituents.[52] Systematic changing of the bite angle is however quite challenging without also altering the effect of steric or electronic properties of the diphosphine.

1.2.2 Hemilabile phosphine ligands

The concept of "hemilabile" ligands was first introduced by Jeffrey and Rauchfuss in 1979.[53] These ligands have at least two chemically inequivalent modes of binding to a metal centre, one of which has the ability to be displaced but can subsequently recoordinate when required, while the other(s) remain bound (Figure 1.6).

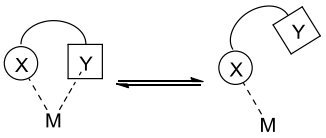
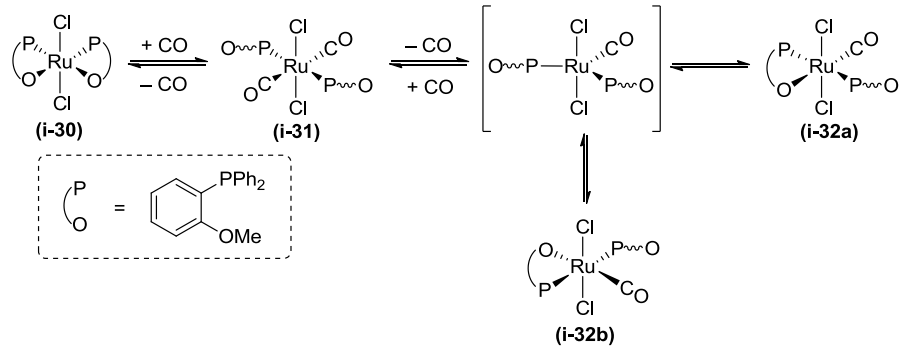


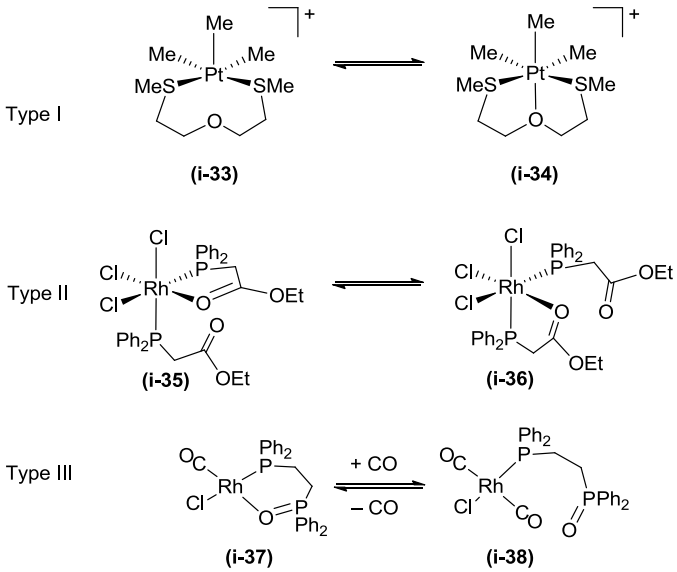
Figure 1.6 Hemilability of atom Y at the metal centre, M, while atom X remains bound.

Rauchfuss illustrated this concept using the *o*-(diphenylphosphino) anisole ligand coordinated to Ru. Upon addition of CO to $Ru\{PPh_2(o\text{-}MeOC_6H_4)\}_2Cl_2$ **(i-30)**, three carbonylated products **(i-31)** and **(i-32a/b)** are observed in equilibrium with one another (interconversion between isomers of **i-32** takes place *via* a 5-coordinate trigonal bipyramidal intermediate) (Scheme 1.7). The weak Ru-O interactions in **i-30** were further illustrated by their bond lengths in the X-ray structure (2.299 and 2.257 Å) which are significantly longer than the sum of the covalent radii (1.99 Å).[53]



Scheme 1.7 Reactivity of $Ru\{PPh_2(o\text{-}MeOC_6H_4)\}_2Cl_2$ **(i-30)** with CO.

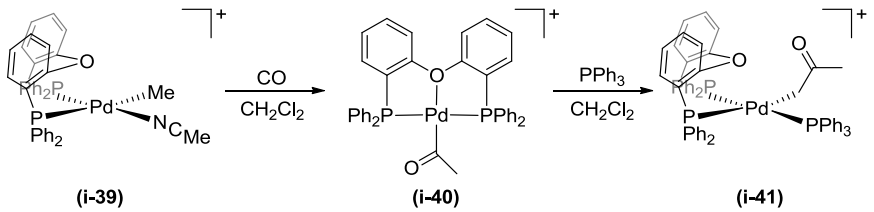
Hemilabile behaviour is now classified into three distinct types: (*e.g.* Scheme 1.8). Type I hemilability is commonly found in metal complexes which have a range of coordination numbers available and thus permit spontaneous interconversion between ligands possessing multiple coordination modes. It also encompasses dinuclear and cluster structures. Type II hemilability defines the intramolecular competition between ligands for coordination to a metal centre whilst Type III involves the reversible coordination of an external ligand to invoke hemilabile behaviour of another.



Scheme 1.8 Classes of hemilability.[54,55,56] $[BF_4]^-$ anion not shown.

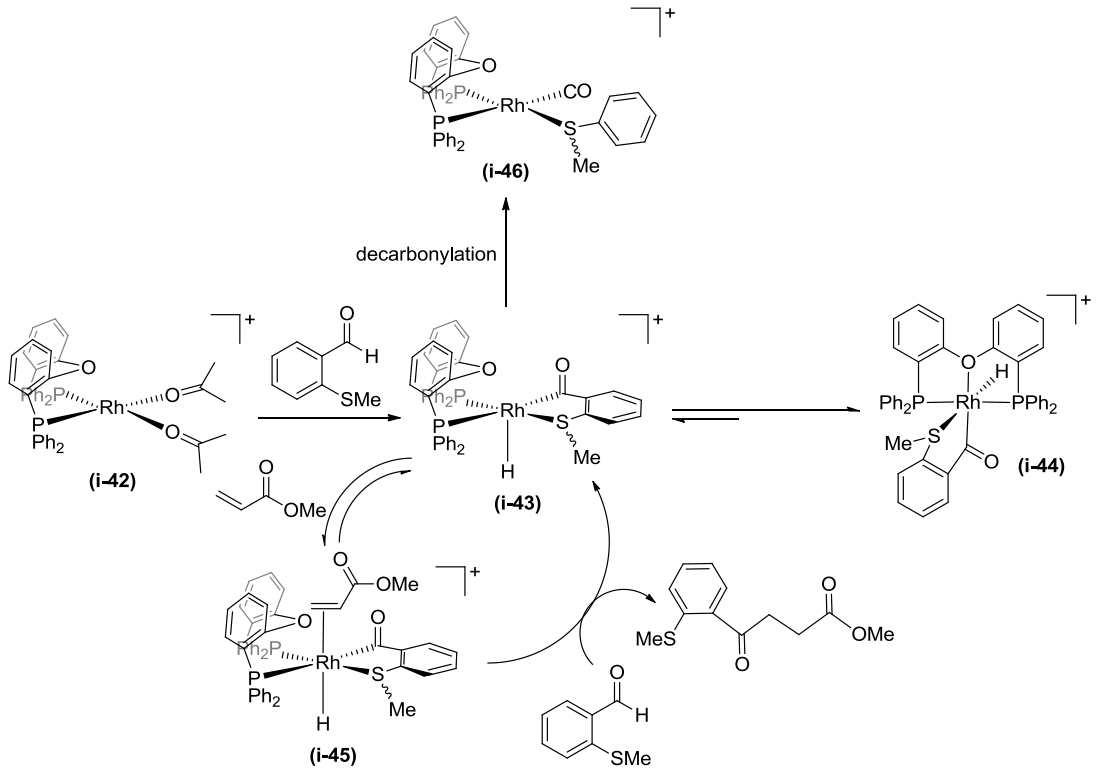
An extenstive list of ligands capable of acting in a hemilabile manner exist.[57] Discussion here will focus on POP diphosphine ligands where an oxygen atom has been shown to act as a

hemilabile donor. The use of DPEphos (bis(2-diphenylphosphinophenyl)-ether))[58] and XANTphos (9,9-dimethyl-4,5-bis-(diphenylphosphino)xanthene)[59] as ligands in transition metal catalysis is very common due their inherent ability to adopt a range of geometries as a result of their wide bite angle and their ability to help stabilise reactive intermediates.[60] The group of van Leeuwen has contributed considerably to this field in the past decade.[61] In 2003 van Leeuwen *et al.* first showed the ability for the DPEphos oxygen atom to reversibly coordinate to Pd depending on the reaction conditions (**i-39-41**, Scheme 1.9).[62].



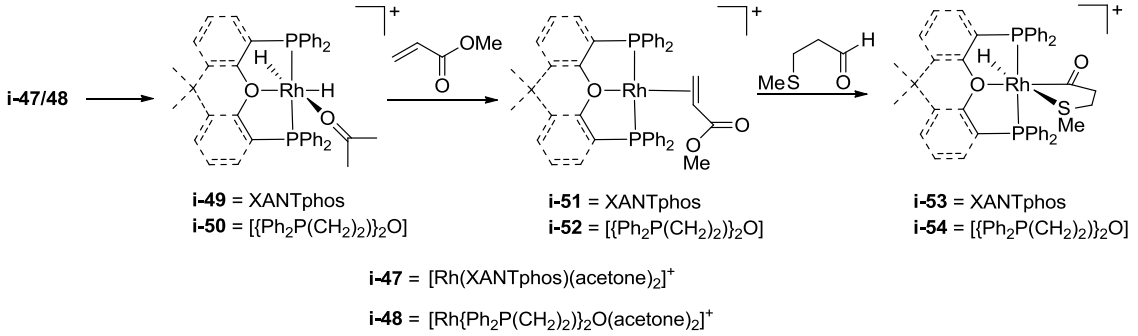
Scheme 1.9 The hemilabile nature of DPEphos using cationic Pd. Anions not shown.

Weller *et al.* have applied this concept in the hydroacylation reaction of alkenes with β-S-substitued aldehydes using a [Rh($\kappa^2_{(PP)}$-DPEphos)(acetone)$_2$][BAr$^F_4$] **(i-42)** precursor.[63] Through a combination of NMR spectroscopy, mass spectrometry and X-ray crystallography the authors identified key intermediates in the catalytic cycle showing Type III hemilability of the DPEphos ligand (Scheme 1.10).[64]



Scheme 1.10 Hydroacylation of $MeSC_6H_4CHO$ with $H_2C{=}CHCOOCH_3$ by **i-42**. Anions not shown.

In the proposed mechanism of hydroacylation using **i-42**, the free site in **(i-43)** is necessary for reductive decarbonylation **(i-46)** which is a competing deactivation pathway to hydroacylation. Coordination of the oxygen atom of the DPEphos ligand to the metal centre **(i-44)** slows decarbonylation but still allows catalysis to proceed by reversibly coordinating and allowing the alkene to bind. Total conversion to the product of hydroacylation is achieved in catalysis with **i-42** at 5 mol% loading after an hour. In a comparative study with the non-hemilabile diphosphine dppe, catalyst turnover is considerably reduced as a result of the diphosphine ligand being unable to stabilise the acyl hydride intermediate (*c.f.* **(i-43)**).[63] Screening of XANTphos and POP′ ($[Ph_2P(CH_2)_2]_2O$) ligands in this system found that these ligands preferentially form $\kappa^3_{(POP)}$-bound complexes with the oxygen atom remaining bound once coordinated which resulted in the generation of robust complexes in solution and considerably slowed catalyst turnover (Scheme 1.11).[65] The tendency of the oxygen to act in a non-hemilabile fashion in these systems is suggested to be the reason for this attenuation in catalysis.

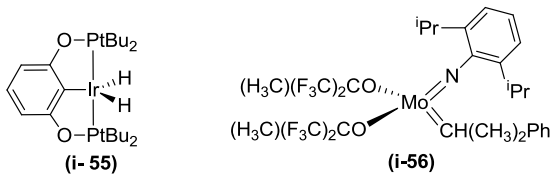


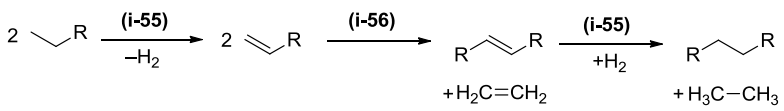
Scheme 1.11 *Trans* spanning $\kappa^3_{(POP)}$-bound structures are preferred by XANTphos and POP' ligands. $[BAr^F_4]^-$ anions not shown.

1.3 Dehydrogenation and dehydrocoupling

1.3.1 Alkane dehydrogenation

The importance of alkenes as a chemical feedstock for the synthesis of a plethora of organic molecules is well documented.[66,67,68] Efficient alkane dehydrogenation to afford alkenes is an important step with regard to this effort in an era where green chemistry is a dominant topic.[69] Significant progress in this field has been made in recent years, which is best highlighted by Goldman and Brookhart's work. In a tandem one pot process, acceptorless dehydrogenation of *n*-alkanes to afford alkenes by an Ir catalyst **(i-55)** can then be increased in molecular weight using a Schrock Mo-based initiator **(i-56)** before rehydrogenation of the newly formed alkenes back to alkanes by the Ir catalyst (Scheme 1.12).[70]





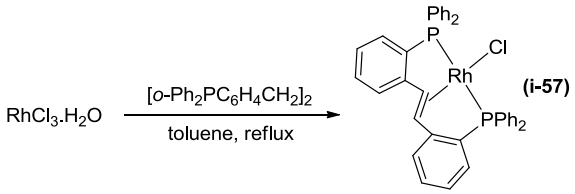
Scheme 1.12 Goldman and Brookhart's catalytic alkane metathesis.

There remains however sufficient scope for the discovery of novel atom economic catalytic processes which can effect dehydrogenation in more complex substrates. One example is the dehydrogenation of alkyl phosphines to alkenyl phosphines by transition metals which has been

known for over forty years.[71,72] Recent work has shown that dehydrogenation of alkyl phosphine ligands requires relatively mild conditions.[12,73] It has also begun to attract significant interest as it places useful functionality on the alkyl phosphine which can be exploited to enhance selectivity and reactivity in catalysis when coordinated to a transition metal.[74,75,76] Highlighted in this introduction are contributions by several groups in this area towards 1,4-addition reactions,[12,77,78] Suzuki-Miyaura coupling,[79] hydrogenation of imines,[80] functionalisation of nitrogen heterocycles,[81,82] allylic alkylations[83] and dehydrogenative silylation[84] using such ligands. (Section 1.3.2.1)

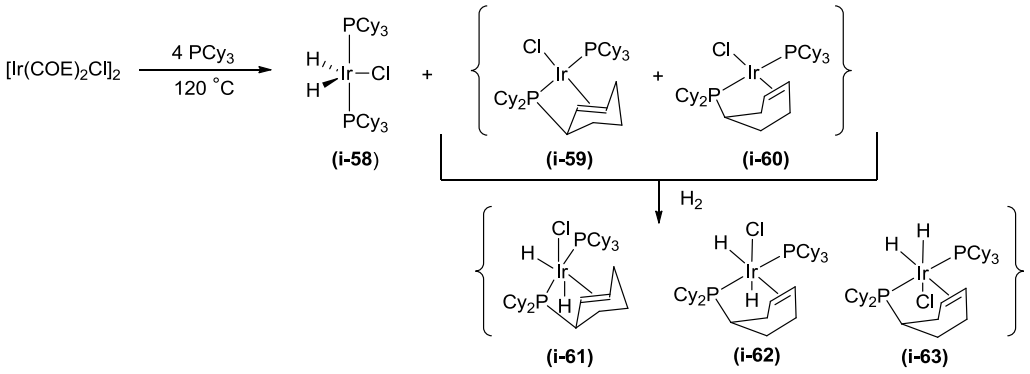
1.3.2 Intramolecular alkyl phosphine dehydrogenation

In 1969 Whimp and coworkers first demonstrated that the 2,2'-bis(diphenylphosphino)dibenzyl ligand could undergo metal-based dehydrogenation to form a chelate phosphine-alkene complex **(i-57)** in the presence of either Rh(I) or Rh(III) precursors (Scheme 1.13).[71] No dehydrogenation of this ligand was observed with equivalent Ir complexes.[85]



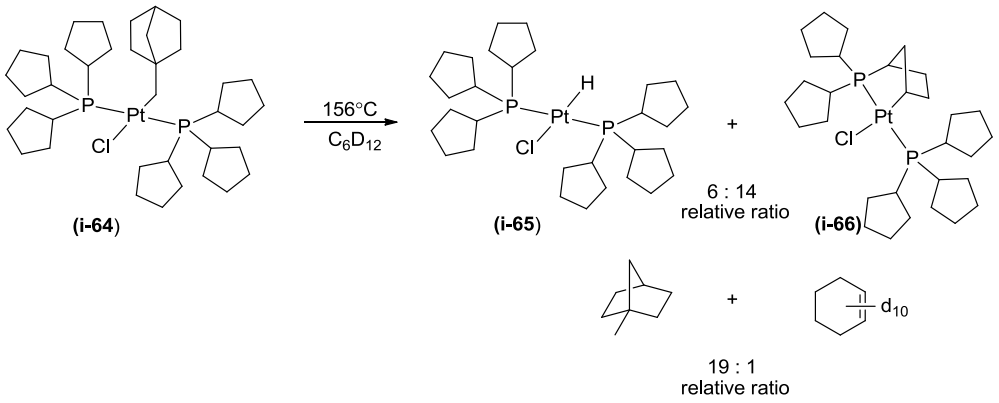
Scheme 1.13 Synthesis of RhCl(*o*-$Ph_2PC_6H_4$-CH=$CHC_6H_4PPh_2$-*o*) **(i-57)**. ($Rh(PPh_3)_3Cl$ or $[Rh(COD)Cl]_2$ can also be used separately as alternatives to $RhCl_3$. H_2O).

Five years later Vrieze *et al.* found a tricyclohexylphosphine Ir complex **(i-58)** to undergo a dehydrogenation of a cyclohexylphosphine ligand to yield 2,3- **(i-59)** and 3,4- **(i-60)** cyclohexene isomers (Scheme 1.14).[86]



Scheme 1.14 Partial dehydrogenation of a tricyclohexylphosphine ligand by Ir. COE = cyclooctene.

Upon subsequent hydrogenation, NMR spectroscopy revealed that the double bond remained bound to the metal centre with the formation of several hydride isomers **(i-61-63)**. Dehydrogenation of tricyclohexylphosphine with Rh also gave rise to a single isomeric product equivalent to **i-59**. In 1986 Whitesides *et al.* postulated the cyclometallation of a C-H bond **(i-66)** in tricyclopentylphosphine from the thermal decomposition of a *trans*-chloro(1-norbornylmethyl)bis(tricyclopentylphosphine)platinum compound **(i-64)** (Scheme 1.15).

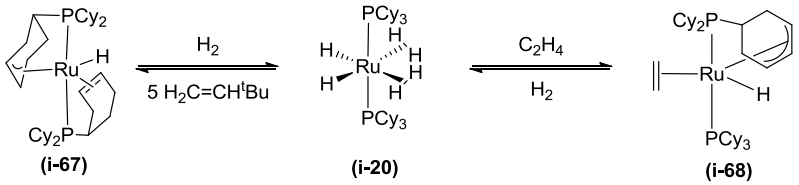


Scheme 1.15 C-H activation of a Pt(II)-biscyclopentyl phosphine complex **(i-64)**.

NMR spectroscopic data were however not sufficient to define the exact structure of the novel complex. Deuterium labelling experiments using $PCyp_3(d_{27})$ found that reactivity with the cyclohexane solvent to form methylnorbornene was favoured upon characterisation of the observed by-products. This points to the transfer of hydrogen (deuterium) from the tricyclopentylphosphine to produce methylnorbornene as a result of C-H activation occurring at

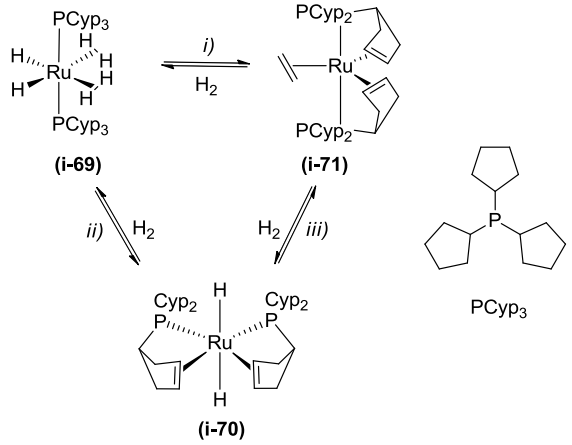
the metal centre when $PCyp_3$ is reacted in C_6D_{12}.[87] Similar conclusions were drawn from the thermal decomposition of a bis(tricyclopentylphosphine)platinacyclopentane complex.[88]

Sabo-Etienne *et al.* have shown that tricyclohexylphosphine on a Ru centre can undergo dehydrogenation to form an η^3 – bound complex **(i-68)** (Scheme 1.16).[73] This complex is the result of an intramolecular dehydrogenation of $Ru(PCy_3)_2(H)_2(\eta^2\text{-}H_2)_2$ **(i-20)** promoted by ethene, which acts as a sacrificial hydrogen acceptor.



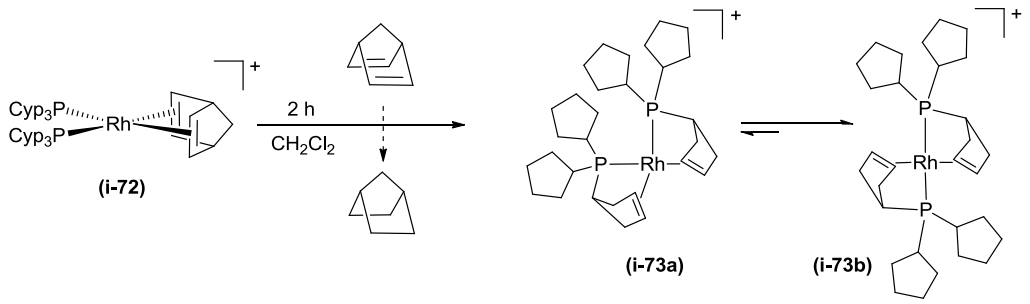
Scheme 1.16 Intramolecular dehydrogenation of $Ru(PCy_3)_2(H)_2(\eta^2\text{-}H_2)_2$ **(i-20)** using a hydrogen acceptor.

Further studies found that **i-20** is an active catalyst for the dehydrogenative silylation of ethene to vinylsilane[84] and the first complex to undergo C-H activation of a cyclohexyl ring from both tricyclohexylphosphines present in the complex in the presence of a hydrogen acceptor (*i.e. tert*-butylethylene, tbe) to form **i-67**.[73] Following on from this discovery, the tricyclopentylphosphine ($PCyp_3$) analogue $Ru(PCyp_3)_2(H)_2(\eta^2\text{-}H_2)_2$ **(i-69)**[89] was also shown to undergo reversible intramolecular dehydrogenation with a cyclopentyl substituent on both phosphine ligands using an ethene atmosphere forming **i-70** initially and **i-71** over 48 hours (Scheme 1.17).[90]



Scheme 1.17 Reversible C-H activation of $PCyp_3$; *i)* C_2H_4, 48 h, *ii)* C_2H_4, 2 min, *iii)* C_2H_4, 48 h.

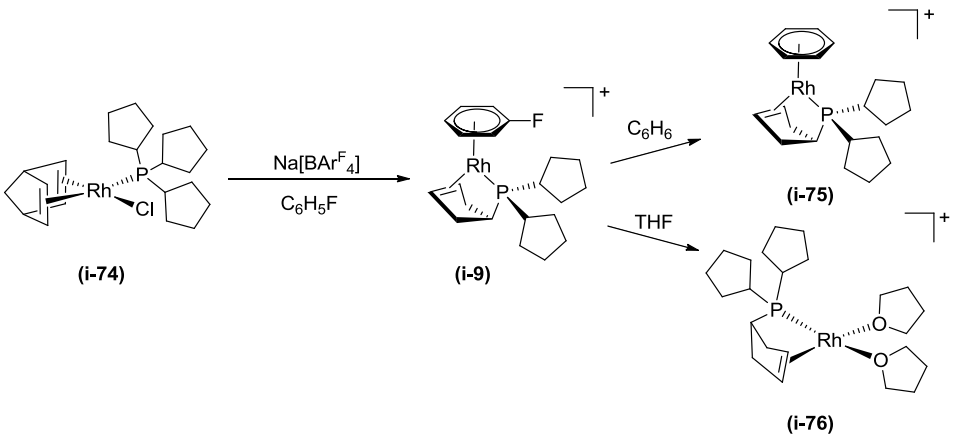
The reuptake of hydrogen from **i-71** to **i-69** was found to occur over 2.5 hours. The authors go on to suggest the potential of this route for hydrogen storage in C-H bonds.



(i-72) (i-73a) (i-73b)

Scheme 1.18 Formation of *cis*- and *trans*- isomers of $[Rh\{PCyp_2(\eta^2\text{-}C_5H_7)\}_2][BAr^F{}_4]$ **(i-73a/b)**. $[BAr^F{}_4]^-$ anions not shown.

Concurrent with Sabo-Etienne and co-workers, research within the Weller group reported intramolecular dehydrogenation of cyclopentyl groups in cationic Rh-phosphine complexes. The reaction of $[Rh(NBD)Cl]_2$ with tricyclopentylphosphine and $Na[BAr^F{}_4]$ yields $[Rh(NBD)(PCyp_3)_2][BAr^F{}_4]$ **(i-72)**, which over the course of two hours converts into a mixture of two isomeric complexes in equilibrium with each other, each of which have undergone a dehydrogenation of a cyclopentyl group on each of the two phosphines; *cis*-$[Rh\{PCyp_2(\eta^2\text{-}C_5H_7)\}_2][BAr^F{}_4]$ **(i-73a)** and *trans*-$[Rh\{PCyp_2(\eta^2\text{-}C_5H_7)\}_2][BAr^F{}_4]$ **(i-73b)** (Scheme 1.18). **i-73b** dominates when left for 48 hours at room temperature (ratio **i-73b**: **i-73a** = 3:1) or upon heating to 40°C (ratio **i-73b**: **i-73a** = 4:1) indicating a high barrier to reorganisation of the ligands. In this reaction norbornadiene acts as the hydrogen acceptor.[91]

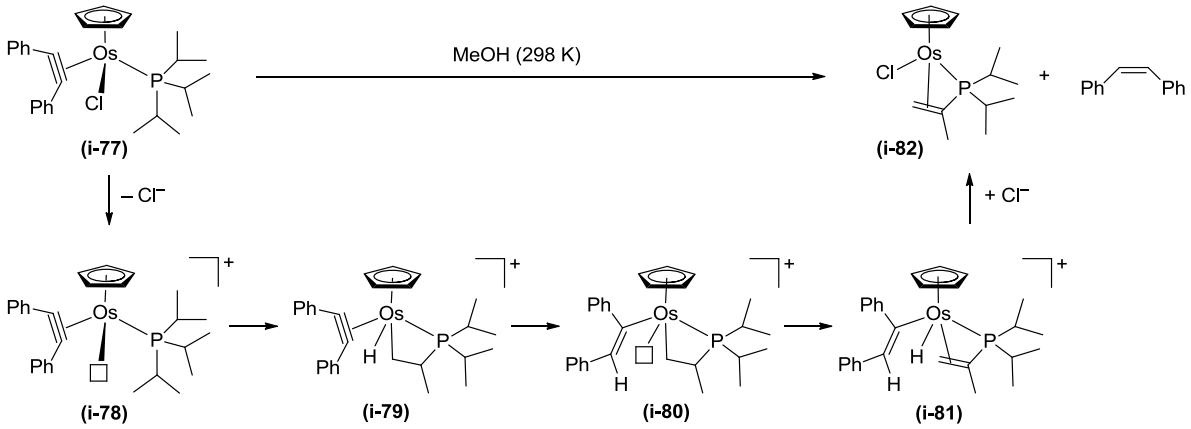


(i-74) (i-9) (i-75) (i-76)

Scheme 1.19 Formation of complexes **i-9** and **i-75/76**. $[BAr^F{}_4]^-$ anions not shown.

This intramolecular dehydrogenation was also found to occur in mono-phosphine complexes.[12] Reaction of the norbornadiene complex [Rh(NBD)($PCyp_3$)Cl] **(i-74)** in C_6H_5F solvent forms [Rh(η^6–C_6H_5F){$PCyp_2$(η^2–C_5H_7)}][BAr^F_4] **(i-9)**. Complex **i-9** reacts with benzene or THF by substitution of the weakly bound C_6H_5F ligand to form [Rh(η^6–C_6H_6){$PCyp_2$(η^2–C_5H_7)}][BAr^F_4] **(i-75)** and [Rh(THF)$_2${$PCyp_2$(η^2–C_5H_7)}][BAr^F_4] **(i-76)** respectively (Scheme 1.19). **i-9** and **i-76** have been shown to be effective catalysts in 1,4 addition reactions.[12]

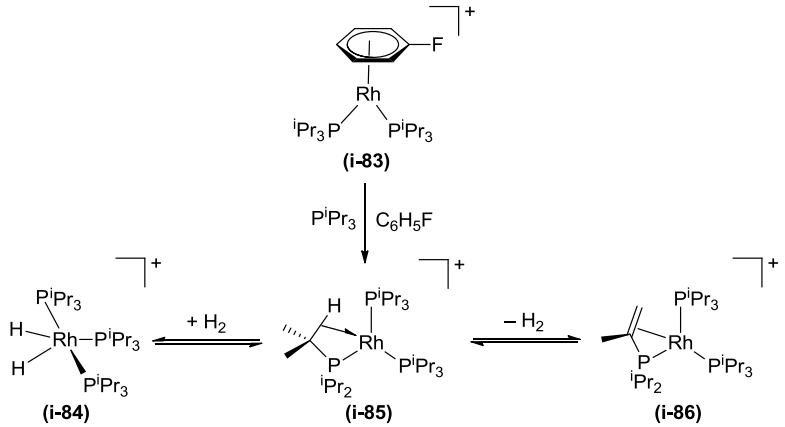
Dehydrogenation of isopropylphosphine using an alkyne as a hydrogen acceptor has been discussed by Estruelas and co-workers using Os complex OsCpCl(η^2-PhC≡CPh)(P^iPr_3) **(i-77)** following the decoordination of the chloride atom in methanol (Scheme 1.20).[92]



Scheme 1.20 Intramolecular dehydrogenation of a coordinated isopropylphosphine ligand.

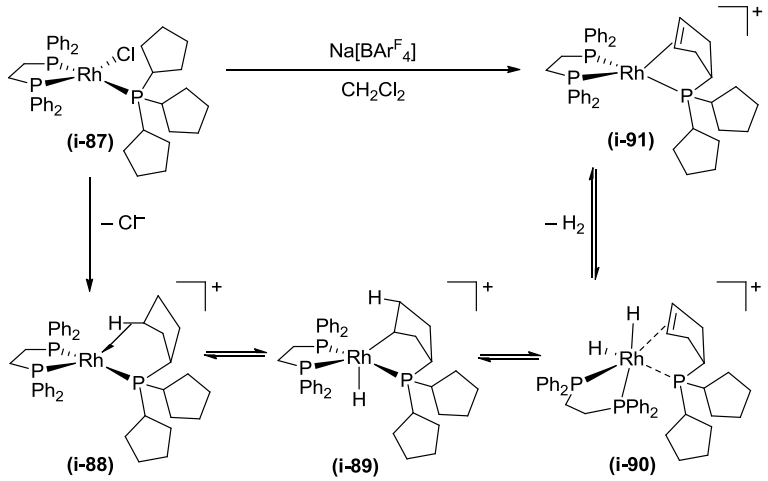
The hemilabile nature of the coordinated vinylphosphine of **i-82** has been exploited to participate in C-C coupling reactions of terminal alkynes and benzonitriles.[93] Glaser and Tilley have also fully characterised an analogous, though cationic, Os complex with a coordinated dehydrogenated isopropylphosphine ligand [Os(η^5-C_5Me_5)$(H)_2${$^iPr_2P$(η^2-MeC=CH_2)}][$B(C_6F_5)_4$] formed as a consequence of halide extraction and without the need for a sacrificial hydrogen acceptor.[94]

Spontaneous, acceptorless dehydrogenation of isopropylphosphine has also been observed by Chaplin and Weller from a cationic triisopropylphosphine Rh complex with a β-CH-agostic interaction from one of the isopropyl groups **(i-85)** (Scheme 1.21).[95] Computational studies have indicated that although γ-C-H activation is possible, dehydrogenation to **(i-86)** goes exclusively *via* the β-CH-agostic complex **(i-85)**.



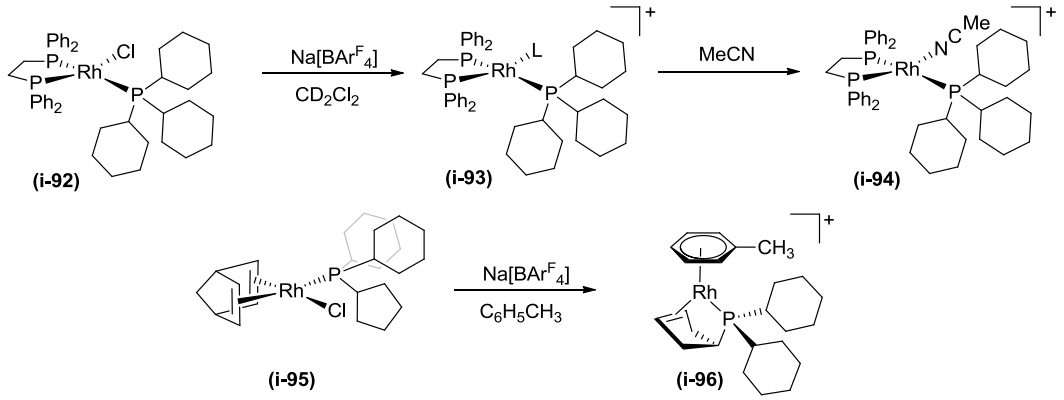
Scheme 1.21 Dehydrogenation of isopropylphosphine *via* a β-H-agostic complex **(i-85)**. $[BAr^F{}_4]^-$ anions not shown.

Remarkably, reaction of $Rh(Ph_2P(CH_2)_2PPh_2)(PCyp_3)Cl$ **(i-87)** with $Na[BAr^F{}_4]$ in CH_2Cl_2 yields $[Rh(Ph_2P(CH_2)_2PPh_2)\{PCyp_2(\eta^2\text{–}C_5H_7)\}][BAr^F{}_4]$ **(i-91)** which also contains a chelating phosphine-alkene ligand formed as a consequence of acceptorless dehydrogenation of the cyclopentyl moiety (Scheme 1.22).



Scheme 1.22 Suggested mechanism for the dehydrogenation of **i-87** to **i-91**.

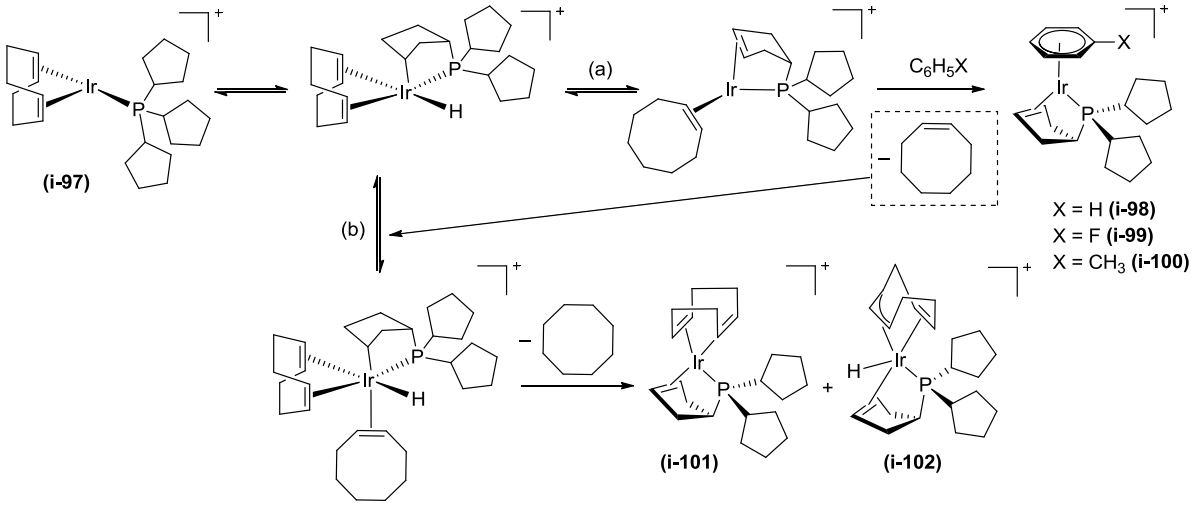
The formation of **i-91** from **i-87** reaches completion in 5 minutes at room temperature, in quantitative yield by NMR spectroscopy and has been probed mechanistically by DFT calculations.[91] The overall mechanism for this example of acceptorless intramolecular alkyl dehydrogenation is also shown in Scheme 1.22. Stepping through the mechanism, removal of the chloride by $Na[BAr^F_4]$ leaves a vacant coordination site at the metal centre which promotes C-H activation of a cyclopentyl group **(i-88)** to form an alkyl hydride **(i-89)**. Subsequent β-hydride elimination results in the formation of a Rh *trans* dihydride, which upon a *trans-cis* isomerisation **(i-90)** (the rate determining step according to computational studies), can reductively eliminate to release hydrogen and form the final phosphine-alkene coordinated complex **(i-91)**. Of particular significance to the idea of hydrogen storage in alkanes, **i-91** has been found to reversibly uptake a total of three equivalents of hydrogen in both solution and solid states.[96] This ability to store and release hydrogen however represents a very modest 0.35 % (w/w) of the complex which makes it unviable as a means to support practical applications.



Scheme 1.23 (top) Dehydrogenation of PCy_3 does not take place; (bottom) Selective dehydrogenation of the cyclopentyl group in **i-95** yields **i-96**. L = solvent or agostic interaction.

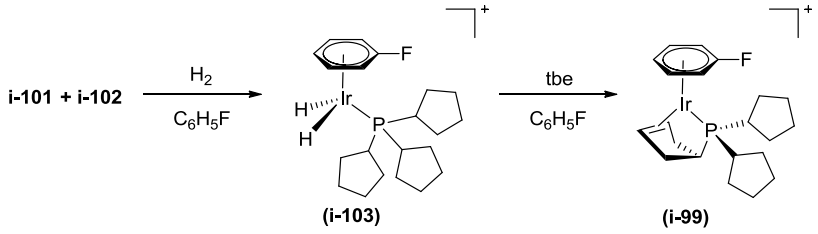
Unlike the Ru chemistry as reported by Sabo-Etienne, the equivalent tricyclohexylphosphine Rh complex, $Rh(NBD)(PCy_3)Cl$ **(i-92)**, does not undergo dehydrogenation of the cyclohexyl moieties and a comparison experiment with the mixed phosphine complex $Rh(NBD)(PCy_2Cyp)Cl$ **(i-95)** shows that upon the addition of $Na[BAr^F_4]$ in toluene, the sole

product is a consequence of exclusive dehydrogenation of the cyclopentyl group; $[Rh(C_6H_5CH_3)\{PCy_2(\eta^2\text{–}C_5H_7)\}][BAr^F{}_4]$ **(i-96)** (Scheme 1.23).[91]



Scheme 1.24 Proposed routes for the formation of **i-98-100. [**$BAr^F{}_4]^-$ anions not shown.

Parallel chemistry has been observed on moving from Rh to Ir. Addition of $Na[BAr^F{}_4]$ to $Ir(COD)(PCyp_3)Cl$ in arene solvent generates $\{Ir(COD)(PCyp_3)\}^+$ **(i-97)** and results in the production of cationic Ir η^6-bridged arene complexes **(i-98-100)** with a coordinated phosphine-alkene as a result of sequential C-H activation and β-hydrogen elimination processes on one of the cyclopentyl ligands (Scheme 1.24).[97] Alongside the formation of **i-98-100** (pathway a), $[Ir(\eta^2\text{:}\eta^2\text{-}C_8H_{12})\{PCyp_2(\eta^2\text{-}C_5H_7)\}][BAr^F{}_4]$ **(i-101)** and $[IrH(\eta^2\text{:}\eta^3\text{-}C_8H_{11})\{PCyp_2(\eta^2\text{-}C_5H_7)\}][BAr^F{}_4]$ **(i-102)** are also observed as a consequence of a competitive alternate pathway (b) whereby a displaced cyclooctene ligand can compete with the loss of hydrogen from the cyclooctadiene complex.



Scheme 1.25 Improved method for the formation of **(i-99)**. $[BAr^F{}_4]^-$ anions not shown.

The quantitative formation of **i-99** however can be achieved upon the addition of tbe to [Ir(η^6-C_6H_5F)($PCyp_3$)$(H)_2$][$BAr^F{}_4$] **(i-103)**, itself made from the hydrogenation of a mixture of **i-101** and **i-102** (Scheme 1.25).

1.3.2.1 Phosphine-alkene ligands in catalysis

The combination of a strong σ-donor phosphorus ligand and the immediacy of an alkene ligand setup coordination to a metal centre and give greater potential for subsequent efficient (enantioselective) catalysis over just alkene coordination alone as a result of being able to form stable, but sufficiently reactive, precursors and intermediates (Figure 1.7).

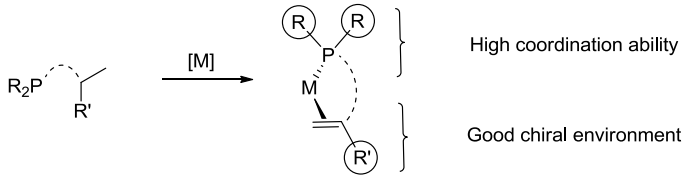
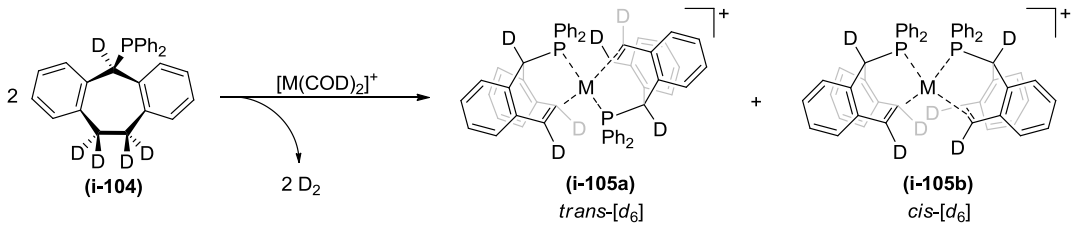


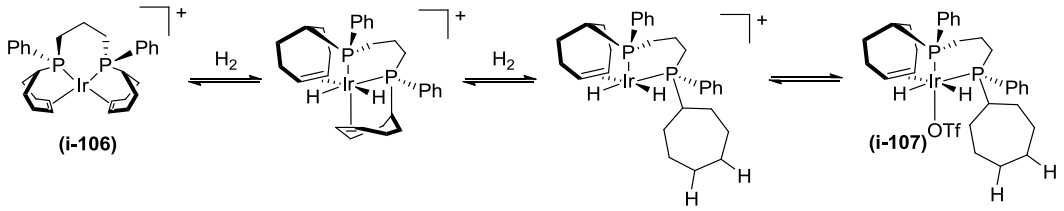
Figure 1.7 Example of phosphine-alkene coordination at a metal centre.

Grützmacher and co-workers have synthesised a range of (5*H*-dibenzo[*a*,*d*]cyclohepten-5-yl)-phosphine alkene ligands (PALs) over the last decade and have developed their coordination to both Rh and Ir principally to investigate the redox activity of unusual Rh(0) and Ir(0) complexes.[98]



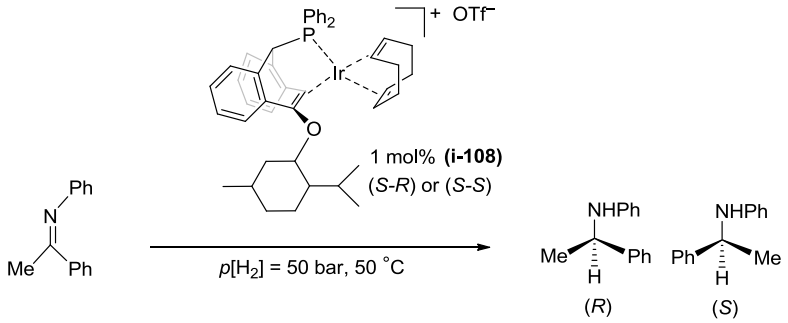
Scheme 1.26 Dehydrogenation of a X_2-tropp^R ligand by Rh and Ir, here X= D. Anions not shown.

The stable first generation X_2-tropp^R ligand **(i-104)** (tropp^R; R = phosphorus bound substituent, X = H/D) has been shown to undergo acceptorless dehydrogenation to the chelating phosphine-alkene ^{C}tropp^{Ph} ligand in the presence of Rh(I) and Ir(I) species **(i-105a/b)** (Scheme 1.26)[99] and can be rehydrogenated in the case of chiral [Ir(^{C}tropp^{Ph})$_2$]OTf **(i-106)** (Scheme 1.27).[100]



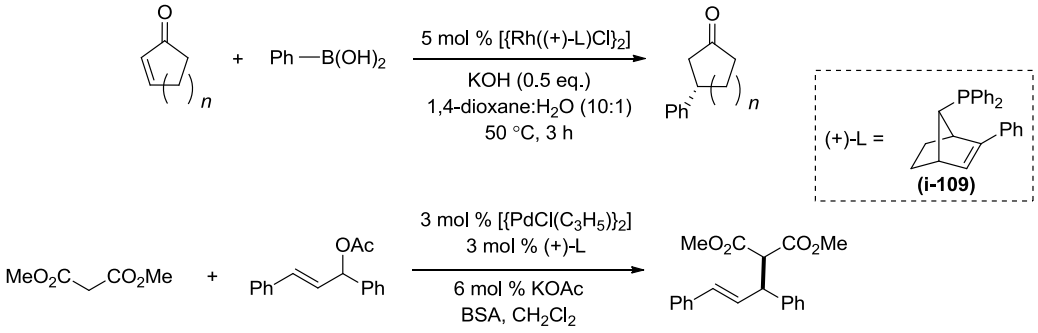
Scheme 1.27 Reversible hydrogenation of a chiral chelating tropp ligand.

[Ir(^{C}tropp^{Ph})$_2$]OTf **(i-106)** incorporates a second generation phenyl-substituted chiral tropp ligand and is competent in the catalytic hydrogenation of 1-octene and cyclooctene, imines and several esters though with a very modest enantiomeric excess.[101] More effectively, chiral tropp based complexes of this variety have also been found to be active catalysts for the 1,4-conjugative addition of phenylboronic acid to α,β-unsaturated carbonyl compounds yielding substituted ketones with excellent enantiomeric selectivity following on from previous work on Suzuki-Miyaura Pd cross coupling.[101] A Rh phosphine-alkene complex based on binaphthyl has also been remarked to show similar reactivity.[102]



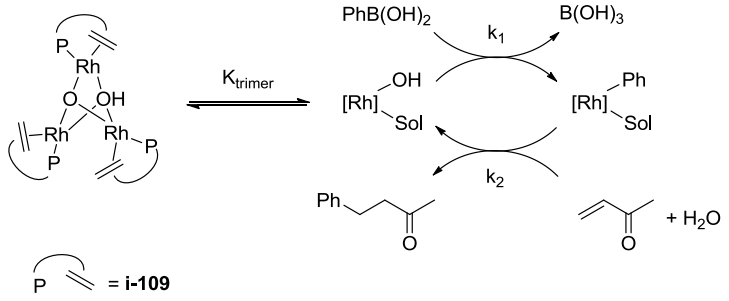
Scheme 1.28 Enantioselective hydrogenation of phenyl(1-phenylethylidene)amine with **i-108**.

Other Ir chiral tropp-type complexes containing a bound mentholate (*R*-/ *S*-) moiety (*e.g.* **i-108**) have also shown promising activity in catalytic imine hydrogenations with the highest enantiomeric excess (86 %) reached with PhN=CMePh and the *R,R* enantiomer of the (10-menthyloxy-5*H*-dibenzo[*a,d*]cyclohepten-5-yl)diphenylphosphine ligand (Scheme 1.28).[80]



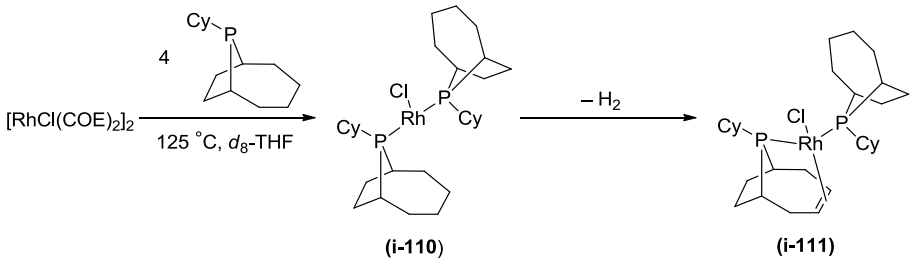
Scheme 1.29 (top) Rh catalysed 1,4-addition of boronic acids to unsaturated ketones using chelated phosphine-alkene ligand **i-109**; (bottom) Pd catalysed allylic alkylation using **i-109**. BSA = Bis(trimethylsilyl)acetamide.

Synchronously with the work of Grützmacher, Hayashi *et al.* published the synthesis of chiral phosphine-alkene ligands based on a norbornene scaffold (*e.g.* **(i-109)**).[77] These chiral ligands, which are achieved following an eight step procedure, are also active in the Rh catalysed Hayashi-Miyaura coupling[78] as described above and the Pd catalysed allylic alkylation of 1,3-diphenyl-2-propenyl acetate (Scheme 1.29).[83]



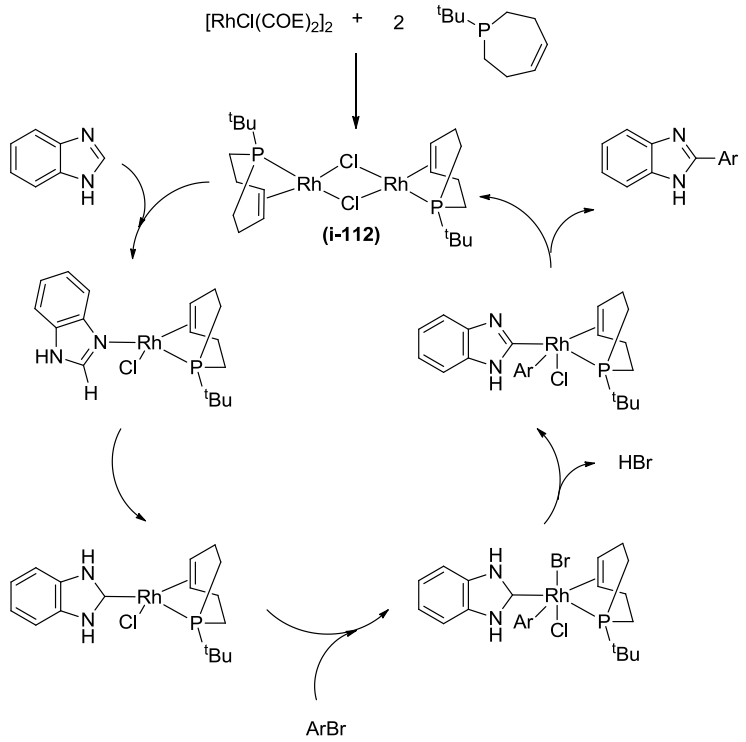
Scheme 1.30 Suggested catalytic cycle for the Rh phosphine-alkene catalysed 1,4-addition of phenylboronic acid to methyl vinyl ketone. Sol = coordinated solvent molecule.

In-depth kinetic analysis has suggested that the mechanism for the 1,4-addition reactions incorporating **i-109** involves a trimer-monomer rather than a dimer-monomer equilibrium as a result of the calculated order dependence of the catalyst (0.4). (Scheme 1.30)[78].



Scheme 1.31 Synthesis of a neutral Rh bis-phoban complex containing a chelating dehydrogenated phoban ligand **(i-111)**.

Ellman and co-workers have recently reported the intramolecular dehydrogenation of Rh phoban complexes during azole arylation catalysis (Scheme 1.31).[81] Isolation of the phosphine-alkene complexes (*e.g.* **i-111**) and independent catalytic studies has shown that the superior activity of these species is due to the formation of these PAL complexes rather than the steric and electronic properties of the phoban ligands alone.

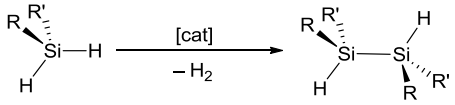


Scheme 1.32 Proposed mechanism for the functionalisation of a nitrogen heterocycle by a Rh phosphepine dimer **(i-112)**.

An extension of this work saw the development of phosphepine ligands which mimic phoban ligands and revealed improved activity and selectivity for arylation over an undesired

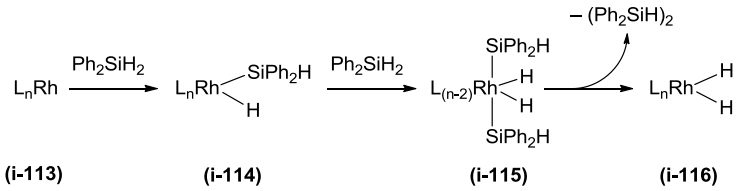
hydrodehalogenation side reaction.[82] The hypothesised mechanism for this process from a Rh phosphepine dimer **(i-112)** incorporates the formation of an *N*-heterocyclic carbene which sets up the metal centre ideally for oxidative addition of the aryl bromide, however this is yet to be experimentally ratified (Scheme 1.32).

1.3.3 Dehydropolymerisation of silanes



Scheme 1.33 A representative example of silane dehydrocoupling for primary (R = H, R' = alkyl, aryl) and secondary (R and R' = alkyl, aryl) silanes.

The dehydrogenative coupling of secondary silanes (*e.g.* Scheme 1.33) has precedence as far back as 1973 when Ojima *et al.* formed $(SiPh_2H)_2$ in 38 % yield from Ph_2SiH_2 with Wilkinson's Catalyst (0.1 mol%).[103] This area was further developed in the 1980's using Ti and Zr derivatives.[104,105] Today, industrial scale preparation of polysilanes is achieved by the Würtz coupling of diorganodihalosilanes using molten sodium,[106] but transition metal catalysis is considered as the most efficient alternative.[107]



Scheme 1.34 Curtis-Epstein mechanism for dehydrogenative coupling of Ph_2SiH_2 *via* a Rh(III) dihydride species.

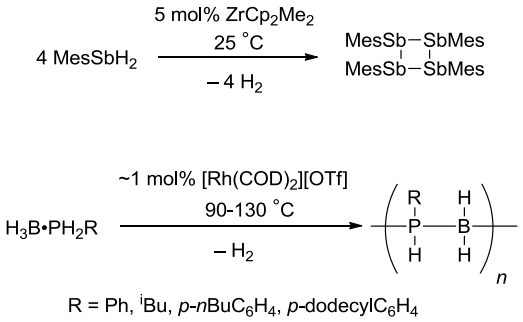
The generally accepted mechanism for silane dehydrocoupling is that devised by Curtis and Epstein (Scheme 1.34).[108] Addition of two equivalents of diphenylsilane to **i-113** results in the generation of a complex with two separate M-$SiPh_2H$ bonds **(i-115)** which then reductively eliminates $(SiPh_2H)_2$ to form **i-116**. Silyl(silylene) intermediates have also been eluded to in several mechanisms,[109,110,111,112] including a recent study of the mechanism of dehydrocoupling

of secondary silanes using Wilkinson's catalyst which has concluded that a Rh hydride species is the active catalyst.[113]

1.3.4 Dehydrogenation and dehydrocoupling of amine-boranes

1.3.4.1 Introduction

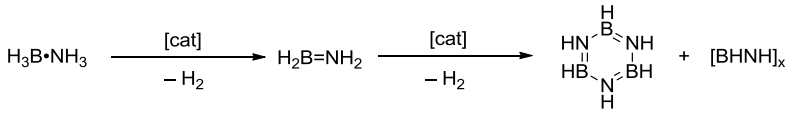
The dehydrocoupling of main group elements with the concomitant release of hydrogen is an important method for the creation of an E-E bond. Processes for a variety of Group 13-15 elements have been discovered but it is beyond the scope of this introduction to discuss them all in detail here (Scheme 1.35).[114,115]



Scheme 1.35 Representative examples of the dehydrocoupling of Group 13-15 elements.

Evolution of hydrogen as a by-product of dehydrocoupling makes compounds of high gravimetric hydrogen capacity which can efficiently release it interesting with regard to chemical hydrogen storage efforts.[116,117] Ammonia-borane (AB, $H_3B{\cdot}NH_3$) is a lead player in this field as it contains 19.6 wt % hydrogen which is sufficiently above that needed for use on a practical scale (9 wt % hydrogen by 2015 as stipulated by US Department of Energy for the storage and delivery of such a hydrogen storage system) and has provoked intense study in recent years.[118,119,120,121,122] The dehydrogenation and dehydrocoupling of AB forms borazine and highly insoluble polymers as products (Scheme 1.36).[123] The main drawback of AB is the difficulty in rehydrogenating the B-N polymeric products of dehydrocoupling.[124] Only in the process of writing this introduction has the first example of rehydrogenation of these polymeric

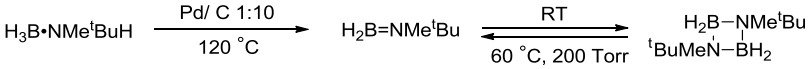
materials to AB using hydrogen (sourced from hydrazine and liquid ammonia) been published in Science.[125]



Scheme 1.36 Dehydrogenation and dehydrocoupling of AB to form borazine and polymeric material.

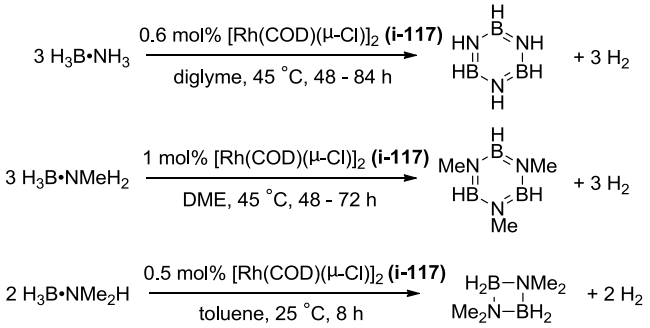
1.3.4.2 Early examples

The dehydrogenation and dehydrocoupling of AB is easily achieved at elevated temperature (100-150 °C).[126] Interest in transition metal promoted dehydrogenation and dehydrocoupling of AB and its amine-borane derivatives has only taken hold in the past decade.[127] The first example of a transition metal complex catalysing the dehydrogenation of an amine-borane was that reported by Roberts and co-workers in 1989.[128] Heating $H_3B{\cdot}NMe^tBuH$ at 120°C under argon using Pd/C resulted in the dehydrogenation of the amine-borane to form $H_2B{=}NMe^tBu$ which rapidly dimerised at room temperature to yield $[H_2BNMe^tBu]_2$ (Scheme 1.37). Upon heating the dimer to 60 °C it was found to convert back to the monomeric complex.



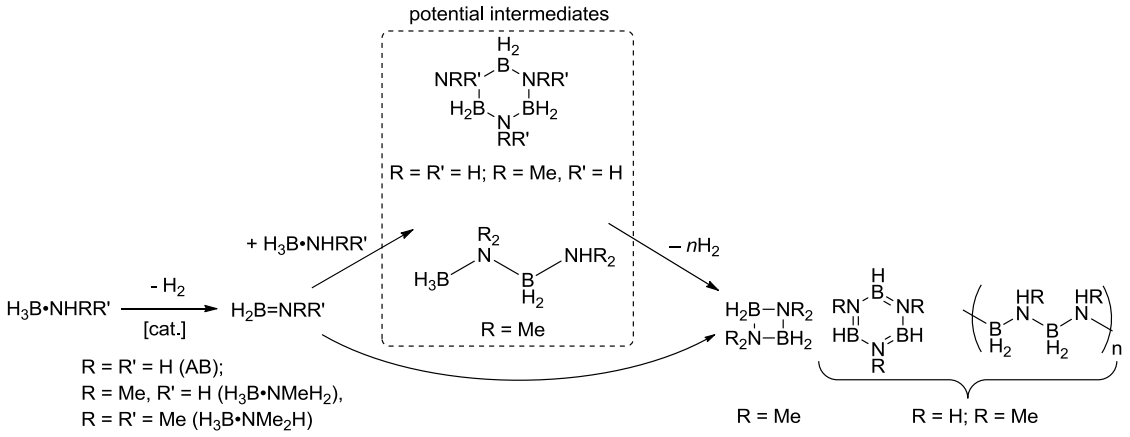
Scheme 1.37 Dehydrogenation of $H_3B{\cdot}NMe^tBuH$.

It was not until 2001 that the next example of a transition metal promoting dehydrogenation of an amine-borane was reported by Manners *et al.* as part of a wider study on dehydrocoupling catalysis.[129] $H_3B{\cdot}NMe_2H$, which quantitatively loses hydrogen upon heating to 130 °C to form the dimeric species $[H_2BNMe_2]_2$ as the sole product, was observed to dehydrocouple at just 25 °C using $[Rh(COD)(\mu\text{-}Cl)]_2$ **(i-117)** at 0.5 mol% loading (Scheme 1.38).



Scheme 1.38 The first examples of transition metal catalysed formation of the products of AB, $H_3B{\cdot}NMeH_2$ and $H_3B{\cdot}NMe_2H$ dehydrocoupling.

Further research showed that dehydrocoupling was not limited to this particular amine-borane with $H_3B{\cdot}NH_3$ and $H_3B{\cdot}NMeH_2$ forming trimeric products upon addition of **i-117** under the same conditions (Scheme 1.38), a transformation that was only previously possible upon heating the precursors to over 100 °C.[130] A continuation of this work saw dehydrogenation strategies extend to potential oligomeric intermediates in amine-borane dehydrocoupling (Scheme 1.39).[114] $H_3B{\cdot}NMe_2BH_2{\cdot}NMe_2H$, although not observed in catalysis to form $[H_2BNMe_2]_2$ with **i-117**, was independently synthesised and subsequently reacted under catalytic conditions (**i-117**, 1.5 mol%, 25 °C). Total conversion to $[H_2BNMe_2]_2$ was observed after 48 hours. $[H_2B{\cdot}NMeH]_3$ was observed as an intermediate in the dehydrocoupling of $H_3B{\cdot}NMeH_2$ to $[HBNMe]_3$ and was also found to be equally competent in the slow (45 °C, 40 h) catalytic dehydrogenation to form $[HBNMe]_3$ when added in the absence of $H_3B{\cdot}NMeH_2$.

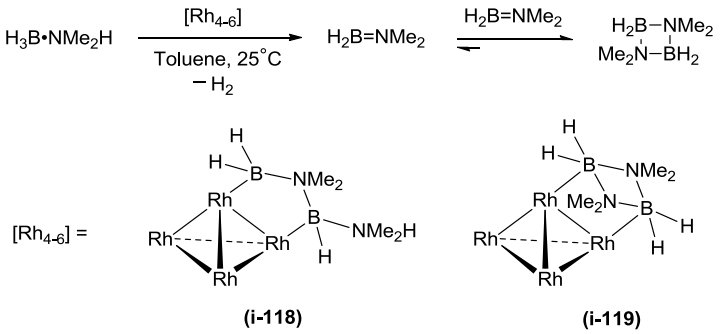


Scheme 1.39 Dehydrogenation of amine-boranes to form dehydrocoupled products with the aid of a catalyst.

Since 2004 a number of homogeneous systems have been discovered which have further improved the efficiency of dehydrocoupling and have begun to improve the understanding of the mechanism[126] (Section 1.3.4.3). These will thus be the main focus of this part of the introduction. The dehydrogenation and dehydrocoupling of $H_3B{\cdot}NMe_2H$ is a simple system to model as $[H_2BNMe_2]_2$ is the sole final product of the reaction and is easily identifiable by NMR spectroscopy as well as being soluble in common solvents.[129] Trimers and polymers which result from the dehydrogenation and dehydrocoupling of $H_3B{\cdot}NMeH_2$ and AB frequently suffer solubility problems and exhibit broad peaks by NMR spectroscopy.[114] Techniques such as IR spectroscopy, Gel Permeation Chromatography (GPC) and Dynamic Light Scattering (DLS) have been used for their characterisation although definitive characterisation is still problematic.[123]

In 2005 Autrey and co-workers reported that the dehydrogenation and dehydrocoupling of $H_3B{\cdot}NMe_2H$ to form $[H_2BNMe_2]_2$ using $[Rh(COD)(\mu\text{-}Cl)]_2$ **(i-117)**, under similar conditions to Manners' first report, was in fact as a result of the formation of a soluble Rh_6 cluster which forms rapidly upon addition of $H_3B{\cdot}NMe_2H$ and not an active heterogeneous catalyst as suggested by Manners.[131] A combination of X-ray absorption fine structure spectroscopy (XAFS) and ^{11}B NMR spectroscopy revealed that over a 45 minute period, after which 45% of $H_3B{\cdot}NMe_2H$ has reacted, the soluble Rh_6 cluster is the major species present in solution and that only after this time is an insoluble precipitate observed. Further work by the same group also showed that Rh_4 to Rh_6 clusters form cleanly from their Rh precursors and that they could be the active catalyst for the dehydrogenation process, although again, more simple monomeric fragments could not be definitively ruled out.[132] In addition, combining the XAFS data with computational calculations on $Rh_4(CO)_{12}$ (which has a similar coordination number to that found for the clusters in this study) suggests the coordination modes of the amine-borane to the cluster as depicted in Scheme 1.40; where the dimeric product **(i-119)** and linear diborazane **(i-118)** bridge two metal atoms. Monodentate coordination of an amino- or amine-borane fragment

is discounted as the Rh-N distances are too long compared to experimental data with model complexes.



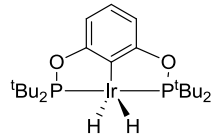
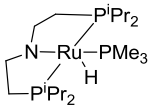
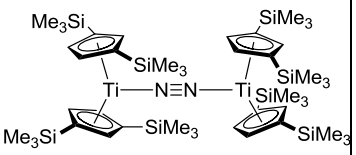
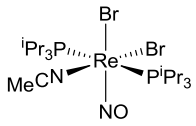
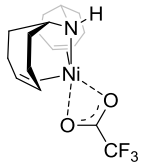
Scheme 1.40 The active catalyst for the dehydrogenation of $H_3B{\cdot}NMe_2H$ with $Rh_{4\text{-}6}$ clusters is likely to involve clusters with both linear diborazane **(i-118)** and dimer coordination **(i-119)**.

Significantly, the observance of a B-N containing intermediate, $H_2B{=}NMe_2$, was noted for the first time for the dehydrocoupling of $H_3B{\cdot}NMe_2H$ by ^{11}B NMR spectroscopy. Its inverse relationship with the concentration of $H_3B{\cdot}NMe_2H$ suggested that a second order process to form $[H_2BNMe_2]_2$ was operating (Scheme 1.40).

1.3.4.3 Catalytic systems

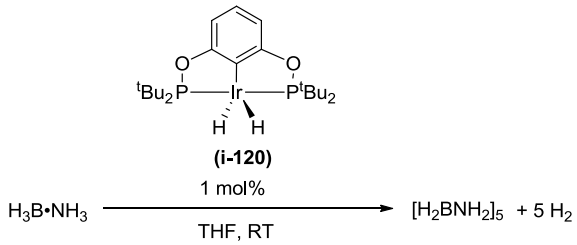
A summary of the most significant advances in the development of dehydrogenation and dehydrocoupling catalysts for AB, $H_3B{\cdot}NMeH_2$ and $H_3B{\cdot}NMe_2H$ is given in Table 1.1. The range of reaction times illustrated by the catalysts suggests that one overarching general mechanism for the process of dehydrogenation and dehydrocoupling of amine-boranes does not exist. Key ideas associated with each catalyst which provide insight into the mechanisms operating are highlighted where necessary in subsequent sections.

Table 1.1 Representative examples of amine-borane (AB/ MMAB/ DMAB) dehydrogenation and dehydrocoupling catalysts discussed in this introduction. NHC = (1,3,4-triphenyl-4,5-dihydro-1*H*-1,2,4-triazol-5-ylidene). Conversion percentage based on consumption of starting material.

	Substrate	Solvent	Conditions	Loading (mol%)	Time	Conversion	Ref.
 **(i-120)**	AB	C_6D_6	25ºC	1 0.25	4 mins 30 mins	100% 100%	133
$[Cr(CO)_6]$ **(i-121)**	DMAB MMAB	THF	8ºC, hυ	5	1 h	100% 98%	148
 **(i-122)**	DMAB	THF	25ºC	0.5	75 secs	70%	151
 **(i-123)**	DMAB	C_6D_6	23ºC	2	6 mins	80 %	162
$[Sc\{N\{SiHMe_2\}_2\}_3(THF)_2]$ **(i-124)**	DMAB	THF	60ºC	3	1 h	100%	177
$[Rh(P^iBu_3)_2][BAr^F{}_4]$ **(i-125)**	DMAB	1,2-$C_6H_4F_2$	25ºC	5	35 mins	100%	139
 **(i-126)**	DMAB	Dioxane	85ºC	1	4 h	99%	156
 **(i-127)**	DMAB	THF	25ºC	0.3	90 secs	100%	158
$Ni(NHC)_2$ **(i-128)**	AB	C_6D_6/ diglyme	60ºC	10	4 h	100%	155
$TiCp_2Cl_2$ 2^nBuLi **(i-129)**	DMAB	Toluene	20ºC	2	4 h	100%	121
$[Rh(1,5\text{-}COD)(\mu\text{-}Cl)]_2$ **(i-117)**	DMAB	Toluene	25ºC	5	< 2 h	100%	124
	MMAB	Monoglyme	45ºC	1	48-72 h	100%	
	AB	Diglyme	45ºC	0.6	48-84 h	100%	
$[FeCp(CO)_2]_2$ **(i-130)**	DMAB	THF	20ºC, hυ	5	4 h	100%	168
	MMAB	THF	20ºC, hυ	5	3 h	90%	
	AB	THF	20ºC, hυ	5	1 h	100 %	

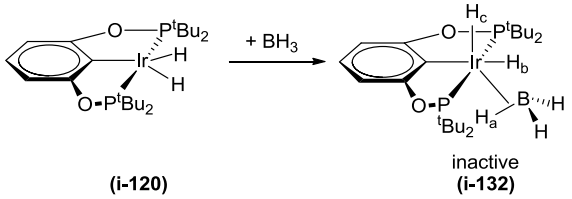
The benchmark in the dehydrogenation and dehydrocoupling catalysis of AB has come from work by Heinekey *et al.* who developed an Ir pincer complex capable of efficient dehydrogenation of AB at previously unprecedented rates and mild conditions in 2006.[133] At 1

mol% loading of catalyst Ir(POCOP)H_2 **(i-120)** (POCOP = [η^3-1,3-(OP^{t}Bu$_2$)$_2$C$_6$H$_3$]) dehydrogenation of AB is complete after just 4 minutes at room temperature to form a product suggested to be a cyclic pentamer $[H_2BNH_2]_5$ (Scheme 1.41).



Scheme 1.41 Dehydrogenation and dehydrocoupling of AB with Heinekey's Ir POCOP catalyst **(i-120)**.

Further reduction in the catalyst loading to give effective catalysis was achieved, which resulted in a lengthening of the reaction time (~15 minutes at 0.5 mol%, ~ 30 minutes at 0.25 mol% catalyst loading). NMR spectroscopy reveals that **i-120** is completely consumed upon the addition of AB to form a species suggested to be Ir(POCOP)H_4 which itself decreases in concentration as the reaction progresses to form an inactive complex assigned as Ir(POCOP)(H)(BH_4). Studies with **i-120** in 2008 found it to be an equally impressive catalyst in the dehydrocoupling of $H_3B{\cdot}NMeH_2$ to form a range of cyclic and oligomeric products of varied molecular weight.[134] The structure of Ir(POCOP)(H)(BH_4) was reassessed in 2008 by the same group and was suggested to be best described as a σ-BH_3 adduct; Ir(POCOP)$(H)_2$(BH_3) **(i-132)** as a consequence of low temperature NMR spectroscopy (Scheme 1.42).[135]



Scheme 1.42 Decomposition of **i-120** as a result of B-N bond cleavage results in the formation of **i-132**

1.3.4.4 Amine-borane σ-complexes and their role in dehydrocoupling processes

σ-borane complexes (R_2B-H) like **i-132** are relatively common in the literature in comparison with those of σ-amine-boranes, $H_3B{\cdot}NR_3$,[36,136,137] which have been suggested as key

intermediates in the dehydrogenation and dehydrocoupling of amine-boranes.[138,139] The characterisation and subsequent reactivity of these species has been the subject of significant recent research both experimentally and computationally but is frequently hampered by their inherent high reactivity.[140] The isoelectronic nature of amine-boranes to alkanes has also fuelled the drive for research into these ligands as they are likely to behave and interact in a similar manner to transient alkene analogues towards organometallic fragments.[42] Model ligands such as tertiary amine-boranes have proved the most useful in this regard as they coordinate in the same mode as their more reactive primary and secondary counterparts but do not undergo dehydrocoupling as a result of lacking an N-H bond (Figure 1.8).[138,141,142,143] Progress in the related field of phosphine-borane dehydrocoupling has also been made as result of isolating such complexes.[144]

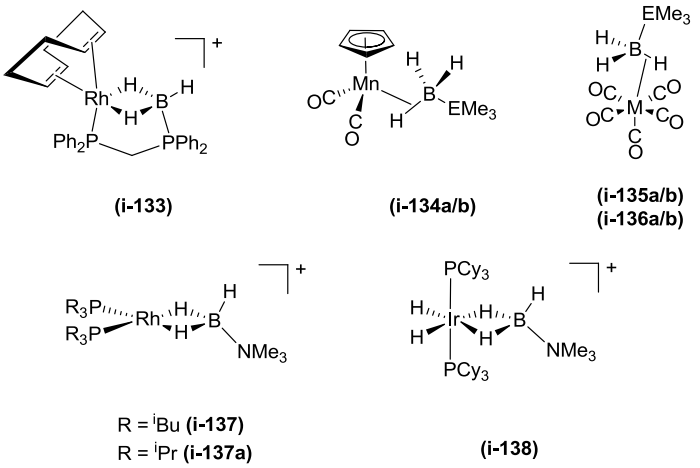


Figure 1.8 Examples of tertiary amine- and phosphine-borane complexes. M = Cr **(i-135)**/ W **(i-136)**; E = N **(a)** / P **(b)**. Anions not shown.

Shimoi and co-workers first reported conclusive characterisation of amine-borane coordination to transition metal complexes in 1999.[141] Photolysis of $[M(CO)_6]$ (M = Cr **(i-121)**, W) in the presence of $H_3B{\cdot}NMe_3$ results in the evolution of CO and the coordination of $H_3B{\cdot}NMe_3$ to quantitatively form $[M(CO)_5(\eta^1\text{-}H_3B{\cdot}NMe_3)]$ **(i-135a/136a)** as stable but air sensitive solids (Figure 1.8). The coordinated $H_3B{\cdot}NMe_3$ ligand was crystallographically characterised and shown to bind to the metal through only one of the B-H bonds in a 3c-2e bond with a long M-B

bond length suggesting a relatively weak interaction {*e.g.* Cr-B 2.873(15) Å}. Room temperature ^{1}H NMR spectroscopy found the proton signals assigned to the H_3B moiety of **i-135a** as a broad quartet [δ −3.3 {*J*(BH) 86 Hz}], the B-H coupling constant not differing significantly from the free ligand {*J*(BH) 98 Hz} consistent with a weak interaction. Low temperature ^{1}H NMR spectroscopy of these complexes did not resolve separate resonances for the bridging and terminal BH protons even at −80 °C indicating that the fluxional process operating is still faster than the NMR timescale at this temperature. The weak interaction of the $H_3B{\cdot}NMe_3$ ligand and the metal is further illustrated upon the addition of benzene solvent to the isolated solid which results in decomposition of the complex and the observance of free ligand in solution. The coordination of $H_3B{\cdot}NMe_3$ to the {$M(CO)_5$} fragment is mainly due to σ-donation from the amine-borane as the B-H group is a weak π-acceptor, a consequence of the B-H σ* orbital being too high in energy to enable backdonation of electron density from the metal centre (Figure 1.9).[141]

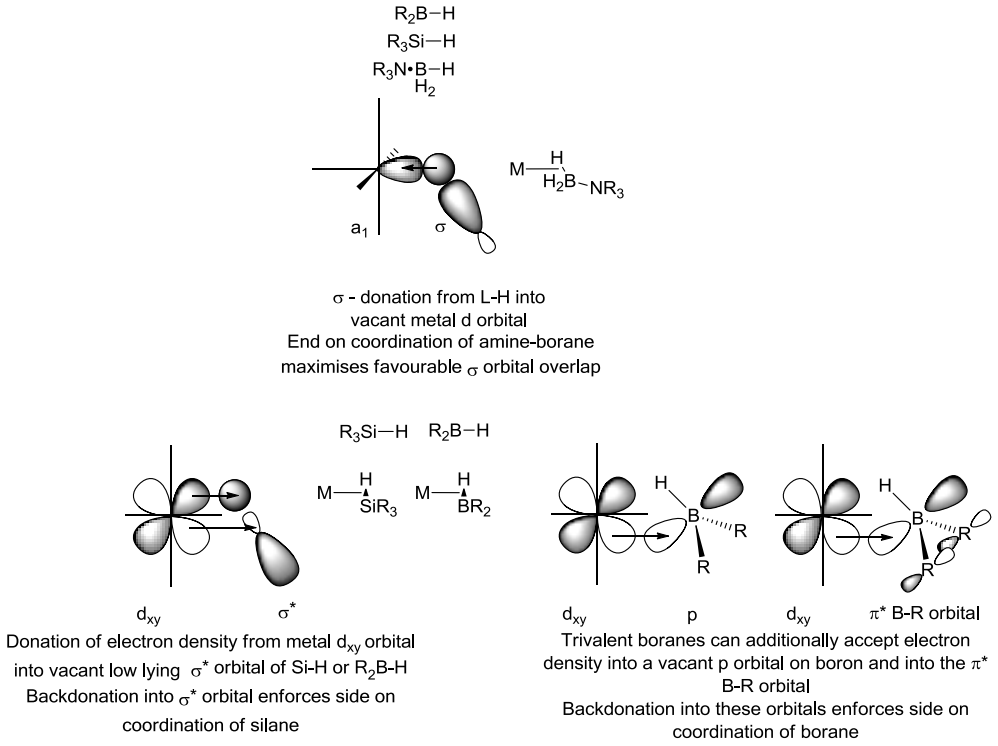
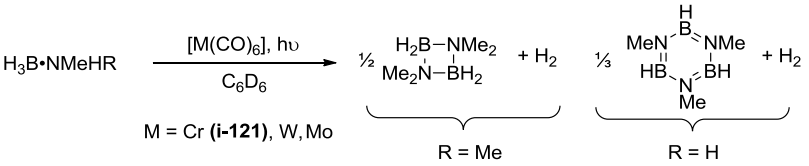


Figure 1.9 The role of σ and σ* orbitals in determining the bond strength of a σ interaction. For amine-boranes backdonation, as shown for the Si-H and R_2B-H interaction, is negligible and so end on coordination of the ligand is preferred.

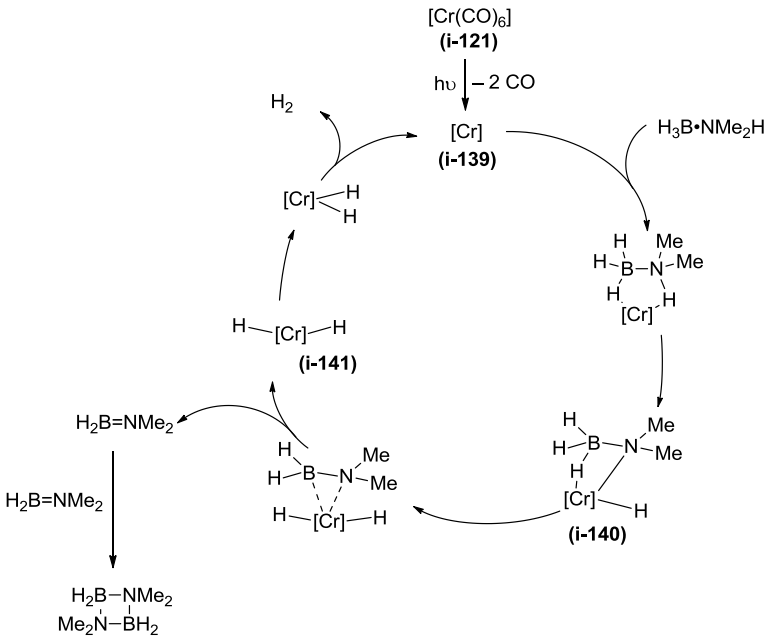
Silanes, dihydrogen ligands and trivalent boranes are better π-acceptors as a result of the σ* / p orbital being lower in energy and as a result form more stable complexes.[7,136] $H_3B{\cdot}NMe_3$ complexes using $\{MnCp(CO)_2\}$[145] and $\{Ru(C_5R_5)(PMe_3)_2\}^+$ (R = H/ Me)[146] fragments related to **i-135a** were subsequently discovered by the same group and found to show the same end on binding motif found upon coordination to the $\{M(CO)_5\}$ fragment. This geometry is adopted in favour of the side on construction observed for silanes and trivalent boranes. End-on coordination of the ligand minimises steric repulsion and is favoured as backdonation is considered negligible. With silanes and trivalent boranes, side on coordination competes for an approach that favours backdonation into a low lying σ*/ p orbital (Figure 1.9).[147]



Scheme 1.43 Dehydrogenation and dehydrocoupling of $H_3B{\cdot}NMe_2H$ and $H_3B{\cdot}NMeH_2$ respectively using Shimoi's system.

In 2009 Shimoi *et al.* extended his initial work with tertiary substrates to include the catalytic reactivity of $[M(CO)_6]$ (M = Cr **(i-121)**, W, Mo) towards primary and secondary amine-boranes $H_3B{\cdot}NMeH_2$ and $H_3B{\cdot}NMe_2H$ (Scheme 1.43).[148] Photolysis of $[Cr(CO)_6]$ **(i-121)** at 0.6 mol% loading with respect to the amine-borane substrate results in the catalytic formation of $[HBNMe]_3$ from $H_3B{\cdot}NMeH_2$ and $[H_2BNMe_2]_2$ from $H_3B{\cdot}NMe_2H$. A complex assigned as $[Cr(CO)_5(\eta^1\text{-}H_3B{\cdot}NMe_2H)]$ is observed by NMR spectroscopy immediately upon photolysis of **i-121** with $H_3B{\cdot}NMe_2H$ which then rapidly reacts on to yield $H_2B{=}NMe_2$ and $[H_2BNMe_2]_2$, the latter of which is also postulated to coordinate to the $\{Cr(CO)_5\}$ fragment in a similar manner to **i-135a** (Figure 1.8). DFT calculations on this system suggest that the active species is actually a $\{Cr(CO)_4\}$ fragment **(i-139)** which dehydrogenates $H_3B{\cdot}NMe_2H$ *via* an intramolecular process which initiates by N-H activation to form **(i-140)**. This is followed by B-H activation and subsequent elimination of aminoborane $H_2B{=}NMe_2$ to generate a Cr tetracarbonyl dihydride complex **(i-141)** which loses hydrogen upon isomerisation to regenerate **i-139** (Scheme 1.44).

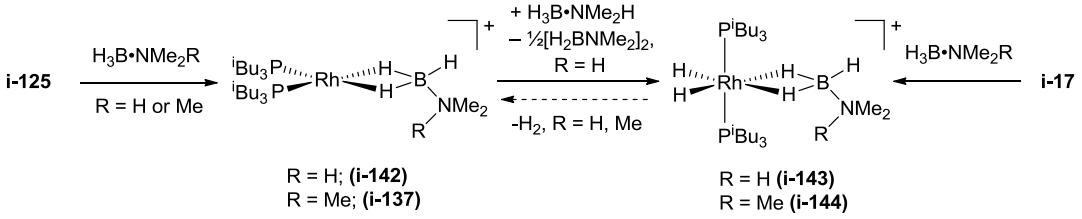
Consequently according to the authors, η^1-amine-borane complexes lie outside the catalytic cycle and merely act as a reservoir for the $\{Cr(CO)_5\}$ fragment.



Scheme 1.44 Shimoi's proposed catalytic cycle for the dehydrogenation of $H_3B{\cdot}NMe_2H$ by a $Cr(CO)_6$ pre-catalyst **(i-121)**. [Cr] = $\{Cr(CO)_4\}$ **(i-139)**.

The mechanism for the dehydrocoupling of amine-boranes highlighted in Shimoi's work above has only just started to receive preliminary investigations. Research in the Weller group in this area using the low coordinate complex $[Rh(P^iBu_3)_2][BAr^F{}_4]$ **(i-125)** began in 2008 to investigate the mechanism of the dehydrogenation and dehydrocoupling of $H_3B{\cdot}NMe_2H$ to give $[H_2BNMe_2]_2$.[138] Addition of 2 equivalents of $H_3B{\cdot}NMe_2H$ to **i-125** in 1,2-$C_6H_4F_2$ solution results in the rapid generation of σ-complex $[Rh(P^iBu_3)_2(\eta^2\text{-}H_3B{\cdot}NMe_2H)][BAr^F{}_4]$ **(i-142)**. The lifetime of this species is extremely short ($t_{½}$ ~ 1 minute) before it goes on to form $[Rh(P^iBu_3)_2(H)_2(\eta^2\text{-}H_3B{\cdot}NMe_2H)][BAr^F{}_4]$ **(i-143)** and $[H_2BNMe_2]_2$ (Scheme 1.45). A very similar complex $[Rh(IMes)_2(H)_2(H_3B{\cdot}NH_2{}^tBu)][BAr^F{}_4]$ (IMes = *N*,*N*-bis(2,4,6-trimethylphenyl)imidazol-2-ylidene) has since been characterised by Aldridge *et al.*[149] Addition of only one equivalent of $H_3B{\cdot}NMe_2H$ to **i-125** slowed dehydrocoupling sufficiently to permit the solution characterisation of **i-142** at low temperature. Reacting $H_3B{\cdot}NMe_3$ with **i-125** results in the formation of $[Rh(P^iBu_3)_2(\eta^2\text{-}H_3B{\cdot}NMe_3)][BAr^F{}_4]$ **(i-137)** which is stable and does not

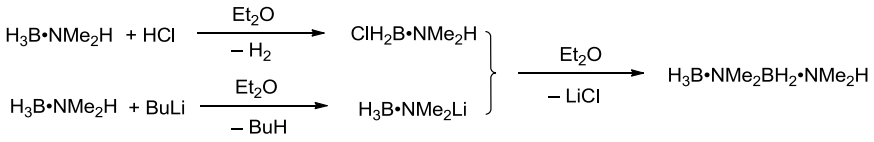
react further due to the inability of $H_3B{\cdot}NMe_3$ to dehydrogenate. The dihydride complex $[Rh(P^iBu_3)_2(H)_2(\eta^2\text{-}H_3B{\cdot}NMe_3)][BAr^F{}_4]$ **(i-144)** could be synthesised by the addition of $H_3B{\cdot}NMe_3$ to $[Rh(P^iBu_3)_2(H)_2][BAr^F{}_4]$ **(i-17)** (Scheme 1.45). A related cationic Ir bis-phosphine dihydride complex $[Ir(PCy_3)_2(H)_2(\eta^2\text{-}H_3B{\cdot}NMe_3)][BAr^F{}_4]$ **(i-138)** has also been isolated.[143]



Scheme 1.45 σ-complexes of $H_3B{\cdot}NMe_2H$ and $H_3B{\cdot}NMe_3$ using the $\{Rh(P^iBu_3)_2\}^+$ fragment derived from **(i-125)**. $[BAr^F{}_4]^-$ anions not shown.

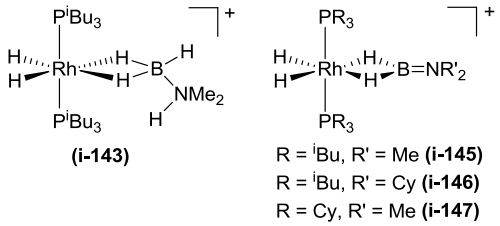
Each of complexes **i-125**, **i-143** and **i-144** are active catalysts in the dehydrogenation and dehydrocoupling of $H_3B{\cdot}NMe_2H$ with a turnover number of 34 h^{-1} (5 mol%, 1,2-$C_6H_4F_2$, 25 °C) in an open system under argon. In a sealed NMR tube at the same catalyst loading, catalysis is remarkably slower (2 h^{-1}) which is suggested to be due to catalyst inhibition as a result of the build up of hydrogen from the dehydrogenation process. Mercury poisoning tests and a non-sigmoidal kinetic profile suggest that this system is not heterogeneous. Monitoring the reaction by ^{11}B NMR spectroscopy reveals that the linear diborazane, $H_3B{\cdot}NMe_2BH_2{\cdot}NMe_2H$,[139] grows in and is consumed over the same timespan for total consumption of $H_3B{\cdot}NMe_2H$ to form $[H_2BNMe_2]_2$.* $H_3B{\cdot}NMe_2BH_2{\cdot}NMe_2H$ has also been observed as an intermediate in the dehydrocoupling of $H_3B{\cdot}NMe_2H$ with a photogenerated $TiCp_2$ homogeneous catalyst in work by Manners and co-workers[150] as well as with a [Ru(H)(PMe_3)(PNP)] {PNP = $N(CH_2CH_2P^iPr_2)_2$} catalyst **(i-122)** developed by Schneider.[151] Its independent synthesis was originally reported in 1999 by a non-catalytic route from $[Na\{(H_3B)_2NMe_2\}]$ using $ZrCl_4$,[152] and improved upon by Manners in 2003 (Scheme 1.46).[114]

* The linear diborazane was initially assigned as $[H_2BNMe_2]_3$ as the second BH_3 resonance of $H_3B{\cdot}NMe_2BH_2{\cdot}NMe_2H$ is hidden underneath the BH_3 resonance of $H_3B{\cdot}NMe_2H$.



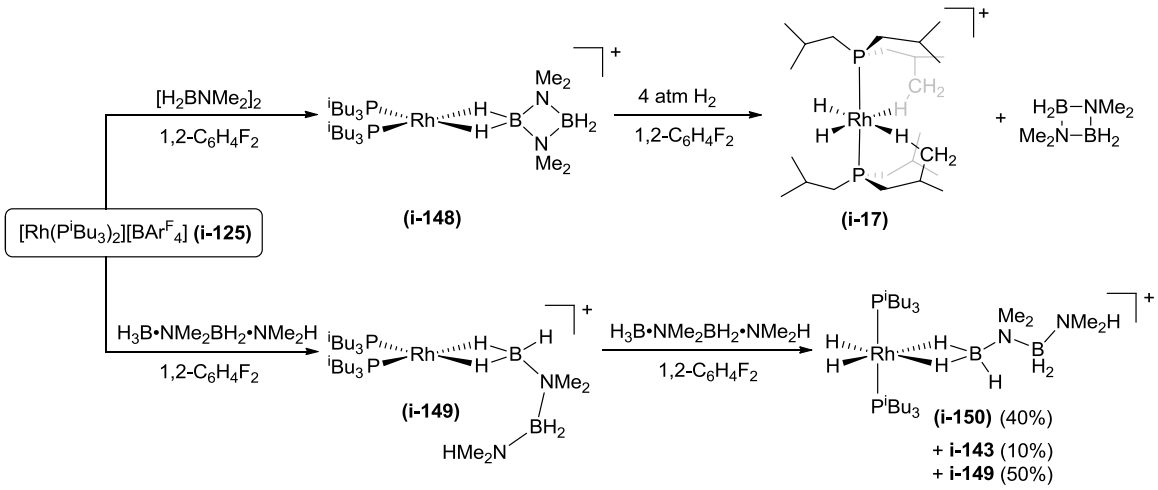
Scheme 1.46 Manners' synthesis of $H_3B{\cdot}NMe_2BH_2{\cdot}NMe_2H$.

Near the completion of $H_3B{\cdot}NMe_2H$ dehydrocoupling, using **i-143**, only the catalyst and another spectroscopically characterised complex $[Rh(P^iBu_3)_2(H)_2(\eta^2\text{-}H_2B{=}NMe_2)][BAr^F{}_4]$ **(i-145)** are observed by NMR spectroscopy (Scheme 1.47). Complex **i-143** diminishes in concentration when catalysis is complete suggesting that it is a catalyst resting state and **i-145** is the final product. The spectroscopic characteristics of **i-145** correlate well with the analogous $[Rh(P^iBu_3)_2(H)_2(\eta^2\text{-}H_2B{=}NCy_2)][BAr^F{}_4]$ **(i-146)**[138] and $[Rh(PCy_3)_2(H)_2(\eta^2\text{-}H_2B{=}NMe_2)][BAr^F{}_4]$ **(i-147)**[143] (which have been independently prepared) suggesting that $H_2B{=}NMe_2$ plays a crucial role in catalysis.



Scheme 1.47 Organometallic intermediates in dehydrocoupling of $H_3B{\cdot}NMe_2H$ **(i-143)** and **(i-145)** and related aminoborane complexes **(i-146)** and **(i-147**). $[BAr^F{}_4]^-$ anions not shown.

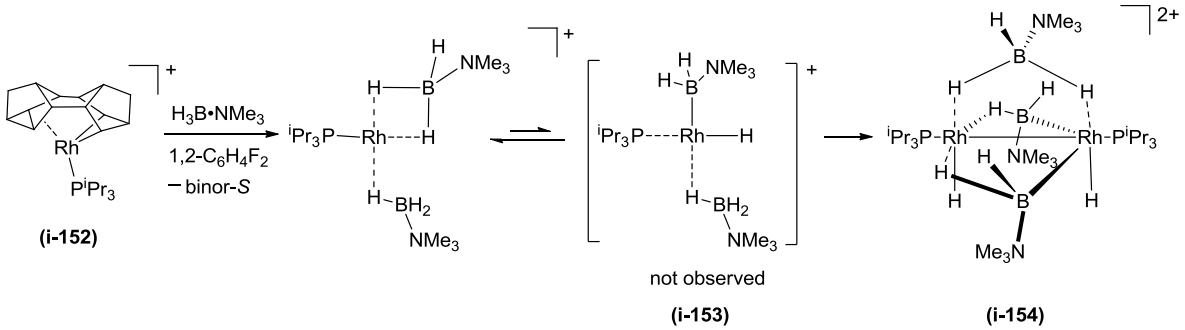
Stoichiometric reactivity of intermediate $H_3B{\cdot}NMe_2BH_2{\cdot}NMe_2H$ and the product $[H_2BNMe_2]_2$ with **i-125** reveals that both are able to coordinate to form η^2-amine-borane species $[Rh(P^iBu_3)_2\{(\eta^2\text{-}H_2BNMe_2)_2\}][BAr^F{}_4]$ **(i-148)** and $[Rh(P^iBu_3)_2(\eta^2\text{-}H_3B{\cdot}NMe_2BH_2{\cdot}NMe_2H)][BAr^F{}_4]$ **(i-149)** respectively. Significantly **i-148** is unable to form the corresponding Rh(III) complex under a hydrogen atmosphere and results in the reformation of **i-17** (Scheme 1.48). **i-149** can form $[Rh(P^iBu_3)_2(H)_2(\eta^2\text{-}H_3B{\cdot}NMe_2BH_2{\cdot}NMe_2H)][BAr^F{}_4]$ **(i-150)** upon the addition of excess $H_3B{\cdot}NMe_2BH_2{\cdot}NMe_2H$ and is discussed later (Scheme 1.54).



Scheme 1.48 Stoichiometric addition of the product and intermediates of the dehydrocoupling of $H_3B{\cdot}NMe_2H$ to **i-125**. $[BAr^F{}_4]^-$ anions not shown.

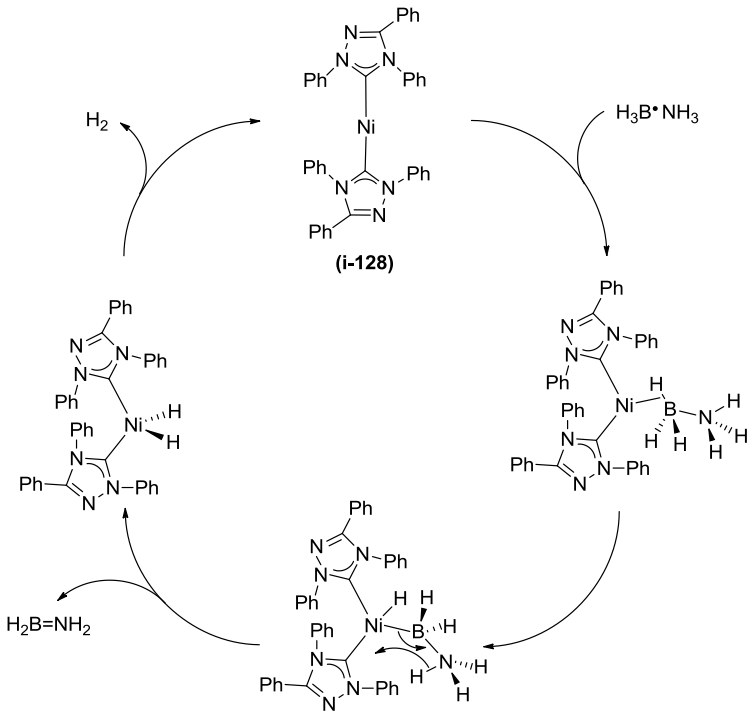
Further studies by Weller *et al.* found that the dehydrocoupling of $H_3B{\cdot}NMe_2H$ is not limited to **i-125** and its derivatives. $[Rh(\eta^6\text{-}1,2\text{-}C_6H_4F_2)(P^iPr_3)_2][BAr^F{}_4]$ **(i-151)** was also found to be catalytically active in this process although at a more modest rate at 5 mol% catalyst loading (100% conversion to $[H_2BNMe_2]_2$ after 300 minutes in an open system, TOF = 4 h^{-1}).[153] As with catalysis with **i-125**, intermediate $H_3B{\cdot}NMe_2BH_2{\cdot}NMe_2H$ is observed, however in a sealed system $[Rh(P^iPr_3)_2(H)_2(\eta^2\text{-}H_3B{\cdot}NMe_2H)]$ is the only observed organometallic species during the course of the reaction which suggests that this complex is the resting state in the catalytic cycle. $[Rh(PR_3)(\text{binor-}S)][BAr^F{}_4]$ {R = ^{i}Pr **(i-154)**/ Cy **(i-155)**} (binor-*S* = 1,2,4,5,6,8-dimetheno-*S*-indacene) was used as a latent source of $\{Rh(PR_3)\}^+$ by the same authors given its known ability to reductively eliminate the norbornadiene dimer (binor-*S*) upon addition of a competitive Lewis base.[27,30] Addition of $H_3B{\cdot}NMe_3$ to this fragment results in the formation of dimeric base stabilised boryl complexes which contain two $H_3B{\cdot}NMe_3$ ligands that bridge the two metal centres coordinating through one 3c-2e σ-bond and one α-B agostic interaction having undergone B-H activation as characterised by X-ray crystallography (*e.g.* **i-154** Scheme 1.49).[154] A third $H_3B{\cdot}NMe_3$ ligand bridges both metal centres coordinated to each through an η^1-B-H σ-bond. X-ray crystallographic data illustrates these different coordination modes perfectly with

different Rh-B distances for each interaction {Rh1-B1 2.747 (5) Å, Rh1-B2 2.086 (5) Å, Rh2-B2 2.217 (4) Å}. *In situ* formation of **i-154** suggests that it is formed *via* intermediate complex $[Rh(P^iPr_3)(H_3B{\cdot}NMe_3)_2][BAr^F{}_4]$ **(i-153)** (Scheme 1.49). Complexes **i-152** and **i-154** are both homogeneous but slow catalysts (100 % conversion to $[H_2BNMe_2]_2$ observed after 15 h at 20 mol% loading, sealed system) for the dehydrogenation and dehydrocoupling of $H_3B{\cdot}NMe_2H$.



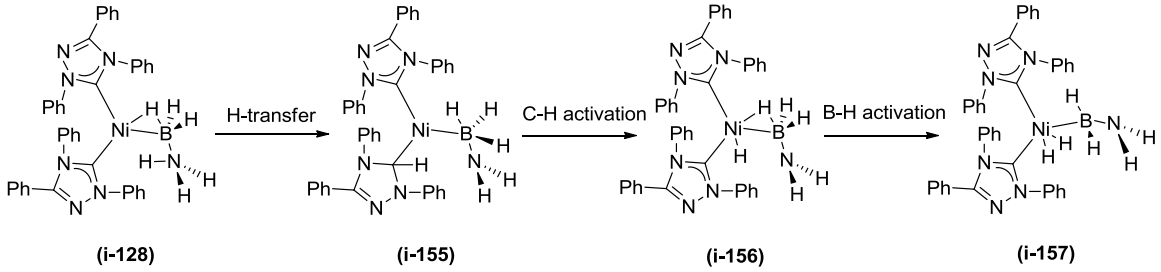
Scheme 1.49 Synthesis of **i-154**. $[BAr^F{}_4]^-$ anions not shown.

On reporting the first example for a first row transition metal to act as a catalyst for the dehydrogenation and dehydrocoupling of AB using $Ni(NHC)_2$ **(i-128)** (NHC = 2,2'-bis-(1,3,4-triphenyl-4,5-dihydro-1H-1,2,4-triazol-5-ylidene), Baker and co-workers postulated a mechanism involving the formation of a σ-complex followed by B-H activation and β-hydride elimination from the N-H moiety (Scheme 1.50).[155]



Scheme 1.50 Baker's mechanism for the dehydrogenation of $H_3B{\cdot}NH_3$ to $H_2B{=}NH_2$ using an *in situ* generated nickel *N*-heterocyclic carbene complex **(i-128)**.

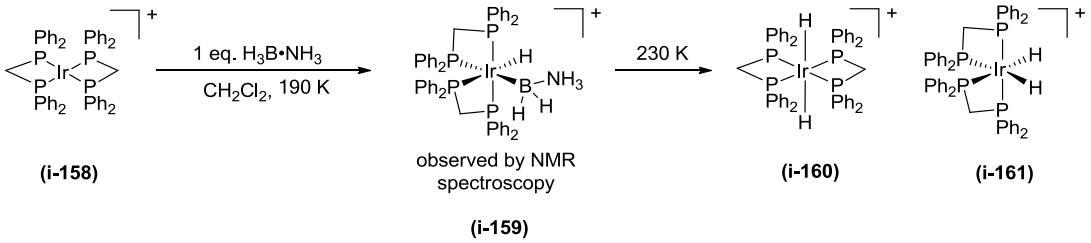
Similar kinetic isotope effects are observed when using $H_3B{\cdot}ND_3$, $D_3B{\cdot}NH_3$ and $D_3B{\cdot}ND_3$ which suggests that the rate of the latter two steps is comparable meaning N-H activation could precede that of B-H activation and that both are rate determining. Jiang and Berke share this mechanistic analogy in the dehydrogenation of $H_3B{\cdot}NMe_2H$ by Re(I) nitrosyl complexes to effect an olefin transfer hydrogenation (*e.g.* **i-126** Table 1.1).[156] Computational analysis by Yang and Hall using Baker's complex **(i-128**) proposes that the first step for the dehydrogenation of AB is proton transfer from the nitrogen to the carbene moiety to form **i-155** which is followed by its subsequent transfer to the metal **(i-156)** *via* a C-H activation step (Scheme 1.51).[157] Only then is the hydrogen on the boron postulated to transfer to the metal to generate H_2 and the aminoborane **(i-157)**.



Scheme 1.51 Hall's computed mechanism for the dehydrogenation of $H_3B{\cdot}NH_3$ with $Ni(NHC)_2$ **(i-128)**.

One of the most efficient $H_3B{\cdot}NMe_2H$ dehydrogenation and dehydrocoupling catalysts to date has been recently reported by Grützmacher and co-workers using a paramagnetic Ni(I) NHC precatalyst which contains a chelating olefin (**(i-127)** Table 1.1).[158] The exact mechanism and nature of the active catalyst however has not been identified, with Ni(0) not discounted as a catalyst.

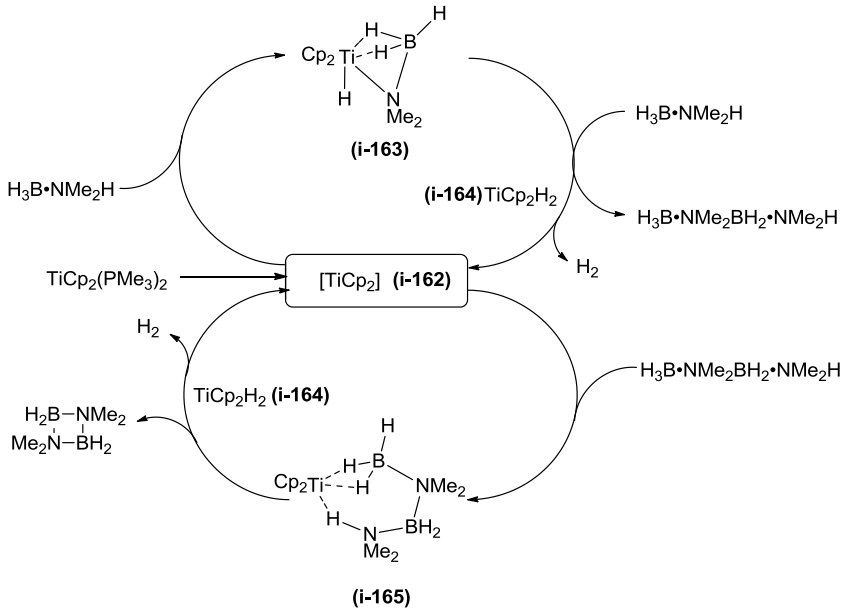
DFT calculations by the group of Peruzzini have shown that with $[Ir(dppm)_2][OTf]$ **(i-158)**, AB undergoes initial B-H oxidative addition on the metal centre to form $[Ir(dppm)(H)(H_2B{\cdot}NH_3)][OTf]$ **(i-159)**.[159] This complex, which is also observed by NMR spectroscopy, is only stable at low temperature (190 K) and reacts further to yield two dihydride isomers **i-160** and **i-161** on warming to 230 K (Scheme 1.52).



Scheme 1.52 Oxidative addition of AB observed at 190 K using $[Ir(dppm)_2][OTf]$ **(i-158)**. $[OTf]^-$ anions not shown.

Manners and co-workers have also reported the homogeneous catalysis of an *in situ* generated $[TiCp_2]$ fragment **(i-162)** towards both the dehydrogenation and dehydrocoupling of $H_3B{\cdot}NMe_2H$ to $[H_2BNMe_2]_2$ and the dehydrogenation of the more sterically encumbered amine-

borane $H_3B{\cdot}N^iPr_2H$ to $H_2B{=}N^iPr_2$, which exists as a stable monomer.[150] DFT calculations by Luo and Ohno using **i-162** for the dehydrogenation of $H_3B{\cdot}NMe_2H$ suggested that $H_2B{=}NMe_2$ is formed catalytically by the metallocene complex and then proceds, uncatalysed, to dimerise in a 2+2 cycloaddition to form $[H_2BNMe_2]_2$.[160] Recent experimental work by Lloyd-Jones and Manners has however discounted this mechanism in favour of that illustrated in Scheme 1.53 which involves the formation of $H_3B{\cdot}NMe_2BH_2{\cdot}NMe_2H$ as an intermediate followed by its metal promoted reductive cyclisation to form $[H_2BNMe_2]_2$.[161]

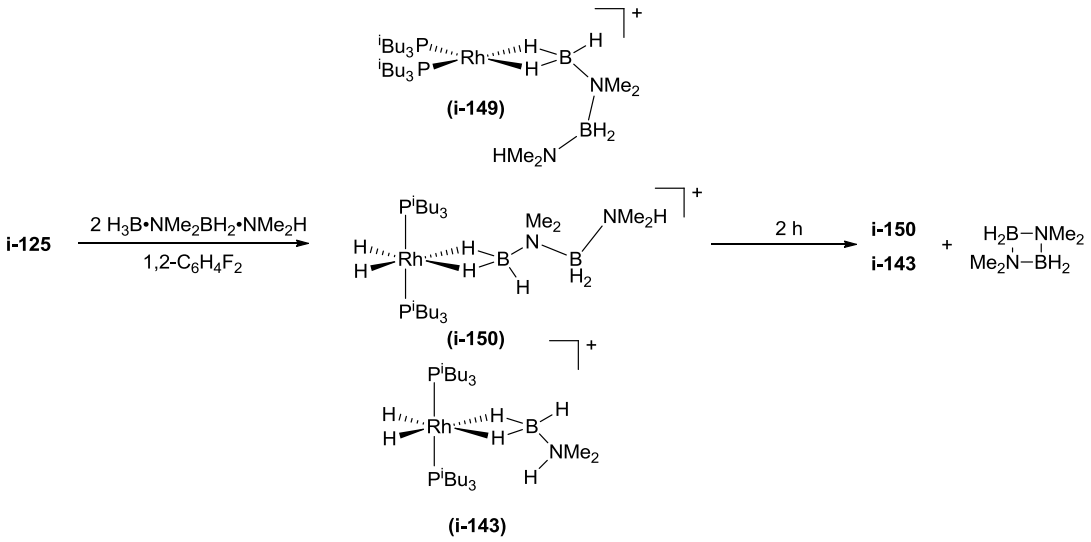


(i-165)

Scheme 1.53 Lloyd-Jones and Manners' mechanism for the dehydrogenation of $H_3B{\cdot}NMe_2H$ to $H_2B{=}NMe_2$ by an *in situ* generated $TiCp_2$ catalyst **(i-162)**.

Work with analogous metallocene complexes has been carried out by Chirik *et al.* who found a silyl-substituted titanocene dinitrogen complex (**(i-123)** (Table 1.1)) to be the most effective for the dehydrogenation of $H_3B{\cdot}NMe_2H$.[162] Zirconocene derivatives are less effective catalysts which is thought to be as a result of the rapid formation of borohydride complexes which were isolated and characterised post reaction. The proposed mechanism for the dehydrogenation of $H_3B{\cdot}NMe_2H$ with the metallocene complexes is similar to that reported by Baker with B-H activation occurring prior to N-H activation.

DFT calculations on the Weller $\{Rh(P^iBu_3)_2\}^+$ system by Hall *et al.* have recently concluded that the lowest energy pathway proceeds by initial B-H oxidative addition/ N-H transfer or N-H activation followed by B-H transfer to give the coordinated aminoborane complex $[Rh(P^iBu_3)_2(H)_2(\eta^2\text{-}H_2B{=}NMe_2)][BAr^F{}_4]$ **(i-145)**.[139] Loss of H_2 and then dissociation of $H_2B{=}NMe_2$ (or *vice versa*) results in dimerisation of $[H_2BNMe_2]_2$ and regeneration of $[Rh(P^iBu_3)_2][BAr^F{}_4]$ **(i-125)**. The role of $H_3B{\cdot}NMe_2BH_2{\cdot}NMe_2H$ was further investigated experimentally. $[Rh(P^iBu_3)_2(\eta^2\text{-}H_3B{\cdot}NMe_2BH_2{\cdot}NMe_2H)][BAr^F{}_4]$ **(i-149)**, although stable in solution, reacts on to ultimately yield $[H_2BNMe_2]_2$ in the presence of an excess of $H_3B{\cdot}NMe_2BH_2{\cdot}NMe_2H$. **i-143**, **i-150** and free $H_2B{=}NMe_2$ are also observed during the reaction indicating that B-N bond cleavage must be taking place (Scheme 1.54). These results suggest that a simple intramolecular "on metal" mechanism for dehydrocoupling is not operating in this system.

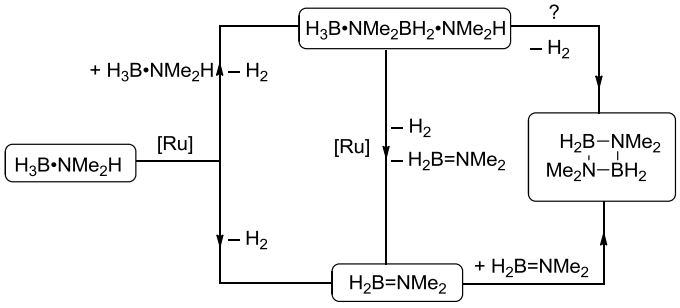


Scheme 1.54 Addition of a small excess of $H_3B{\cdot}NMe_2BH_2{\cdot}NMe_2H$ to **i-125** results in turnover to form $[H_2BNMe_2]_2$ as well as the formation of complexes **i-143**, **i-149** and **i-150**. $[BAr^F{}_4]^-$ anions not shown.

Addition of $H_3B{\cdot}NMe_2BH_2{\cdot}NMe_2H$ to **i-149** or $[Rh(\eta^6\text{-}C_6H_4F_2)(P^iBu_3)_2][BAr^F{}_4]$ **(i-166)** (5 mol%, 1,2-$C_6H_4F_2$, 298 K, sealed NMR tube) results in its slow catalytic turnover to form $[H_2BNMe_2]_2$ which is complete after 70 hours (TOF = 0.3 h^{-1}) a rate comparable to that observed when the equivalent B-N concentration of $H_3B{\cdot}NMe_2H$ is employed (**i-166**, 2.5 mol%

1,2-$C_6H_4F_2$, 298 K, sealed NMR tube, complete after 80 hours). These findings suggest that the dehydrocoupling of $H_3B{\cdot}NMe_2BH_2{\cdot}NMe_2H$ is the rate determining step.

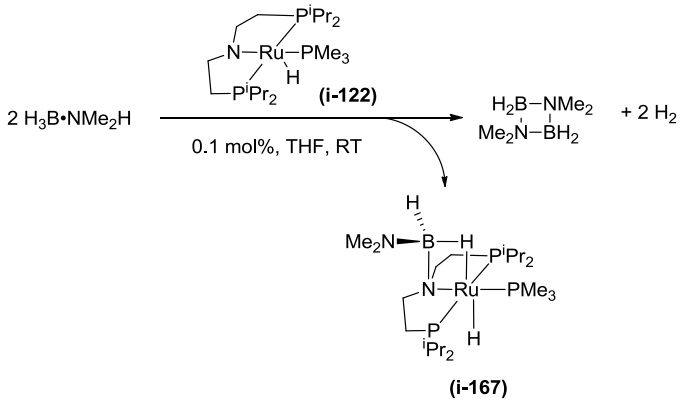
Mechanistic insight by Schneider and co-workers has predominantly focussed on the role of the intermediate amine-borane species $H_2B{=}NMe_2$ and $H_3B{\cdot}NMe_2BH_2{\cdot}NMe_2H$ observed during the dehydrocoupling catalysis of $H_3B{\cdot}NMe_2H$ with [Ru(H)(PMe_3)(PNP)] **(i-122)**.[151] Their thesis is that the formation of $H_3B{\cdot}NMe_2BH_2{\cdot}NMe_2H$ is a consequence of a metal-based process given that the dimerisation of $H_2B{=}NMe_2$ to afford $[H_2BNMe_2]_2$ is known to be fast and that thermochemical calculations predict that a kinetic barrier prevents "off metal" reactivity of $H_2B{=}NMe_2$ and $H_3B{\cdot}NMe_2H$ dehydrocoupling to form $H_3B{\cdot}NMe_2BH_2{\cdot}NMe_2H$ (Scheme 1.55).



Scheme 1.55 Mechanistic model for the dehydrogenation and dehydrocoupling of $H_3B{\cdot}NMe_2H$ to form $[H_2BNMe_2]_2$.

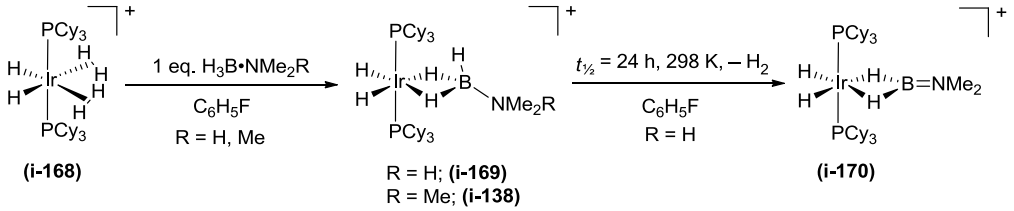
Furthermore, increased concentrations of substrate $H_3B{\cdot}NMe_2H$ yield a lower concentration ratio for $[H_3B{\cdot}NMe_2BH_2{\cdot}NMe_2H]$:$[H_2B{=}NMe_2]$ (0.44 at 0.54 M $H_3B{\cdot}NMe_2H$ *viz.* 4.09 at 0.1 M $H_3B{\cdot}NMe_2H$ after 3 minutes) which supports the argument of an increased metal *vs.* amine-borane concentration favouring the formation of $H_3B{\cdot}NMe_2BH_2{\cdot}NMe_2H$ as a result of a metal species being involved in the dehydrocoupling. These results contrast a related computational study by Musgrave *et al.* which suggests that free AB can react with free $H_2B{=}NH_2$ to form $H_3B{\cdot}NH_2BH_2{\cdot}NH_3$.[163] The ability for $H_3B{\cdot}NMe_2BH_2{\cdot}NMe_2H$ to cyclise directly to $[H_2BNMe_2]_2$ with the aid of the metal catalyst was not directly probed. Interestingly, deactivation in Schneider's system is noted to produce a four membered borametallacycle **(i-167)** (Scheme 1.56) incorporating aminoborane $H_2B{=}NMe_2$ which coordinates to Ru through a σ-B-H

interaction and additionally to the nitrogen of the PNP ligand backbone. **i-167** is also observed to be catalytically active to the dehydrogenation and dehydrocoupling of $H_3B{\cdot}NH_3$ with the aminoborane ($H_2B{=}NMe_2$) remaining coordinated during catalysis and not substituting for $H_2B{=}NH_2$.



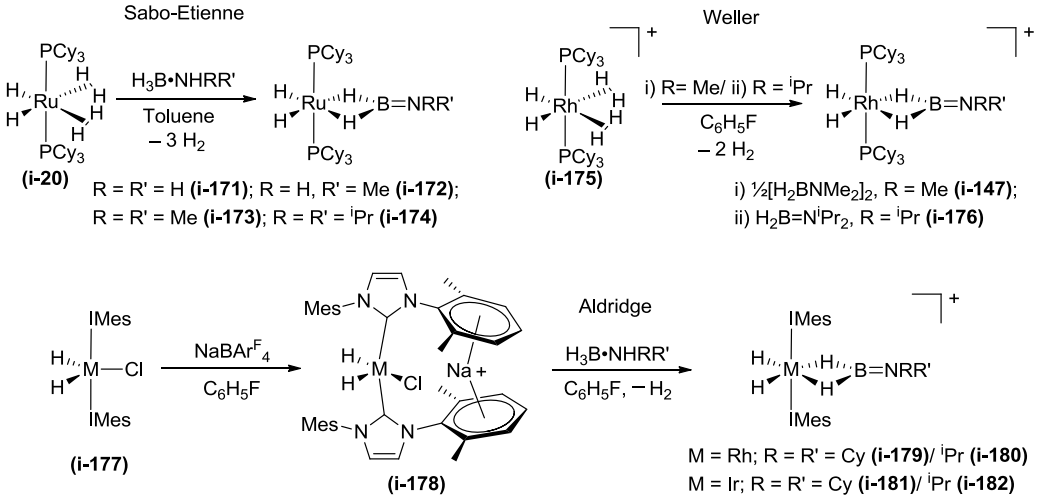
Scheme 1.56 Dehydrocoupling of $H_3B{\cdot}NMe_2H$ with Schneider's Ru catalyst **(i-122)**.

To further probe the metal involvement in the dehydrogenation and dehydrocoupling of $H_3B{\cdot}NMe_2H$, work within the Weller group has investigated the Ir bis(phosphine) dihydride complex $[Ir(PCy_3)_2(H)_2(\eta^2\text{-}H_2)_2][BAr^F{}_4]$ **(i-168)** which can lose hydrogen to form $\{Ir(PCy_3)_2(H)_2\}^+$, a latent 14-electron low coordinate fragment related to $\{Rh(P^iBu_3)_2\}^+$. Addition of one equivalent of $H_3B{\cdot}NMe_2H$ to **i-168** results in the initial formation of σ-complex $[Ir(PCy_3)_2(H)_2(\eta^2\text{-}H_3B{\cdot}NMe_2H)][BAr^F{}_4]$ **(i-169)** as observed by NMR spectroscopy however this complex reacts on ($t_{½}$ = 24 h) to form the aminoborane complex $[Ir(PCy_3)_2(H)_2(\eta^2\text{-}H_2B{=}NMe_2)][BAr^F{}_4]$ **(i-170)** a result which prevents the isolation of pure **i-169** in the solid-state (Scheme 1.57).[143] This species is analogous to the Rh complex **(i-145)** observed at the end of $H_3B{\cdot}NMe_2H$ catalysis with **i-125**[139] and shares similar characteristics to the coordinated $H_2B{=}N^iPr_2$ complex **(i-176)** (Scheme 1.58).[164]



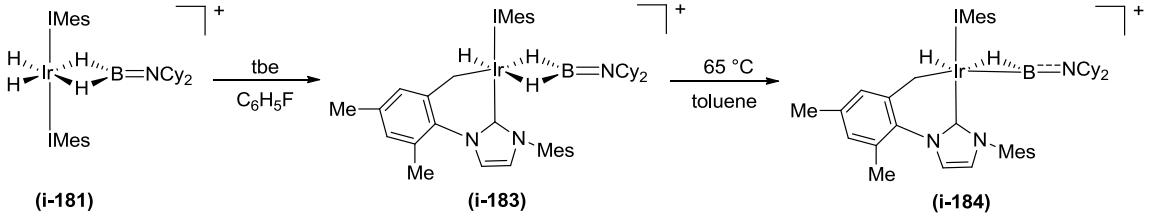
Scheme 1.57 Formation of the respective σ-complexes **i-169** and **i-138**. $[BAr^F_4]^-$ anions not shown.

Aminoborane complexes have also received attention from the groups of Sabo-Etienne (Ru)[165] and Aldridge (Rh / Ir)[149] who have highlighted the favourable coordination of this variety of ligand to late transition metal fragments (Scheme 1.58). Sabo-Etienne *et al.* have concurrently reported the formation of a range of bis-σ-aminoborane complexes (**i-171-174**) upon addition of the parent amine-borane to $Ru(PCy_3)_2(H)_2(\eta^2\text{-}H_2)_2$ **(i-20)**, however the further reactivity of these species in catalysis was not discussed.[166] Aldridge and co-workers obtain complexes **i-179-82** upon the dehydrogenation of $H_3B{\cdot}NR_2H$ (R = ^{i}Pr, Cy) with **i-178** at 2 mol% loading (Scheme 1.58).[149]



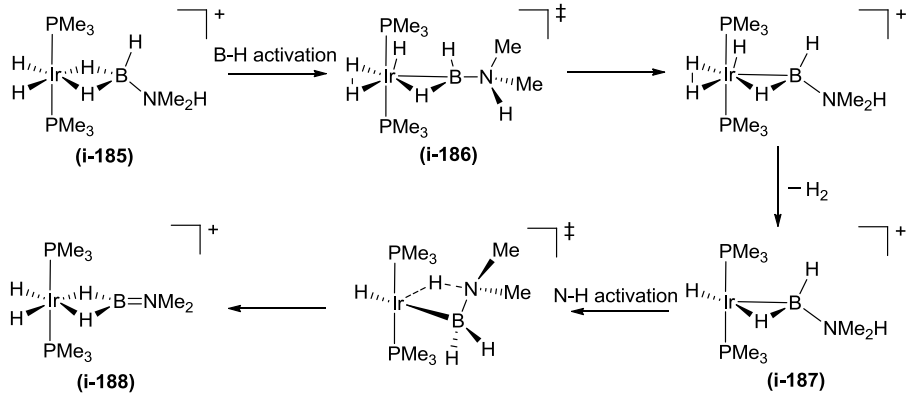
Scheme 1.58 Formation of aminoborane complexes. $[BAr^F_4]^-$ anions not shown.

Intriguingly **i-181** has been shown to undergo another sequential C-H activation and dehydrogenation step to afford **i-184**, which can be described as either a base stabilised borylene or an α-agostic boryl species (Scheme 1.59).[142]



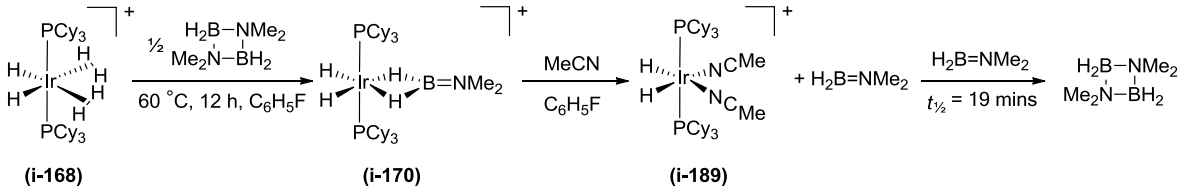
Scheme 1.59 Aldridge's dehydrogenation of a coordinated aminoborane **(i-181)**. $[BAr^F_4]^-$ anions not shown.

DFT calculations for the dehydrogenation in $[Ir(PMe_3)_2(H)_2(\eta^2\text{-}H_3B{\cdot}NMe_2H)]^+$ **(i-185)** to form $[Ir(PMe_3)_2(H)_2(\eta^2\text{-}H_2B{=}NMe_2)]^+$ **(i-188)** found that the dehydrogenation process is most likely to occur along a pathway first involving B-H activation to form **(i-186)** followed by loss of H_2 to yield **(i-187)** and then finally N-H activation. This was supported by a KIE experiment with $H_3B{\cdot}NMe_2D$ that yielded a slower rate of dehydrogenation to form **i-188** requiring an activation energy of 126.3 kJ mol^{-1} (Scheme 1.60).



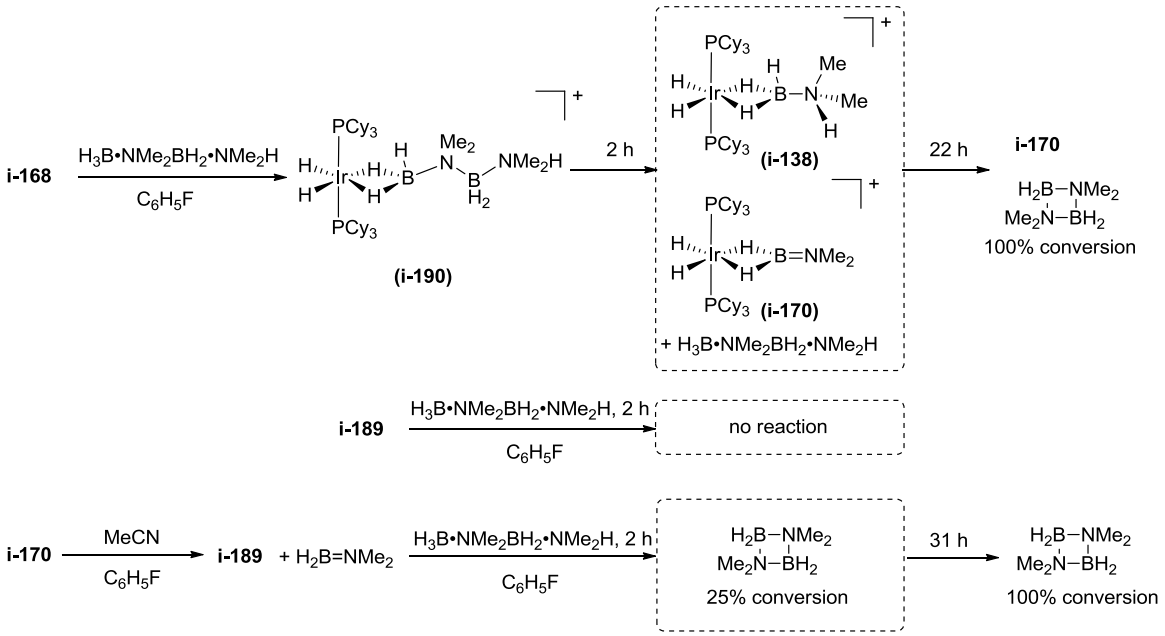
Scheme 1.60 Weller and Macgregor's mechanism for the dehydrogenation of **i-185** to **i-188**.

Addition of the product, $[H_2BNMe_2]_2$, to $[Ir(PCy_3)_2(H)_2(\eta^2\text{-}H_2)_2][BAr^F_4]$ **(i-168)** in a 2:1 ratio respectively results in the slow (12 hours, 60°C) trapping of $H_2B{=}NMe_2$ (formed by retrodimerisation of the cyclic dimer) by the $\{Ir(PCy_3)_2(H)_2\}^+$ fragment to form $[Ir(PCy_3)_2(H)_2(\eta^2\text{-}H_2B{=}NMe_2)][BAr^F_4]$ **(i-170)** (Scheme 1.61). Addition of MeCN to **i-170** results in the formation of $[Ir(PCy_3)_2(H)_2(MeCN)_2][BAr^F_4]$ **(i-189)** (a non-kinetically relevant $H_3B{\cdot}NMe_2H$ dehydrogenation catalyst) and the release of $H_2B{=}NMe_2$ which then goes on to dimerise.



Scheme 1.61 Retrodimerisation of $[H_2BNMe_2]_2$ by the $\{Ir(PCy_3)_2(H)_2\}^+$ fragment and liberation of $H_2B{=}NMe_2$ which dimerises in an off metal process. $[BAr^F{}_4]^-$ anions not shown.

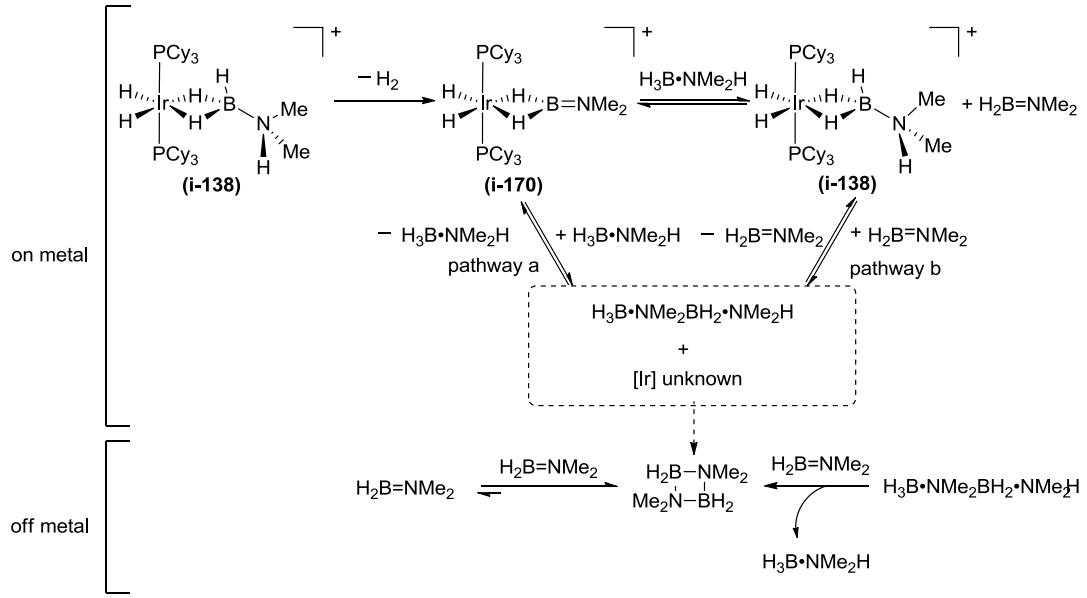
Addition of $H_3B{\cdot}NMe_2H$ to **i-170** results in the observation of $H_3B{\cdot}NMe_2BH_2{\cdot}NMe_2H$ after 30 minutes which is not observed upon the addition of $H_3B{\cdot}NMe_2H$ to $H_2B{=}NMe_2$ generated from the addition of acetonitrile to **i-170**. This further supports Schneider's observation that $H_3B{\cdot}NMe_2BH_2{\cdot}NMe_2H$ is formed by an "on metal" process which is not possible with **i-189** as acetonitrile prevents the coordination of aminoborane.[151]



Scheme 1.62 Investigating the role of $H_3B{\cdot}NMe_2BH_2{\cdot}NMe_2H$ in the dehydrogenation and dehydrocoupling of $H_3B{\cdot}NMe_2H$ with the $\{Ir(PCy_3)_2(H)_2\}^+$ fragment. $[BAr^F{}_4]^-$ anions not shown.

Addition of a small excess of $H_3B{\cdot}NMe_2BH_2{\cdot}NMe_2H$ to **i-168** results in the initial formation of $[Ir(PCy_3)_2(H)_2(\eta^2\text{-}H_3B{\cdot}NMe_2BH_2{\cdot}NMe_2H)][BAr^F{}_4]$ **(i-190)**, with the gradual formation (24 hours) of $[H_2BNMe_2]_2$. **i-138** and **i-170** are observed during the reaction after 2 hours proving that B-N bond scission must be taking place (Scheme 1.62). Addition of

$H_3B{\cdot}NMe_2BH_2{\cdot}NMe_2H$ to **i-189** shows no reaction after 2 hours whilst its addition to **i-189** and free $H_2B{=}NMe_2$ results in 25 % conversion of $H_3B{\cdot}NMe_2BH_2{\cdot}NMe_2H$ to $[H_2BNMe_2]_2$ in the same timeframe which is eventually complete after 31 hours. These data point to competitive "non-metal" promoted reactivity of $H_3B{\cdot}NMe_2BH_2{\cdot}NMe_2H$ with $H_2B{=}NMe_2$ which has also been suggested to occur in the dehydrocoupling of AB with $H_3B{\cdot}NH_2BH_2{\cdot}NH_3$ and $H_2B{=}NH_2$, as alluded to previously, but independently, by Musgrave[163] and Baker.[167]



Scheme 1.63 On and off metal pathways for the dehydrogenation and dehydrocoupling of $H_3B{\cdot}NMe_2H$ by the $\{Ir(PCy_3)_2(H)_2\}^+$ fragment. $[BAr^F{}_4]^-$ anions not shown.

Scheme 1.63 summaries these observations and suggests that the metal fragment is involved in all intermediary steps apart from the dimerisation of $H_2B{=}NMe_2$ to $[H_2BNMe_2]_2$. Manners *et al.* have also suggested that the metal does not play a role in the dimerisation of $H_2B{=}NMe_2$ in their recent work using $[FeCp(CO)_2]_2$ **(i-130)** (Table 1.1).[168] Non-metal based formation of oligomeric species in the dehydrocoupling of $H_3B{\cdot}NMe_2H$ using different combinations of frustrated Lewis pairs has also been independently reported by Bercaw[169] and Manners.[170]

Precedent for pathway a (Scheme 1.63) has been observed in the related reactivity of $H_3B{\cdot}NMe_2H$ with amidoboranes as reported by the groups of Harder (Ca[171,172]/ Mg[173]/ Zn[174]) and Roesler (Zr[175]). Examples of isolated amidoborane complexes are shown in Figure 1.10.

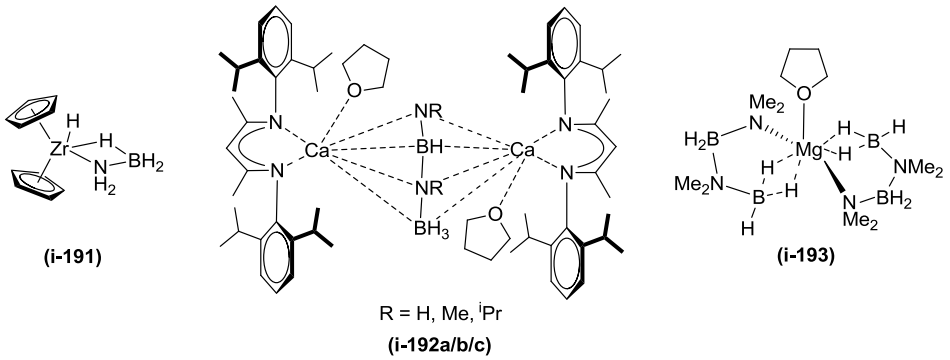
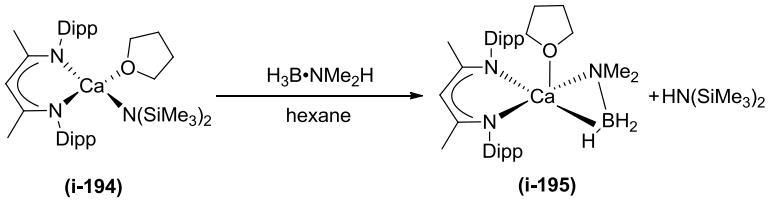


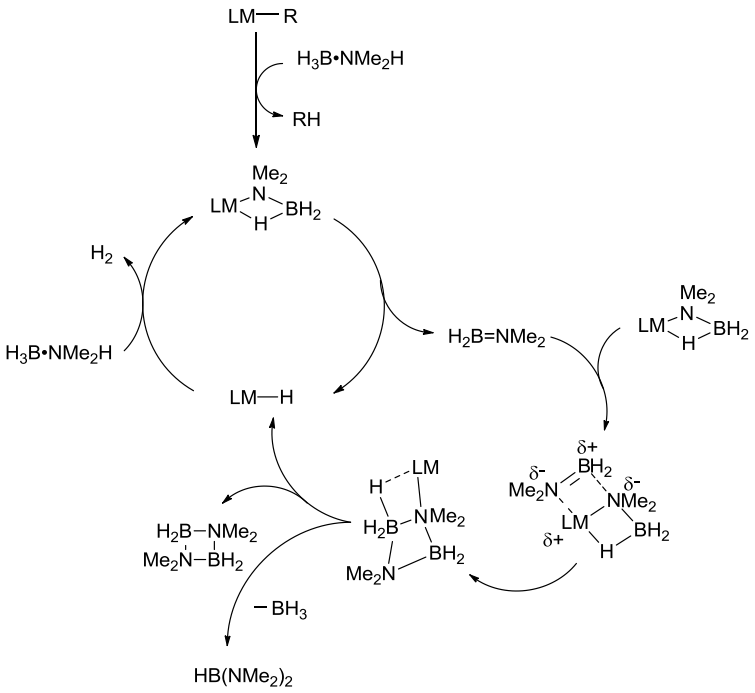
Figure 1.10 Amidoborane complexes of Roesler **(i-191)**, Harder **(i-192a/b/c)** and Hill **(i-193)**.

Work by Hill and co-workers has found that addition of one equivalent of $H_3B{\cdot}NMe_2H$ to a Ca β-diketiminate complex $[HC\{(Me)Dipp)\}_2Ca\{N(SiMe_3)_2\}(THF)]$ **(i-194)** (Dipp = 2,6-di-iso-propylphenyl) gives the quantitative formation of $[HC\{(Me)CN(Dipp)\}_2Ca\{NMe_2BH_3\}(THF)]$ **(i-195)** (Scheme 1.64).[176]



Scheme 1.64 Synthesis of complex **i-195**.

Catalytic reactivity of **i-194** and an analogous Mg species forms the $[H_3B{\cdot}NMe_2BH_2{\cdot}NMe_2]^-$ anion as an intermediate in dehydrocoupling before ultimately forming $[H_2BNMe_2]_2$. In the case Mg, an organometallic complex where this anion coordinates through both the terminal nitrogen and boron atoms was isolated (**i-193**, Figure 1.10). The mechanism proposed for these group 2 d^0 complexes invokes N-H activation at the metal which protonates $(SiMe_3)_2NH$ as the first step, followed by B-H activation and β-hydride elimination to form $H_2B{=}NMe_2$. This free aminoborane can react further with the amidoborane complex to form the coordinated anionic oligomeric species which can β-hydride eliminate to form $[H_2BNMe_2]_2$ or β-hydride eliminate and lose a BH_3 unit to form $HB(NMe_2)_2$ to leave a metal hydride species which is also catalytically active (Scheme 1.65).



Scheme 1.65 Hill's mechanism for the dehydrogenation and dehydrocoupling of $H_3B{\cdot}NMe_2H$ with amidoborane complexes. M = Ca, Mg, Sc, Y.

Work by the same group has found similar reactivity for related Sc (*e.g.* **i-124** Table 1.1) and Y complexes.[177] $HB(NMe_2)_2$ and $B_2H_5(\mu\text{-}NMe_2)$[178] have previously been observed as minor components of the dehydrocoupling of $H_3B{\cdot}NMe_2H$ in the Rh, Ru and Ti catalytic systems aforementioned.[139,150,151] An Al complex which coordinates $HB(NMe_2)_2$ has recently been isolated as a by-product of the dehydrocoupling of $H_3B{\cdot}NMe_2H$ with $Al(NMe_2)_3$.[179]

1.4 References

[1] Collman, J. P.; Hegedus, L. S.; Norton, J. R.; Finke, R. G. *Principles and Applications of Organotransition Metal Chemistry*; University Science: Mill Valley, CA, 1987.

[2] Crabtree, R. H. *Acc. Chem. Res.* **1979,** *12,* 331-358.

[3] Scott, N. M.; Dorta, R.; Stevens, E. D.; Correa, A.; Cavallo, L.; Nolan, S. P. *J. Am. Chem. Soc.* **2005,** *127,* 3516-3526.

[4] Budzelaar, P. H. M.; Moonen, N. N. P.; de Gelder, R.; Smits, J. M. M.; Gal, A. W. *Eur. J. Inorg. Chem.* **2000,** 753-769.

[5] Zhao, P.; Krug, C.; Hartwig, J. F. *J. Am. Chem. Soc.* **2005,** *127,* 12066-12073.

[6] Holland, P. L.; Cundari, T. R.; Perez, L. L.; Eckert, N. A.; Lachicotte, R. J.; *J. Am. Chem. Soc.* **2002,** *124,* 14416-14424.

[7] Crabtree, R. H. *The Organometallic Chemistry of the Transition Metals, Fourth Edition;* John Wiley & Sons: Hoboken, NJ, 2005.

[8] Brookhart, M.; Grant, B.; Volpe, A. F. Jr. *Organometallics* **1992,** *11,* 3920-3922.

[9] Butts, M. D.; Scott, B. L.; Kubas, G. J. *J. Am. Chem. Soc.* **1996,** *118,* 11831-11843.

[10] For some early examples see: (a) Crabtree, R. H.; Hlatky, G. G.; Parnell, C. P.; Segmüller, B. E.; Uriarte, R. *J. Inorg. Chem.* **1984,** *23,* 354-358. (b) Luo, X.-L.; Schulte, G. K.; Crabtree, R. H. *Inorg. Chem.* **1990**, *29*, 682-686.

[11] Willems, S. T. H.; Budzelaar, P. H. M.; Moonen, N. N. P.; de Gelder, R.; Smits, J. M. M.; Gal, A. W. *Chem. Eur. J.* **2002,** *8,* 1310-1320.

[12] Douglas, T. M.; Le Nôtre, J.; Brayshaw, S. K.; Weller, A. S. *Chem. Commun.* **2006,** 3408-3410.

[13] Tang, C. Y.; Lednik, J.; Vidovic, D.; Thompson, A. L. Aldridge, S. *Chem. Commun.* **2011,** *47,* 2523-2525.

[14] Douglas, T. M.; Molinos, E.; Brayshaw, S. K.; Weller, A. S. *Organometallics* **2007,** *26,* 463-465.

[15] Krossing, I.; Raabe, I.; *Angew. Chem. Int. Ed.* **2004,** *43,* 2066-2090.

[16] Jelenik, T.; Baldwin, P.; Scheidt, W. R.; Reed, C. A. *Inorg. Chem.* **1993,** *32,* 1982-1990.

[17] Chaplin, A. B.; Weller, A. S. *Eur. J. Inorg. Chem.* **2010,** 5124-5128.

[18] Brookhart, M.; Green, M. L. H. *J. Organomet. Chem.* **1983,** *250,* 395-408.

[19] Lein, M. *Coord. Chem. Rev.* **2009,** *253,* 625-634.

[20] Trofimenko, S. *J. Am. Chem. Soc.* **1968,** *90,* 4754-4755.

[21] Bochmann, M. *Organometallics 1: Complexes with Transition Metal M-C σ-bonds;* Oxford University Press 1994.

[22] Omae, I. *J. Organomet. Chem.* **2011,** *696,* 1128-1145.

[23] Cooper, A. C.; Streib, W. E.; Eisenstein, O.; Caulton, K. G. *J. Am. Chem. Soc.* **1997,** *119,* 9069-9070.

[24] Cooper, A. C.; Clot, E.; Huffman, J. C.; Streib, W. E.; Maseras, F.; Eisenstein, O.; Caulton, K. G. *J. Am. Chem. Soc.* **1999,** *121,* 97-106.

[25] Douglas, T. M.; Chaplin, A. B.; Weller, A. S. *Organometallics* **2008,** *27,* 2918-2921.

[26] Chaplin, A. B.; Tonner, R.; Weller, A. S. *Organometallics* **2010,** *29,* 2710-2714.

[27] Chaplin, A. B.; Poblador-Bahamonde, A. I..; Sparkes, H. A.; Howard, J. A. K.; Macgregor, S. A.; Weller, A. S. Chem. Commun. **2009,** 244-246.

[28] Muhoro, C. N.; He, X.; Hartwig, J. F. *J. Am. Chem. Soc.* **1999,** *121,* 5033-5046.

[29] Kubas, G. J. *Metal Dihydrogen and σ-Bond Complexes* Kleuwer Academic/ Plenum Publishers. NY, 2001.

[30] Brayshaw, S. K.; Green, J. C.; Kociok-Köhn, G.; Sceats, E. L.; Weller, A. S. *Angew. Chem. Int. Ed.* **2006,** *45,* 452-456.

[31] Brayshaw, S. K.; Sceats, E. L.;Green, J. C.; Weller, A. S. *Proc. Nat. Acad. Sci.* **2007,** *104,* 6921-6926.

[32] Crabtree, R. H. *Acc. Chem. Res.* **1990,** *23,* 95-101.
[33] Kubas, G. J.; Ryan, R. R.; Swanson, B. I.; Vergamini, P. J.; Wasserman, H. J.; *J. Am. Chem. Soc.* **1984,** *106,* 451-452.
[34] Kubas, G. J. *Chem. Rev.* **2007,** *107,* 4152-4205.
[35] Hebden, T. J.; St. John, A. J.; Gusev, D. G.; Kaminsky, W.; Goldberg, K. I.; Heinekey, D. M. *Angew. Chem. Int. Ed.* **2011,** *50,* 1873-1876.
[36] Alcaraz, G.; Grellier, M.; Sabo-Etienne, S.; *Acc. Chem. Res.* **2009,** *42,* 1640-1649.
[37] Borowski, A. F.; Donnadieu, B.; Daran, J. C.; Sabo-Etienne, S.; Chaudret, B. *Chem. Commun.* **2000,** 543-544.
[38] Hartwig, J. F.; Muhoro, C. N.; He, X.; Eisenstein, O.; Bosque, R.; Maseras, F. *J. Am. Chem. Soc.* **1996,** *118,* 10936-10937.
[39] Pandey, K. K. *Coord. Chem. Rev.* **2009,** *253,* 37-55.
[40] Alcaraz, G.; Clot, E.; Helmstedt, U.; Vendier, L.; Sabo-Etienne, S.; *J. Am. Chem. Soc.* **2007,** *129,* 8704–8705
[41] Hesp, K. D.; Rankin, M. A.; McDonald, R.; Stradiotto, M. *Inorg. Chem.* **2008,** *47,* 7471–7473.
[42] Bernskoetter, W. H.; Schauer, C. K.; Goldberg, K. I.; Brookhart, M. *Science* **2009,** *326,* 553-556.
[43] Perutz, R. N.; Turner, J. J. *J. Am. Chem. Soc.* **1975,** *97,* 4791-4800.
[44] Kelly, J. M.; Hermann, H.; von Gustorf, E. K. *J. Chem. Soc. Chem. Commun.* **1973,** 105-106.
[45] Cowan, A. J.; Portius, P.; Kawanami, H. K.; Jina, O. S.; Grills, D. C.; Sun, X-. Z.; McMaster, J.; George, M. W. *Proc. Natl. Acad. Sci. U.S.A.* **2007,** *104,* 6933-6938.
[46] Ball, G. E.; Brookes, C. M.; Cowan, A. J.; Darwish, T. A.; George, M. W.; Kawanami, H. K.; Portius, P.; Rourke, J. P. *Proc. Natl. Acad. Sci. U.S.A.* **2007,** *104,* 6927-6932.
[47] Evans, D. R.; Drovetskaya, T.; Bau, R.; Reed, C. A.; Boyd, P. D. W. *J. Am. Chem. Soc.* **1997,** *119,* 3633-3634.
[48] Castro-Rodriguez, I.; Nakai, H.; Gantzel, P.; Zakharov, L. N.; Rheingold, A. L.; Meyer, K. *J. Am. Chem. Soc.* **2003,** *125,* 15734-15735.
[49] Tolman, C. A. *Chem. Rev.* **1977,** *77,* 313-348.
[50] Müller, T. E.; Mingos, M. P. *Transition Met. Chem.* **1995,** *20,* 533-539.
[51] van Leeuwen, P. W. N. M.; Kamer, P. C. J.; Reek, J. N. H.; Dierkes, P. *Chem. Rev.* **2000,** *100,* 2741-2769.
[52] Koide, Y.; Bott, S. G.; Barron, A. R. *Organometallics* **1996,** *15,* 2213-2226.
[53] Jeffrey, J. C.; Rauchfuss, T. B. *Inorg. Chem.* **1979,** *18,* 2658-2666.
[54] Braunstein, P.; Matt, D.; Mathey, F.; Thavard, D. *J. Chem. Res. Synop.* **1978,** 232-233.
[55] Wegman, R. W.; Abatjoglou, A. G.; Harrison, A. M. *J. Chem. Soc. Chem. Commun.* **1987,** 1891-1892.
[56] Abel, E. W.; Kite, K.; Perkins, P. S. *Polyhedron* **1987,** *6,* 549-562.
[57] For a review on hemilabile ligands see (a) Braunstein, P.; Naud, F. *Angew. Chem. Int. Ed.* **2001,** *40,* 680-699 and references therein. For some recent examples see (b) Marson, A.; Ernsting, J. E.; Lutz, M.; Spek, A. L.; van Leeuwen, P. W. N. M.; Kamer, P. C. J. *Dalton Trans.* **2009,** 621-633. (c) Hounjet, L. J.; Bierenstiel, M.; Ferguson, M. J.; McDonald, R.; Cowie, M. *Dalton Trans.* **2009,** 4213-4226. (d) Fliedel, C.; Schnee, G.; Braunstein, P. *Dalton Trans.* **2009,** 2474-2476.
[58] For some examples see (a) Kranenburg, M.; Kamer, P. C. J.; van Leeuwen, P. W. N. M. *Eur. J. Inorg. Chem.* **1998,** 155-157. (b) Utsunomiya, M.; Kuwano, R.; Kawatsura, M.; Hartwig, J. F. *J. Am. Chem. Soc.* **2003,** *125,* 5608-5609. (c) Haniti, M.; Hamid, S. A.; Allen, C. L.; Lamb, G. W.; Maxwell, A. C.; Maytum, H. C.; Watson, A. J. A.; Williams, J. M. J. W. *J. Am. Chem. Soc.* **2009,** *131,* 1766-1774.
[59] For some examples see (a) Fox, J. A. M.; Huang, X.; Chieffi, A.; Buchwald, S. L. *J. Am. Chem. Soc.* **2000,** *122,* 1360-1370. (b) Yin, Y.; Buchwald, S. L. *J. Am. Chem. Soc.* **2002,**

124, 6043-6048. (c) Johns, A. M.; Utsunomiya, M.; Incarvito, C. D.; Hartwig, J. F. *J. Am. Chem. Soc.* **2006,** *128,* 1828-1839. (b) Martinelli, J. R.; Watson, D. A.; Freckmann, D. M. M.; Barder, T. E.; Buchwald, S. L. *J. Org. Chem.* **2008,** *73,* 7102-7107.

[60] van Haaren, R. J.; Goubitz, K.; Fraanje, J.; van Strijdonck, G. P. F.; Oevering, H.; Coussens, B.; Reek, J. N. H.; Kamer, P. C. J.; van Leeuwen, P. W. N. M. *Inorg. Chem.* **2001,** *40,* 3363-3372.

[61] Birkholz, M. N.; Freixa, Z.; van Leeuwen, P. W. N. M. *Chem. Soc. Rev.* **2009,** 1099-1118.

[62] van Leeuwen, P. W. N. M.; Zuideveld, M. A.; Swennenhuis, B. H. G.; Freixa, Z.; Kamer, P. C. J.; Goubitz, K.; Fraanje, J.; Lutz, M.; Spek, A. L *J. Am. Chem. Soc.* **2003,** *125,* 5523-5539.

[63] Moxham, G. L.; Brayshaw, S. K.; Woodward, S. L.; Weller, A. S.; Willis, M. C. *Angew. Chem. Int. Ed.* **2006,** *45,* 7618-7622.

[64] Moxham, G. L.; Randell-Sly, H.; Brayshaw, S. K.; Weller, A. S.; Willis, M. C.; *Chem. Eur. J.* **2008,** *14,* 8383-8397.

[65] Pawley, R. J.; Moxham, G. L.; Dallanegra, R.; Chaplin, A. B.; Brayshaw, S. K.; Weller, A. S.; Willis. M. C. *Organometallics* **2010,** *29,* 1717-1728.

[66] Jensen, C. M. *Chem. Commun.* **1999,** 2443-2449.

[67] Zhu, K. M.; Achord, P. D.; Zhang, X. W.; Krogh-Jespersen, K.; Goldman, A. S. *J. Am. Chem. Soc.* **2004,** *126,* 13044-13053.

[68] Dick, A. R.; Sanford, M. S. *Tetrahedron,* **2006,** *62,* 2439-2463.

[69] Dobereiner, G. E.; Crabtree, R. H. *Chem. Rev.* **2009,** *110,* 681-703.

[70] Goldman, A. S.; Roy, A. H.; Huang, Z.; Ahuja, R.; Schinski, W.; Brookhart, M. *Science* **2006,** *312,* 257-261.

[71] Bennett, M. A.; Longstaff, P. A. *J. Am. Chem. Soc.* **1969,** *91,* 6266-6280.

[72] Bennett, M. A.; Clark, P. W.; Robertson, G. B.; Whimp, P. O. *J. Organomet. Chem.* **1973,** 63, C15-C18.

[73] Borowski, A. F.; Sabo-Etienne, S.; Christ, M. L.; Donnadieu, B.; Chaudret, B. *Organometallics* **1996,** *15,* 1427-1434.

[74] Johnson, J. B.; Rovis, T. *Angew. Chem. Int. Ed.* **2008,** *47,* 840-871.

[75] Defieber, C.; Grützmacher, H.; Carreira, E. M. *Angew. Chem. Int. Ed.* **2008,** *47,* 4482-4502.

[76] Pregosin, P. *Chem. Commun.* **2008,** 4875-4884.

[77] Shintani, R.; Duan, W.-L.; Nagano, T.; Okada, A.; Hayashi, T. *Angew. Chem. Int. Ed.* **2005,** *44,* 4611-4614.

[78] Duan, W.-L.; Iwamura, H.; Shintani, R.; Hayashi, T. *J. Am. Chem. Soc.* **2007,** *129,* 2130-2138.

[79] Thoumazet, C.; Ricard, L.; Grützmacher, H.; Le Floch, P. *Chem Commun.* **2005,** 1592-1594.

[80] Maire, P.; Deblon, S.; Breher, F.; Geier, J.; Böhler, C.; Rüegger, H.; Schönberg, H.; Grützmacher, H. *Chem. Eur. J.* **2004,** *10,* 4198-4205.

[81] Lewis, J. C.; Berman, A. M.; Bergman, R. G.; Ellman, J. A. *J. Am. Chem. Soc.* **2008,** *130,* 2493-2500.

[82] Lewis, J. C.; Bergman, R. G.; Ellman, J. A. *Acc. Chem. Res.* **2008,** *41,* 1013-1025.

[83] Shintani, R.; Duan, W.-L.; Okamoto, K.; Hayashi, T. *Tetrahedron Asymmetry* **2005,** *16,* 3400-3405.

[84] Christ, L. M.; Sabo-Etienne, S.; Chaudret, B. *Organometallics* **1995,** *14,* 1082-1084.

[85] Bennett, M. A.; Clark, P. W.; Robertson, G. B.; Whimp, P. O. *Chem Commun.* **1972,** 1011-1012.

[86] Heitkamp, S.; Stufkens, D.J.; Vrieze, K. *J. Organometall. Chem.,* **1978,** *152,* 347-357.

[87] Brainard, R. L.; Miller, T. M.; Whitesides, G. M. *Organometallics* **1986,** *5,* 1481-1490.

[88] Miller, T. M.; Whitesides, G. M. *Organometallics* **1986,** *5,* 1473-1480.

[89] Grellier, M.; Vendier, L.; Chaudret, B.; Albinati, A.; Rizzato, S.; Mason, S. A.; Sabo-Etienne, S. *J. Am. Chem. Soc.,* **2005,** *127,* 17592-17593.

[90] Grellier, M.; Vendier, L.; Sabo-Etienne, S. *Angew. Chem. Int. Ed.* **2007,** *46,* 2613-2615.

[91] Douglas, T. M.; Brayshaw, S. K.; Dallanegra, R.; Kociok-Köhn, G.; Macgregor, S. A.; Moxham, G. L.; Weller, A. S.; Wondimagegn, T.; Vadivelu, P. *Chem. Eur. J.*, **2008**, *14*, 1004-1022.
[92] Baya, M.; Buil, M. L.; Esteruelas, M. A.; Oñate, E. *Organometallics* **2004,** *23,* 1416-1423.
[93] Esteruelas, M. A.; Lopez, A. M. *Organometallics* **2005,** *24,* 3584-3613.
[94] Glaser, P. B.; Tilley, T. D. *Organometallics* **2004,** *23,* 5799-5812.
[95] Chaplin, A. B.; Weller, A. S. *Chem. Commun.* **2009,** 244-246.
[96] Douglas, T. M.; Weller, A. S. *New. J. Chem.,* **2008,** *32,* 966-969.
[97] Moret, S.; Dallanegra, R.; Chaplin, A. B.; Douglas, T. M.; Hiney, R. M. Weller, A. S. *Inorg. Chim. Acta.* **2010,** 574-580.
[98] Schönberg, H.; Boulmaâz, S.; Wörle, M.; Liesum, L.; Schweiger, A.; Grützmacher, H. *Angew. Chem. Int. Ed.* **1998,** *37,* 1423-1426.
[99] Deblon, S.; Liesum, L.; Harmer, J.; Schönberg, H.; Schweiger, A.; Grützmacher, H. *Chem. Eur. J.* **2002,** *8,* 601-611.
[100] Laporte, C.; Büttner, H.; Rüegger, J.; Geier, H.; Schönberg, H.; Grützmacher, H. *Inorg. Chim. Acta.* **2004,** *357,* 1931-1947.
[101] Piras, E.; Läng, F.; Rügger, H.; Stein, D.; Wörle, M.; Grützmacher, H. *Chem. Eur. J.* **2006,** *12,* 5849-5858.
[102] Kasák, P.; Arion, V. B.; Widhalm, M. *Tetrahedron Asymmetry* **2006,** *17,* 3084-3090.
[103] Ojima, I.; Inaba, S.; Kogure, T. *J. Organomet. Chem.* **1973,** *55,* C7-C8.
[104] Aitken, C.; Harrod, J. F.; Samuel, E. J. *J. Organomet. Chem.* **1985,** *279,* C11.
[105] Aitken, C.; Harrod, J. F.; Samuel, E. J. *J. Am. Chem. Soc.* **1986,** *108,* 4059-4066.
[106] Corey, J. Y. *The Chemistry of Organic Silicon Compounds;* Patai, S.; Rappoport, Z. Eds.; John Wiley and Sons: New York, 1989; pp 1-56.
[107] Smith, E. E.; Du, G.; Fanwick, P. E.; Abu-Omar, M. M. *Organometallics* **2010**, *29,* 6527-6533.
[108] Curtis, M. D.; Epstein, P. S. *Adv. Organomet. Chem.* **1981,** *19,* 213-232.
[109] Okazaki, M.; Tobita, H.; Ogino, H. *Dalton Trans.* **2003,** 493-506.
[110] Pannell, K. H.; Brun, M-C.; Sharma, H.; Jones, K.; Sharma, S. *Organometallics* **1994,** *13,* 1075-1077.
[111] Goikhman, R.; Milstein, D. *Chem. Eur, J.* **2006,** *11,* 2983-2988.
[112] Gigler, P.; Bechlars, B.; Herrmann, W. A.; Kühn, F. E. *J. Am. Chem. Soc.* **2011,** *133,* 1589-1596.
[113] Jackson, S. M.; Chisholm, D. M.; McIndoe, J. S.; Rosenberg, L. *Eur. J. Inorg. Chem.* **2011,** 327-330.
[114] Jaska, C. A.; Temple, K.; Lough, A. J.; Manners, I. *J. Am. Chem. Soc.* **2003,** *125,* 9424-9434. and references therein.
[115] Clark, T. J.; Lee, K.; Manners, I. *Chem. Eur. J.* **2006,** *12,* 8634-8648.
[116] Yoon, C. W.; Sneddon, L. G. *J. Am. Chem. Soc.* **2006,** *128,* 13992-13993.
[117] Yoon, C. W.; Carroll, P. J.; Sneddon, L. G. *J. Am. Chem. Soc.* **2009,** *131,* 14101-14110.
[118] Stephens, F. H., Pons, V.; Baker, R. T. *Dalton Trans.* **2007,** 2613-2626.
[119] Smythe, N. C.; Gordon, J. C. *Eur. J. Inorg. Chem.* **2010,** 509-521.
[120] Käß, M.; Friedrich, A.; Drees, M.; Schneider, S. *Angew. Chem. Int. Ed.* **2009,** *48,* 905-907.
[121] Blacquiere, N.; Diallo-Garcia, S.; Gorelsky, S. I.; Black, D. A.; Fagnou, K. *J. Am. Chem. Soc.* **2008,** *130,* 14034-14035.
[122] Conley, B. L.; Williams, T. J. *Chem. Commun.* **2010,** *46,* 4815-4817.
[123] Staubitz, A.; Presa Soto, A.; Manners, I. *Angew. Chem. Int. Ed.* **2008,** *47,* 6212-6215.
[124] Marder, T. B. *Angew. Chem. Int. Ed.* **2007,** *46,* 8116-8118.
[125] Sutton, A. D.; Burrell, A.K.; Dixon, D. A.; Garner, E. B. III; Gordon, J. C.; Nakagawa, T.; Ott, K. C.; Robinson, J. P.; Vasiliu, M. *Science,* **2011,** *331,* 1426-1429.
[126] Hamilton, C. W.; Baker, R. T.; Staubitz, A.; Manners, I. *Chem. Soc. Rev.* **2009,** *38,* 279-293. and references therein.

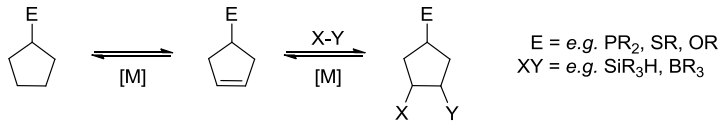
[127] Pons, V.; Baker, R. T. *Angew. Chem. Int. Ed.* **2008,** *47,* 9600-9602.
[128] Green, I. G.; Johnson, K. M.; Roberts, B. P. *J. Chem. Soc. Perkin Trans. II* **1989,** 1963-1989.
[129] Jaska, C. A.; Temple, K.; Lough, A. J.; Manners, I. *Chem. Commun.* **2001,** 962-963.
[130] Jaska, C. A.; Manners, I. *J. Am. Chem. Soc.* **2004,** *126,* 9776-9785.
[131] Chen, Y.; Fulton, J. L.; Linehan, J. C.; Autrey, T. *J. Am. Chem. Soc.* **2005,** *127,* 3254-3255.
[132] Fulton, J. L.; Linehan, J. C.; Autrey, T.; Balasubramanian, M.; Chen, Y.; Szymczak, N. K. *J. Am. Chem. Soc.* **2007,** *129,* 11936-11949.
[133] Denney, M. C.; Pons, V.; Hebden, T. J.; Heinekey, D. M.; Goldberg, K. I. *J. Am. Chem. Soc.* **2006,** *128,* 12048-12049.
[134] Dietrich, B. L.; Goldberg, K. I.; Heinekey, D. M.; Autrey, T.; Linehan, J. C. *Inorg. Chem.* **2008,** *47,* 8583-8585.
[135] Hebden, T. J.; Denney, M. C.; Pons, V.; Piccoli, P. M. B.; Koetzle, T. F.; Schultz, A. J.; Kaminsky, W.; Goldberg, K. I.; Heinekey, D. M. *J. Am. Chem. Soc.* **2008,** *130,* 10812-10820.
[136] Alcaraz, G.; Sabo-Etienne, S. *Coord. Chem. Rev.* **2008,** *252,* 2395-2409.
[137] Pandey, K. K.; *Coord. Chem. Rev.* **2009,** *253,* 37-55.
[138] Douglas, T. M.; Chaplin, A. B.; Weller, A. S. *J. Am. Chem. Soc.* **2008,** *130,* 14432-14433.
[139] Douglas, T. M.; Chaplin, A. B.; Weller, A. S.; Hall, M. B.; Yang, X. *J. Am. Chem. Soc.* **2009,** *131,* 15440.
[140] Alcaraz, G.; Sabo-Etienne, S. *Angew. Chem. Int. Ed.* **2010,** *49,* 7170-7179.
[141] Shimoi, M.; Nagai, S.; Ichikawa, M.; Kawano, Y.; Katoh, K.; Uruichi, M.; Ogino, H. *J. Am. Chem. Soc.* **1999,** *121,* 11704-11712.
[142] Tang, C. Y.; Thompson, A. L.; Aldridge, S. *J. Am. Chem. Soc.* **2010,** *132,* 10578-10591.
[143] Stevens, C. J.; Dallanegra, R.; Chaplin, A. B.; Weller, A. S.; Macgregor, S. A.; Ward, B.; McKay, D.; Alcaraz, G.; Sabo-Etienne, S. *Chem. Eur. J.* **2011,** *17,* 3011-3020.
[144] Staubitz, A.; Robertson, A. P. M.; Sloan, M. E.; Manners, I. *Chem. Rev.* **2010,** *110,* 4023-4078.
[145] Kakizawa, T.; Kawano, Y.; Shimoi, M. *Organometallics* **2001,** *20,* 3211-3213.
[146] Kawano, Y.; Hashiva, M.; Shimoi, M. *Organometallics* **2006,** *25,* 4420-4426.
[147] Fan, M.-F.; Jia, G.; Lin, Z. *J. Am. Chem. Soc.***1996,** *118,* 9915-9921.
[148] Kawano, Y.; Uruichi, M.; Shimoi, M.; Taki, S.; Kawaguchi, T.; Kakizawa, T.; Ogino, H. *J. Am. Chem. Soc.* **2009,** *131,* 14946-14957.
[149] Tang, C. Y.; Thompson, A. L.; Aldridge, S. *Angew. Chem. Int. Ed.* **2010,** *49,* 921-925.
[150] Clark, T. J.; Russell, C. A.; Manners, I. *J. Am. Chem. Soc.* **2006,** *128,* 9582-9583.
[151] Friedrich, A.; Drees, M.; Schneider, S. *Chem. Eur. J.* **2009,** *15,* 10339-10342.
[152] Nöth, H.; Thomas, S. *Eur. J. Inorg. Chem.* **1999,** 1373-1379.
[153] Chaplin, A. B.; Weller, A. S. *Inorg. Chem.* **2010,** *49,* 1111-1121.
[154] Chaplin, A. B.; Weller, A. S. *Angew. Chem. Int. Ed.* **2010,** *49,* 581-584.
[155] Keaton, R. J.; Blacquiere, J. M.; Baker, R. T. *J. Am. Chem. Soc.* **2007,** *129,* 1844-1845.
[156] Jiang, Y.; Berke, H. *Chem. Commun.* **2007,** 3571-3573.
[157] Yang, X.; Hall, M. B. *J. Am. Chem. Soc.* **2008,** *130,* 1798-1799.
[158] Vogt, M.; de Bruin, B.; Berke, H.; Trincado, M.; Grützmacher, H. *Chem. Sci.* **2011,** *2,* 721-723.
[159] Rossin, A.; Caporali, M.; Gonsalvi, L.; Guerri, A.; Lledós, A.; Peruzzini, M.; Zanobini, F. *Eur. J. Inorg. Chem.* **2009,** 3055-3059.
[160] Luo, Y.; Ohno, K. *Organometallics* **2007,** *26,* 3597-3600.
[161] Sloan, M. E.; Staubitz, A.; Clark, T. J.; Russell, C. A.; Lloyd-Jones, G. C.; Manners, I. *J. Am. Chem. Soc.* **2010,** *132,* 3831-3841.
[162] Pun, D.; Lobkovsky, E.; Chirik, P. J. *Chem. Commun.* **2007,** 3297-3299.
[163] Zimmerman, P. M.; Paul, A.; Zhang, Z. Musgrave, C. B. *Inorg. Chem.* **2009,** *48,* 1069-1081.
[164] Alcaraz, G.; Chaplin, A. B.; Stevens, C. J.; Clot, E.; Vendier, L.; Weller, A. S.; Sabo-Etienne, S. *Organometallics* **2010,** *29,* 5591-5595.

[165]Gloaguen, Y.; Alcaraz, G.; Vendier, L.; Sabo-Etienne, S. *J. Organomet. Chem.* **2009,** *694,* 2839-2841.
[166]Alcaraz, G.; Vendier, L.; Clot, E.; Sabo-Etienne, S. *Angew. Chem. Int. Ed.* **2010,** *49,* 918-920.
[167]Pons, V.; Baker, T. R.; Szymczak, N. K.; Heldebrandt, D. J.; Linehan, J. C.; Matus, M. H.; Grant, D. J.; Dixon, D. A.; *Chem. Commun.* **2008,** 6597-6599.
[168]Vance, J. R.; Robertson, A. P. M.; Lee, K.; Manners, I.; *Chem. Eur. J.* **2011,** 17, 4099-4103.
[169]Miller, A. J. M.; Bercaw, J. E. *Chem. Commun.* **2010,** *46,* 1709-1711.
[170]Whittell, G. R.; Balmond, E. I.; Robertson, A. P. M.; Patra, S. K.; Haddow, M. F.; Manners, I. *Eur. J. Inorg. Chem.* **2010,** 3967-3975.
[171]Spielmann, J.; Harder, S.; *J. Am. Chem. Soc.* **2009,** *131,* 5064-5065.
[172]Spielmann, J.; Jansen, G.; Bandmann, H.; Harder, S. *Angew. Chem. Int. Ed.* **2008,** *47,* 6290-6295.
[173]Spielmann, J.; Bolte, M.; Harder, S. *Chem. Commun.* **2009,** 6934-6936.
[174]Spielmann, J.; Piesik, D.; Wittkamp, B.; Jansen, G.; Harder, S. *Chem. Commun.* **2009,** 3455-3456.
[175]Forster, T. D.; Tuononen, H. M.; Parvez, M.; Roesler, R. *J. Am. Chem. Soc.* **2009,** *131,* 6689-6691.
[176]Liptrot, D. J.; Hill, M. S.; Mahon, M. F.; MacDougall, D. J. *Chem. Eur. J.* **2010,** *16,* 8508-8515.
[177]Hill, M. S.; Kociok-Köhn, G.; Robinson, T. P. *Chem. Commun.* **2010,** *46,* 7587-7589.
[178]Gaines, D. F.; Schaeffer, R. *J. Am. Chem. Soc.* **1964,** *86,* 1505-1507.
[179]Cowley, H. J.; Holt, M. S.; Melen, R. L.; Rawson, J. M.; Wright, D. S. *Chem. Commun.* **2011,** *47,* 2682-2684.

2 PHOSPHINE-ALKENE COMPLEXES OF DPEphos AND XANTphos

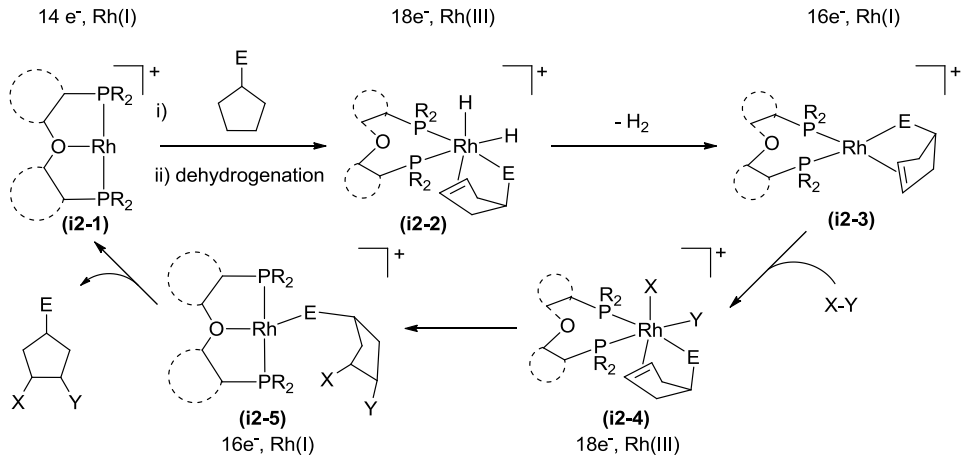
2.1 Introduction

The aim of the work presented in this chapter is to investigate the reactivity and possibility of functionalising the C=C bond formed from the intramolecular dehydrogenation of tethered cyclopentyl groups (Scheme 2.1).



Scheme 2.1 Proposed functionalisation of the cyclopentyl moiety.

The approach will involve the use of metal cations, hemilabile diphosphine ligands DPEphos and XANTphos and new cyclopentyl tethers in the form of ethers and thioethers. Hemilabile ligands, as noted in Chapter 1, have the ability to reversibly coordinate to the metal centre, stabilising highly reactive intermediates and facilitating reactivity in the presence of a more strongly coordinating substrate.[1,2,3] In the dehydrogenation cycle of the cyclopentyl group DPEphos and XANTphos could therefore adopt different geometries and coordination modes to permit both the functionalisation of the C=C bond and the catalytic turnover of the dehydrogenated substrate. (Scheme 2.2). The tether of the cyclopentyl group must be able to coordinate sufficiently to the metal centre but not so strong as to prevent decoordination upon dehydrogenation of the cyclopentyl group. In this regard, the subtle use of oxygen or sulphur over phosphorus may favour a weaker Rh-E interaction and result in catalytic turnover.

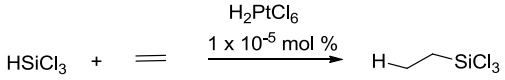


Scheme 2.2 Suggested stabilisation of catalytic cycle by a hemilabile POP ligand. Anions not shown.

The functionalisation of the now well established $PCyp_2(\eta^2\text{-}C_5H_7)$ motif will be investigated with regard to its reactivity with hydrogen, as well as amine-boranes and silanes respectively in the anticipation of hydroboration, hydrosilylation or transfer dehydrogenation of the double bond.

2.1.1 Hydrosilylation of alkenes

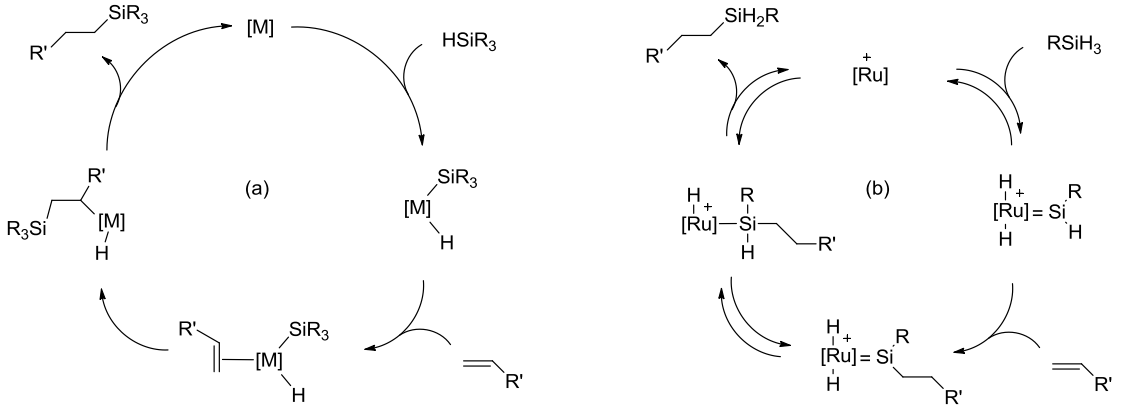
The hydrosilylation of alkenes (addition of a silane across a C=C bond) mediated by transition metals is one example of alkene hydrofunctionalisation[4,5] and is a well-documented method to provide useful synthetic organosilicon frameworks which possess different properties to their carbon based analogues.[6] Cross-linked polysiloxanes, generated from alkyl silane monomers, have wide ranging applications ranging from caulk to aerospace applications[7] while polysilanes are noteworthy because of their inherent conductivity and photophysical properties.[8] Recent efforts have been focused towards fast, asymmetric hydrosilylation.[9]



Scheme 2.3 Hydrosilylation of ethene with trichlorosilane using Speier's Catalyst.

The birth of transition-metal based hydrosilylation occurred in the 1950's using Ir, Ru catalysts and also a Pt chloride salt - chloroplatinic acid (Speier's Catalyst) which has shown remarkable

reactivity at small catalyst loadings (Scheme 2.3).[10] The product distribution of hydrosilylated species has been shown to differ depending on both the silane and catalyst employed suggesting the existence of different mechanisms for hydrosilylation.[11]



Scheme 2.4 (a) Modified Chalk-Harrod mechanism for hydrosilylation of alkenes; (b) Glaser-Tilley mechanism for the hydrosilylation of alkenes using a Ru catalyst to generate silylene intermediates.

The modified Chalk-Harrod mechanism (Scheme 2.4, (a)), which supersedes their first mechanism for hydrosilylation from 1965[12], best describes hydrosilylation catalysis using Rh[13] and concludes that migratory-insertion of the alkene into the Rh-Si bond occurs prior to reductive elimination to yield the C-H bond. The first step of either mechanism is the construction of an M-Si bond through oxidative addition of the silane. M=Si bonds formed as a product of double Si-H bond activation leads to an alternative mechanism. The existence of these highly reactive fragments had been a subject of contention for many years until 2003 when Glaser and Tilley first published a mechanism for the hydrosilylation of alkenes involving the formation of silylene intermediates coordinated to Ru (Scheme 2.4, (b)).[14] Formation of the metal-silylene precedes addition of alkene which critically coordinates to the silicon atom instead of the metal directly. Consequent migratory insertion of the hydrides and then reductive elimination yields the product of hydrosilylation and the regeneration of the catalyst. Transition metal complexes which undergo Si-H bond activation upon addition of silane are well documented,[15,16] especially in the group of Tilley (Figure 2.1).[17]

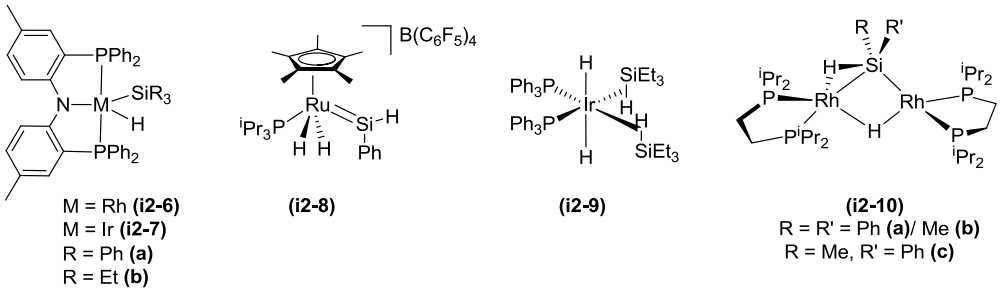


Figure 2.1 Examples of different coordination modes in complexes which have undergone Si-H bond activation.

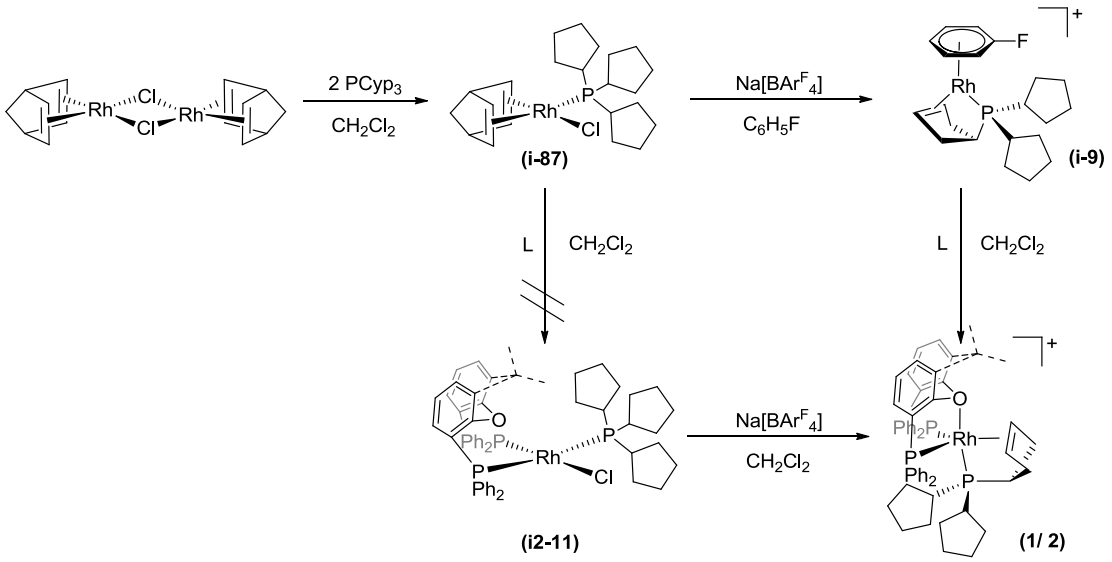
$[RuCp^*(^iPr_3P)(H)_2\{=Si(H)Ph\}\cdot Et_2O][B(C_6F_5)_4]$ **(i2-8)**, shown above without the labile ether ligand, catalyses the hydrosilylation of a wide range of alkenes using primary silanes to selectively form secondary silanes.[18] In 2008 work by Tilley and coworkers produced a second M=Si based catalyst of the family $[(PNP^{iPr})(H)Ir=SiR_2][B(C_6F_5)_4]$, where PNP^{iPr} = $[N(2\text{-}P^iPr_2\text{-}4\text{-}Me\text{-}C_6H_3)_2]^-$, this time capable of anti-Markovnikov selectivity.[19] A key importance of Tilley's complexes is attributed to the positive charge on the metal silylene which helps to promote hydrosilylation as a consequence of the silicon atom being more acidic.[20]

2.2 Results and discussion

2.2.1 Synthesis of complexes $[Rh(POP)\{PCyp_2(\eta^2\text{-}C_5H_7)\}][BAr^F_4]$ (1/ 2)

The Rh(I) diphosphine precursor complex $Rh(DPEphos)(PCyp_3)Cl$ **(i2-11)** was first targeted as a suitable precursor to *fac*-$[Rh(\kappa^3_{(POP)}\text{-}DPEphos)\{PCyp_2(\eta^2\text{-}C_5H_7)][BAr^F_4]$ **(1)** which upon the addition of $Na[BAr^F_4]$ would undergo dehydrogenation of one of the cyclopentyl groups in the same way that $Rh(Ph_2P(CH_2)_2PPh_2)(PCyp_3)Cl$ **(i-87)** forms $[Rh(Ph_2P(CH_2)_2PPh_2)\{PCyp_2(\eta^2\text{-}C_5H_7)][BAr^F_4]$ **(i-91)**.[21] Initial attempts to make **(i2-11)** however were unsuccessful with starting material and some evidence of decomposition to unidentifiable products (Scheme 2.5). Instead *fac*-$[Rh(\kappa^3_{(POP)}\text{-}DPEphos)\{PCyp_2(\eta^2\text{-}C_5H_7)\}][BAr^F_4]$ **(1)** was prepared directly in quantitative yield by the stoichiometric reaction of the preformed dehydrogenated tricyclopentylphosphine C_6H_5F coordinated complex $[Rh(\eta^6\text{-}C_6H_5F)\{PCyp_2(\eta^2\text{-}C_5H_7)\}][BAr^F_4]$ **(i-9)** with 1 equivalent of DPEphos in CH_2Cl_2 solvent at 298 K. The XANTphos complex, *fac*-$[Rh(\kappa^3_{(POP)}\text{-}$

XANTphos){PCyp$_2$(η^2-C$_5$H$_7$)}][BAr$^F_4$] **(2)** was isolated in quantitative yield in an analogous manner (Scheme 2.5).



Scheme 2.5 Synthesis of complexes **1** and **2**. **1**, L = DPEphos; **2**, L= XANTphos. [BAr$^F_4$]$^-$ anions not shown.

Complexes **1** and **2** were characterised by NMR spectroscopy, ESI-MS, microanalysis and single crystal X-ray diffraction. In both complexes a co-ordinated alkene resonance is confirmed by downfield shifts in their respective ^{1}H NMR spectra δ 3.84 (2H) **(1)**; 3.58 (2H) **(2)**. (*c.f.* δ 3.89 (2H) **(i-9)**) **2** also shows two inequivalent methyl environments for the XANTphos backbone δ 1.86 (s, 3H), 1.37 (s, 3H). The ^{13}C{^{1}H} NMR spectra also corroborate the coordination of an alkene [δ 74.9 (br) **(1)**]; [δ 62.2 (apparent q, *J* = 11 Hz) **(2)**]. These shifts are broadly similar to previously reported phosphine-alkene complexes *e.g.* [Rh(η^6-C$_6$H$_5$F){PCyp$_2$(η^2-C$_5$H$_7$)}][BAr$^F_4$] **(i-9)** and [Rh(Ph$_2$P(CH$_2$)$_2$PPh$_2$){PCyp$_2$(η^2-C$_5$H$_7$)][BAr$^F_4$] **(i-91)** *viz.* [δ 65.0 {d, *J*(RhC) 16 Hz)} **(i-9)**]; [δ 96.2 (t, *J* = 9.7 Hz) **(i-91)**].[21] The ^{31}P{^{1}H} NMR spectra show distinct characteristics of A$_2$MX spin systems; two phosphorus environments in a 1:2 ratio at [δ 84.1 {dt, 1P, *J*(RhP) 142 Hz, *J*(PP$_{cis}$) 44 Hz}, 19.0 {dd, 2P, *J*(RhP) 134 Hz, *J*(PP$_{cis}$) 44 Hz} **(1)**], [δ 90.7 {dt, 1P, *J*(RhP) 152 Hz, *J*(PP$_{cis}$) 22 Hz}, 26.6 {dd, 2P, *J*(RhP) 131 Hz, *J*(PP$_{cis}$) 22 Hz} **(2)**]. The ^{31}P-^{31}P coupling constants confirm that the three phosphorus atoms in the two complexes are located *cis* to each other (no large *trans* coupling observed, *e.g.*

[Rh($\kappa^3_{(POP)}$-DPEphos)($COCH_2CH_2SMe$)(H)][*closo*-$CB_{11}H_6Cl_6$] $J(PP_{trans})$ = 305 Hz)[22,23] whilst the coupling pattern (dd / dt) shows that the two diphosphine phosphorus atoms are chemically equivalent due to the existence of a mirror plane in each complex. The modest *cis* coupling constants match well for those found for [*cis*,*cis*-1,3,5-tris{(diphenylphosphino)methyl}cyclohexane]rhodium(I) chloride which also has a similar (*fac*) configuration of phosphine ligands {$J(PP_{cis})$ = 25.8}.[24] Overall these data confirm the proposed structures of **1** and **2** in solution.

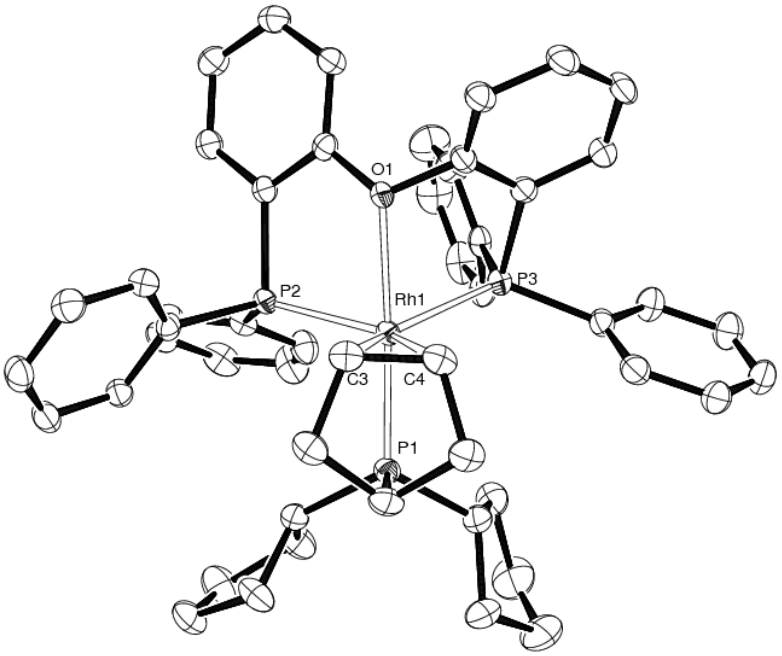


Figure 2.2 Solid-state structure of the cationic portion of **1**. Hydrogen atoms are omitted for clarity. Thermal ellipsoids are presented at the 50 % probability level. Selected bond lengths [Å] and angles [°]: Rh1-P1 2.2256(7), Rh1-P2 2.3270(7), Rh1-P3 2.3969(7), Rh1-O1 2.2503(17), Rh1-C3 2.128(3), Rh1-C4 2.175(3), C3-C4 1.425(4); P1-Rh1-P2 101.00(2), P1-Rh1-P3 108.95(2), P2-Rh1-P3 110.83(2), C3-Rh1-P1 83.67(8), C4-Rh1-P1 82.57(7), C3-Rh1-P2 101.20(8), C4-Rh1-P2 139.55(8), C3-Rh1-P3 141.91(7), C4-Rh1-P3 105.71(8), C3-Rh1-O1 87.09(9), C4-Rh1-O1 90.22(8).

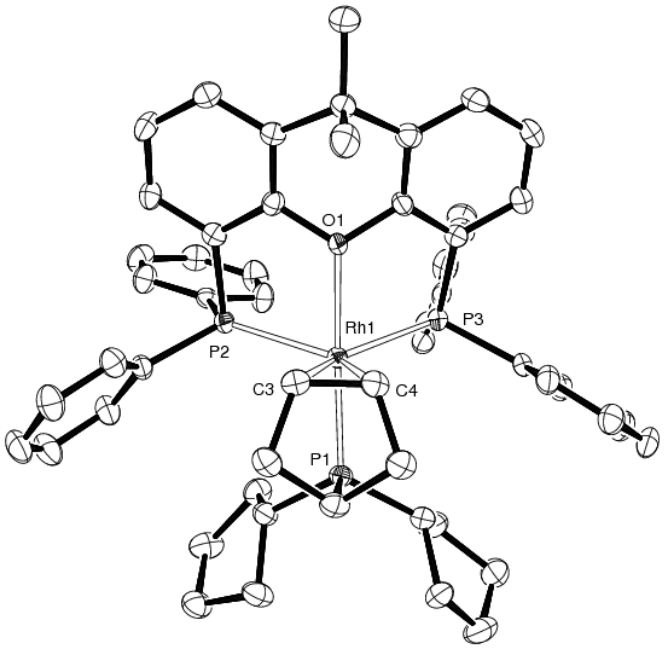
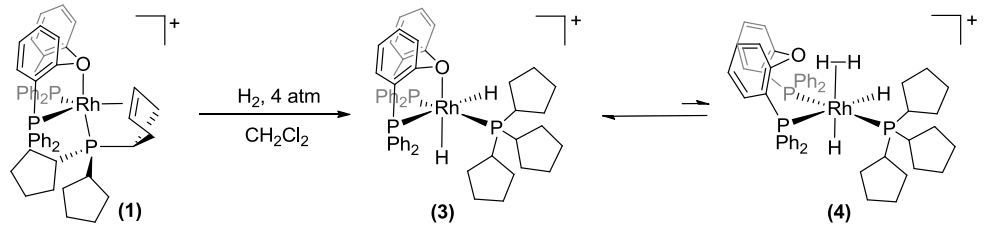


Figure 2.3 Solid-state structure of the cationic portion of **2**. Hydrogen atoms are omitted for clarity. Thermal ellipsoids are presented at the 50 % probability level. Selected bond lengths [Å] and angles [°]: Rh1-P1 2.2285(8), Rh1-P2 2.4007(7), Rh1-P3 2.3529(7), Rh1-O1 2.1837(19), Rh1-C3 2.151(3), Rh1-C4 2.165(3), C3-C4 1.416(4); P1-Rh1-P2 105.87(3), P1-Rh1-P3 103.63(3), P2-Rh1-P3 118.17(3), C3-Rh1-O1 86.81(9), C4-Rh1-O1 87.15(9), C3-Rh1-P1 84.01(8), C4-Rh1-P1 82.29(8), C3-Rh1-P2 93.72(8), C4-Rh1-P2 131.20(8), C3-Rh1-P3 142.61(8), C4-Rh1-P3 105.58(8).

The solid-state structures of complexes **1** and **2** further confirm the geometry of **1** and **2** (Figures 2.2 and 2.3). Both show *pseudo*-trigonal bipyramidal structures with the phosphorus atoms of the diphosphine located in equatorial positions *cis* to each other and *trans* to the alkene which also lies in an equatorial location as expected for a formally d^8 metal centre (*i.e.* Rh(I)) interacting with a π- acceptor with this geometry.[25] The DPEphos and XANTphos oxygen atoms are located in an axial position *trans* to the phosphorus atom of the tricyclopentylphosphine ligand which lies in an axial position as the strongest σ-donor with the shortest Rh-P bonds {Rh1-P1 2.2256(7) Å **(1)**; Rh1-P1 2.2285(8) Å **(2)**}. The solid-state structure of [Rh(NBD)(Me-dpa)][PF_6] {Me-dpa = *N*-(2-pyridylmethyl)-*N*-(6-methyl-2-pyridylmethyl)amine} exhibits similar characteristics.[26] Interestingly the Rh-O bond length for **2** is considerably shorter than that of **1** {2.1837(19) Å **(2)** *vs.* 2.2503(17) Å **(1)**} possibly suggesting a tighter interaction and a stronger Rh-O bond for **2**, which is presumably a result of the more rigid backbone of the

XANTphos ligand compared to DPEphos which enforces the oxygen atom in a position close to the metal. That the *trans* Rh-P1 distances are the same within error {2.2256(7) Å **(1)** *vs.* 2.2285(8) Å **(2)**} as are the Rh-P1 coupling constants of **1** and **2** {142 Hz **(1)**; 152 Hz **(2)**} suggests a similar interaction of the tricyclopentylphosphine in both cases with a similar Rh-O bond strength, even though the distances are different. The C=C bond lengths for the two complexes are also the same within error {1.425(4) Å **(1)** and 1.416(4) Å **(2)**} and again comparable with complexes **i-9** and **i-91** {1.401(4) Å **(i-9)**, 1.372(3) Å **(i-91)**}.[21] 18-electron-5-coordinate Rh(I) species, although not common, are known as both cationic[27,28] and neutral species.[29,30,31]

2.2.2 Reactivity of 1 and 2 with H_2



Scheme 2.6 Hydrogenation of **1** forms an equilibrium between complexes **3** and **4**. $[BAr^F_4]^-$ anions not shown.

Hydrogen can be considered as the simplest example of an XY substrate for the functionalisation of the co-ordinated alkene. Hydrogenation (4 atm, 10 minutes) of **1** at 298 K results in the hydrogenation of the bound alkene, which is characterised by the disappearance of the alkene signal in the ^{1}H NMR spectrum and the generation of [Rh($\kappa^3_{(POP)}$-DPEphos)$(H)_2PCyp_3$][BAr^F_4] **(3)** as the only species (Scheme 2.6). The ^{1}H NMR spectrum of the resulting product shows two broad, integral 1H, hydride environments at 298 K. On cooling to 223 K these resolve into complex signals δ −8.66 ppm {apparent doublet of quintets $J(P_{trans}H)$ 149 Hz, 13 Hz}, δ −22.95 (apparent triplet, J = 26 Hz) (Figure 2.4), which have not shifted appreciably in comparison to the spectrum at 298 K. The significantly large coupling constant for the resonance at δ −8.66 ppm suggests that this hydride is opposite a phosphorus atom. The second hydride resonance does not have an analogous coupling constant of this magnitude thus

identifying it to be opposite the oxygen to fill the octahedral coordination sphere. Being *trans* to a weaker donor is also consistent with the lower frequency shift. The $^{31}P\{^{1}H\}$ spectrum at 248 K shows a doublet of doublets at δ 58.8 and two broader peaks at δ 32.9 and 26.6 in a 1:1:1 ratio. Upon further cooling to 223 K the three environments in the $^{31}P\{^{1}H\}$ NMR spectrum sharpen further to reveal that each phosphorus sees coupling to Rh as well as two inequivalent phosphorus nuclei with a pair of phosphorus atoms lying *trans* to each other and the remaining phosphorus atom in a mutually *cis* orientation to the others (large *trans* coupling constant not observed) confirming the structure of **3** [δ 62.3 {ddd, 1P, $J(PP_{trans})$ 319 Hz, J(RhP) 114 Hz, $J(PP_{cis})$ 18 Hz}, 34.0 {ddd, 1P, $J(PP_{trans})$ 319 Hz, J(RhP) 106 Hz, $J(PP_{cis})$ 22 Hz}, 27.7 {apparent dt, 1P, J(RhP) 104 Hz, $J(PP_{cis})$ 20 Hz}]. In the ^{1}H NMR spectrum at 223 K under a pressure of H_2 (4 atm), in addition to the original hydride signals, three new broad resonances are observed at δ −1.79 (2H), −10.94 (1H) and −13.18 (1H) attributed to the low temperature formation of a dihydrogen dihydride complex, $[Rh(\kappa^2_{(PP)}\text{-DPEphos})(\eta^2\text{-}H_2)(H)_2(PCyp_3)][BAr^F{}_4]$ **(4)** (*vide infra*) in a 17:1 ratio **3**: **4**.

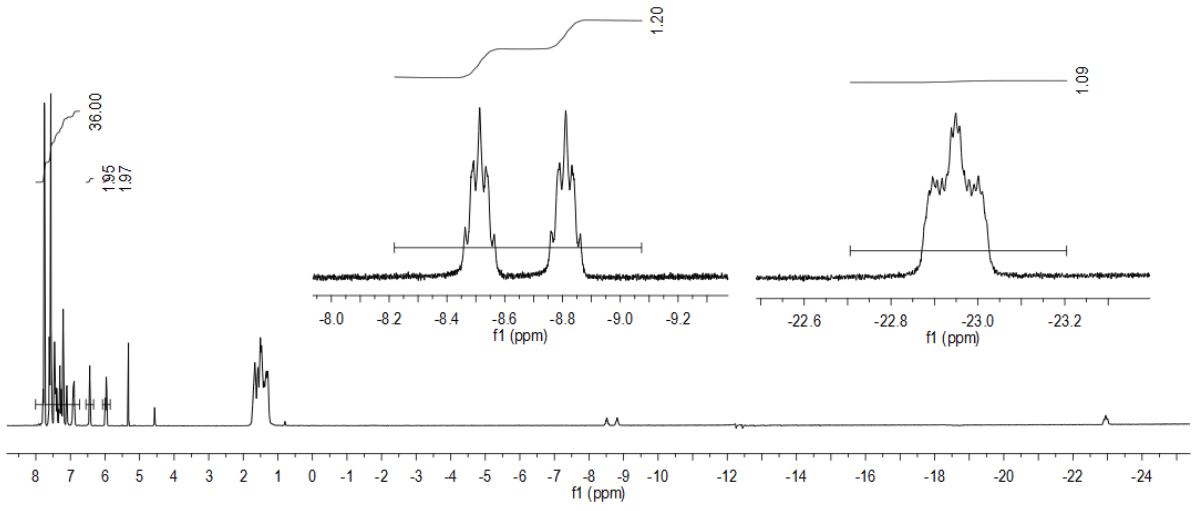


Figure 2.4 ^{1}H NMR spectrum of **3** at 223 K, hydride resonances shown inset (500 MHz, CD_2Cl_2).

Evidence for a dynamic equilibrium between **3** and **4** was obtained by further cooling to 198 K whereby the ratio of complexes **3**:**4** changed to 1:5 respectively. T_1 relaxation measurements for **4** were also gathered at this temperature. The relative 2H integral of **4** at δ −1.79 has a T_1 of 21

ms consistent with a dihydrogen ligand while the low frequency hydride resonances relax at 400 ms, typical of a dihydride[32] {*c.f.* [Rh($Ph_2P(CH_2)PPh_2$)(η^2-H_2)$(H)_2$($PCyp_3$)][BAr^F_4] **(i-98)**, η^2-H_2 19 ms, $(H)_2$ 215 ms (180 K)}[21] and {[Ru($\kappa^3_{(POP)}$-DPEphos)(η^2-H_2)(H)(PPh_3)][BAr^F_4], η^2-H_2 9.6 ms (236 K), $(H)_2$ 324 ms (239 K)}.[33] The solid-state structure of **3**, obtained by crystallisation under an atmosphere of H_2, is consistent with the NMR spectroscopic data for this complex and shows a distorted six coordinate octahedral geometry following the location of both hydride ligands (Figure 2.5). The tricyclopentylphosphine ligand is indeed located *trans* to one phosphorus atoms of the DPEphos ligand (which itself adopts a *fac* geometry at the metal centre) with one of the hydride ligands *trans* to the other phosphorus atom of the diphosphine. The resulting *trans* influence of this hydride ligand is evidenced in the lengthening of the Rh-O bond in comparison with **1** {2.308(2) Å **(3)** *vs.* 2.2503(17) Å **(1)**} and also the longer Rh-P3 bond {2.3514(10) Å} observed with respect to Rh-P1 {2.3135(10) Å} and Rh-P2 {2.3349(10) Å}. The greater steric bulk of the phosphine ligands in comparison with H0A and H0B renders P1-Rh1-P3 and O1-Rh1-P1 larger than 90°. The Rh1-H0A bond distance is relatively short and the same within error to that found in the reported X-ray structure of [Rh($\kappa^3_{(POP)}$-XANTphos)(MeCN)$(H)_2$][BAr^F_4] (1.49(4) Å **(3)** *vs.* 1.482(3) Å).[34] The Rh1-H0B bond length of **3** is somewhat longer (1.54(3) Å) presumably as a result of the *trans* phosphine which is also a good σ-donor and therefore a moderate *trans* influence ligand.

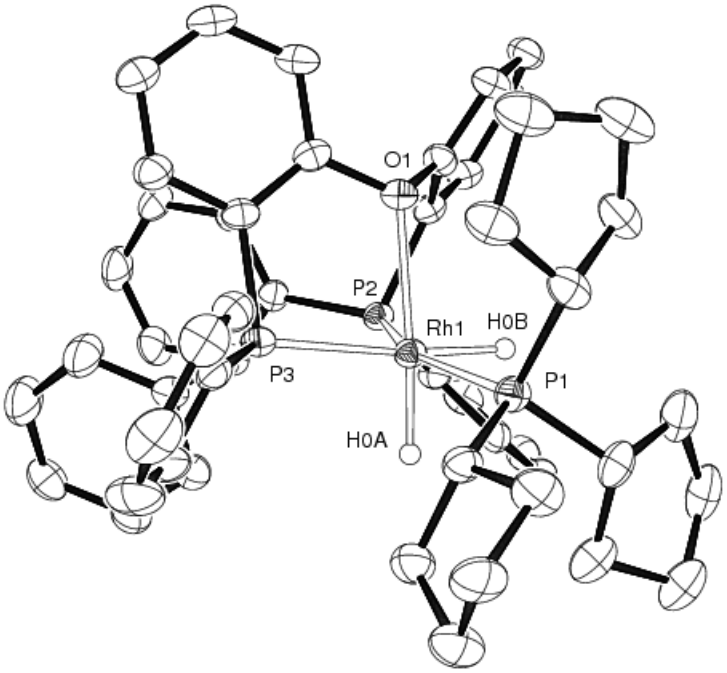
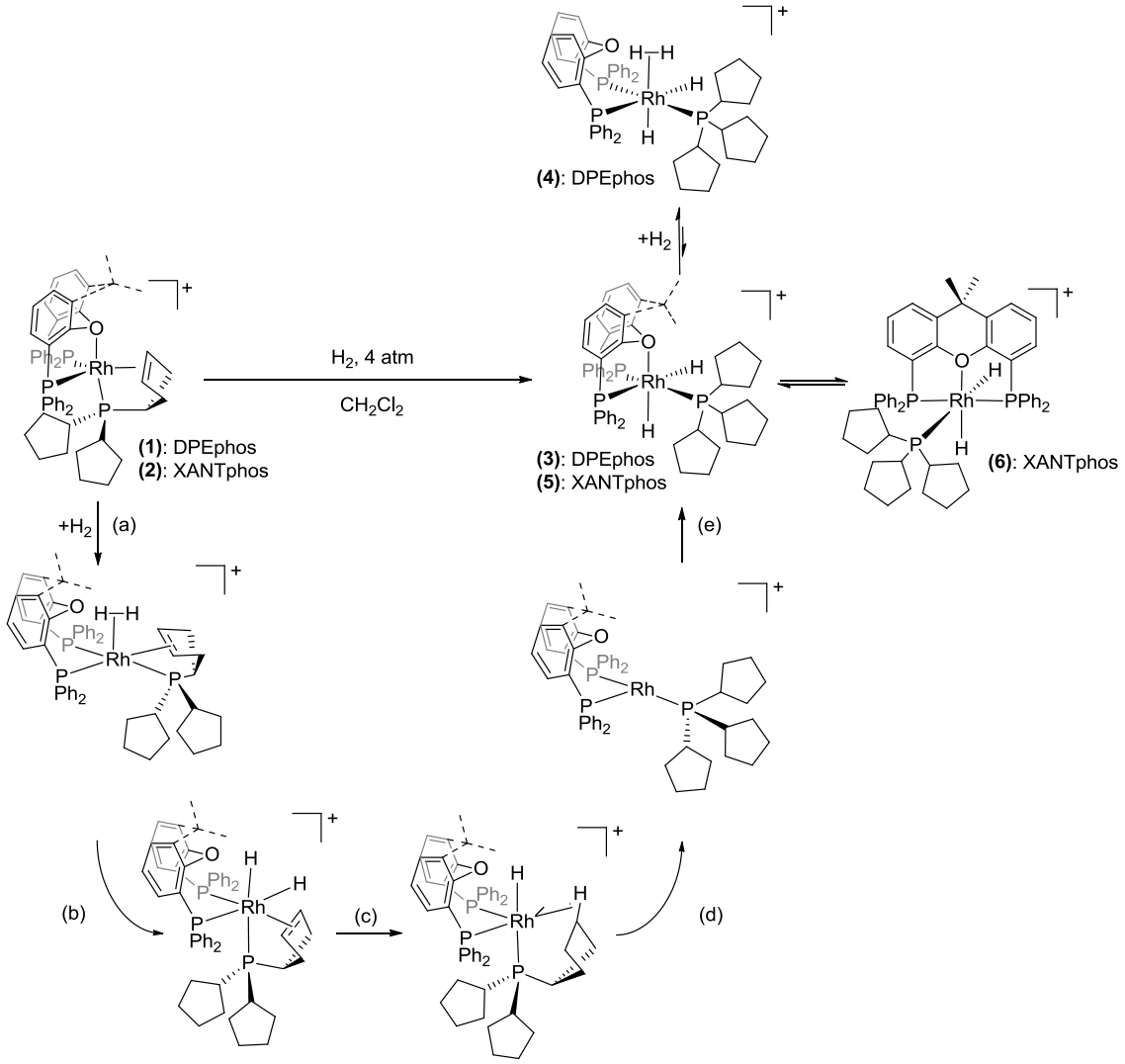


Figure 2.5 Solid-state structure of the cationic portion of **3**. Hydrogen atoms (except hydride ligands) are omitted for clarity. Thermal ellipsoids are presented at the 50 % probability level. Selected bond lengths [Å] and angles [°]: Rh1-P1 2.3135(10), Rh1-P2 2.3349(10), Rh1-P3 2.3514(10), Rh1-O1 2.308(2), Rh1-H0A 1.49(4), Rh1-H0B 1.54(3); P1-Rh1-P2 153.78(4), P1-Rh1-P3 106.99(4), P2-Rh1-P3 99.20(3), O1-Rh1-P1 104.07(7), O1-Rh1-P2 78.42(7), O1-Rh1-P3 81.12(6).

Complex **2** undergoes hydrogenation considerably slower than **1**, and two dihydride isomers *fac*-[Rh($\kappa^3_{(POP)}$-XANTphos)$(H)_2(PCyp_3)$][BAr^F_4] **(5)** and *mer*-[Rh($\kappa^3_{(POP)}$-XANTphos)$(H)_2(PCyp_3)$][BAr^F_4] **(6)** are formed after 5 days at 298 K (*vide infra*) (Scheme 2.7) unlike DPEphos which gives rise to only the *fac*-isomer. As decoordination of the oxygen atom and coordination of H_2 in **1** and **2** is presumably the first step in these reactions, this difference in reaction time further supports the stronger or, at the very least, less flexible nature of the Rh-O bond in **2** compared to **1**. Subsequent oxidative addition of dihydrogen then occurs, *via* a series of suggested unobserved intermediates, to form complexes **3** – **6**.



Scheme 2.7 Proposed mechanism for complexes formed upon hydrogenation of **1** and **2**. $[BAr^F_4]^-$ anions not shown. (a) = addition of H_2, (b) = oxidative addition, (c) insertion, (d) reductive elimination, (e) oxidative addition and isomerisation

The ^{1}H NMR spectra of **5** and **6** are characterised by a pair of hydride environments at 298 K in a 1.7 : 1 ratio respectively, reflecting the formation of two isomers [δ −9.33 {broad d, J(PH$_{trans}$) 143 Hz}; δ −22.19 (br), **(5)**]; [δ −7.93 {apparent dqd, J(PH$_{trans}$) 135 Hz, J(RhH) 13 Hz, J(HH) 5.8 Hz}, −20.49 {m, J(RhH) 29 Hz, J(HH) 6.1 Hz} **(6)**] (Figure 2.6). The difference in chemical shifts between the two hydride environments of each complex reflects the nature of substituent *trans* to it with the more labile oxygen atom of the POP ligand providing least stabilisation resulting in a hydride shift at higher field.[35] To gain a better idea for the magnitude of the complex coupling of the low frequency resonances for **6**, simulation was undertaken; both were

successfully simulated using the gNMR based on two inequivalent phosphorus environments and two inequivalent hydride environments in an $ABMX_2Y$ system.[36]

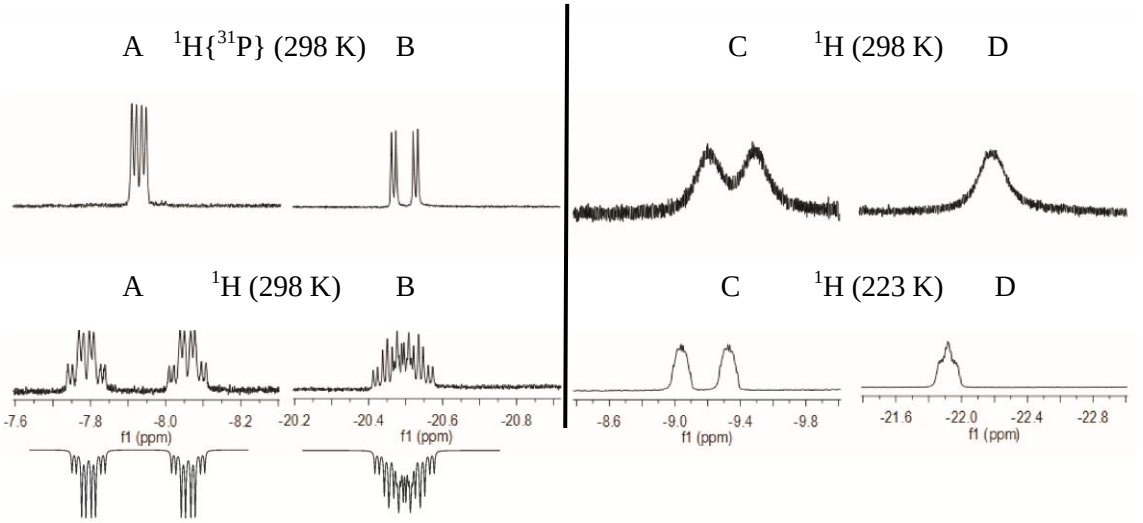


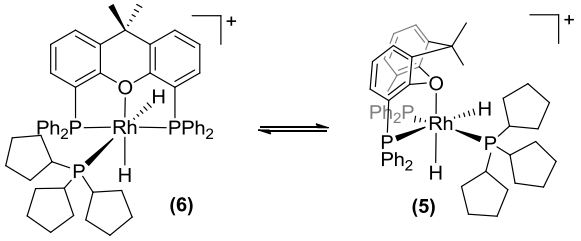
Figure 2.6 A & B: Low frequency ^1H NMR spectra with gNMR simulation (inverted) (bottom) and ^1H $\{^{31}P\}$ NMR spectra for complex **6** at 298 K (top) (500 MHz, CD_2Cl_2). C & D: Low frequency ^1H NMR spectra of **5** at 298 K (top) and 223 K (bottom) (500 MHz, CD_2Cl_2).

The $^{31}P\{^1H\}$ spectrum at 298 K exhibits three phosphorus environments for **5** [δ 50.9 {broad dd,1P, $J(PP_{trans})$ 324 Hz, J(RhP) 110 Hz}, 36.1 {broad dd, 1P, $J(PP_{trans})$ obscured, J(RhP) 112 Hz}, 27.3 {broad d, 1P, J(RhP) 98 Hz}] whilst only two environments for **6** [δ 36.9 {dd, 2P, J(RhP) 114 Hz, $J(PP_{cis})$ 20 Hz}, 20.7 {dt, 1P, J(RhP) 97 Hz, $J(PP_{cis})$ 20 Hz}] are observed. The three inequivalent phosphorus environments observed for **5** show a close resemblance to those observed for **3** suggesting that **5** has similar geometry with the tricyclopentylphosphine coordinating *trans* to a phosphorus atom of the XANTphos backbone. Only two phosphorus environments are observed for isomer **6** with no large *trans* phosphorus coupling constant which is consistent with the two phosphorus atoms of the XANTphos ligand being chemically equivalent with the tricyclopentylphosphine lying mutually *cis* opposite a hydride.

Upon cooling a solution containing a mixture of **5** and **6** from 293 K to 253 K the relative integrals of the hydride resonances changes from 1:2.00, **6**:**5** to 1:1.56, **6**:**5** to favour **6** although **5** is still the major isomer present. This suggests the presence of an equilibrium between the two

species. The equilibrium constant (K_{eq}) was obtained by taking the ratio between the hydride resonances of **5** and **6** at five different temperatures. Plotting ln(K_{eq}) versus the reciprocal of temperature (T^{-1}) yields a van't Hoff plot from which the standard enthalpy (ΔH) and entropy (ΔS) can be calculated from the gradient and y intercept respectively (Figure 2.7). The calculated enthalpy of +4.4 ± 0.2 kJ mol^{-1} for **6** ↔ **5** indicates that the energy difference between the two isomers is small. ΔS is however significant (+21.3 ± 0.6 $JK^{-1}mol^{-1}$) in comparison and therefore is the overriding factor in determining that **5** dominates in solution giving an overall ΔG (298 K) = −1.9 kJ mol^{-1} for **6** ↔ **5**. Tentatively comparing the structures of **5** and **6** sees that **5** is less sterically congested than **6**, which would also lend support for the preferred existence of **5**.

$$K_{eq} = \frac{[\mathbf{5}]}{[\mathbf{6}]}$$



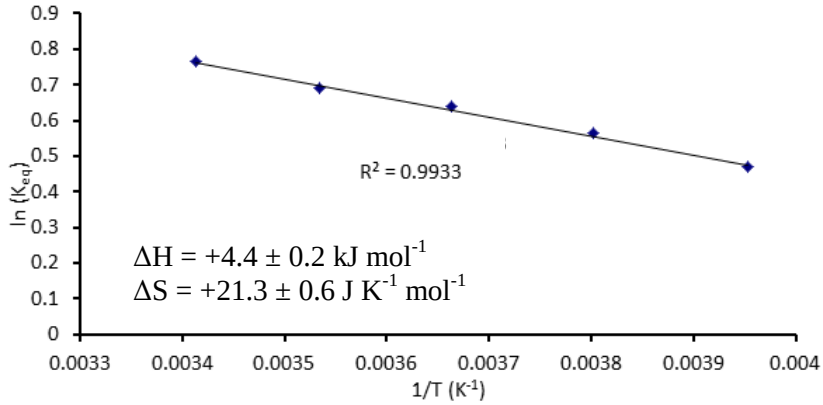
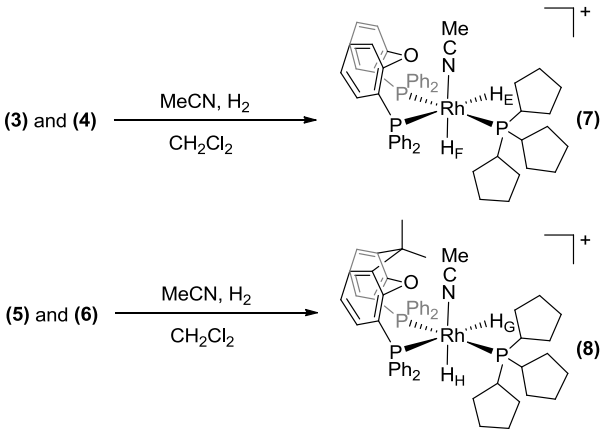


Figure 2.7 van't Hoff plot of **5** and **6** from 293 K to 253K. $[BAr^F_4]^-$ anions not shown.

Addition of an excess of MeCN (approx. 10 eq.) to complexes **3** - **6** in solution under an atmosphere of hydrogen (*vide infra*) yields [Rh($\kappa^2_{(PP)}$-DPEphos)($PCyp_3$)$(H)_2$(MeCN)][BAr^F_4]

(7) and [Rh($\kappa^2_{(PP)}$-XANTphos)($PCyp_3$)$(H)_2$(MeCN)][BAr^F_4] **(8)** in quantitative yield by NMR spectroscopy (Scheme 2.8). The formation of **7** and **8** is demonstrated by ^{1}H NMR spectroscopy (*vide infra*) and by three separate environments in their respective $^{31}P\{^1H\}$ NMR spectra. [δ 50.9 {broad dd, 1P, $J(PP_{trans})$ 357 Hz, J(RhP) 110 Hz}, 32.1 {broad dd, 1P, $J(PP_{trans})$ 358 Hz, J(RhP) 112 Hz}, 22.9 {broad d, 1P, J(RhP) 99 Hz} (**7**)]; [δ 56.6 {ddd, 1P, $J(PP_{trans})$ 365 Hz, J(RhP) 115 Hz, $J(PP_{cis})$ 15 Hz}, 20.0 {ddd, 1P, $J(PP_{trans})$ 365 Hz, J(RhP) 110 Hz, $J(PP_{cis})$ 20 Hz}, 15.3 {ddd, 1P, J(RhP) 92 Hz, $J(PP_{cis})$ 20 Hz, $J(PP_{cis})$ 15 Hz} (**8**)]. In the case of **7** the *cis*-phosphorus coupling is not resolved at 298 K.



Scheme 2.8 Addition of MeCN to complexes **3-6** under a hydrogen atmosphere forms acetonitrile adducts **7** (DPEphos) and **8** (XANTphos). $[BAr^F_4]^-$ anions not shown.

In the ^{1}H NMR spectra of **7** and **8**, sharp hydride resonances with complicated multiplicity are observed which were successfully modelled using gNMR assuming coupling to three inequivalent phosphorus environments, Rh and the other inequivalent hydride (Figure 2.8). Selective $^1H\{^{31}P\}$ NMR spectroscopy experiments removed several orders of fine structure to reveal the H-H and Rh-H coupling constants for the two pairs of hydride signals [{J(HH) ~ J(RhH) = 9 (E)} and {J(HH) 9, J(RhH) 13 (F)} **(7)**]; [{J(HH) ~J(RhH) = 11 (G) and (H)} **(8)**], which demonstrates that the largest coupling for hydrides E and G is due to a *trans* P-H coupling {$J(PH_{trans})$ = 150 Hz and 149 Hz, respectively}.

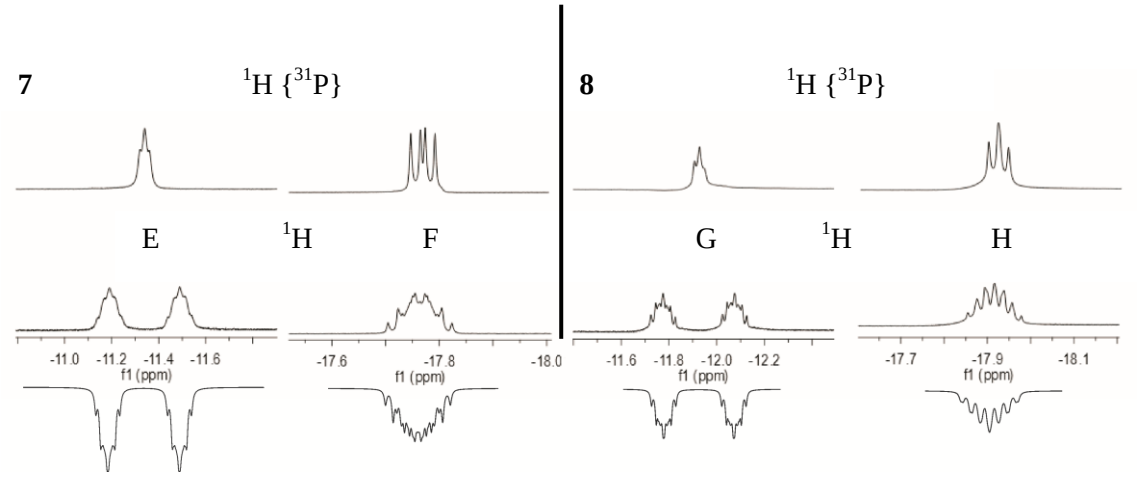
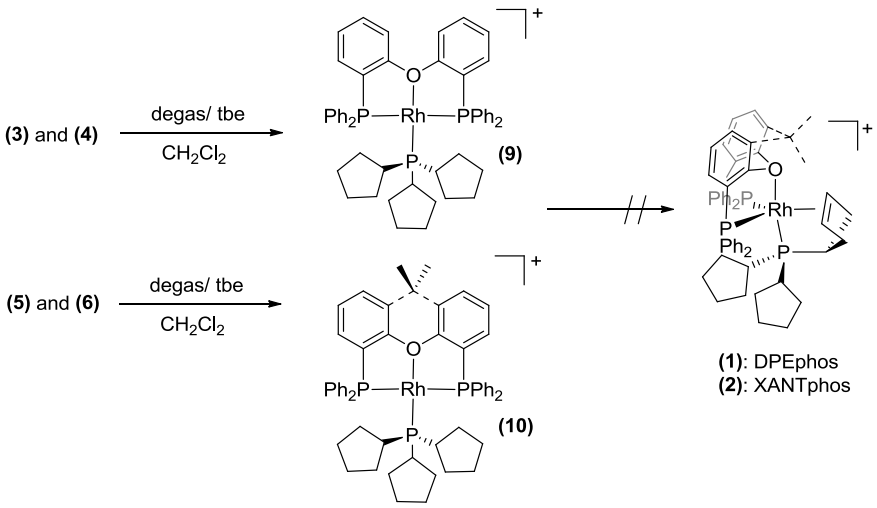


Figure 2.8 Low frequency ^{1}H (bottom) and ^{1}H {^{31}P} (top) NMR spectra of complexes **7** (left) and **8** (right) at 298 K (500 MHz, CD_2Cl_2).

Complexes **3 - 6** are only stable under a hydrogen atmosphere. When placed under vacuum or upon addition of tbe they lose H_2 to form [Rh($\kappa^3_{(POP)}$-DPEphos)($PCyp_3$)][BAr^F_4] **(9)** and [Rh($\kappa^3_{(POP)}$-XANTphos)($PCyp_3$)][BAr^F_4] **(10)** respectively in quantitative yield by NMR spectroscopy (Scheme 2.9). A related $\kappa^3_{(POP)}$-DPEphos Rh(III) octahedral complex, [Rh($\kappa^3_{(POP)}$-DPEphos)($CH_2CH_2CO_2Me$)(COC_2H_4SMe)][$CB_{11}H_6Cl_6$], has previously been shown to have a similarly short lifetime (minutes) in solution.[22] This contrasts to a related Rh(III) bis-phosphine dihydride, [Rh$(H)_2(P^iPr_3)_2$][BAr^F_4], which is stable for over 72 hours under vacuum in solution.[37]



Scheme 2.9 Removal of the hydrogen atmosphere from complexes **3-6** results in the formation of complexes **9** (DPEphos) and **10** (XANTphos). Complexes **1** and **2** cannot be reformed. [BAr^F_4]$^-$ anions not shown.

Interestingly, **5/ 6** (XANTphos) lose H_2 rapidly (one freeze-thaw-degas cycle) while H_2 loss is much slower for **3/ 4** (DPEphos, 5 cycles). The rapid reductive elimination of hydrogen from the XANTphos isomers could be attributed to the release of significant strain in the ligand backbone on moving from a *fac*-$\kappa^3_{(POP)}$ octahedral geometry in **5** and **6** to form the *trans*-$\kappa^3_{(POP)}$ square planar structure of **10**. Increasing the natural bite angle of the diphosphine has been previously shown to increase the rate of reductive elimination in Pd cross-coupling reactions with the best results obtained using the XANTphos ligand and negligible activity observed for DPEphos.[38] The $^{31}P\{^1H\}$ NMR spectra for **9** and **10** reveal two phosphorus environments in a 2:1 ratio showing coupling to ^{103}Rh [δ 48.8 {dt, 1P, *J*(RhP) 190 Hz, *J*(PP_{cis}) 35 Hz}, 33.4 {dd, 2P, *J*(RhP) 156 Hz, *J*(PP_{cis}) 35 Hz} **(9)**]; [δ 44.3 {dt, 1P, *J*(RhP) 193 Hz, *J*(PP_{cis}) 35 Hz}, 33.1 {dd, 2P, *J*(RhP) 156 Hz, *J*(PP_{cis}) 35 Hz} **(10)**]. The solid state structures of **9** and **10** confirm that the complexes exhibit square planar geometries (sum of the angles around the Rh centre = 359.99° and 361.15° respectively) (Figures 2.9 and 2.10). The phosphorus atoms of the diphosphines are approaching a *trans* configuration {156.61(5)° **(9)**; 158.409(7)°, **(10)**} while the Rh-O bond distance in **9** is significantly shorter than in **1** {2.189(3) Å **(9)** *vs.* 2.2503(17) Å **(1)**} on moving to this Rh(I) 16 electron species whilst that for **10** lengthens compared to **2** {2.222(5) Å **(10)** *vs.* 2.1837(19) Å **(2)**}. Interestingly, examples of tridentate coordination of POP type ligands are scarce in the literature[39] however these X-ray data compare favourably with two complexes containing $\kappa^3_{(POP)}$-*trans* spanning POP ligands [Rh($\kappa^3_{(POP)}$-($Ph_2P(CH_2)_2O(CH_2)_2PPh_2$))(CO)][$PF_6$] and [Rh($\kappa^3_{(POP)}$-XANTphos)(CO)][$BF_4$] which also exhibit square planar geometries and have similar POP ligand bite angles {165.9(1)° and 164.42(4)° respectively} about the metal centre.[40,41] Work within our group has recently characterised related Rh and Ir XANTphos complexes.[34,42] The rigidity of the XANTphos ligand in coordination to Rh has been previously noted as a large contributing factor to the observed linear selectivity in the hydroformylation of styrene.[43] The stability of **9** and **10** is demonstrated by their lack of further reactivity with regard to the dehydrogenation of the tricyclopentylphosphine (to **1** and **2**). Even when heating at 313 K in the presence of tbe as a

hydrogen acceptor. This could possibly be rationalised by the tight κ^3-$_{(POP)}$ coordination of the diphosphine ligand (which would have to be displaced by a weak agostic C-H bond for dehydrogenation to occur) and stable Rh(I) 16-electron cationic species.

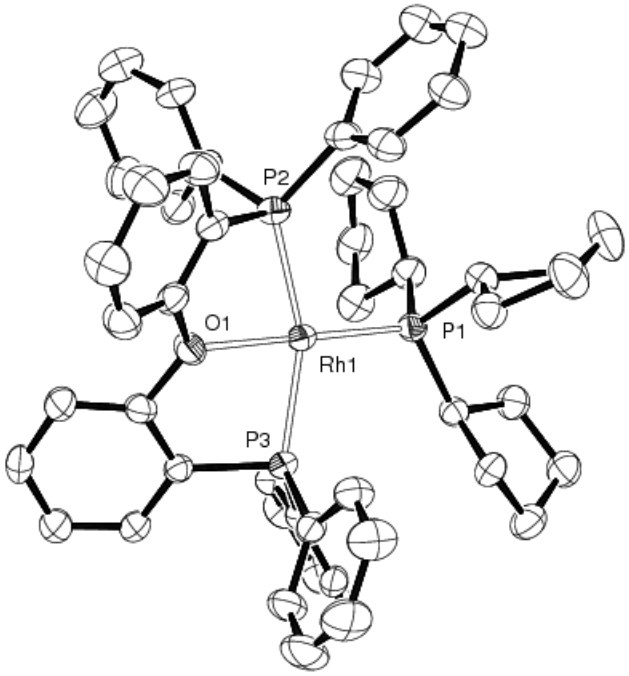


Figure 2.9 Solid-state structure of the cationic portion of **9**. Hydrogen atoms are omitted for clarity. Thermal ellipsoids are presented at the 50 % probability level. Selected bond lengths [Å] and angles [°]: Rh1-P1 2.2375(13), Rh1-P2 2.3247(12), Rh1-P3 2.2678(12), Rh1-O1 2.189(3); P1-Rh1-P2 102.71(5), P1-Rh1-P3 100.67(4), P2-Rh1-P3 156.61(5), O1-Rh1-P1 178.89(10), O1-Rh1-P2 77.27(9), O1-Rh1-P3 79.34(9).

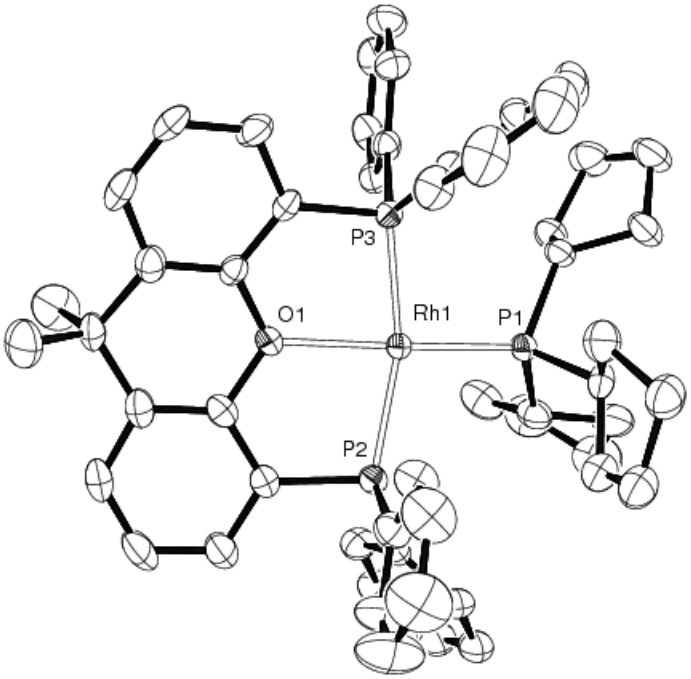
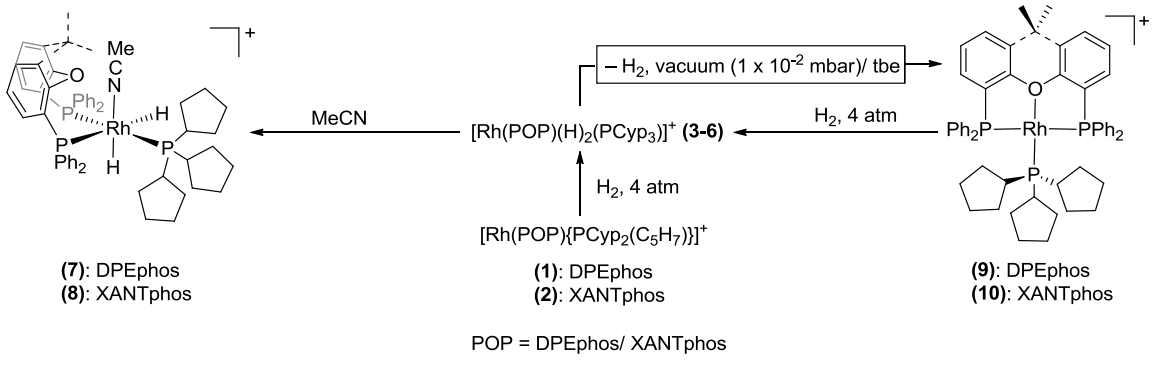


Figure 2.10 Solid-state structure of the cationic portion of **10**. Hydrogen atoms are omitted for clarity. Thermal ellipsoids are presented at the 50 % probability level. Selected bond lengths [Å] and angles [°]: Rh1-P1 2.2458(19), Rh1-P2 2.2985(19), Rh1-P3 2.2659(19), Rh1-O1 2.222(5); P1-Rh1-P2 101.07(7), P1-Rh1-P3 97.83(7), P2-Rh1-P3 158.40(7), O1-Rh1-P1 174.08(15), O1-Rh1-P2 80.80(14), O1-Rh1-P3 81.45(14).

Placing **9** and **10** under a hydrogen atmosphere (4 atm) resulted in the reformation of mixtures of **3** and **4 (9)** and **5** and **6 (10)**, respectively both within 5 minutes - easily recognised by the change in colour of the solution from orange to colourless. A summary of the reactivity of complexes **1-10** is shown in Scheme 2.10 with the $^{31}P\{^{1}H\}$ NMR spectra of complexes **1**, **2** and **7-10** shown in Figure 2.11.



Scheme 2.10 Onward reactivity of complexes **1** and **2**. $[BAr^{F}_{4}]^{-}$ anion for complexes **7-10** not shown.

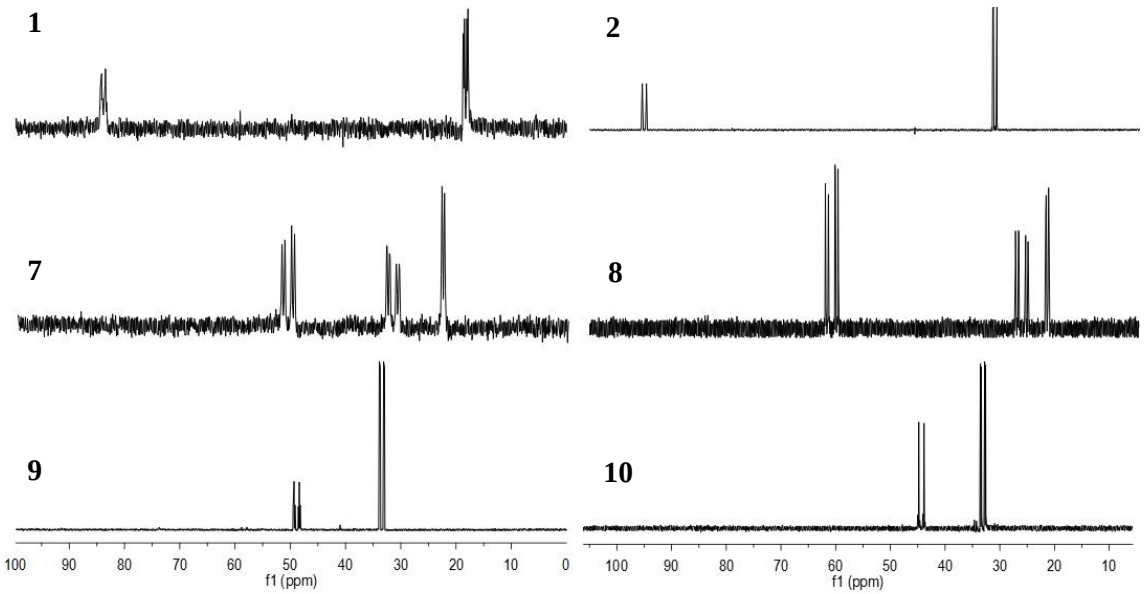
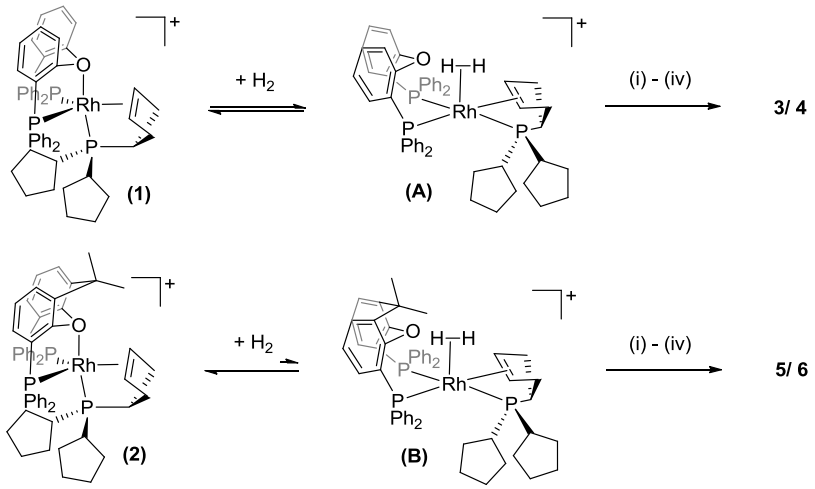


Figure 2.11 ^{31}P $\{^{1}H\}$ NMR spectra of complexes **1**,**2** and **7**-**10** at 298 K (202 MHz, CD_2Cl_2). $[BAr^F_4]^-$ anions not shown.

It is interesting to note the large difference in reactivity between the DPEphos and XANTphos complexes with hydrogen and towards reductive elimination. Complexes containing chelating POP ligands commonly coordinate in a $\kappa^3_{(POP)}$ manner although the oxygen atom can be displaced with a strong coordinating ligand or solvent molecule.[44] Their inherent stability is also determined by their natural bite angles; DPEphos = 102°, XANTphos = 111°[45] which generally favour *mer* geometries (with the phosphorus atoms in a *trans* position) upon coordination to the metal; particularly the larger bite angle XANTphos ligand. $\kappa^3_{(POP)}$-*fac* coordination geometries as found in **1** and **2** are less common although they have been observed in neutral Ru complexes *e.g. fac*-[$RuCl_2$($\kappa^3_{(POP)}$-DPEphos)(DMSO)] by Balakrishna and co-workers[46] and have also been suggested to stabilise cationic trigonal bipyramidal Pd species in the cross-coupling of *sec*-butyl magnesium chloride with bromobenzene.[47] To coordinate dihydrogen, **1** and **2** must decoordinate the oxygen of the POP ligand to form a $\kappa^2_{(PP)}$-5 coordinate structure **(A/ B)** (Scheme 2.11). XANTphos, with the wider natural bite angle compared to DPEphos, is more reluctant to do this as it results in greater steric pressure on the rigid backbone. DPEphos is

more flexible and therefore can more easily stabilise a $\kappa^2_{(PP)}$-5 coordinate geometry **(A)** resulting in faster reactivity to form **3/ 4** than observed for the formation of **5/ 6** from **2** (Scheme 2.11).

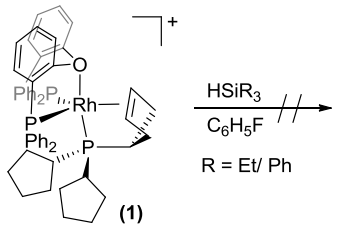


Scheme 2.11 $\kappa^3_{(POP)}$ *vs.* $\kappa^2_{(PP)}$ DPEphos and XANTphos coordination. (i) = oxidative addition, (ii) insertion, (iii) reductive elimination, iv) oxidative addition and isomerisation. $[BAr^F_4]^-$ anions not shown.

The features of these ligands are further illustrated in the stability of complexes **3-6** to reductive elimination of dihydrogen. **5/ 6** lose hydrogen immediately to favour the $\kappa^3_{(POP)}$-*trans* spanning square planar Rh(I) complex **10** (XANTphos) whilst **3/ 4** require several freeze/ pump/ thaw degas attempts and tbe to gain quantitative conversion to **9** (DPEphos) as the XANTphos complex has a strong preference to lie in a *trans*-$\kappa^3_{(POP)}$ geometry. Stabilisation of a square planar Pd complex by tridentate *trans* XANTphos coordination compared to bidentate *cis* preference for DPEphos has been previously been noted by van Leeuwen *et. al.* as a reason for reduced activity using XANTphos in the amination of aryl triflates.[48] Investigations by van Leeuwen *et al.* into the steric role played by the R substituents of diphosphine ligands has concluded that *mer*-$\kappa^3_{(POP)}$ octahedral geometries are favoured over *fac*-$\kappa^3_{(POP)}$ octahedral geometries with bulkier ligands.

2.2.3 Reactivity of complexes 1 and 2 with silanes

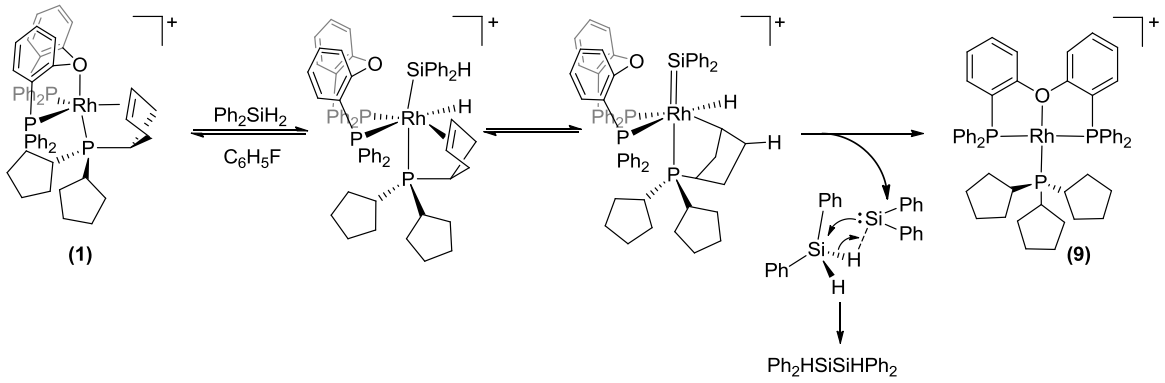
Having characterised the reactivity of **1** and **2** towards hydrogen, the potential to carry out hydrosilylation reactions with the tethered alkene of **1** was attempted. This was initially probed using tertiary silanes Et_3SiH and Ph_3SiH (Scheme 2.12). No reaction was observed in either case upon stoichiometric addition or the addition of a small excess of either silane in C_6H_5F solvent at 298 K over the period of 48 hours.



Scheme 2.12 Addition of triethyl- or triphenyl-silane to **1** in C_6H_5F showed no sign of reaction. $[BAr^F_4]^-$ anion not shown.

Addition of 1 equivalent of the more reactive secondary silane Ph_2SiH_2 to complex **1** in C_6H_5F solution surprisingly resulted in quantitative formation of complex **9** after 8 hours by NMR spectroscopy. Addition of 2 equivalents of Ph_2SiH_2 to **1** again afforded **9** cleanly with the concomitant appearance of disilane $(SiPh_2H)_2$ [δ 5.38 (s), C_6H_5F][49] in addition to free Ph_2SiH_2 as determined by ^1H NMR spectroscopy, although the characteristic silicon satellites of this species were too weak to be observed. This suggests that transformation of **1** to **9** occurs by transfer hydrogenation using Ph_2SiH_2 as the hydrogen source. In the presence of excess silane, $(SiPh_2H)_2$ appears to be the major by-product. $(SiPh_2H)_2$ is however not formed under stoichiometric conditions, suggesting that the mechanism operating is more complicated. Addition of 0.5 equivalents of Ph_2SiH_2 to **1** yielded incomplete conversion to **9** with **1** remaining in a 1:1.3 **(1)**:**(9)** ratio with no disilane observed. Presumably in the absence of excess Ph_2SiH_2, the reactive silylene ($SiPh_2$) generated on dehydrogenation to form **9** dissociates and decomposes in solution (Scheme 2.13). These results are in line with those reported by Milstein *et al.* who used $Rh(^iPr_3P)_2(H)_2(OTf)$ in the dehydrocoupling reaction of Ph_2SiH_2 to $(SiPh_2H)_2$ and found no equivalent dehydrocoupling reaction with Ph_3SiH.[50] Milstein proposed that the

Curtis-Epstein mechanism (See introduction, Scheme 1.34) for dehydrogenative coupling of Ph_2SiH_2 could be ruled out on the grounds that oxidative addition of two molecules of Ph_3SiH should promote dehydrocoupling meaning that the existence of two hydrogen atoms per silane must have an effect. Subsequent studies showed conclusive evidence for an alternative mechanism involving the loss of a silylene fragment which reacts further with free Ph_2SiH_2 to form $(SiPh_2H)_2$ with no observed intermediates. A similar mechanism has been offered for the catalytic dehydrocoupling of stannanes by hafnium complexes (Scheme 2.13).[51]



Scheme 2.13 Suggested mechanism for the formation of **9** and $(SiPh_2H)_2$. $[BAr^F_4]^-$ anions not shown.

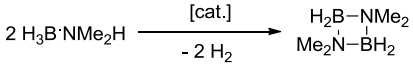
To further investigate the incorporation of hydrogen into the tricyclopentylphosphine motif, **1** was reacted with 1 equivalent of Ph_2SiD_2. ^2H NMR spectroscopy confirmed that deuterium had become integrated into the tricyclopentylphosphine ligand with the observance of alkyl peaks $\delta(^2H)$ 1.86 – 0.70. Further deuteration crossover studies using equimolar quantities of Ph_2SiH_2 and Ph_2SiD_2 were thwarted by the appearance of $SiPh_2HD$ upon stoichiometric addition of Ph_2SiD_2 to **1** indicating that scrambling is occurring between the tricyclopentylphosphine and diphenylsilane at 298 K.

Quantitative formation of **9** was also observed upon the addition of $PhSiH_3$ (1 equivalent) to **1** after an hour. Upon addition of 2 equivalents of $PhSiH_3$ to **2**, incomplete consumption of the starting organometallic complex was observed even after the course of two weeks. This sluggish reactivity with the most reactive silane, again highlights the favoured $\kappa^3_{(POP)}$-*fac vs.* $\kappa^2_{(PP)}$-*cis*

geometry of the XANTphos ligand in these complexes and thus deterred us from investigating the further reactivity of **2**.

2.2.4 Reactivity of 1 with amine-boranes.

Given the ability for primary and secondary silanes to act as sources of hydrogen and in turn form dehydrocoupled products with **1**, amine-boranes were subsequently probed to see if similar reactivity was observed. $H_3B{\cdot}NMe_2H$ (DMAB), a secondary amine-borane, is well documented (significantly by research carried out in the Weller group[52,53]) to undergo metal-mediated loss of hydrogen and dehydrocouple to form $[H_2BNMe_2]_2$ as the sole amine-borane product (Scheme 2.14). Mechanistic studies for the dehydrogenation and dehydrocoupling process of $H_3B{\cdot}NMe_2H$ including observed intermediates is discussed at length in Chapters 3 and 4 and therefore will not be further detailed here.



Scheme 2.14 Dehydrogenation and dehydrocoupling of $H_3B{\cdot}NMe_2H$ to form $[H_2BNMe_2]_2$.

Addition of $H_3B{\cdot}NMe_2H$ (2 equivalents) to **1** resulted in the hydrogenation of the alkene and quantitative formation of **9** after 2 hours with the formation of $[H_2BNMe_2]_2$ [δ +5.40 {t, *J*(BH) 113 Hz}] and complete consumption of $H_3B{\cdot}NMe_2H$ [δ −13.0 {q, *J*(BH) 96 Hz}] by ^{11}B NMR spectroscopy. The continued turnover of the amine-borane substrate (unlike that found in the case of Ph_2SiH_2) prompted us to test **1** again in open system catalysis as a build-up in hydrogen pressure is known to inhibit the rate of dehydrogenation catalysis.[52] 100 μL aliquots of the reaction were taken at intervals, quenched with MeCN and frozen at 77 K before analysis by ^{11}B NMR spectroscopy. Complete conversion of $H_3B{\cdot}NMe_2H$ to $[H_2BNMe_2]_2$ was found to occur after 150 minutes, TOF = 8 h^{-1} (**1**, 5 mol% 1,2-$C_6H_4F_2$, 298 K, 0.07 M $H_3B{\cdot}NMe_2H$) showing that **1** is a capable catalyst (Figure 2.12), but one which is not as efficient as $[Rh(P^iBu_3)_2][BAr^F{}_4]$ **(i-125)**[52] TOF = 34 h^{-1} (5 mol%, 1,2-$C_6H_4F_2$, 298 K, 0.196 M $H_3B{\cdot}NMe_2H$) or indeed [Rh(diphosphine)(η^6-C_6H_5F)][$BAr^F{}_4$] pre-catalysts **(11, 12, 25** and **26)** at the same

loading as is discussed in Chapter 4. No other B-N intermediate species were observed during catalysis. The lack of reactivity for **1** with $SiPh_3H$ was mirrored with tertiary amine-borane $H_3B{\cdot}NMe_3$ (TMAB), which similarly showed no reactivity with **1**.

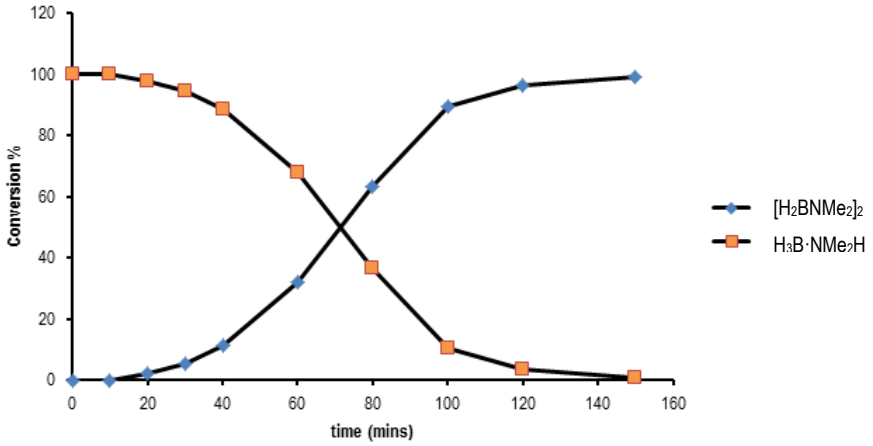
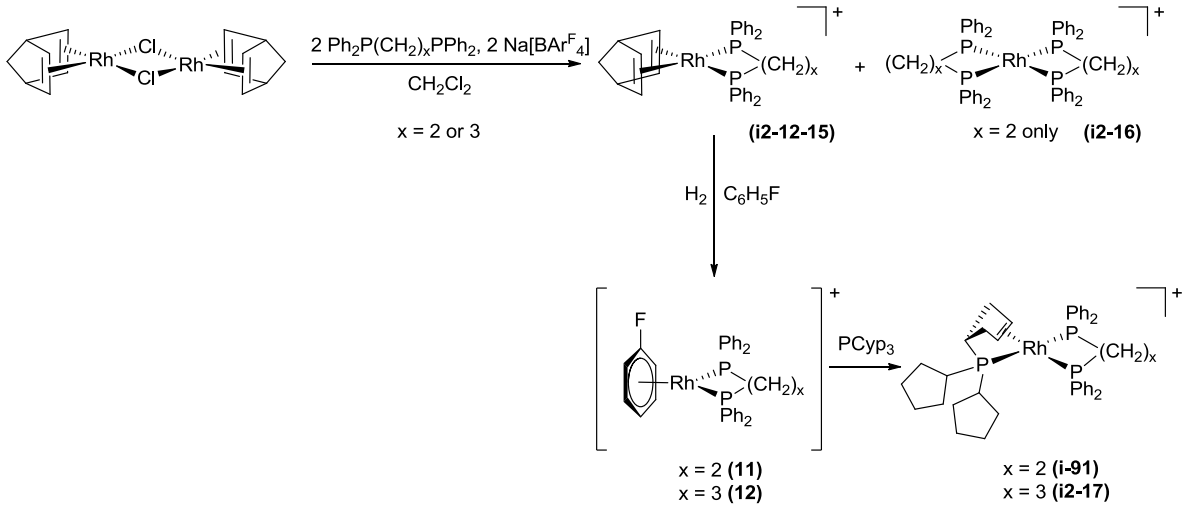


Figure 2.12 Plot of dehydrocoupling of $H_3B{\cdot}NMe_2H$ to form $[H_2BNMe_2]_2$ with **1** (5 mol%, 1,2-$C_6H_4F_2$, 298 K).

2.2.5 Dehydrogenation of cyclopentylthioether ligands

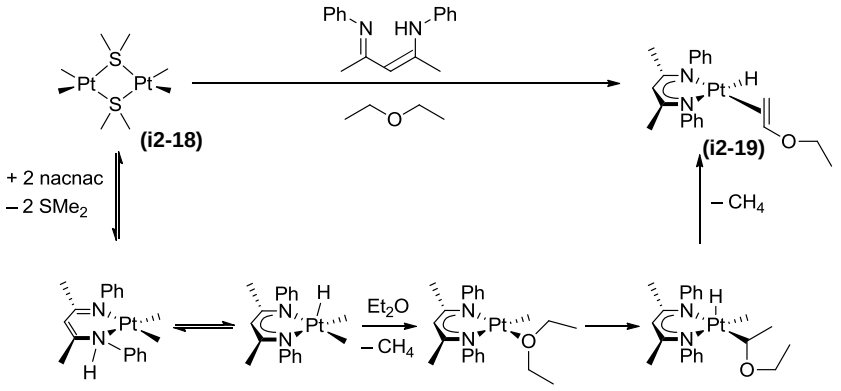
As an extension to the aforementioned work with the chelating phosphine-alkene, the acceptorless dehydrogenation of the cyclopentyl groups using other tethering groups was investigated in collaboration with Ben Pilgrim and Prof. T. J. Donohoe (Oxford). The rapid dehydrogenation of tricyclopentylphosphine by the $\{Rh(dppe)\}^+$ fragment to form $[Rh(Ph_2P(CH_2)_2PPh_2)\{PCyp_2(\eta^2\text{-}C_5H_7)\}][BAr^F{}_4]$ **(i-91)** prompted us to explore whether this chemistry could be extended to other chelating diphosphine fragments. Different Rh precursors were first prepared to enable the screening of potential ligands.



Scheme 2.15 A new route to phosphine-alkene complexes **i-91** and **i2-17**. $[BAr^F_4]^-$ anions not shown.

An alternative route to **(i-91)**, from that previously reported,[21] was developed involving hydrogenation of isolated $[Rh(NBD)(Ph_2P(CH_2)_2PPh_2)][BAr^F_4]$ **(i2-12)** in C_6H_5F, followed by addition of $PCyp_3$ (Scheme 2.15). The intermediate complex $[Rh(Ph_2P(CH_2)_2PPh_2)(\eta^6\text{-}C_6H_5F)][BAr^F_4]$ **(11)** has a labile C_6H_5F ligand, which is displaced by the strong σ-donor $PCyp_3$, which can then undergo acceptorless dehydrogenation as seen before to form **i-91**, thanks to the available coordination site *trans* to one of the phosphines of the dppe ligand. The larger scale use of this procedure is limited by the unwanted formation of $[Rh(Ph_2P(CH_2)_2PPh_2)_2][BAr^F_4]$ **(i2-16)** [$\delta^{31}P\{^1H\}$ 57.9 {d, *J*(RhP) 133 Hz}] [54] during the preparation of $[Rh(NBD)(Ph_2P(CH_2)_2PPh_2)][BAr^F_4]$ **(i2-12)** from $[Rh(NBD)Cl]_2$, dppe and $Na[BAr^F_4]$. Purification of this mixture was very challenging. The best method for making **i2-12** is actually *via* the addition of NBD to a complex formed from reacting $[Rh(Ph_2P(CH_2)_2PPh_2)Cl]_2$ and $Na[BAr^F_4]$ in C_6H_5F.[34] Altering the diphosphine to 1,3-bis(diphenylphosphino)propane, dpp_{prop}, was found to avoid the problem of forming the bis-chelating diphosphine complex. Presumably the increased NBA of the chelating diphosphine, 86° (dppe) *vs.* 91° (dpp_{prop}),[39] disfavours bis-chelation due to the orientation of the phenyl groups and steric hinderance. Hydrogenation of precursor $[Rh(NBD)(Ph_2P(CH_2)_3PPh_2)][BAr^F_4]$ **(i2-13)** in C_6H_5F followed by addition of a small excess of tricyclopentylphosphine shows evidence for a coordinated alkene δ 4.69 (*c.f.* δ 4.89 for **i-91**) in the ^1H NMR spectrum, whilst the $^{31}P\{^1H\}$ spectrum exhibits three sets of doublet of

doublets of doublets [δ 66.4 {$J(PP_{trans})$ 283 Hz, J(RhP) 127 Hz, $J(PP_{cis})$ 36 Hz}, 12.7 {$J(PP_{trans})$ 283 Hz, J(RhP) 122 Hz, $J(PP_{cis})$ 52 Hz}; 5.3 {J(RhP) 152 Hz, $J(PP_{cis})$ 52 Hz, $J(PP_{cis})$ 36 Hz}] consistent with coordination of an additional phosphine ligand and again similar to the environments observed for **i-91**. These data suggested one of the cyclopentyl ligands had undergone dehydrogenation. This was corroborated by ESI-MS that presents a parent ion m/z = 751.2264 (calc. 751.2259) as expected for the formation of $[Rh(Ph_2P(CH_2)_3PPh_2)\{PCyp_2(\eta^2\text{-}C_5H_7)\}][BAr^F{}_4]$ **(i2-17)** (Scheme 2.15). As with the dppe system, immediate dehydrogenation of a cyclopentyl group occurs without the need for a sacrificial hydrogen acceptor due to the vacant site left by the departure of the labile C_6H_5F ligand. The full characterisation of η^6-C_6H_5F complexes **11** and **12** is discussed later in Chapter 4 (Section 4.2.1). Changing the cyclopentyl tether to sulphur and oxygen was then investigated using the $\{Rh(Ph_2P(CH_2)_3PPh_2)\}^+$ fragment given the ability for this fragment to successfully dehydrogenate $PCyp_3$ and the easier synthesis of the η^6-C_6H_5F precursor complex compared to the $\{Rh(Ph_2P(CH_2)_2PPh_2)\}^+$ fragment.



Scheme 2.16 Dehydrogenation of diethyl ether by $Pt_2Me_4(\mu\text{-}SMe_2)_2$ **(i2-18)**.

Metal-thioether and -ether linkages are known to form weaker bonds to transition metals than their metal-phosphine counterparts. Dehydrogenation of ethers using transition metal catalysts has been the subject of recent research.[55, 56] Kinetic studies of the dehydrogenation of diethylether using Pt nacnac complexes, *e.g.* **(i2-18)** by Templeton and co-workers suggest the mechanism shown in Scheme 2.16. This first involves the coordination of diethylether to Pt through the oxygen followed by C-H activation of the diethylether at the α-position which is the rate determining step. Elimination of methane and a second C-H activation of the diethylether

form the coordinated alkenylether complex **(i2-19)**. Dehydrogenation of thioethers is, to our knowledge, unknown.

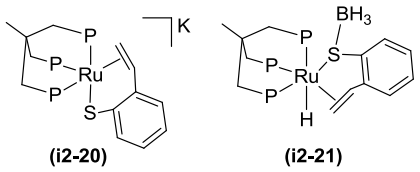


Figure 2.13 Examples of Bianchini's complexes that coordinate to the metal through both the sulphur atom and the alkene.

Transition metal monothioether coordination, although relatively scarce, has also been reported,[22,23] *e.g.* Rh(PNP)S^{i}Pr$_2$ (PNP = [(^{i}Pr$_2$P(C$_6$H$_3$CH$_3$))$_2$N]$^-$),[57] whilst η^2-coordination of thiophene through both the sulphur and alkenyl moieties has been characterised in solution by the group of Bianchini using Rh, Ir and Ru TRIPHOS complexes (*e.g.* **i2-20** and **i2-21** Figure 2.13).[58,59,60] OCyp$_2$ **(I)**, SCyp$_2$ **(II)** and SCypPh **(III)** were targeted as ligands to best fit our goal and were synthesised by Ben Pilgrim (Figure 2.14).

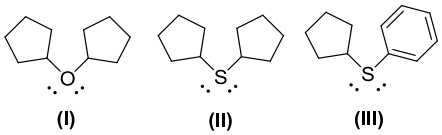
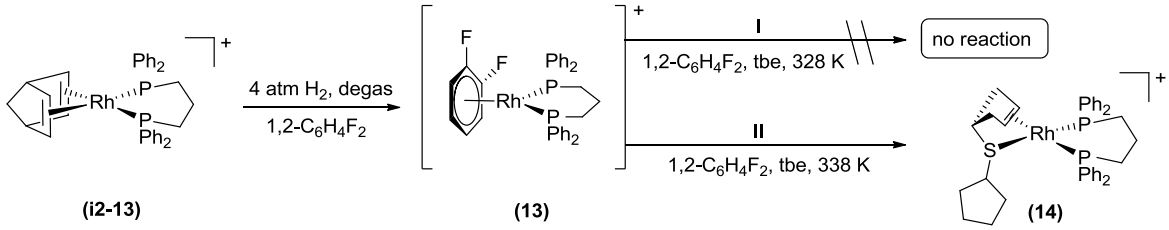


Figure 2.14 Ligands synthesised to target further dehydrogenation of the cyclopentyl moiety.

Hydrogenation of [Rh(NBD)(Ph$_2$P(CH$_2$)$_3$PPh$_2$)][BAr$^{F}_4$] **(i2-13)** (4 atm, 1,2-C$_6$H$_4$F$_2$) results in the formation of a complex with coordinated 1,2-C$_6$H$_4$F$_2$ analogous to **12**, [Rh(η^6-C$_6$H$_4$F$_2$)(Ph$_2$P(CH$_2$)$_3$PPh$_2$)][BAr$^{F}_4$] **(13)** (Scheme 2.17). The ^{1}H NMR spectrum of **13** shows two resonances shifted to lower frequency to free solvent [δ 6.07 (m, 2H, C$_6$H$_4$F$_2$), 5.70 (m, 2H, C$_6$H$_4$F$_2$)] whilst the ^{31}P{^{1}H} spectrum shows one environment [δ 25.2 {d, *J*(RhP) 195 Hz}]. ESI-MS was also consistent with its formation and showed a parent mass ion m/z = 629.1168 (calc. 629.0840) for the {Rh(η^6-C$_6$H$_4$F$_2$)(Ph$_2$P(CH$_2$)$_3$PPh$_2$)}$^+$ fragment. 1,2-C$_6$H$_4$F$_2$ was used instead of C$_6$H$_5$F as it has previously been noted to have weaker binding to Rh thus aiding coordination of these ligands *c.f.* [Rh(η^6-C$_6$H$_4$F$_2$)(P^{i}Bu$_3$)$_2$][BAr$^{F}_4$] **(i-166)** that rapidly dissociates 1,2-C$_6$H$_4$F$_2$ when dissolved in 1,2-C$_2$H$_4$Cl$_2$.[53] Stoichiometric addition of **I** to **13** (1,2-C$_6$H$_4$F$_2$, excess tbe) showed no evidence for the coordination or dehydrogenation of the ether ligand by

^{1}H and ^{31}P{^{1}H} spectroscopy over 24 hours even when heated to 328 K. Clearly the interaction of the oxygen with the metal centre is too weak to displace even the weakly coordinating 1,2-$C_6H_4F_2$.

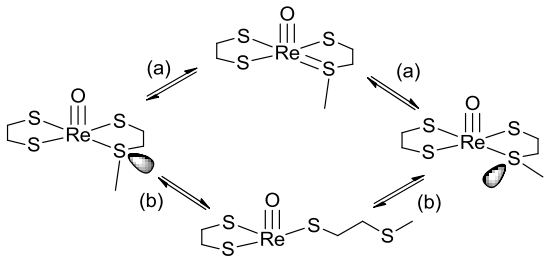


(i2-13) (13) (14)

Scheme 2.17 Reactivity of **I** and **II** with **13**. $[BAr^{F}_{4}]^{-}$ anions not shown.

Addition of **II** (1.1 equivalents) and tbe to a solution of **13** in 1,2-$C_6H_4F_2$ at 298 K also gave no observable thioether coordination by NMR spectroscopy. However, heating to 338 K for 18 hours in the presence of excess tbe resulted in the anticipated dehydrogenation and the formation of $[Rh(Ph_2P(CH_2)_3PPh_2)\{S(C_5H_9)(\eta^2\text{-}C_5H_7)\}][BAr^{F}_{4}]$ **(14)** (Scheme 2.17), presumably following the same mechanism as already outlined for the formation of **i-91** (Chapter 1, Scheme 1.22). The ^{1}H NMR spectrum of **14** at 298 K shows a very broad resonance (δ 4.59, fwhm = 150 Hz) in the region expected for a coordinated alkene signal, two sharp resonances for the two cyclopentyl *ipso*-CH signals (δ 3.22, 3.03) and broad resonances for the remaining alkyl signals of the cyclopentyl groups and diphosphine ligand backbone (δ 2.86 – 0.66). The ^{31}P{^{1}H} NMR spectrum of **14** is, however, sharp with two distinct environments for the two inequivalent phosphorus atoms [δ 22.3 {dd, *J*(RhP) 150 Hz, *J*(PP_{cis}) 55 Hz}, 3.4 {dd, *J*(RhP) 152 Hz, *J*(PP_{cis}) 55 Hz}] (Figure 2.16, *vide infra*). Cooling to 200 K freezes out the broad signals in the ^{1}H NMR spectrum yielding two separate resonances each of integral 1H for the alkene (δ 4.69, 4.34) and unique sets of peaks for the saturated and unsaturated cyclopentyl rings. This decrease in temperature apparently halts a fluxional process that is occurring at room temperature. This process would likely involve a thioether intermediate that incorporates an sp^2-sulphur atom, which is stabilised by a (p-d)π interaction with the transition metal centre and a strong Rh-S interaction as has been suggested previously (Scheme 2.18).[22,61] Inversion *via* decoordination of

sulphur, inversion and rotation of the ligand and finally recoordination to the metal centre has also been observed with Re[62] and Ir[63] SPS complexes.



Scheme 2.18 Possible routes for sulphur inversion with Espenson's complexes.[61]

The structure of $[Rh(Ph_2P(CH_2)_3PPh_2)\{S(C_5H_9)(\eta^2\text{-}C_5H_7)\}][BAr^F{}_4]$ **(14)** was elucidated by diffusion of pentane into a 1,2-$C_6H_4F_2$ solution of **14** which yielded X-ray diffraction quality crystals (Figure 2.15). The coordinated alkene C=C distance is the same within error to that found for **i-91**[21] {1.380(7) Å **(14)** *vs.* 1.372(3) Å **(i-91)**}. The Rh-S distance is comparable to that found in the solid-state structure of a similar Rh(I) diphosphine thioether complex $[Rh(CO)(DPEphos)(EtSMe)][\textit{closo}\text{-}CB_{11}H_6Cl_6]$ {2.3850(10) Å **(14)** *vs.* 2.3694(11) Å}.[22]

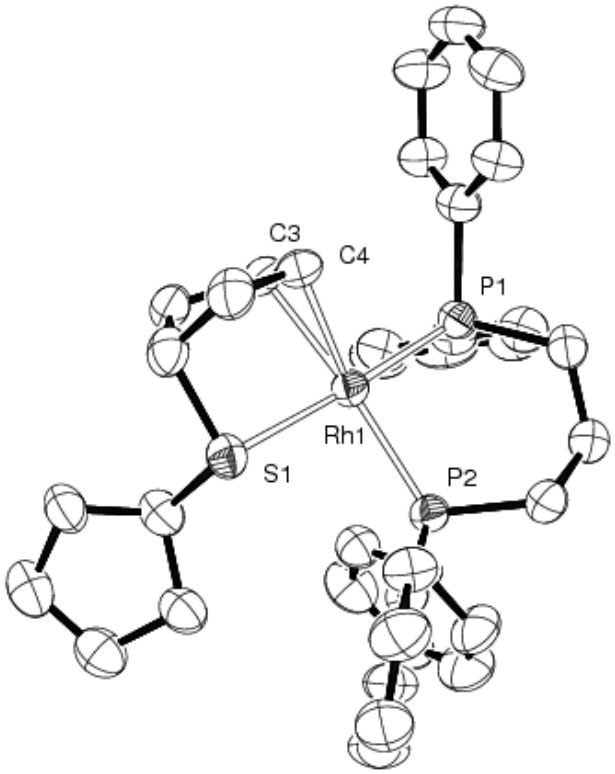
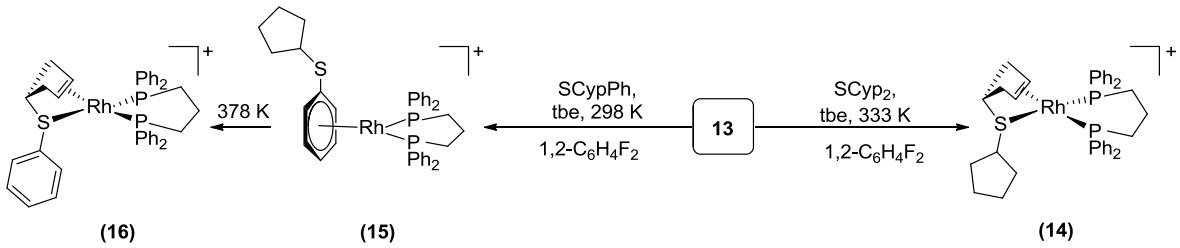


Figure 2.15 Solid-state structure of the cationic portion of **14**. Hydrogen atoms are omitted for clarity. Thermal ellipsoids are presented at the 50 % probability level. Selected bond lengths [Å] and angles [°]:Rh1-P1 2.2597(10), Rh1-P2 2.3050(10), Rh1-S1 2.3850(10), Rh1-C4 2.215(4), Rh1-C3 2.230(4), C3-C4 1.380(7); P1-Rh1-P2 89.91(4), P1-Rh1-S1 176.65(4), P2-Rh1-S1 93.42(4), C4-Rh1-C3 36.17(17), C4-Rh1-P1 93.83(13), C3-Rh1-P1 91.80(12), C4-Rh1-P2 152.23(13), C3-Rh1-P2 171.21(12), C4-Rh1-S1 83.39(13), C3-Rh1-S1 84.86(12).

To supplement the solid-state structure and confirm that dehydrogenation of thioether **II** had occured, 10 equivalents of tetra-n-butylammonium fluoride (TBAF) were added to a solution of **14** which resulted in the dissociation of the ligand from the metal centre with the observance of a signal of integral 2H assigned to the C=C resonance of the free thioethercyclopentene ligand (δ 5.68). Independent synthesis of SCyp(*cyclo*-C_5H_7) **(II')** and comparison of the ^{1}H NMR chemical shifts confirmed that this ligand had been formed. Addition of **II'** to **13** yields an identical species in both the ^{1}H and ^{31}P{^{1}H} NMR spectra. Importantly, in terms of atom efficient processes, complete acceptorless formation of **14** was achieved upon heating the reaction without tbe to 333 K in an NMR tube and freeze/ pump/ thaw degassing at several intervals to remove the build-up of evolved hydrogen. Efforts to make this process catalytic

were however unsuccessful as upon addition of **II** in excess (10 eq.) to **13** in the presence of excess tbe at 333 K did not result in turnover to form **II'**.



Scheme 2.19 Synthesis of complexes **14-16**.

Stoichiometric addition of **III** to **13** under the same conditions at room temperature gave a set of new high frequency signals in the ^{1}H NMR spectrum, consistent with the coordination of the phenyl group to the Rh centre [δ 6.47 {t, *J*(HH) 6 Hz, 1H}, 5.70 {apparent doublet, *J*(HH) 6 Hz, 2H}, 5.47 {t, *J*(HH) 6 Hz, 2H}] and correlate well to the signals seen for other cationic η^6-coordinated arene Rh(I) species, *e.g.* [Rh(η^6-C_6H_6){PCyp$_2$(η^2-C_5H_7)}][BAr$^F{}_4$] **(i-75)** (Chapter 1, Scheme 1.19).[64] No alkene signals were observed, only a doublet [δ 25.4 {*J*(RhP) 196 Hz}] is evident in the ^{31}P{^{1}H} NMR spectrum suggesting the clean formation of only one new complex; [Rh(Ph$_2$P(CH$_2$)$_3$PPh$_2$){S(η^6-C_6H_5)(C_5H_9)}][BAr$^F{}_4$] **(15)**. Heating this 1,2-$C_6H_4F_2$ solution to 378 K in a sealed New Era high pressure NMR tube resulted in the formation of a new complex with similar ^{31}P{^{1}H} resonances to **14**: [δ 23.1 {dd, *J*(RhP) 153 Hz, *J*(PP$_{cis}$) 54 Hz}, 1.8 {dd, *J*(RhP) 148 Hz, *J*(PP$_{cis}$) 54 Hz}] (Figure 2.16) and two broad alkene resonances in the ^{1}H NMR spectrum {δ 5.00 (1H), 4.23 (1H)} that sharpen on cooling to 200 K. ESI-MS of this solution gives a parent mass ion corresponding to a cationic Rh complex consistent with the formation of [Rh(Ph$_2$P(CH$_2$)$_3$PPh$_2$){S(C_6H_5)(η^2-C_5H_7)}][BAr$^F{}_4$] **(16)** (m/z = 691.1204, calc. 691.1219).

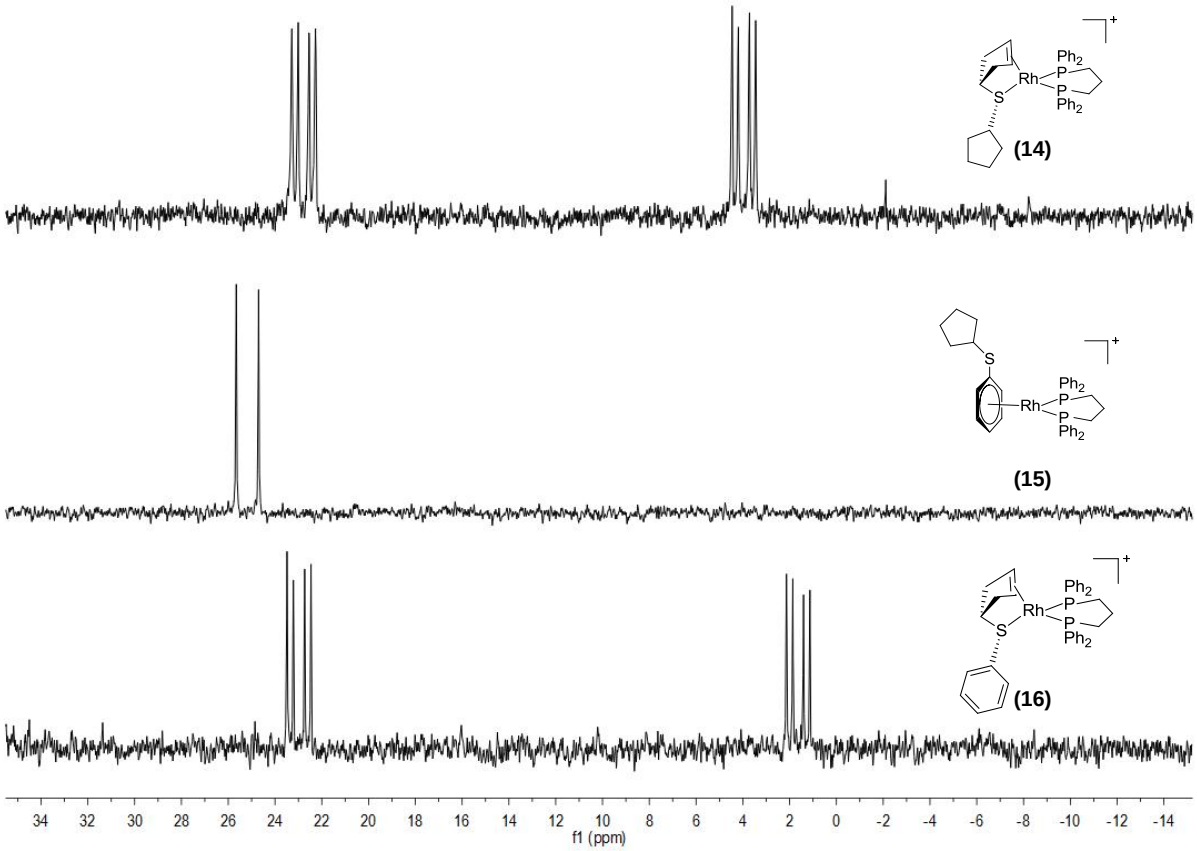


Figure 2.16 $^{31}P\{^{1}H\}$ NMR spectra of complexes **14-16** (202 MHz, 1,2-$C_6H_4F_2$). $[BAr^F{}_4]^-$ anions not shown.

Addition of a small excess of **III** to **13** (378 K, 1,2-$C_6H_4F_2$) in the presence of excess tbe did not result in catalytic turnover of **III** to form **III'** to any significant extent. This suggests that once the sulphur ligand is bound to the metal centre the Rh-S bond is too strong to decoordinate to permit the coordination of a new thioether ligand much like the Rh-P bond with $PCyp_3$. Interesting, in the hydroacylation catalysis of alkynes using sulphur tethered aldehydes and a $\{Rh(diphosphine)\}^+$ pre-catalyst, Willis and co-workers report the catalytic formation of sulphur-tethered ketones containing an alkene.[65,66] This illustrates that with a subtle change in the substrate, $\{Rh(diphosphine)\}^+$ fragments can yield catalytic turnover to form this variety of ligand.

2.3 Conclusions and future work

This work has revealed different reactivity patterns in the hemilabile nature of DPEphos and XANTphos ligands in the hydrogenation and dehydrogenation chemistry of tricyclopentylphosphine ligands. In particular XANTphos complexes are characterised by a less labile oxygen atom compared to DPEphos. The coordinated alkene in **1** and **2** could be hydrogenated using H_2 however much slower reactivity was observed for **2** compared to **1**. Attempts to hydrosilylate the coordinated alkene in complex **1** instead resulted in transfer hydrogenation, which could similarly be achieved using $H_3B{\cdot}NMe_2H$.

Due to the strong chelating effects of the phosphorus and sulphur donor atoms of phosphine ($PCyp_3$) and thioethers (**II** and **III**) it is difficult to envisage the possibility of achieving efficient catalytic dehydrogenation of cyclopentyl groups with these base sets. Attempting to solve this problem by using a weaker donor atom (oxygen) did not result in dehydrogenation indicating the fine balance in the system between coordination of the tether and activity. Choosing substrates which have different electronic properties, *e.g.* electronwithdrawing groups, to weaken the Rh-P/S bond strength, or alternatively bulkier spectator groups, such as adamantane, may force the decoordination of the dehydrogenated cyclopentyl ligand upon dehydrogenation resulting in catalytic turnover (*e.g.* Figure 2.17). Alternatively, the use of a cyclopentyl ring on a chiral thioether/ phosphine coordinated to a Rh complex with a chiral anion remains to be investigated. Such second generation complexes could reveal interesting enantioselective catalytic properties.

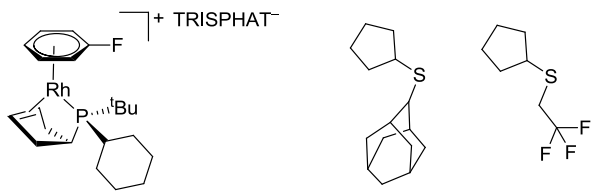


Figure 2.17 Examples of a new chiral complex (left) and thioether ligands (right).

2.4 References

[1] Jiménez, M. V.; Pérez-Torrente, J. J.; Bartolomé, M. I.; Gierz, V.; Lahoz, F. J.; Oro, L. A. *Organometallics,* **2008,** *27,* 224-234.

[2] Chen, G.; Lam, W. H.; Fok, W. S.; Lee, H. W.; Kwong, F. Y. *Chem. Asian J.* **2007,** *2,* 306-313.

[3] Chikkali, S. H.; Gudat, D.; Lissner, F.; Nieger, *M.;* Schleid, T. *Dalton Trans.*, **2007,** 3906-3913.

[4] Labinger, J. A.; Bercaw, J. E. *Nature* **2002,** *417,* 507-514.

[5] Goldberg, K. I.; Goldman, A. S. *Activation and Functionalisation of C-H bonds;* American Chemical Society, Washington, 2004, Vol. 885.

[6] Marciniec, B. *Comprehensive Handbook on Hydrosilylation;* Pergamon Press: Oxford, NY, 1992.

[7] Hartwig, J. F. *Organotransitionmetal chemistry: From Bonding to Catalysis;* Sausalito, Ca: University Science Books 2009 pp1-1127.

[8] Rosenberg, L. *Macromol. Symp*. **2003,** *196,* 347-353.

[9] Comte, V.; Balan, C.; Le Gendre, P.; Moïse, C. *Chem Commun,* **2007,** 713-715.

[10] Speier, J. L. *Adv. Organomet. Chem.* **1979,** *17,* 407-447.

[11] Garcia, J.; Meyer, D. J. M.; Guillaneux, D.; Moreau, J. J. E.; Wong Chi Man, M. *J. Organomet. Chem.* **2009,** *694,* 2427-2433 and references therein.

[12] Chalk, A. J.; Harrod, J. F.; *J. Am. Chem. Soc.* **1965,** *87,* 16-21.

[13] Sakaki, S.; Sumimoto, M.; Fukuhara, M.; Sugimoto, M.; Fujimoto, H.; Matsuzaki, S. *Organometallics*, **2002,** *21,* 3788-3802.

[14] Glaser, P. B.; Tilley, T. D. *J. Am. Chem. Soc.* **2003,** *125,* 13640-13641.

[15] Corey, J. Y.; Braddock-Wilking, J. *Chem. Rev.* **1999,** *99,* 175-292.

[16] Lin, Z. *Chem. Soc. Rev.* **2002,** *31,* 239-245.

[17] Calimano, E.; Tilley, T. D. *Dalton Trans.* **2010,** *39,* 9250-9263 and references therein.

[18] Waterman, R.; Hayes, P. G.; Tilley, T. D. *Acc. Chem. Res.* **2007,** *40,* 712-719.

[19] Calimano, E.; Tilley, T. D. *J. Am. Chem. Soc.* **2008,** *130,* 9226-9227.

[20] Hayes, P. G.; Beddie, C.; Hall, M. B.; Waterman, R.; Tilley, T. D. *J. Am. Chem. Soc.* **2006,** *128,* 428-429.

[21] Douglas, T. M.; Brayshaw, S. K.; Dallanegra, R.; Kociok-Köhn, G.; Macgregor, S. A.; Moxham, G. L.; Weller, A. S. Wondimagegn, T.; Vadivelu, P. *Chem. Eur. J.* **2008,** *14,* 1004-1022.

[22] Moxham, G. L.; Randell-Sly, H. E.; Brayshaw, S. K.; Woodward, R. L.; Weller, A. S.; Willis, M. C. *Angew. Chem. Int. Ed.* **2006,** *45,* 7618-7622.

[23] Moxham, G. L.; Randell-Sly, H. E.; Brayshaw, S. K.; Weller, A. S.; Willis, M. C. *Chem. Eur. J.* **2008,** *14,* 8383-8397.

[24] Mayer, H. A.; Kaska, W. C.; *Chem. Ber.* **1990,** *123,* 1827-1831.

[25] Rossi, A. R.; Hoffmann, R. *Inorg. Chem.* **1975,** *14,* 365-374.

[26] Hetterscheid, D. G. H; Smits, J. M. M.; de Bruin, B. *Organometallics* **2004,** *23,* 4236-4246.

[27] Haines, L. M. *Inorg. Chem.* **1971,** *10,* 1685.

[28] Rivers, J. H.; Jones, R. A. *Chem. Commun.* **2010,** *46,* 4300-4302.

[29] Price, A. J.; Ciancanelli, R.; Noll, B. C.; Curtis, C. J.; Dubois, D. L.; Dubois, M. R. *Organometallics* **2002,** *21,* 4833-4839.

[30] Choi, J.-C.; Sakakura, T. *Organometallics* **2004,** *23,* 3756-3758.

[31] Sangtrirutnugul, P.; Stradiotto, M.; Tilley, T. D. *Organometallics* **2006,** *25,* 1607-1617 and references therein.

[32] Crabtree, R. H. *Angew. Chem, Int. Ed. Engl.* **1993,** *32,* 789-805.

[33] Ledger, A. E. W.; Moreno, A.; Ellul, C. E.; Mahon, M. F.; Pregosin, P. S.; Whittlesey, M.K.; Williams, J. M. J. *Inorg. Chem.* **2010,** *49,* 7244-7256.

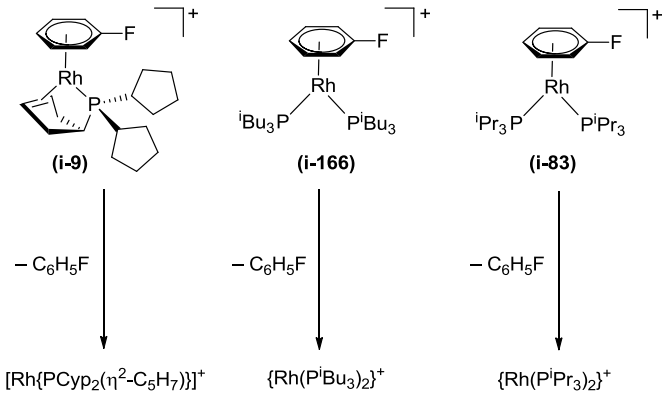
[34] Pawley, R. J.; Moxham, G. L.; Dallanegra, R.; Chaplin, A. B.; Brayshaw, S. K.; Weller, A. S.; Willis, M. C. *Organometallics,* **2010,** *29,* 1717-1728.

[35] Cooper, A. C.; Eisenstein, O.; Caulton, K. G. *New J. Chem.* **1998,** 307-309.
[36] Budzelaar, P. gNMR, 4.0; Cherwell Scientific Publishing, Oxford, 1997.
[37] Chaplin, A. B.; Weller, A. S. *Inorg. Chem.* **2010,** *49,* 1111-1121.
[38] Mispelaere-Canivet, C.; Spindler, J. F.; Perrio, S.; Beslin, P.; *Tetrahedron,* **2005,** *61,* 5253-5259.
[39] Birkholz, M.-N.; Freixa, Z.; van Leeuwen, P. W. N. M. *Chem. Soc. Rev.* **2009,** *38,* 1099-1118.
[40] Alcock, N. W.; Brown, J. M; Jeffrey, J. C. *J. Chem. Soc. Dalton Trans.* **1976,** 583-588.
[41] Sandee, A. J.; van der Veen, L. A.; Reek, J. N. H.; Kamer, P. C. J.; Lutz, M.; Spel, A. L.; van Leeuwen, P. w. N. M. *Angew. Chem. Int. Ed.* **1999,** *38,* 3231-3235.
[42] Pontiggia, A. J.; Chaplin, A. B.; Weller, A. S. *J. Organomet. Chem.* **2011,** in the press.
[43] Kranenburg, M.; van der Burgt, Y. E. M.; Kamer, P. C. J.; van Leeuwen, P. W. N. M. *Organometallics* **1995,** *14,* 3081-3089.
[44] Zuideveld, M. A.; Swennenhuis, B. H. G.; Boele, M. D. K.; Guari, Y.; van Strijdonck, G. P. F.; Reek, J. N. H.; Kamer, P. C. J.; Goubitz, K.; Fraanje, J.; Lutz, M.; Spek, A. L.; van Leeuwen, P. W. N. M. *J. Chem. Soc. Dalton Trans.* **2002,** 2308-2317.
[45] van der Veen, L. A.; Keeven, P. K.; Schoemaker, G. C.; Reek, J. N.H.; Kamer, P. C. J.; van Leeuwen, P. W. N. M.; Lutz, M.; Spek, A.L. *Organometallics* **2000**, *19,* 872-883.
[46] Venkateswaran, R.; Mague, J. T.; Balakrishna, M. S. *Inorg. Chem.* **2007,** *46,* 809-817.
[47] Kranenburg, M. Kamer, P. C. J.; van Leeuwen, P. W. N. M. *Eur. J. Inorg. Chem.* **1998,** 155-157.
[48] Guari, Y.; van Strijdonck, G. P. F.; Boele, M. D. K.; Reek, J. N. H.; Kamer, P. C. J.; van Leeuwen, P. W. N. M. *Chem. Eur. J.* **2001,** *7,* 475-482.
[49] Lappert, M. F.; Maskell, R. K. *J. Organomet. Chem.* **1984,** *264,* 217-228.
[50] Goikhman, R.; Milstein, D. *Chem. Eur. J.* **2005,** *11,* 2983-2988.
[51] Neale, N. R.; Tilley, T. D. *J. Am. Chem. Soc.* **2002,** *124,* 3802.
[52] Douglas, T. M.; Chaplin, A. B.; Weller, A. S. *J. Am. Chem. Soc.* **2008,** *130,* 14432-14433.
[53] Douglas, T. M.; Chaplin, A. B.; Weller, A. S.; Hall, A. B.; Yang, X. *J. Am. Chem. Soc.* **2009,** *131,* 15440-15456.
[54] Ernsting, J. M.; Elsevier, C. J.; de Lange, W. G. J.; Timmer, K. *Magn. Res. Chem.* **1991,** *29,* 118-124.
[55] Whited, M. T.; Zhu, Y.; Timpa, S. D.; Chen, C.-H.; Foxman, B. M.; Ozerov, O. V.; Grubbs, R. H. *Organometallics* **2009,** *28,* 4560-4570.
[56] West, N. M.; White, P. S.; Templeton, J. L. *J. Am. Chem. Soc.* **2007,** *29,* 12372-12373.
[57] Gatard, S.; Guo, C.; Foxman, B. M.; Ozerov, O. V. *Organometallics* **2007,** *26,* 6066-6075 and references therein.
[58] Bianchini, C.; Meli, A.; Moneti, S.; Vizza, F. *Organometallics* **1998,** *17,* 2636-2645.
[59] Bianchini, C.; Masi, D.; Meli, A.; Peruzzini, M.; Vizza, F.; Zanobini, F. *Organometallics* **1998,** *17,* 2495-2502.
[60] Bianchini, C.; Meli, A. *Acc. Chem. Res.* **1998,** *31,* 109-116.
[61] Shan, X.; Espenson, J. H. *Organometallics* **2003,** *22,* 1250-1254 and references therein.
[62] Abel, E. W.; Ellis, D.; Orrell, K. G. *J. Chem. Soc., Dalton Trans.***1992,** 2243-2249.
[63] Klerman, Y.;Ben-Ari, E.;Diskin-Posner, Y.; Leitus, G.; Shimon, L. J. W.; Ben-David, Y.; Milstein, D. *Dalton Trans.* **2008,** 3226–3234.
[64] Douglas, T. M.; Le Nôtre, J.; Brayshaw, S. K.; Frost, C. G.; Weller, A. S. *Chem. Commun.* **2006,** 3408-3410.
[65] González-Rodríguez, C.; Parsons, S. R.; Thompson, A. L.; Willis, M. C. *Chem. Eur. J.* **2010,** *16,* 10950-10954.
[66] Parsons, S. R.; Hooper, J. F.; Willis, M. C. *Org. Lett.* **2011,** *13,* 998-1000.

3 DEHYDROCOUPLING OF AMINE-BORANES WITH THE $\{Rh(PR_2(\eta^2\text{-}C_5H_7)\}^+$ FRAGMENT

3.1 Introduction

Despite significant research over the last five years, mechanistic data on the dehydrogenation and dehydrocoupling of amine-boranes is sparse (*c.f.* Chapter 1, section 1.3.4.4). As outlined in Chapter 1, the $\{Rh(PR_3)_2\}^+$ fragment has been found to act as a low coordinate fragment that can accommodate the coordination of amine- and aminoboranes and catalyse the dehydrocoupling of $H_3B{\cdot}NMe_2H$ to $[H_2BNMe_2]_2$. The $[Rh\{PCyp_2(\eta^2\text{-}C_5H_7)\}]^+$ fragment, discussed in Chapter 2, is a more open bis-chelating fragment in comparison to $\{Rh(PR_3)_2\}^+$ and is therefore potentially more accessible to coordination of amine-boranes. It was therefore decided to investigate the dehydrocoupling of amine-boranes. (Scheme 3.1)



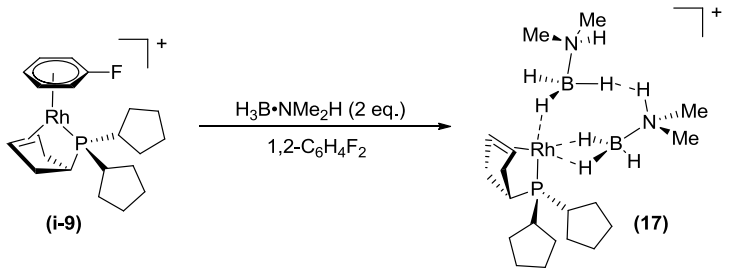
Scheme 3.1 Latent sources of reactive 12-electron fragments from **i-9**, **i-166** and **i-83**. $[BAr^F{}_4]^-$ anions not shown.

This chapter discusses examples of isolated and fully characterised cationic Rh(I) complexes coordinating amine-borane substrates and intermediates with the discovery of a novel coordination mode of amine-boranes at a transition metal centre. Their onward reactivity (*e.g.* in catalysis) has been investigated to help further understand the complex mechanism of dehydrocoupling.

3.2 Results and discussion

3.2.1 Reactivity of i-9 with amine-boranes

Addition of $H_3B{\cdot}NMe_2H$ (2 equivalents) to **i-9** in 1,2-$C_6H_4F_2$ solvent (Scheme 3.2) resulted in the immediate total consumption of $H_3B{\cdot}NMe_2H$ [δ^{11}B −12.8 {q, *J*(BH) 96 Hz}]. The products of dehydrogenation and dehydrocoupling; $H_2B{=}NMe_2$ [δ^{11}B +38 {t, *J*(BH) 113 Hz}] and $[H_2BNMe_2]_2$ [δ^{11}B +5.4 {t, *J*(BH) 113 Hz}] were not observed. Instead, a broad signal was observed at δ −20.3 in the ^{11}B NMR spectrum. Together with this, the $^{31}P\{^1H\}$ NMR spectrum showed quantitative formation of a new complex [δ 105.3 {d, *J*(RhP) 165 Hz}], while the ^{1}H NMR spectrum exhibited a broad resonance {δ −0.64 (6H)} characteristic of the coordination of amine-borane (*H*$_3$B), *c.f.* $[Rh(P^iBu_3)_2(\eta^2\text{-}H_3B{\cdot}NMe_2H)][BAr^F{}_4]$ **(i-142)** [δ −2.13 (br s, 3H, η^2-*H*$_3$B)].[1] The relative 6H integral, suggested the coordination of two molecules of $H_3B{\cdot}NMe_2H$ to the metal, as did those of the downfield broad N*H* (δ 4.08 (2H)) and N*Me*$_2$ [δ 2.60 {d, *J*(HH) 6 Hz), 12H}] signals (Figure 3.2). The alkenyl resonance (δ 3.64, 2H) was also still present indicating that transfer hydrogenation had not taken place.



Scheme 3.2 Addition of 2 equivalents of $H_3B{\cdot}NMe_2H$ to **i-9** forms bis-σ-amine-borane complex **17**. $[BAr^F{}_4]^-$ anions not shown.

This complex was found to be highly temperature, moisture and air sensitive as repeated attempts to isolate it at ambient temperature using Schlenk line techniques were unsuccessful and resulted in its rapid decomposition. Carrying out this synthesis completely inside a glove box in 1,2-$C_6H_4F_2$ solvent and layering with pentane at 238 K however allowed the isolation of this material and crystals suitable for X-ray diffraction analysis from which the structure of

$[Rh\{PCyp_2(\eta^2\text{-}C_5H_7)\}(\eta^1\text{-}H_3B{\cdot}NMe_2H)(\eta^2\text{-}H_3B{\cdot}NMe_2H)][BAr^F{}_4]$ **(17)** was obtained (Figure 3.1).

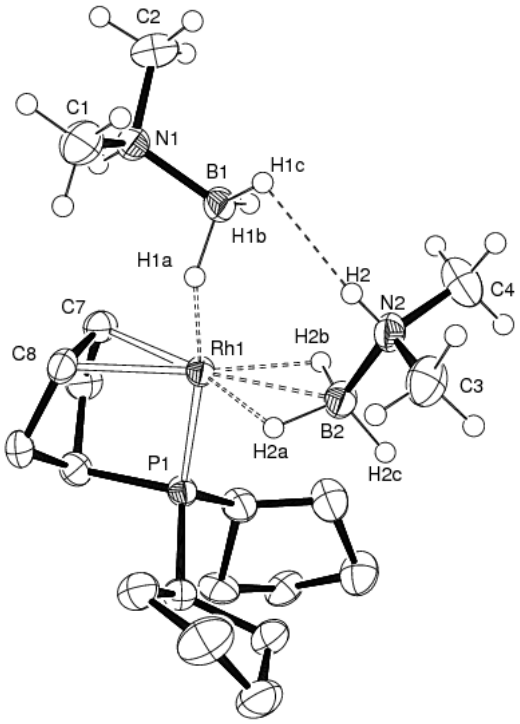


Figure 3.1 Solid-state structure of the cationic portion of **17**. Thermal ellipsoids are presented at the 50 % probability level. Minor disordered components not shown. Selected bond lengths [Å]: Rh1-B1 2.661(3), Rh1-B2 2.282(3), Rh1-P1 2.2197(6), Rh1-C7 2.106(2), Rh1-C8 2.121(2), C7-C8 1.417(3).

The structure of **17** shows that two molecules of $H_3B{\cdot}NMe_2H$ are bound to the metal in two different coordination modes and that the phosphine-alkene motif is retained with a C=C distance of 1.417(3) Å (C7 – C8) reminiscent of that found for **(1)** and **(2)** (Chapter 2). The *pseudo*-octahedral Rh(I) centre has one molecule of $H_3B{\cdot}NMe_2H$ bound in an equatorial position with two 3c-2e Rh-H-B bonds with the other amine-borane located in an apical position and bound through just one 3c-2e Rh-H-B bond. The location of all the hydrogen atoms associated with the H_3B components in this structure verifies the two distinct coordination modes η^1-H_3B and η^2-H_3B. Analysis of the Rh-B bond lengths of the two coordination modes suggests that the η^2-H_3B interaction is stronger with a shorter Rh-B distance compared to that found in the η^1-H_3B interaction [2.661(3) Å (η^1-H_3B) *vs.* 2.282(3) Å (η^2-H_3B)]. These

differences correlate well with other known structures of η^1 and η^2 bound amine-borane complexes *e.g.* $[RuCp(PMe_3)_2(\eta^1\text{-}H_3B{\cdot}NMe_3)][BAr^F{}_4]$ Ru-B = 2.648(3) Å[2] and $[Rh(P^iBu_3)_2(\eta^2\text{-}H_3B{\cdot}NMe_3)][BAr^F{}_4]$ **(i-137)** Rh-B = 2.180(4) Å.[1] Of particular note is the existence of a non-classical hydrogen bond between a B*H* (H1c) of the η^1 bound ligand and the N*H* (H2) of the η^2 bound ligand which has a distance of 2.12(4) Å. This distance is comparable with the reported distance of the hydrogen bonds of the free amine-borane in its crystal lattice (δ 1.95/ 2.08 Å)[3,4] suggesting a similar interaction in the metal coordination sphere. Low temperature (200 K, CD_2Cl_2) $^1H\{^{11}B\}$ NMR spectroscopy of the isolated crystalline material freezes out the fluxional process affecting the Rh-H_3B signals observed at 298 K, which are now observed as two resonances [δ −1.49 (br, 3H, η^1-H_3B); −1.63 (br, 2H, η^2-H_3B)], the former assigned to the η^1 bound $H_3B{\cdot}NMe_2H$ ligand, which is still undergoing site exchange between terminal and bridging hydrides, with the second assigned to the η^2 bound H_3B for which this fluxional process is halted (Figure 3.2). The terminal RhH_2BH resonance was not located in the ^{1}H NMR spectrum presumably as it is very broad. It would be expected to resonate (δ +4 – +6).[5] The terminal RhH_2BH resonance for coordinated $H_3B{\cdot}NMe_3$ in $[Rh(P^iPr_3)_2(\eta^2\text{-}H_3B{\cdot}NMe_3)][BAr^F{}_4]$ **(i-137a)** lies significantly downfield in comparison to the metal bound RhH_2BH resonances in the ^{1}H NMR spectrum at 190 K [δ +4.43 RhH_2BH (1H) *vs.* −6.91 RhH_2BH (2H)].[6]

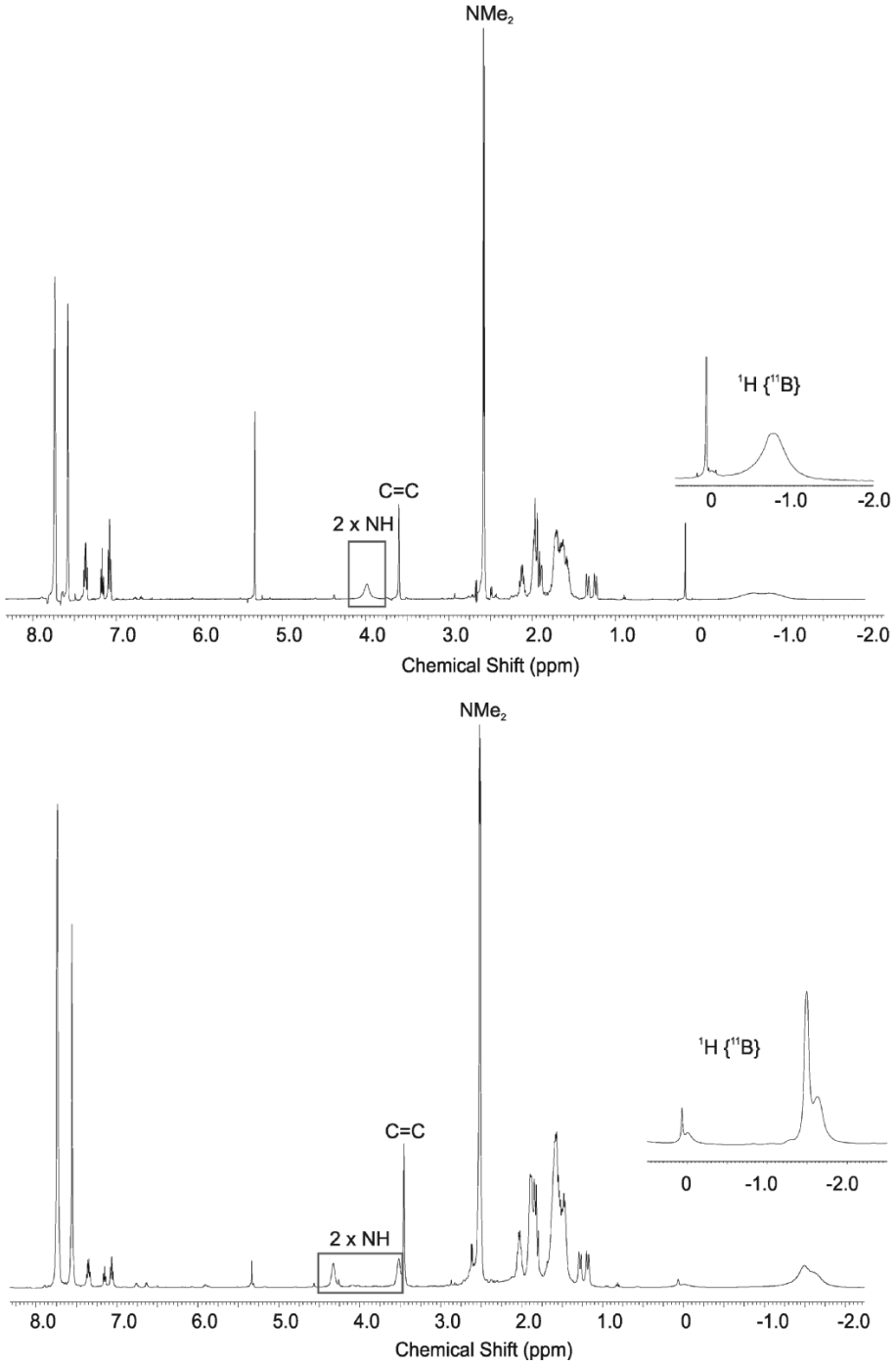


Figure 3.2 ^{1}H and $^{1}H\{^{11}B\}$ NMR spectra of **17** at 298 K (top) and 225 K (bottom) (500 MHz, CD_2Cl_2).

Significantly, the N*H* signal splits into two separate signals at 225 K [δ 4.33 (br, 1H), 3.52 (br, 1H)] indicating two different amine-borane environments. The resonance assigned to **17** in the ^{11}B NMR spectrum broadened further upon cooling, as could be expected, due to the

considerable quadropolar broadening of this nucleus on decreasing temperature. ESI-MS of **17** in 1,2-$C_6H_4F_2$ yielded the parent mass ion (*m/z* = 457.2647, calc. 457.2563; **B**) as well as masses attributed to the loss of one molecule of $H_3B{\cdot}NMe_2H$ from **17** (*m/z* = 398.1720, calc. 398.1653; **A**) and the formation of a dimer whose mass correlates to $[\{Rh(PCyp_2C_5H_7)\}_2(C_6H_4F_2)(HBNMe_2)]^+$ (*m/z* = 848.2836, calc. 848.2452; **C**), presumably resulting from gas phase reactivity in the mass spectrometer (Figure 3.3). Microanalysis of **17** was not possible as the sample melts on warming to room temperature.

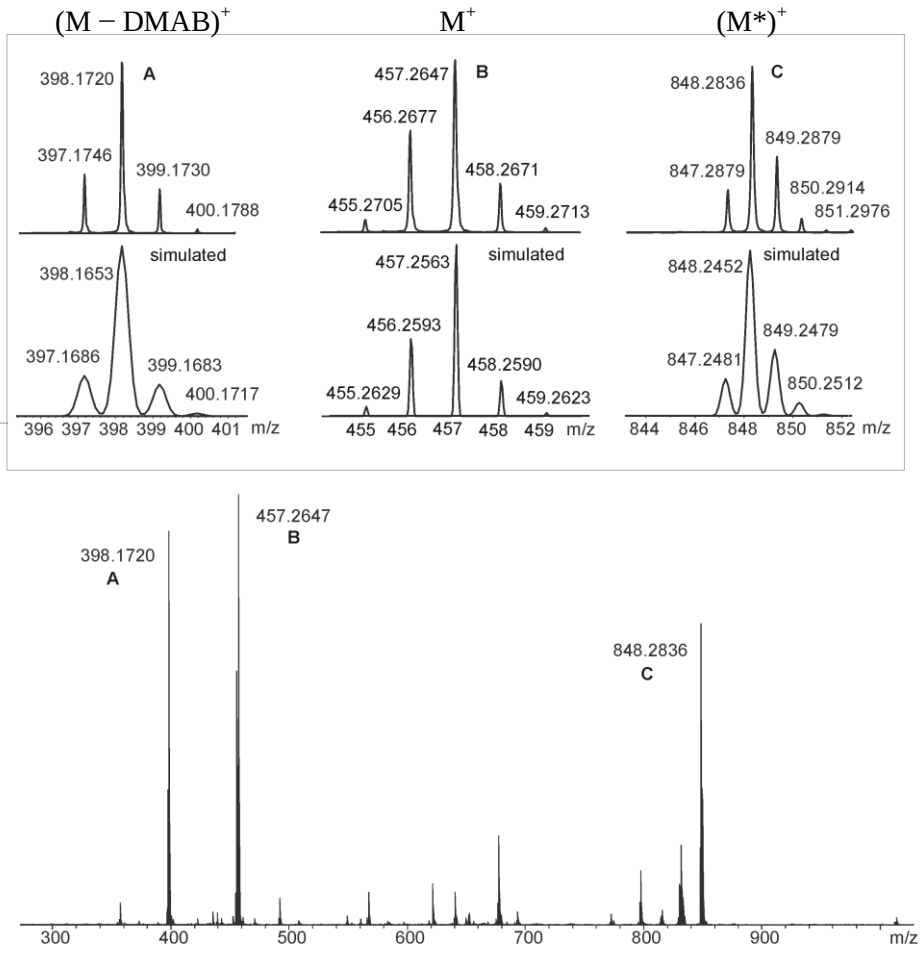
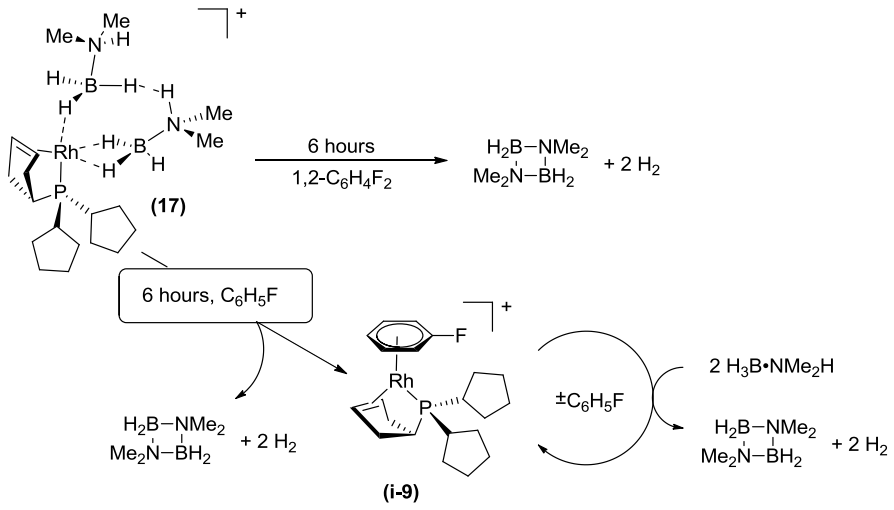


Figure 3.3 ESI-MS of **17**. A $(M^+-DMAB) = [Rh(PCyp_2C_5H_7)(H_3B{\cdot}NMe_2H)]^+$;B $(M^+) = [Rh(PCyp_2C_5H_7)(H_3B{\cdot}NMe_2H)_2]^+$; C $(M^*)^+ = [\{Rh(PCyp_2C_5H_7)\}_2(C_6H_4F_2)(HBNMe_2)]^+$.



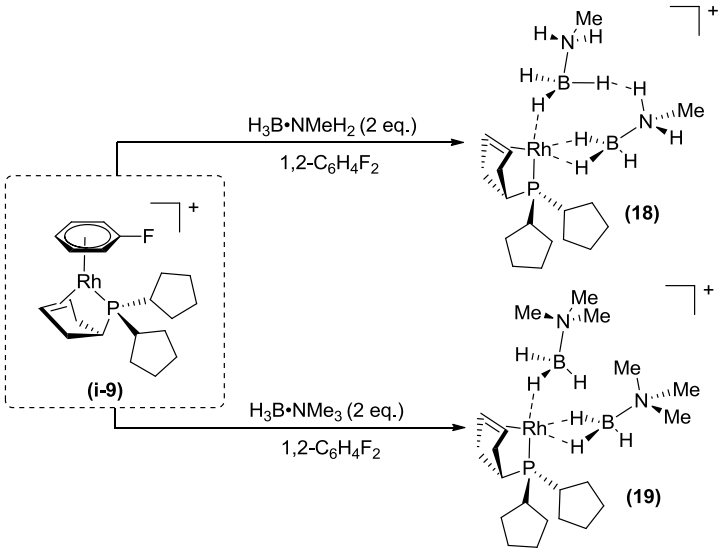
Scheme 3.3 Onward reactivity of complex **17**. $[BAr^F_4]^-$ anions not shown.

Redissolving crystals of **17** in 1,2-$C_6H_4F_2$ solvent and leaving to stand for a period of 6 hours resulted in the generation of $[H_2BNMe_2]_2$ as observed by ^{11}B NMR spectroscopy (Scheme 3.3). No significant B-N or organometallic intermediates were observed over this time frame by NMR spectroscopy. This result suggests that "on metal" dehydrogenation and dehydrocoupling of $H_3B{\cdot}NMe_2H$ is potentially taking place. Further mechanistic analysis with a deuterium analogue of $H_3B{\cdot}NMe_2H$ ($H_3B{\cdot}NMe_2D$) was not conclusive in determining the path of the evolved hydrogen, whilst no other organometallic products were observed during the 6 hours taken to form the products of dehydrocoupling.[*] Dissolving **17** in C_6H_5F however did result in regeneration of **i-9** upon the dehydrocoupling of $H_3B{\cdot}NMe_2H$ to form $[H_2BNMe_2]_2$ (6 hours) which then was able to undergo additional catalysis on the addition of more $H_3B{\cdot}NMe_2H$ to the same solution. This represents a possible "catch and release" process (Scheme 3.3).[7]

Similar to with $H_3B{\cdot}NMe_2H$, **i-9** was reacted with $H_3B{\cdot}NMe_3$ and $H_3B{\cdot}NMeH_2$ under the same conditions resulting in the rapid formation of $[Rh\{PCyp_2(\eta^2\text{-}C_5H_7)\}(\eta^1\text{-}H_3B{\cdot}NMeRR')(\eta^2\text{-}H_3B{\cdot}NMeRR')][BAr^F_4]$ {R = R' = H **(18)**; R = R' = Me **(19)**} in quantitative yield by NMR

[*] The only crystallographically characterised η^6-1,2-$C_6H_4F_2$ complex has been isolated by our group: $[Rh(P^iBu_3)_2(\eta^6\text{-}C_6H_4F_2)][BAr^F_4]$ **(i-166)**. Addition of 1,2-$C_2H_4Cl_2$ or C_6H_5F to this complex results in rapid dissociation of 1,2-$C_6H_4F_2$ and coordination of these solvents.

spectroscopy (Scheme 3.4). **18** is the first example of $H_3B{\cdot}NMeH_2$ coordination to a transition metal complex.



Scheme 3.4 Synthesis of bis-σ-amine-borane complexes **18** and **19**. $[BAr^F{}_4]^-$ anions not shown.

The respective $^{31}P\{^1H\}$ NMR spectra of **18** and **19** each show a doublet [δ 104.7, *J*(RhP) 168 Hz **(18)**], [δ 108.6, *J*(RhP) 174 Hz **(19)**] while the ^{11}B spectra show broad resonances [δ –16.9 **(18)**, –6.3 **(19)**], which are comparable to that found for **17**. The ^1H NMR spectra at 298 K are broadly similar, although **19** does not contain a N*H* signal with its N*Me*$_3$ signal observed as a singlet (δ 2.69), whilst the N*Me*H_2 signal for **18** is observed as a broad triplet [δ 2.60 {*J*(HH) 5 Hz}]. The NMe*H*$_2$ signal of **18** is a broad resonance [δ 3.76 (br, 4H, 2×N*H*$_2$)], which resolves into two separate resonances at 200 K [δ 4.00 (br, 2H, N*H*$_2$), 3.51 (br, 2H, N*H*$_2$)]. Only one N*Me* signal is observed at low temperature (δ 2.63, s, 18H) for **19**. Each of the *H*$_3$B resonances for **18** and **19** is broad and integrates to six protons at room temperature. On cooling to 200 K those for **19** freeze out, into a 3:2 ratio by $^1H\{^{11}B\}$ NMR spectroscopy as seen for **17**. At this temperature, those for **18** are observed as a broad five proton signal (3H + 2H coincidence) with the remaining terminal B*H* unobserved. Interestingly, the formation of bis-σ- amine-borane adduct **19** suggests that the hydrogen bond found between the two amine-borane ligands in complexes **17** and **18** (*vide infra*) is not necessary for the formation of these complexes, as

hydrogen bonding is not possible in **19**. Unlike **17**, ESI-MS of **18** and **19** gave mass spectra whose predominant mass ion was the difluorobenzene fragment $[Rh(C_6H_4F_2)\{PCyp_2(C_5H_7)\}]^+$ (*m/z* = 453.1024, calc. 453.1030), with each of the complexes having lost their two coordinated amine-borane ligands in favour of the solvent. The structures of **18** (Figure 3.4) and **19** (Figure 3.5) were obtained upon crystallisation under the same conditions as **17** and were similarly thermally unstable in the solid state.

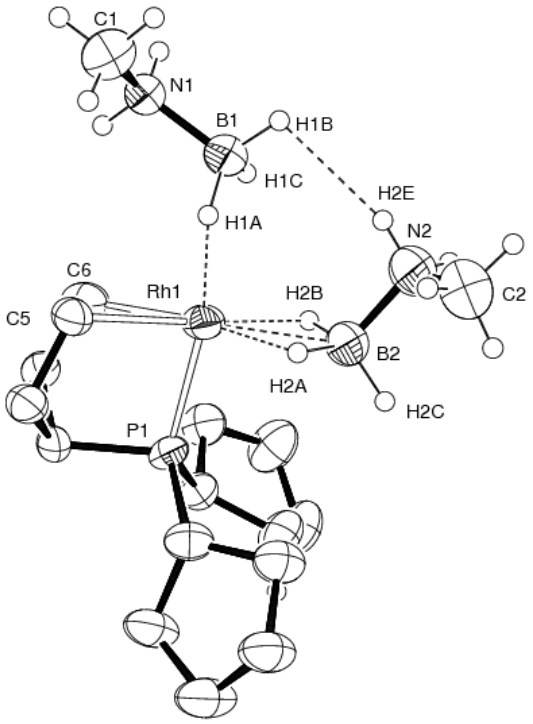


Figure 3.4 Solid-state structure of the cationic portion of **18**. Thermal ellipsoids are presented at the 50 % probability level. Minor disordered components not shown. Selected bond lengths [Å]: Rh1-B1 2.642(11), Rh1-B2 2.289(6), Rh1-P1 2.2377(12), Rh1-C5 2.111(3), Rh1-C6 2.112(3), C5-C6 1.411(10), H2e-H1b 2.22 (calcd).

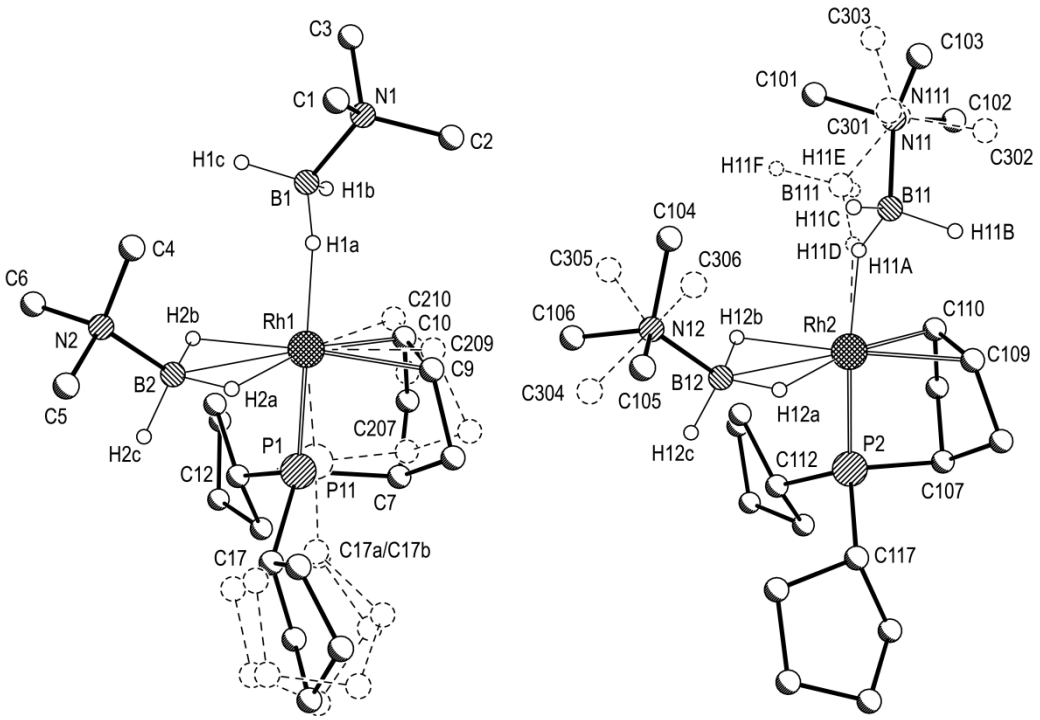


Figure 3.5 Molecular structure of the cationic portion of **19** showing two independent molecules from the asymmetric unit in a ball and stick representation. Minor disordered components drawn with dashed lines and atoms. Most H atoms omitted for clarity. Selected bond lengths [Å]: (left): Rh1-P1 2.223(2), Rh1-P11 2.219(3), Rh1-B1 2.766(7), Rh1-B2 2.310(7), Rh1-C9 2.112(4), Rh1-C10 2.115(4), Rh1-C209 2.115(5), Rh1-C210 2.115(5), C9-C10 1.444(10), C209-C210 1.41(2); (right): Rh2-P2 2.2185(12), Rh2-B11 2.815(12), Rh2-B111 2.313(6), Rh2-C109 2.109(5), Rh2-C110 2.107(5), C109-C110 1.413(7).

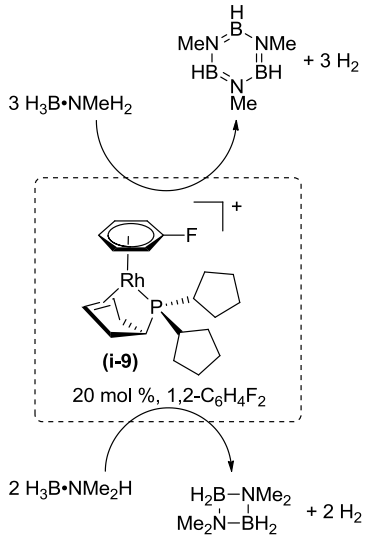
Two independent molecules of **19** appear in the asymmetric unit cell, exhibiting significant disorder in the phosphine (Rh1), amine-borane (Rh2) and solvent molecules present, which were successfully modelled. Table 3.1 shows that the respective η^1- and η^2- Rh···B interactions for complexes **17** and **18** are the same within error. Those for **19** are appreciably longer hinting at a weaker interaction with the $H_3B{\cdot}NMe_3$ ligand, presumably due to the increased steric bulk imposed by the additional methyl group which further constrains the geometry of the complex. Bond distances for **19** are quoted as averages due to the two independent molecules in the unit cell and significant disorder.

Table 3.1 Selected bond distances of complexes **17-19**.

Complex	H-H Bond Length (Å)	η^1-Rh···BH_3 Bond Length (Å)	η^2-Rh···BH_3 Bond Length (Å)
17	2.2 (calcd)	2.642 (11)	2.289 (6)
18	2.12 (4)	2.661 (3)	2.282 (3)
19	n/a	2.80 (avg.)	2.31 (avg.)

Upon dissolving **19** in 1,2-$C_6H_4F_2$ solvent, the complex was found to be unchanged over a period of 48 hours by NMR spectroscopy. This is consistent with the inability for $H_3B{\cdot}NMe_3$ to undergo dehydrogenation and similar stability was observed with $[Rh(PR_3)_2(\eta^2\text{-}H_3B{\cdot}NMe_3)][BAr^F{}_4]$ (R = ^{i}Bu **(i-137)**, ^{i}Pr **(i-137a)**).[1,8] Complex **18** however behaved in an analogous manner to **17** in solution, resulting in the dehydrogenation and dehydrocoupling of $H_3B{\cdot}NMeH_2$ to form trimethylborazine, $[HBNMe]_3$ [δ 33.4, {*J*(BH) 134 Hz}] as the major inorganic product by ^{11}B NMR spectroscopy over 6 hours. Some additional unresolved signals (δ −8) were also observed as a minor product however their further characterisation by ^{1}H NMR spectroscopy was hampered by the cyclopentylphosphine resonances (δ 2 – 0).

3.2.2 Amine-borane dehydrocoupling catalysis with i-9



Scheme 3.5 $H_3B{\cdot}NMe_2H$ and $H_3B{\cdot}NMeH_2$ catalysis with **i-9** at 20 mol% loading. $[BAr^F{}_4]^-$ anions not shown.

Complexes **17-19** represent the first examples of bis-σ-amine-borane coordination to a metal fragment. Interestingly, the involvement of bis-σ-complexes in the dehydrocoupling of $H_3B{\cdot}NMe_2H$ has been rejected in Ohno's computational model using $TiCp_2$ as their formation was not energetically or kinetically favourable.[9] Conversely, in the recent experimental and kinetic study by Manners *et al.* on the same system, a bis-σ-amine-borane complex is suggested to form initially upon addition of $H_3B{\cdot}NMe_2H$ to $TiCp_2$.[10] Hill and co-workers have also recently reported the metal assisted dehydrocoupling of two molecules of the related amine-borane $H_3B{\cdot}N(CH_2)_4H$ to form $[H_3B{\cdot}N(CH_2)_4BH_2{\cdot}N(CH_2)_4]^-$ coordinated to a Mg β-diketiminato complex.[11]

The ultimate formation of the products of dehydrocoupling with **17** and **18** led us to investigate the catalytic activity of **i-9** towards $H_3B{\cdot}NMe_2H$ and $H_3B{\cdot}NMeH_2$ respectively (Scheme 3.5). Dehydrocoupling (**(i-9)** 20 mol%, 1,2-$C_6H_4F_2$, 298 K) to yield $[H_2BNMe_2]_2$ and $[HBNMe]_3$ respectively was found to reach completion (~ 94 %) after 12 hours. This slow dehydrocoupling with this catalyst also presumably reflects the ability to isolate intermediate complexes **17** and **18**. The time/composition plot for the catalysis of **i-9** (20 mol%) with $H_3B{\cdot}NMe_2H$ is shown in Figure 3.6.

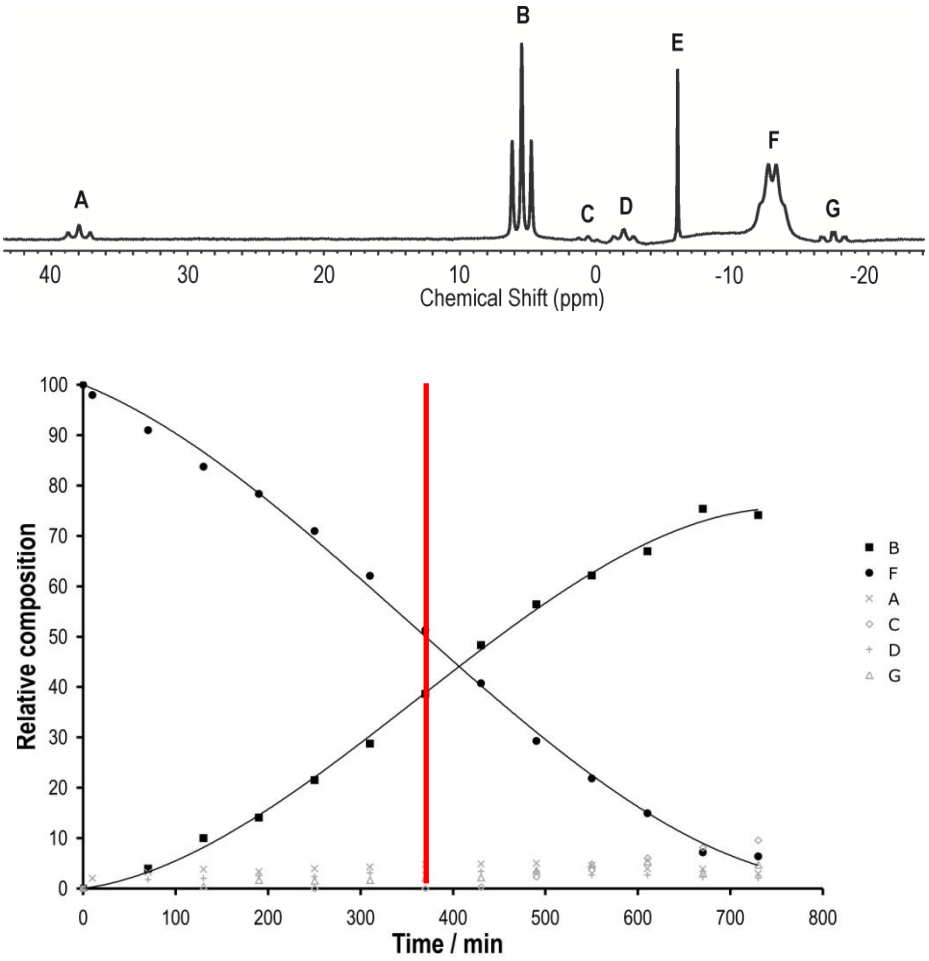


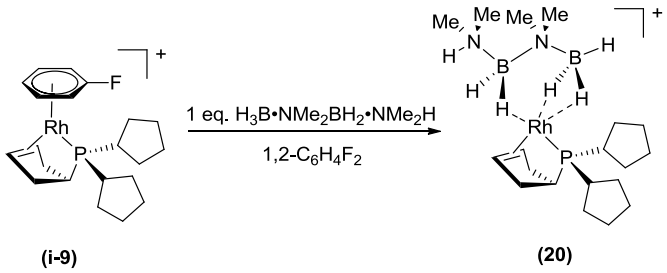
Figure 3.6 ^{11}B NMR spectrum of H_3BNMe_2H catalysis with **i-9** after 370 minutes, indicated by vertical line on time concentration plot (top). Time composition plot for the dehydrogenation and dehydrocoupling of $H_3B{\cdot}NMe_2H$ with **i-9** at 20 mol% catalyst loading in 1,2-$C_6H_4F_2$ (bottom). **A** = $H_2B{=}NMe_2$, **B** = $[H_2BNMe_2]_2$, **C** = unidentified species (δ 1 ppm), **D** = unidentified species (δ -2 ppm), **E** = $[BAr^F{}_4]^-$, **F** =$H_3B{\cdot}NMe_2H$, **G** = $(\mu\text{-}NMe_2)B_2H_5$. Lines drawn are for clarity only and are third-order polynomials.

To help ascertain the nature of the active catalyst, Hg (100 µL) was added to the catalytic mixture at the start of the reaction and the formation of $[H_2BNMe_2]_2$ monitored by ^{11}B NMR spectroscopy by taking 200 µL aliquots of the reaction mixture and quenching the catalyst with dppe. Hg addition was not observed to attenuate catalysis in comparison to a control. This, along with a non-sigmoidal time composition profile suggests that catalysis is homogeneous rather than heterogeneous (Chapter 4 discusses these tests in considerable detail).[12,13] The

absence of oligomeric species $H_3B{\cdot}NMe_2BH_2{\cdot}NMe_2H$ and $[H_2B{\cdot}NMeH]_3$ in the dehydrogenation and dehydrocoupling catalysis of $H_3B{\cdot}NMe_2H$ and $H_3B{\cdot}NMeH_2$ respectively with **i-9** is intriguing given that other related systems report their formation and eventual consumption during catalysis,[14,15,16] especially as in the case of **17**, $H_3B{\cdot}NMe_2BH_2{\cdot}NMe_2H$ would formally result from the simple loss of H_2 which might, on first inspection, be enabled by the hydrogen bond. With a view to further understanding the mechanism of the dehydrocoupling process the reactivity of **i-9** towards these oligomeric species was undertaken.

3.2.3 Reactivity of i-9 with $H_3B{\cdot}NMe_2BH_2{\cdot}NMe_2H$

$H_3B{\cdot}NMe_2BH_2{\cdot}NMe_2H$ was synthesised using the literature protocol from the reaction of $H_3B{\cdot}NMe_2Li$ and $H_2ClB{\cdot}NMe_2H$ generated *in situ* from the reaction of $H_3B{\cdot}NMe_2H$ and ^nBuLi and HCl (in Et_2O) respectively (Chapter 1, Section 1.3.4.4, Scheme 1.46).[17]

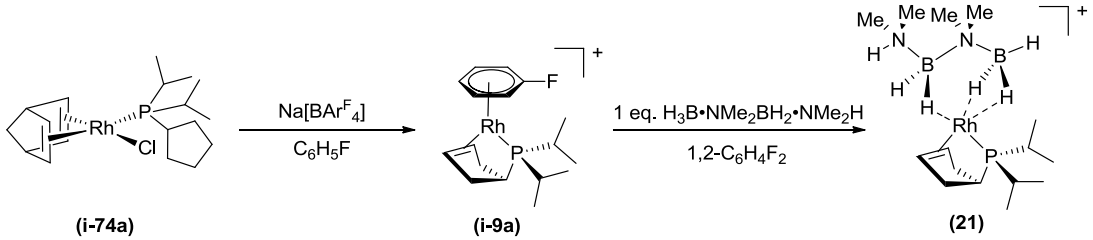


Scheme 3.6 Addition of $H_3B{\cdot}NMe_2BH_2{\cdot}NMe_2H$ to **i-9** results in the formation of $[Rh\{PCyp_2(\eta^2\text{-}C_5H_7)\}(\eta^2\text{-}:\eta^1\text{-}H_3B{\cdot}NMe_2BH_2{\cdot}NMe_2H)][BAr^F{}_4]$ **(20)**. $[BAr^F{}_4]^-$ anions not shown.

Stoichiometric addition of $H_3B{\cdot}NMe_2BH_2{\cdot}NMe_2H$ (1 equivalent) to **i-9** (Scheme 3.6) yielded the quantitative formation of a new species by NMR spectroscopy which, as for complexes **17-19**, was shown clearly by $^{31}P\{^1H\}$ NMR spectroscopy with the appearance of a new doublet further downfield to **i-9** [δ 114.6 {*J*(RhP) 170 Hz}]. The ^{11}B NMR spectrum shows a single broad peak centred at δ −4.3 which lies in between the BH_2 [δ +2.5 {t, *J*(BH) 107 Hz}] and BH_3 [δ −12.8 {q, *J*(BH) 94 Hz}] resonances found for free ligand. The ^1H NMR spectrum showed the appearance of two broad resonances in a 3:2 ratio assigned to the coordination of both the BH_3 and BH_2 components of $H_3B{\cdot}NMe_2BH_2{\cdot}NMe_2H$ [δ +0.10 {br, *J*(BH) 111 Hz, 3H}, −1.94

{br, *J*(BH) 117 Hz, 2H}]. These signals sharpen dramatically on decoupling the quadropolar boron nucleus with the former becoming a doublet *J*(RhH) = 21 Hz. Two N*Me*$_2$ environments are observed [δ 2.75 {d, *J*(HH) 5 Hz, 6H}; 2.67 (s, 6H)] along with one N*H* resonance [δ 4.19 (br s, 1H)]. Upon cooling to 200 K, the B*H*$_3$ signal at δ^1H +0.10 collapses into a very broad relative 2H integral (δ^1H −1.30) indicating that a fluxional process involving the B*H*$_3$ component has been halted, the terminal B*H* resonance however remained unidentified. The B*H*$_2$ resonance however does not change chemical shift or shape on cooling. All evidence thus pointed towards the formation of [Rh{PCyp$_2$(η^2-C$_5$H$_7$)}(η^2:η^1- H$_3$B·NMe$_2$BH$_2$·NMe$_2$H)][BAr$^F_4$] **(20)** (Scheme 3.6). This was further confirmed by ESI-MS with a parent mass ion *m/z* = 455.2420 (calc. 455.2406) with the correct isotope pattern being observed. Two Rh complexes of H$_3$B·NMe$_2$BH$_2$·NMe$_2$H have been reported; [Rh(P^{i}Bu$_3$)$_2$(H$_3$B·NMe$_2$BH$_2$·NMe$_2$H)][BAr$^F_4$] **(i-149)** and [Rh(P^{i}Bu$_3$)$_2$(H$_2$)(H$_3$B·NMe$_2$BH$_2$·NMe$_2$H)][BAr$^F_4$] **(i-150)**. Both show only a broad integral 3H resonance for the η^2-*H*$_3$B coordinated component in the ^{1}H NMR spectrum at 298 K [δ −2.31 **(i-149)**, −0.75 **(i-150)**], that of the B*H*$_2$ moiety could not be definitively assigned and it is speculated to be broad or obscured under other aliphatic peaks.[14] Two resonances in the high field region of the ^{1}H NMR spectrum of **20**, suggests that both boron moieties are bound to the metal centre. The observation of only one ^{11}B environment suggests that both the *B*H$_2$ and *B*H$_3$ resonances are coincident. The same resonances were very broad for **i-149** (δ +26.0, +3.9) and unobserved for **i-150**.[14] A greater change in ^{11}B chemical shift from free ligand is therefore observed for the *B*H$_3$ moiety of **20** (δ −12.8 (free) *vs.* + 4.2 (bound)) suggestive of a strong Rh···H$_2$BH interaction, presumably through η^2 coordination in comparison to **17-19**. Binding of the BH$_2$ to the metal centre through an η^1-Rh···HBH interaction would lead to an 18-electron complex. Crystals suitable for X-ray diffraction were obtained upon generating **20** *in situ* in 1,2-C$_6$H$_4$F$_2$ solution and layering with pentane at 238 K, however extensive disorder of the sample prevented definitive structural characterisation. This problem led us to use the related [Rh{P^{i}Pr$_2$(η^2-C$_5$H$_7$)}]$^+$ fragment to help characterise this bonding mode. This fragment was generated *in situ* from [Rh(η^6-C$_6$H$_5$F){P^{i}Pr$_2$(η^2-C$_5$H$_7$)}][BAr$^F_4$] **(i-9a)** made in an analogous

manner to **i-9**,[18] from the norbornadiene precursor [Rh(NBD)(P^iPr_2Cyp)][BAr^F_4] **(i-74a)**, originally synthesised by Jennifer Tsim (Part II student, Weller group) (Scheme 3.7).



(i-74a) **(i-9a)** **(21)**

Scheme 3.7 Synthesis of complex **21**. [BAr^F_4]$^-$ anions not shown.

The NMR data for **21** are similar to that observed for **20**. The ^{1}H NMR spectrum of **21** shows two broad peaks in a 3:2 ratio [δ +0.12 {br, *J*(BH) 110 Hz, 3H, B*H*$_3$}, −2.14 {br, *J*(BH) 119 Hz, 2H, B*H*$_2$}] (Figure 3.7) whilst the ^{31}P{^{1}H} spectrum contains a doublet [δ 123.0 {d, *J*(RhP) 176 Hz}] and a single broad signal (δ −4.3) is observed in the ^{11}B NMR spectrum.

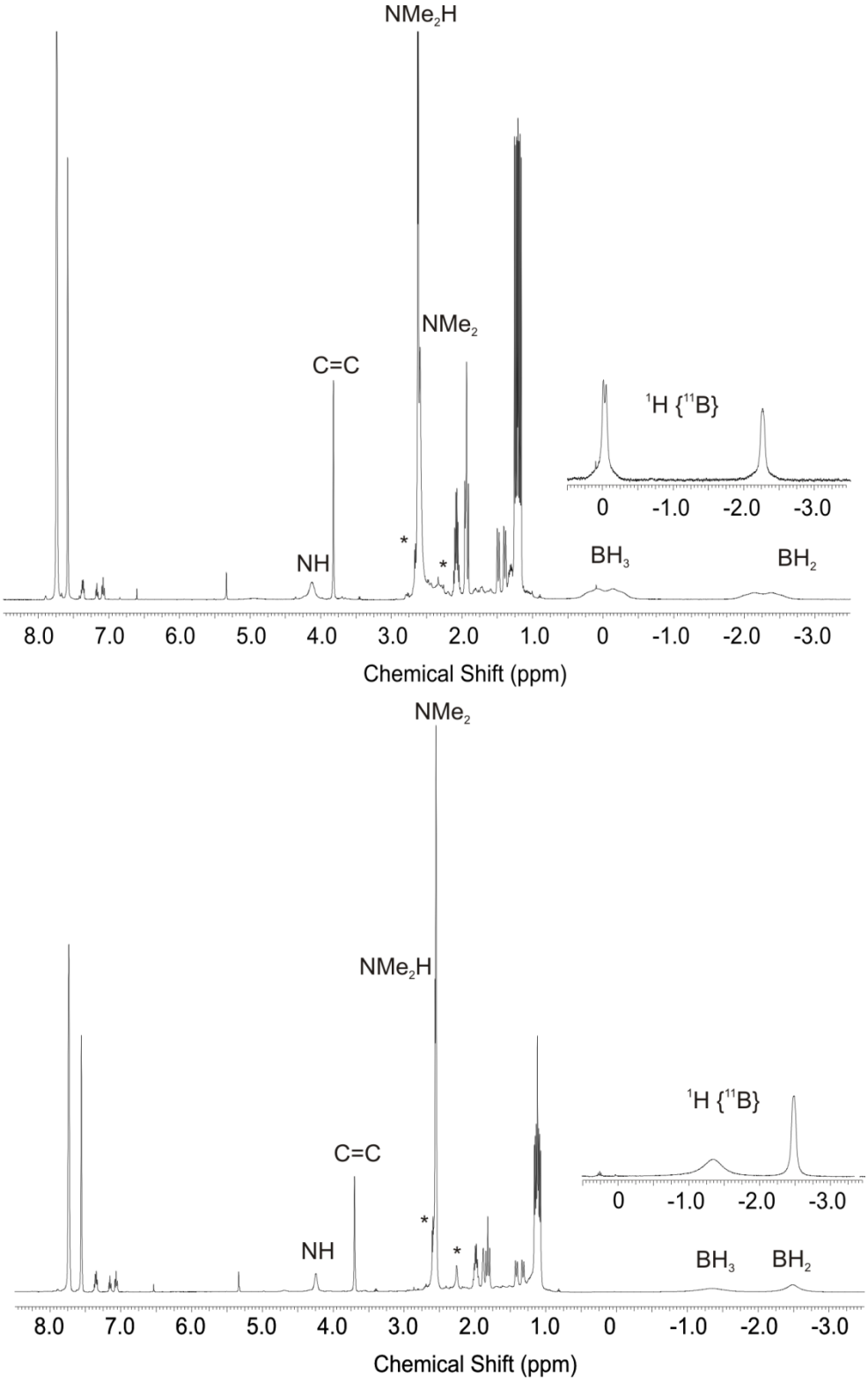


Figure 3.7 (top): ^{1}H NMR spectrum of **21** at 298 K, $^{1}H\{^{11}B\}$ spectrum shown inset. (bottom): ^{1}H NMR spectrum of **21** at 200 K, $^{1}H\{^{11}B\}$ spectrum shown inset (500 MHz, CD_2Cl_2). * = free $H_3B{\cdot}NMe_2BH_2{\cdot}NMe_2H$.

Crystallisation of **21** yielded X-ray quality crystals which now did not have significant disorder in the cation and from which the structure in Figure 3.8 was obtained.

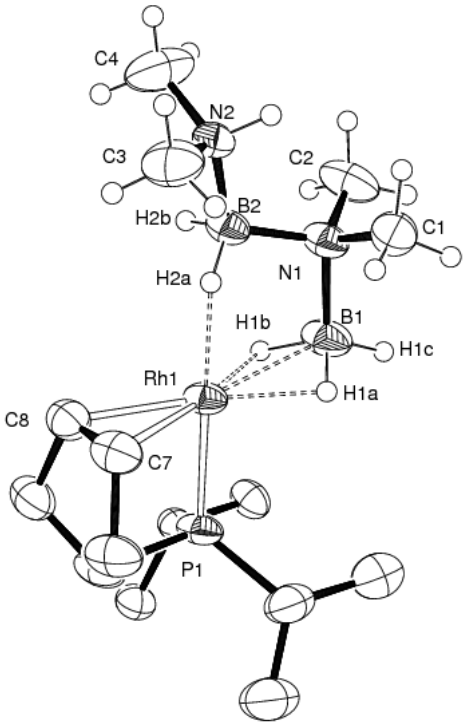


Figure 3.8 Solid-state structure of the cationic portion of **21**. Thermal ellipsoids are presented at the 50 % probability level. Selected bond lengths [Å] and angles (°): Rh1-B1 2.242(5), Rh1-B2 2.626(4), Rh1-H1A 1.85(5), Rh1-H1B 1.84(5), Rh1-H2A 1.96(4), Rh1-C7 2.107(4), Rh1-C8 2.121(4), Rh1-P1 2.2058(9); B2-N1-B1 103.3(3), N1-B2-N2 112.7(3), N1-B1-Rh1 103.1(3), Rh1-H2A-B2, 23.3(13).

Figure 3.8 shows that **21** exhibits a *pseudo*-octahedral geometry with Rh1-C7/8 and Rh1-P1 distances consistent with other phosphine-alkene complexes of this type [Rh-C7/8 {2.114(4) Å (avg.)}; Rh1-P1 2.058(9) Å] *c.f.* [Rh(η^6-C_6H_5F){P^iPr_2(η^2-C_5H_7)}][BAr^F_4] **(i-9a)** [Rh-C7/8 {2.129(4) Å }; Rh1-P1 2.2507(11) Å]. The $H_3B{\cdot}NMe_2BH_2{\cdot}NMe_2H$ ligand is coordinated to the Rh phosphine-alkene fragment *via* both boron moieties in a η^1-H_2B: η^2-H_3B fashion, very similar to that observed for bis-σ amine-borane complexes **17-19**. The η^1-H_2B···Rh bond distance of **21** is comparable to that observed for the η^1-H_3B···Rh bond length of **17** {2.661(3) Å **(17)** *vs.* 2.626(4) Å **(21)**} as is the η^2-H_3B···Rh distance {2.282(3) Å **(17)** *vs.* 2.242(5) Å **(21)**}. The η^2-H_3B···Rh interaction of [Rh(P^iBu_3)$_2$(η^2- $H_3B{\cdot}NMe_2BH_2{\cdot}NMe_2H$)][$BAr^F_4$] **(i-149)** is of a similar magnitude within experimental error {2.184(9) Å}.[14]

Isolated **20** or **21** dissolved in 1,2-$C_6H_4F_2$ were stable in solution over a period of 48 hours. This is in contrast to **17** which goes on to form $[H_2BNMe_2]_2$ in 6 hours. This suggests that $H_3B{\cdot}NMe_2BH_2{\cdot}NMe_2H$ is *not* formed on the metal during the dehydrocoupling on **17**, consistent with neither **20** nor the free ligand being observed during the dehydrocoupling of $H_3B{\cdot}NMe_2H$ to $[H_2BNMe_2]_2$ with **i-9**. Addition of excess $H_3B{\cdot}NMe_2BH_2{\cdot}NMe_2H$ (5/2 equivalents) to **20** however results in the slow (96 hours) dehydrogenation and dehydrocoupling to form $[H_2BNMe_2]_2$ (Figure 3.9), which is considerably slower than the dehydrocoupling of $H_3B{\cdot}NMe_2H$ to $[H_2BNMe_2]_2$ with **i-9** (20 mol%, 298 K, 1,2-$C_6H_4F_2$), which is complete after 13.5 hours (Figure 3.6). Products of B-N bond cleavage ($H_2B{=}NMe_2$ [δ^{11}B +38 {t, *J*(BH) 123 Hz}], $HB(NMe_2)_2$ [δ^{11}B +29 {d, *J*(BH) 125 Hz}], $B_2H_5(\mu\text{-}NMe_2)$ [δ^{11}B −17 {td, *J*(BH) 133 Hz, 30 Hz}]) are present during the dehydrocoupling of $H_3B{\cdot}NMe_2BH_2{\cdot}NMe_2H$ with **20** and also in the catalytic dehydrocoupling of $H_3B{\cdot}NMe_2H$ with **i-9** (Figure 3.6). Although $H_3B{\cdot}NMe_2BH_2{\cdot}NMe_2H$ is not observed in the dehydrocoupling of $H_3B{\cdot}NMe_2H$ with **i-9**, this could be evidence for the scission of $H_3B{\cdot}NMe_2BH_2{\cdot}NMe_2H$ present at low concentration.

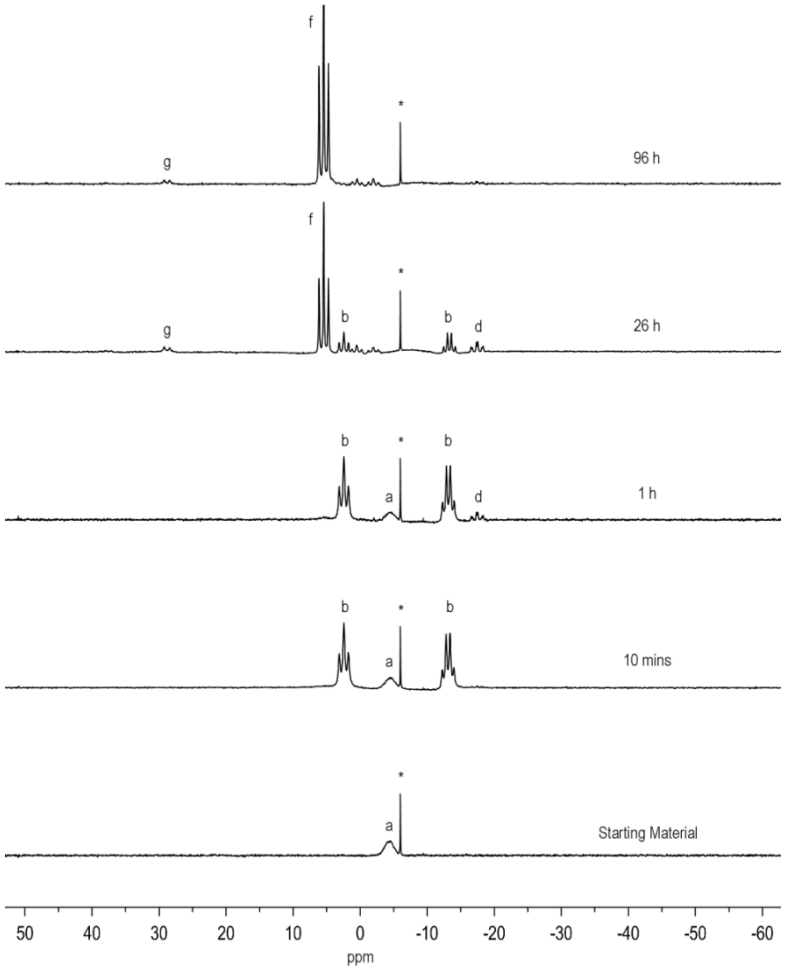
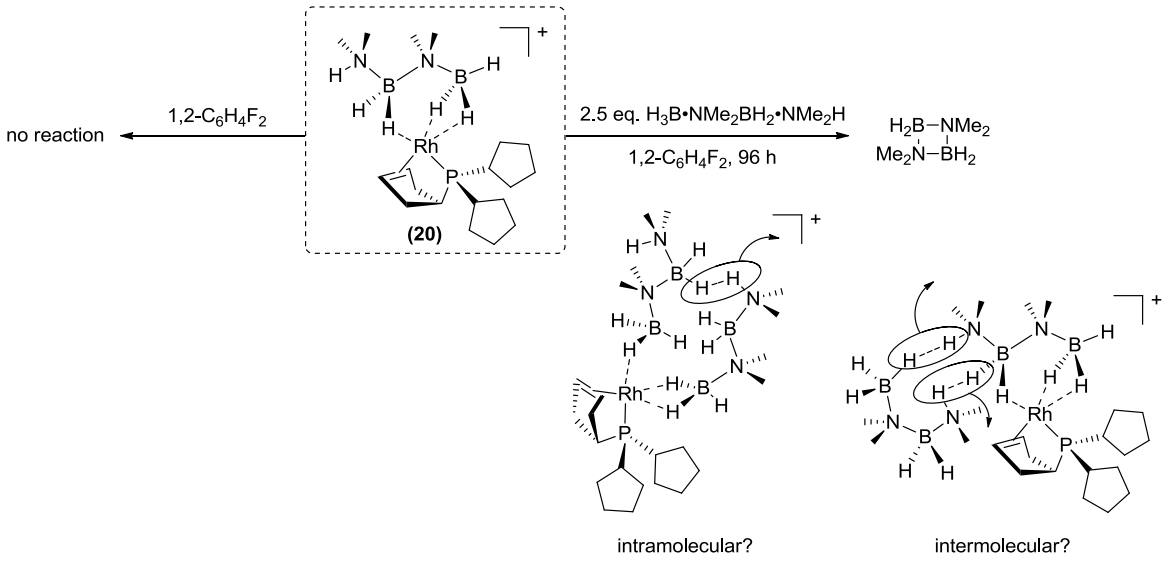


Figure 3.9 ^{11}B NMR spectra (160 MHz, 1,2-$C_6H_4F_2$) of the catalytic dehydrocoupling of $H_3B{\cdot}NMe_2BH_2{\cdot}NMe_2H$ with **20** (20 mol % relative to $H_3B{\cdot}NMe_2H$, 1,2-$C_6H_4F_2$). a = **20**, b = $H_3B{\cdot}NMe_2BH_2{\cdot}NMe_2H$, c = $H_3B{\cdot}NMe_2H$, d = $B_2H_5(\mu\text{-}NMe_2)$, e = $H_2B{=}NMe_2$, f = $[H_2BNMe_2]_2$, g = $(\mu NMe_2)_2BH$, * = $[BAr^F{}_4]^-$.

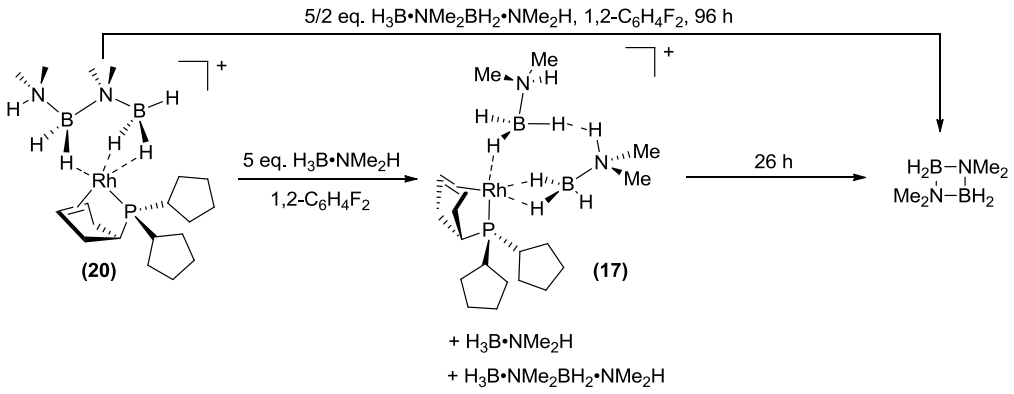
$[Rh(P^iBu_3)_2(H_3B{\cdot}NMe_2BH_2{\cdot}NMe_2H)][BAr^F{}_4]$ **(i-149)** shows similar stability to **20** and does not dehydrocouple to $[H_2BNMe_2]_2$ until excess $H_3B{\cdot}NMe_2BH_2{\cdot}NMe_2H$ is added.[14] The reason for this instability in the presence of excess ligand is unclear. One potential rationale is that a second $H_3B{\cdot}NMe_2BH_2{\cdot}NMe_2H$ unit could coordinate forming a hydrogen bonding interaction like the bis-σ-$H_3B{\cdot}NMe_2H$ motif and result in onward reactivity (Scheme 3.8). Alternatively an intermolecular process could be operating. Both presumably could result in the scission of $H_3B{\cdot}NMe_2BH_2{\cdot}NMe_2H$ to form $H_2B{=}NMe_2$ and $H_3B{\cdot}NMe_2H$, the former dimerising to form $[H_2BNMe_2]_2$ while the latter proceeds to dehydrocouple on the $[Rh\{PCyp_2(\eta^2\text{-}C_5H_7)\}]^+$ fragment. Metal promoted B-N bond cleavage of $H_3B{\cdot}NMe_2BH_2{\cdot}NMe_2H$ to form $H_2B{=}NMe_2$ and $H_3B{\cdot}NMe_2H$ has been reported in several catalyst systems.[14,15,19] The observance of the

products of B-N bond cleavage ($H_2B{=}NMe_2$ and $B_2H_5(\mu\text{-}NMe_2)$) during catalysis support this argument. Reaction of $H_2B{=}NMe_2$ with $H_3B{\cdot}NMe_2BH_2{\cdot}NMe_2H$ has also been suggested in work within the Weller group.[19]



Scheme 3.8 The suggested onward reactivity of complex **20.** $[BAr^F{}_4]^-$ anions not shown.

To further investigate the role of $H_3B{\cdot}NMe_2BH_2{\cdot}NMe_2H$ in the dehydrocoupling of $H_3B{\cdot}NMe_2H$, five equivalents of $H_3B{\cdot}NMe_2H$ were added to **20**. $^{31}P\{^1H\}$ NMR spectroscopy revealed the dissociation of $H_3B{\cdot}NMe_2BH_2{\cdot}NMe_2H$ and the coordination of $H_3B{\cdot}NMe_2H$ by the disappearance of the resonance of **20** [δ 114.6 {d, *J*(RhP) 170 Hz}] and the appearance of a resonance at δ 105.3 {d, *J*(RhP) 165 Hz} assigned to the coordinated bis-σ-amine-borane motif **(17)**. Analysis by ^{11}B NMR spectroscopy after 10 minutes confirms this as the broad signal of **20** (δ −4.3) is no longer present, with free $H_3B{\cdot}NMe_2BH_2{\cdot}NMe_2H$ observed, best indicated by the BH_2 resonance [δ +2.5 {t, *J*(BH) 107 Hz}] (Figure 3.10).



Scheme 3.9 A summary of the reactivity of **20**. $[BAr^{F}_{4}]^{-}$ anions not shown.

Dehydrogenation and dehydrocoupling of $H_3B{\cdot}NMe_2H$ and the liberated $H_3B{\cdot}NMe_2BH_2{\cdot}NMe_2H$ continues over 26 hours to near completion (Figure 3.10). Catalysis using $H_3B{\cdot}NMe_2BH_2{\cdot}NMe_2H$ and **20** (Figure 3.9) leads to a similar degree of conversion after 96 hours as summarised in Scheme 3.9. These data are consistent with $H_3B{\cdot}NMe_2BH_2{\cdot}NMe_2H$ being a viable kinetic intermediate with this system, although it is not formed simply by H_2 loss from **17** nor is it observed during the dehydrocoupling of $H_3B{\cdot}NMe_2H$.

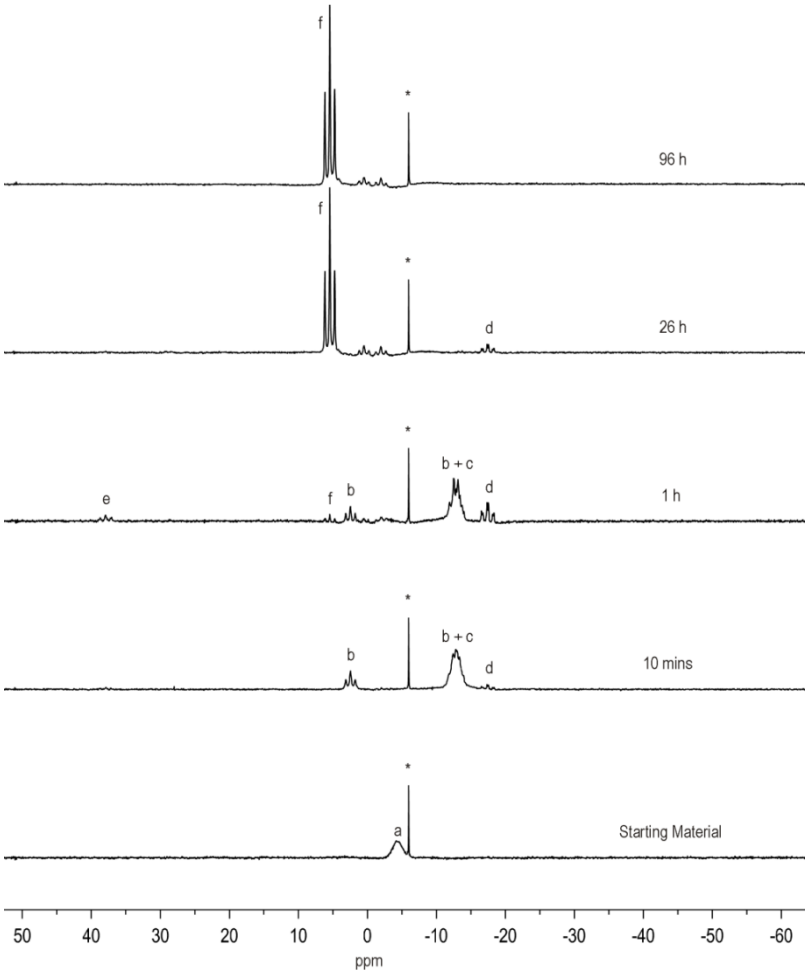


Figure 3.10 ^{11}B NMR spectra (160 MHz, 1,2-$C_6H_4F_2$) of the catalytic dehydrocoupling of $H_3B{\cdot}NMe_2H$ with **20** (20 mol %, 1,2-$C_6H_4F_2$, 160 MHz). a = **20**, b = $H_3B{\cdot}NMe_2BH_2{\cdot}NMe_2H$, c = $H_3B{\cdot}NMe_2H$, d = $B_2H_5(\mu\text{-}NMe_2)$, e = $H_2B{=}NMe_2$, f = $[H_2BNMe_2]_2$, g = $(\mu NMe_2)_2BH$, * = $[BAr^F{}_4]^-$.

3.2.4 Reactivity of i-9 with $[H_2B{\cdot}NMeH]_3$

$[H_2B{\cdot}NMeH]_3$ was synthesised using a preparative procedure developed by Paine and co-workers by heating $H_3B{\cdot}NMeH_2$ at reflux overnight in DME.[20] $[H_2B{\cdot}NMeH]_3$ exists as two isomers; the *eea* and *eee* forms (Figure 3.11).

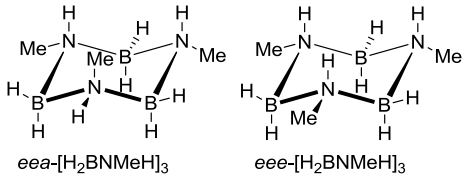
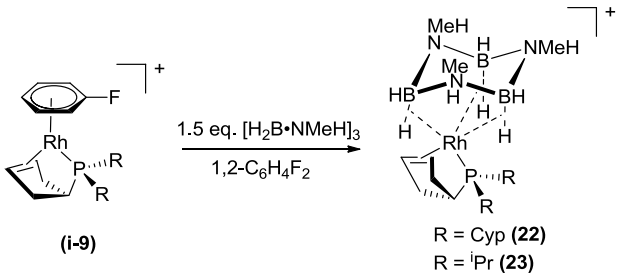


Figure 3.11 The *eea*- and *eee*- isomers of $[H_2B{\cdot}NMeH]_3$.

The *eee* isomer forms as the major product of the synthesis and was isolated in its pure form following recrystallization from benzene. Addition of *eee*-$[H_2B{\cdot}NMeH]_3$ (1.5 equivalents due to limited solubility of the trimeric species in 1,2-$C_6H_4F_2$) resulted in the quantitative formation of $[Rh\{\eta^1\text{-}\eta^1\text{-}\eta^1\text{-}(H_2B{\cdot}NMeH)_3\}\{PCyp_2(\eta^2\text{-}C_5H_7)\}][BAr^F{}_4]$ **(22)** (Scheme 3.10).



Scheme 3.10 Synthesis of complexes **22** (R = Cyp) and **23** (R = ^{i}Pr). $[BAr^F{}_4]^-$ anions not shown.

At room temperature the ^{1}H NMR spectrum of **22** shows a broad signal (δ −3.16, 3H) consistent with three bound Rh*H*BH protons undergoing site exchange (Figure 3.11). Cooling the solution to 200 K halts this process with two broad signals observed [δ −1.08 (br, 2H, Rh*H*BH), −8.31 (br, 1H, Rh*H*BH)]. ^{1}H{^{11}B} NMR spectroscopy at 298 K sharpens the Rh*H*BH relative 3H signal and reveals the remaining three terminal RhHB*H* protons [δ 2.63 (br d, *J* = 9 Hz)] which are presumably too broad to see in the ^{1}H NMR spectrum. The NH protons appear as a broad singlet (δ 3.26) slightly downfield from the N*Me* signal to which it couples [δ 2.73 {d, *J*(HH) 5 Hz}]. The alkene resonance is observed [δ 3.81 (s, 2H)]. The ^{31}P{^{1}H} NMR spectrum displays a doublet [δ 113.1 {*J*(RhP) 161 Hz}] with a broad resonance (δ −5.3) observed by ^{11}B NMR spectroscopy. Crystallisation of **22** yielded X-ray quality crystals that had similar problems with disorder as **20**. Again the equivalent complex $[Rh\{\eta^1\text{-}\eta^1\text{-}\eta^1\text{-}(H_2B{\cdot}NMeH)_3\}\{P^iPr_2(\eta^2\text{-}C_5H_7)\}][BAr^F{}_4]$ **(23)** was synthesised upon the reaction of **i-9a** with $[H_2B{\cdot}NMeH]_3$ and exhibited similar spectroscopic characteristics (Table 3.2, Figure 3.12).

Table 3.2 Comparison of the NMR data of complexes **22** and **23**. Coupling constants in Hz. All chemical shifts recorded in 1,2 $C_6H_4F_2$ solvent at designated frequencies: ^{1}H 500 MHz, ^{31}P{^{1}H} 202 MHz, ^{11}B 160 MHz.

Complex	^{1}H (δ Rh*H*BH)	^{1}H(δ NH)	^{1}H (δ NMe)	δ ^{31}P{^{1}H}	δ ^{11}B
22	−3.16 (br, 3H)	3.26 (br s, 3H)	2.73 {d, *J*(HH) 5, 9H}	113.1 {d, *J*(RhP) 161}	−5.3 (br)
23	−3.32 {q, *J*(BH) 87, 3H}	3.31 (br s, 3H)	2.71 {d, *J*(HH) 6, 9H}	120.7 {d, *J*(RhP) 165}	−5.2{br dd, *J*(BH) 118, 87}

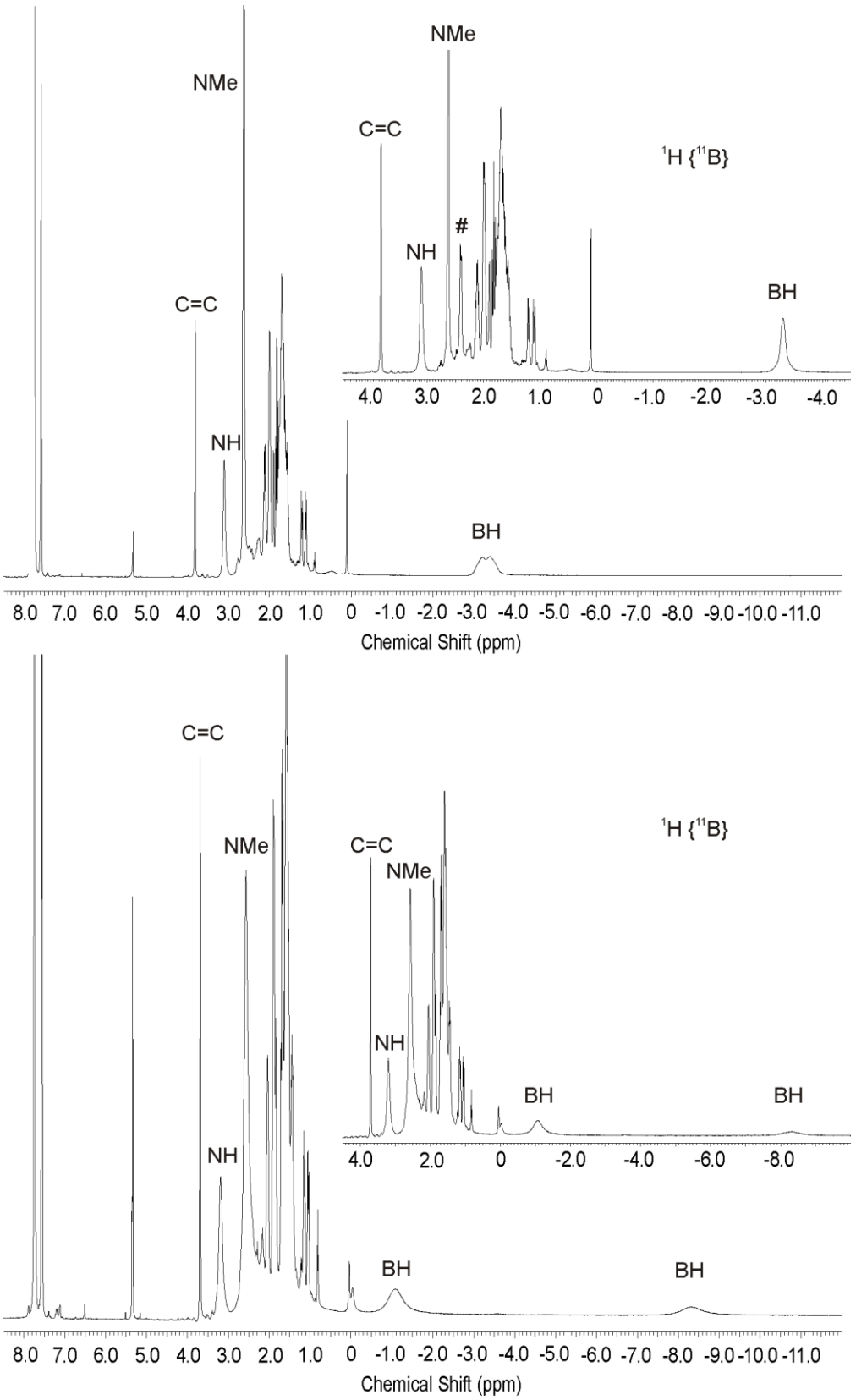


Figure 3.12 (top) ^{1}H NMR spectrum of **22** at 298 K with ^{1}H{^{11}B} spectrum shown inset. (bottom) ^{1}H NMR spectrum of **22** at 200 K with ^{1}H{^{11}B} spectrum shown inset (500 MHz, CD_2Cl_2). # = New BH resonance found as a result of the ^{11}B decoupling.

The structure of **23** shows that the trimeric $[H_2B{\cdot}NMeH]_3$ ligand acts to cap the phosphine-alkene motif which is itself retained and exhibits metrics similar to that for **22**. This coordination mode is comparable to that observed in $Mn(CO)_3(B_3H_8)$ where the $B_3H_8^-$ anion also coordinates to the Mn atom through three B-H bonds.[21] All three η^1-Rh···B interactions are relatively long {2.693(4) – 2.808(4) Å} although similar to that calculated for the η^1-Rh···B of **19** {2.80 Å (avg.)}. The *eee*-conformation of the ligand is also retained upon coordination with both the B-N distances {1.556(6) – 1.575(8) Å (free) *vs.* 1.566(5) – 1.576(5) Å **(23)**} and N-B-N angles {108.9(4)° avg. (free) *vs.* 109.4(3) ° avg. **(23)**} being similar to those found for the free ligand (Figure 3.13).[20]

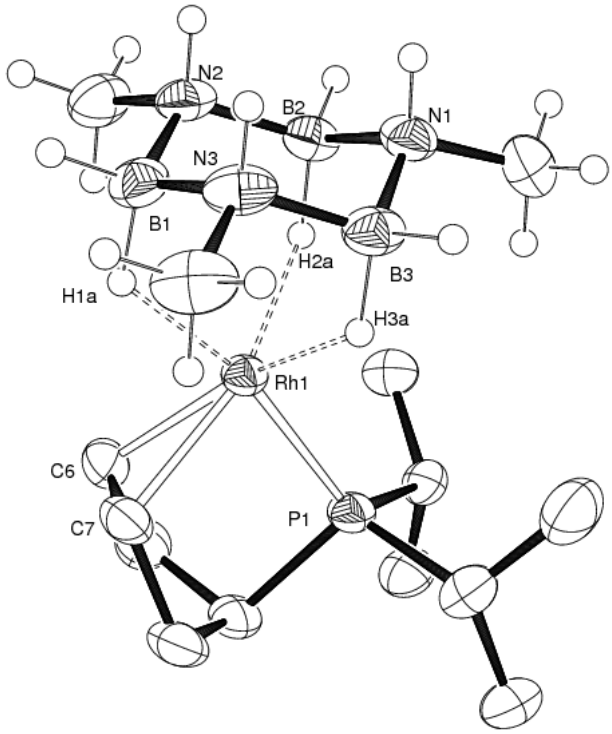
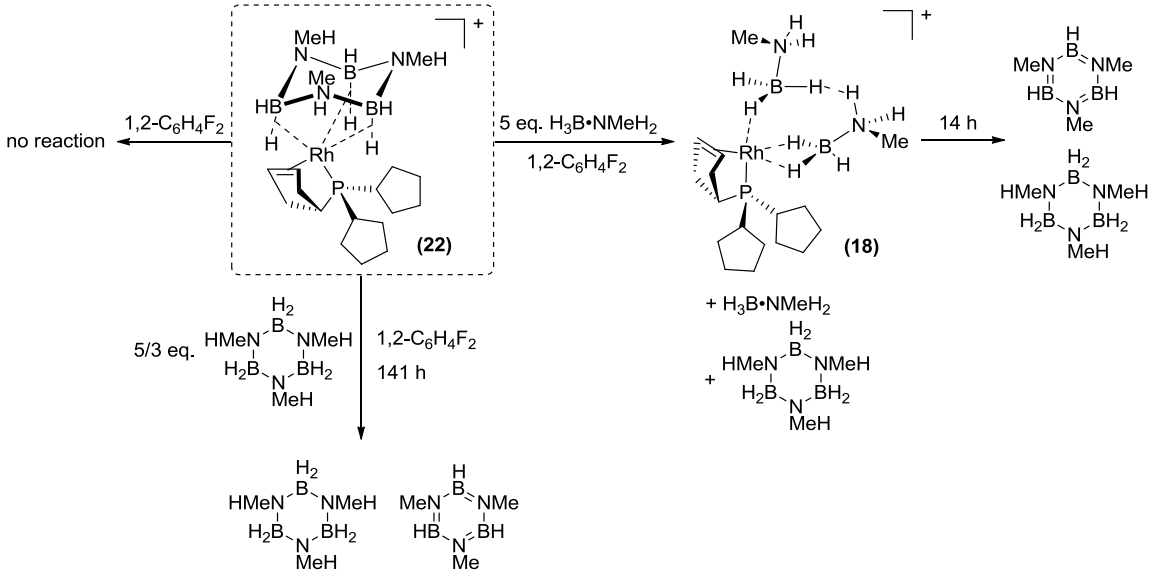


Figure 3.13 Solid-state structure of the cationic portion of **23**. Thermal ellipsoids are presented at the 50 % probability level. Selected bond lengths [Å] and angles (°): Rh1-B1, 2.693(4); Rh1-B2, 2.808(4); Rh1-B3, 2.761(4); Rh1-H1A, 1.84(4); Rh1-H2A, 1.94(4); Rh1-H3A, 1.86(4); Rh1-P1, 2.2354(8); Rh1-C6, 2.096(3); Rh1-C7, 2.094(3); B1-N2-B2, 112.9(3); B2-N1-B3, 111.7(3); B3-N3-B1, 112.6(3); Rh1-H1A-B1, 123(3); Rh1-H2A-B2, 128(3); Rh1-H3A-B3, 128(3).

Isolated **22** or **23** dissolved in 1,2-$C_6H_4F_2$ show no further reactivity after 48 hours, as is observed for **20** and **21**. This suggests that a simple intramolecular dehydrogenation of

$[H_2B{\cdot}NMeH]_3$ on the metal centre to form $[HBNMe]_3$ is not taking place. Addition of 5/3 equivalents of *eee*-$[H_2B{\cdot}NMeH]_3$ to **22** results in very slow dehydrogenation to form $[HBNMe]_3$, which is incomplete after 141 hours (Scheme 3.11 and Figure 3.14). A doped mixture containing both the *eee*- and *eea*-$[H_2B{\cdot}NMeH]_3$ isomers (*eee*-: *eea*-,1:2) showed no difference in ratio of the isomers over the same period of reactivity indicating that both isomers have the same affinity for the dehydrocoupling process with this system.



Scheme 3.11 Onward reactivity of complex **22**. $[BAr^F{}_4]^-$ anion not shown.

Addition of $H_3B{\cdot}NMeH_2$ (20 mol%) to **22** resulted in the dehydrogenation and dehydrocoupling of the amine-borane to form a significantly larger quantity of $[HBNMe]_3$ over 141 hours compared with the reaction of **22** with same B-N concentration of $[H_2B{\cdot}NMeH]_3$. Reliable ratios based on relative integrals are however not possible due to the insolubility of $[H_2B{\cdot}NMeH]_3$ in solution thus preventing kinetic analysis. $^{31}P\{^1H\}$ NMR spectroscopy after 10 minutes reveals that at this concentration, $H_3B{\cdot}NMeH_2$ binds preferentially to the $[Rh\{PCyp_2(\eta^2\text{-}C_5H_7\}]^+$ fragment with the disappearance of the doublet assigned to the coordination of $[H_2B{\cdot}NMeH]_3$ [δ 113.1 {d, *J*(RhP) 161 Hz}] in favour of the doublet associated with the formation of bis-σ-amine-borane complex of $H_3B{\cdot}NMeH_2$ [δ 104.7, {*J*(RhP) 168 Hz}

(18)]. This is further supported by the ^{11}B NMR spectrum at this time which shows a clear triplet for the $[H_2B{\cdot}NMeH]_3$ signal [δ −4.3 {*J*(BH) 104 Hz}] and the disappearance of the broad resonance (δ −5.3) associated with the bound ligand. Crucially after 14 hours, ^{11}B NMR spectroscopy identifies that all $H_3B{\cdot}NMeH_2$ has been consumed to leave $[H_2B{\cdot}NMeH]_3$ still present (Figure 3.14). These data suggest that with this system $[H_2B{\cdot}NMeH]_3$ is not a viable kinetic intermediate for the dehydrogenation and dehydrocoupling of $H_3B{\cdot}NMeH_2$.

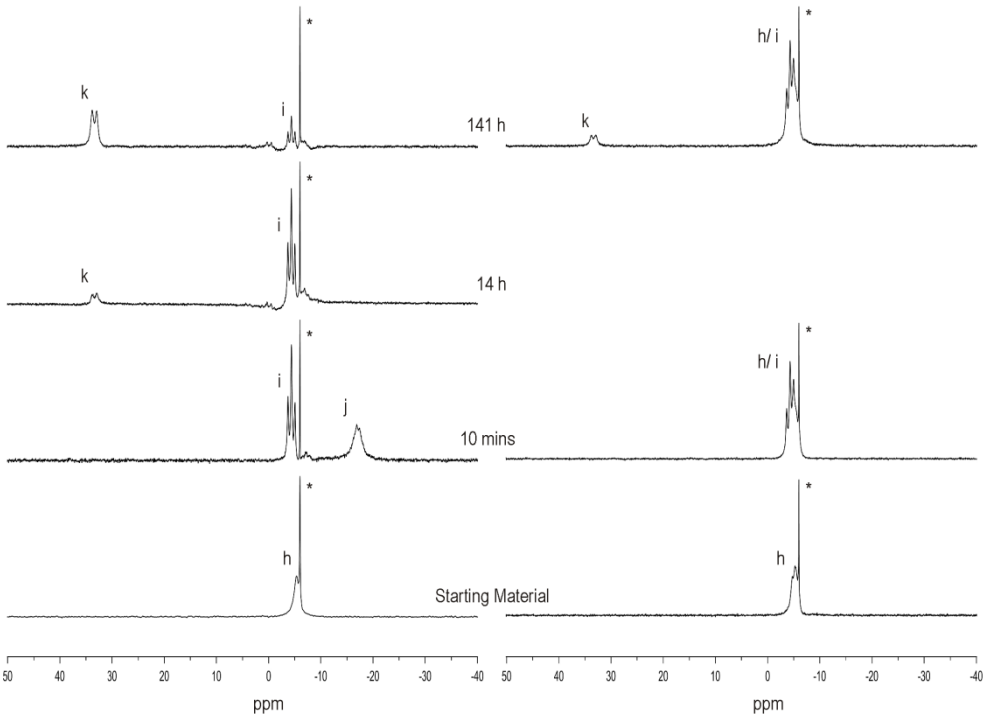


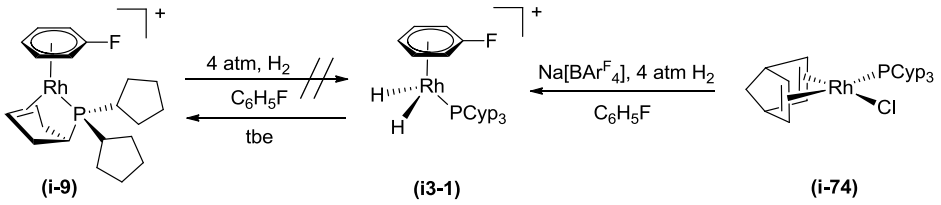
Figure 3.14 Left: ^{11}B NMR spectra (160 MHz, 1,2-$C_6H_4F_2$) of the catalytic dehydrocoupling of $H_3B{\cdot}NMeH_2$ with **22** (20 mol %, 1,2-$C_6H_4F_2$). Right: ^{11}B NMR spectra (160 MHz, 1,2-$C_6H_4F_2$) of the catalytic dehydrocoupling of $[H_2B{\cdot}NMeH]_3$ with **22** (20 mol % relative to $H_3B{\cdot}NMeH_2$, 1,2-$C_6H_4F_2$). h = **22**, i = $[H_2B{\cdot}NMeH]_3$, j = $H_3B{\cdot}NMeH_2$, k = $[HBNMe]_3$, * = $[BAr^F{}_4]^-$.

3.2.5 A view to a mechanism for the dehydrocoupling of $H_3B{\cdot}NMe_2H$ and $H_3B{\cdot}NMeH_2$ with i-9

Complexes **i-9, 17, 18, 20** and **22** are active pre-catalysts in the dehydrogenation and dehydrocoupling of $H_3B{\cdot}NMe_2H$ (**i-9**, **17**, **20**) and $H_3B{\cdot}NMeH_2$ (**i-9**, **18**, **22**), all be it relatively inefficient ones in comparison to others found in the literature (See Chapter 1, Table 1.1).[15,22,23,24,25] The ability to isolate stable amine-borane complexes based on the [Rh{$PCyp_2$(η^2-

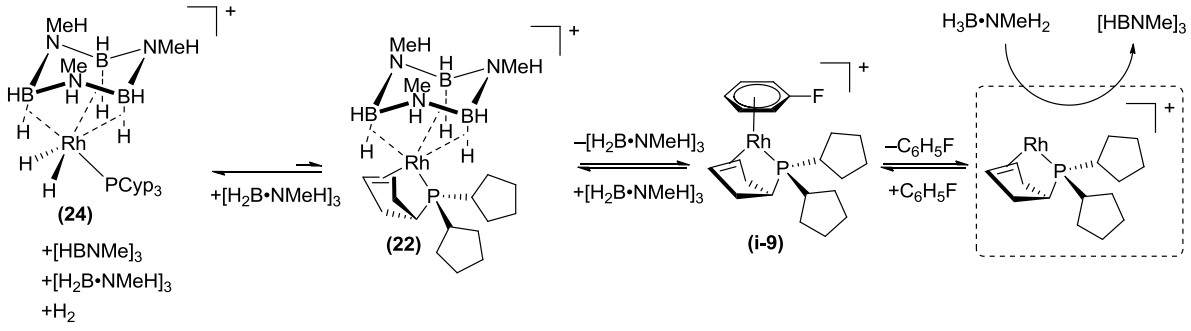
$C_5H_7)\}]^+$ fragment reflects this. The lack of observed intermediates under catalytic conditions mean a concrete mechanism is difficult to postulate with this system.

Interestingly, placing the parent complex **i-9** under hydrogen (4 atm, C_6H_5F, 77 K) does not result in the hydrogenation of the phosphine-alkene ligand (to give *e.g.* $[Rh(\eta^6\text{-}C_6H_5F)(PCyp_3)(H)_2][BAr^F{}_4]$ **(i3-1)** or the observance of any notable change by NMR spectroscopy. Clearly oxidative addition of H_2 and hydrogenation of the alkene is not favourable under these conditions. Work carried out by Douglas and Weller found that **i3-1** can be prepared directly from the addition of $Na[BAr^F{}_4]$ to $Rh(NBD)(PCyp_3)Cl$ **(i-74)** under a hydrogen atmosphere (Scheme 3.12).[26]



Scheme 3.12 **i-9** does not undergo hydrogenation to form **i3-1** although **i3-1** can be synthesised *via* an alternative route. $[BAr^F{}_4]^-$ anions not shown.

Complex **i3-1** is stable under argon and does not spontaneously undergo elimination of H_2 to permit dehydrogenation of the cyclopentyl moiety. This step requires the addition of a hydrogen acceptor (tbe) thus indicating a significant barrier to dehydrogenation in solution. Complex **i3-1** could then be expected to be observed at the end of dehydrocoupling catalysis with $H_3B{\cdot}NMe_2H$ and $H_3B{\cdot}NMeH_2$ if the $\{Rh(PCyp_3)(H)_2\}^+$ fragment was present at low amine-borane (high fluorobenzene) concentration. As the final product is **i-9** in $H_3B{\cdot}NMe_2H$ dehydrocoupling, this suggests that the phosphine-alkene fragment $[Rh\{PCyp_2(\eta^2\text{-}C_5H_7)\}]^+$ remains intact during catalysis in this system as a bidentate ligand and does not act as a transfer hydrogenation catalyst with hydrogenation of the phosphine-alkene (See Chapter 2). However during the slow dehydrogenation of $[H_2B{\cdot}NMeH]_3$ to $[HBNMe]_3$ with **i-9**, a complex assigned as $[Rh(\eta^1{:}\eta^1{:}\eta^1\text{-}H_2B{\cdot}NMeH)_3(H)_2(PCyp_3)][BAr^F{}_4]$ **(24)** is observed (Scheme 3.13).



Scheme 3.13 Formation of **24** upon addition of excess $[H_2BNMeH]_3$ to **22** and incomplete formation of $[HBNMe]_3$ hints that the dehydrocoupling of $H_3B{\cdot}NMeH_2$ by **i-9** operates by a different mechanism.

The ^1H NMR spectrum of **24** shows a broad relative integral 3H resonance at the same chemical shift as **22** with an additional relative 2H resonance further upfield [δ −18.74 (t, *J* = 20 Hz)]. The $^{31}P\{^1H\}$ NMR spectrum displays a doublet [δ 83.5 *J*(RhP) 147 Hz] with a coupling constant consistent with the formation of a cationic Rh(III) complex, *c.f.* $[Rh(\eta^6\text{-}C_6H_5F)(PCyp_3)(H)_2][BAr^F{}_4]$ **(i3-1)** (*J*(RhP) 145 Hz).[26] The ^{11}B NMR spectrum was inconclusive due to the presence of excess $[H_2B{\cdot}NMeH]_3$ and $[HBNMe]_3$ in catalysis. ESI-MS of the catalytic mixture gave a parent mass ion with an isotope pattern consistent with **24** (m/z = 472.2752 calc. 472.2842). After 141 hours in the catalysis of $[H_2B{\cdot}NMeH]_3$ with **22**, **24** is the only organometallic species observed by NMR spectroscopy. This suggests that loss of hydrogen from **24** is slow at best and that it may be forming as a preferred by-product of the reaction through a different mechanism to the dehydrocoupling of $H_3B{\cdot}NMeH_2$ to $[HBNMe]_3$ and therefore acts to trap the $\{Rh(PCyp_3)(H)_2\}^+$ fragment preventing further dehydrogenation of the cycloborazane. This fits with the absence of $[H_2B{\cdot}NMeH]_3$ in catalysis with $H_3B{\cdot}NMeH_2$ and it therefore not being a kinetically relevant intermediate.

The absence of $H_3B{\cdot}NMe_2BH_2{\cdot}NMe_2H$ and $[H_2B{\cdot}NMeH]_3$ in the dehydrogenation and dehydrocoupling catalysis of $H_3B{\cdot}NMe_2H$ and $H_3B{\cdot}NMeH_2$ respectively with **i-9** is intriguing given that they are observed as intermediates in other related systems.[10,14,15,19,23] A recent publication by Manners has found that $[\{FeCp(CO)_2\}_2]$ **(i-130)** is inactive to the

dehydrogenation and dehydrocoupling of $H_3B{\cdot}NMe_2BH_2{\cdot}NMe_2H$ despite being an active catalyst for the dehydrocoupling of $H_3B{\cdot}NMe_2H$ to $[H_2BNMe_2]_2$.[16] The fact that the complexes involving coordination of $H_3B{\cdot}NMe_2BH_2{\cdot}NMe_2H$ and $[H_2B{\cdot}NMeH]_3$ (**20** and **22**) are not observed in catalysis of the parent amine-boranes suggest that they are not formed in any significant quantity. This is further ratified by their independent dehydrocoupling taking longer in each case. $H_3B{\cdot}NMe_2BH_2{\cdot}NMe_2H$ however appears a kinetically viable intermediate on the timescale of catalysis while $[H_2B{\cdot}NMeH]_3$ does not. The presence of small amounts of the products of B-N bond cleavage in the dehydrocoupling of $H_3B{\cdot}NMe_2H$ with **i-9/ 17/ 20** also tentatively support the role of $H_3B{\cdot}NMe_2BH_2{\cdot}NMe_2H$ as an intermediate at low concentration.

3.3 Conclusions

The $[Rh\{PR_2(\eta^2\text{-}C_5H_7)\}]^+$ (R = Cyp, ^{i}Pr) fragment is a low coordinate 12-electron motif which has been shown to coordinate two molecules of amine-borane in an unprecedented coordination mode. Complex **18** is the first fully characterised example of $H_3B{\cdot}NMeH_2$ coordination to a transition metal. Complexes **17** and **18** show evidence for a hydrogen bonding interaction between the amine-borane ligands however this interaction is not compulsory for this coordination mode to be adopted given the formation of **19**. **17** and **18** proceed slowly to give $[H_2BNMe_2]_2$ and $[HBNMe]_3$ respectively in the absence of excess amine-borane, suggesting they are potential intermediates in the mechanism. Coordination of $H_3B{\cdot}NMe_2BH_2{\cdot}NMe_2H$ and $[H_2B{\cdot}NMeH]_3$ to the $[Rh\{PR_2(\eta^2\text{-}C_5H_7)\}]^+$ fragment resulted in stable complexes **20-23**, in contrast to **17** and **18**. Catalytic dehydrocoupling of these substrates using the $[Rh\{PR_2(\eta^2\text{-}C_5H_7)\}]^+$ fragment results in the formation of $[H_2BNMe_2]_2$ and $[HBNMe]_3$ respectively; $H_3B{\cdot}NMe_2BH_2{\cdot}NMe_2H$ at a rate which is consistent with it being a viable B-N intermediate in catalytic dehydrocoupling of $H_3B{\cdot}NMe_2H$ and $[H_2B{\cdot}NMeH]_3$ at a rate which is not kinetically relevant to the dehydrocoupling of $H_3B{\cdot}NMeH_2$.

3.4 References

[1] Douglas, T. M.; Chaplin, A. B.; Weller, A. S.; *J. Am. Chem. Soc.* **2008,** *130,* 14432-14433.
[2] Kawano, Y.; Hashiva, M.; Shimoi, M. *Organometallics* **2006,** *25,* 4420-4426.
[3] Klooster, W. T.; Koetzle, T. F.; Siegbahn, P. E. M.; Richardson, T. B.; Crabtree, R. H. *J. Am. Chem. Soc.* **1999,** *121,* 6337-6343.
[4] Aldridge, S.; Downs, A. J.; Tang, C. Y.; Parsons, S.; Clarke, M. C.; Johnstone, R. D. L.; Robertson, H. E.; Rankin, D. W. H.; Wann, D. A. *J. Am. Chem. Soc.* **2009,** *131,* 2231-2243.
[5] Chaplin, A. B.; Weller, A. S. *Angew. Chem. Int. Ed.* **2010,** *49,* 581-584.
[6] Chaplin, A. B.; Poblador-Bahamonde, A. I.; Sparkes, H. A.; Howard, J. A. K.; Macgregor, S. A.; Weller, A. S. *Chem. Commun.* **2009,** 244-246.
[7] Rifat, A.; Kociok-Köhn, G.; Steed, J. W.; Weller, A. S. *Organometallics* **2004,** *23,* 428-432.
[8] Chaplin, A. B.; Weller, A. S. *Inorg. Chem.* **2010,** *49,* 1111-1121.
[9] Luo, Y.; Ohno, K. *Organometallics* **2007,** *26,* 3597-3600.
[10] Sloan, M. E.; Staubitz, A.; Clark, T. J.; Russell, C. A.; Lloyd-Jones, G. C.; Manners, I. *J. Am. Chem. Soc.* **2010,** *132,* 3831-3841.
[11] Hill, M. S.; Hodgson, M.; Liptrot, D. J.; Mahon, M. J. *Dalton. Trans.* **2011,** *ASAP.*
[12] Jaska, C. A.; Manners, I. *J. Am. Chem. Soc.* **2004,** *126,* 9776-9785.
[13] Widegren, J. A.; Finke, R. G. *J. Mol. Catal. A: Chem.* **2003,** *198,* 317-341.
[14] Douglas, T. M.; Chaplin, A. B.; Weller, A. S.; Hall, M. B.; Yang, X. *J. Am. Chem. Soc.* **2009,** *131,* 15440.
[15] Friedrich, A.; Drees, M.; Schneider, S. *Chem. Eur. J.* **2009,** *15,* 10339-10342.
[16] Vance, J. R.; Robertson, A. P. M.; Lee, K.; Manners, I.; *Chem. Eur. J.* **2011,** *17,* 4099-4103.
[17] Jaska, C. A.; Temple, K.; Lough, A. J.; Manners, I. *J. Am. Chem. Soc.* **2003,** *125,* 9424-9434. and references therein.
[18] Douglas, T. M.; Le Nôtre, J. M.; Brayshaw, S. K.; Frost, C. G.; Weller, A. S. *Chem. Commun.* **2006,** 3408-3410.
[19] Stevens, C. J.; Dallanegra, R.; Chaplin, A. B.; Weller, A. S.; Macgregor, S. A.; Ward, B.; McKay, D.; Alcaraz, G.; Sabo-Etienne, S. *Chem. Eur. J.* **2011,** *17,* 3011-3020.
[20] Narula, C. K.; Janik, J. F.; Duesler, E. N.; Paine, R. T.; Schaeffer, R. *Inorg. Chem.* **1986,** *25,* 3346-3349.
[21] Gaines, D. F.; Hildebrandt, S. J. *Inorg. Chem.* **1978,** *17,* 794-806.
[22] Sloan, M. E.; Clark, T. J.; Manners, I. *Inorg. Chem.* **2009,** *48,* 2429-2435.
[23] Miller, A. J. M.; Bercaw, J. E. *Chem. Commun.* **2010,** *46,* 1709-1711.
[24] Pun, D.; Lobkovsky, E.; Chirik, P. J. *Chem. Commun.* **2007,** 3297-3299.
[25] Vogt, M.; de Bruin, B.; Berke, H.; Trincado, M.; Grützmacher, H. *Chem. Sci.* **2011,** *2,* 721-723.
[26] Douglas, T. M.; Brayshaw, S. K.; Dallanegra, R.; Macgregor, S. A.; Moxham, G. L.;Kociok-Köhn, G.; Vadivelu, P.; Weller, A. S.; Wondimagegn, T. *Chem. Eur. J.* **2008,** *14,* 1008-1022.

4 DEHYDROCOUPLING OF AMINE-BORANES WITH THE {Rh(diphosphine)}$^+$ FRAGMENT

4.1 Introduction

From Chapter 3 it is evident that the [Rh{$PR_2(\eta^2\text{-}C_5H_7)$}]$^+$ (R = Cyp, ^{i}Pr) fragment is capable of the dehydrogenation and dehydrocoupling of the amine-boranes $H_3B{\cdot}NMe_2H$ and $H_3B{\cdot}NMeH_2$ to their respective products all be it at a very slow rates and high catalyst loadings. To further investigate the catalytic ability of low coordinate cationic Rh complexes, chelating diphosphines were targeted as an alternative chelating ligand to the phosphine-alkene motif. The bite angle Rh-P-C of the PAL in [Rh($Ph_2P(CH_2)_2PPh_2$){$PCyp_2(\eta^2\text{-}C_5H_7)$}][$BAr^F_4$] **(i-91)** is 84°, which is similar to that reported for the NBA of the chelating diphosphine, dppe (86°).[1] The steric profile at the metal centre is however very different for the two motifs (Figure 4.1).

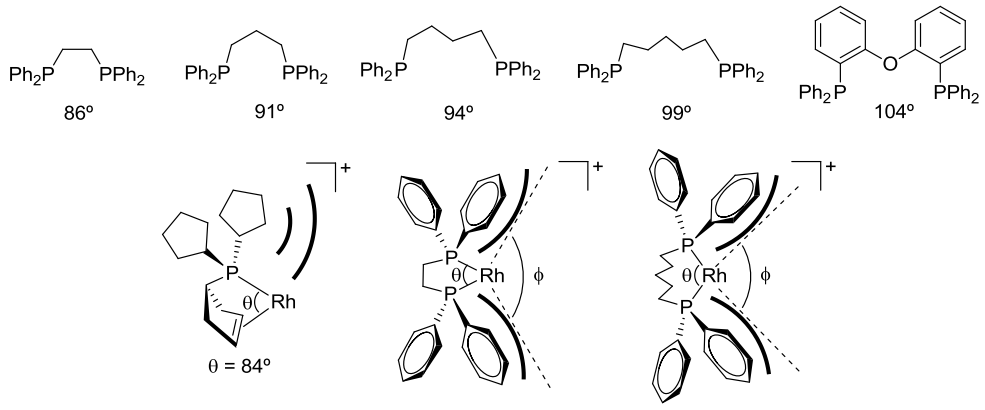


Figure 4.1 (top) NBAs of diphosphine ligands dppe, dpp_{prop}, dppb, dpp_{pent} and DPEphos. (bottom) Bite angle made by the phosphine-alkene and the Rh centre (θ) along with Rh{$PCyp_2(\eta^2\text{-}C_5H_7)$}/ dppe/ dpp_{pent} pocket angles (ϕ). Anions not shown.

Studies of the effects of changing the bite angle of chelating diphosphines in catalysis are abundant in the literature, *e.g.* in hydroformylation,[2,3,4] hydrocyanation[5,6] and cross-coupling reactions,[7,8,9] but not in amine-borane dehydrogenation and dehydrocoupling catalysis. In order to observe the effect of the bite angle it is necessary to keep the electronic and steric

components of the system the same as these have repeatedly been shown to cause remarkable differences in both rate and selectivity.[10] Sequentially changing the ligand in this way is also likely to affect the accessibility of the metal centre to the coordination of substrate, which is best described by the pocket angle (Chapter 1, section 1.21). Increasing the bite angle, decreases the pocket angle and makes the coordination of substrate more difficult. A larger bite angle (smaller pocket angle) could also sterically favour reductive elimination over a smaller bite angle. With these ideas in mind, this chapter describes a comparative study of amine-borane dehydrocoupling catalysis with a series of Rh(I) chelating diphosphine complexes whose diphosphine backbone chain length differs by a CH_2 unit; dppe, dpp_{prop}, dppb and dpp_{pent} (DPEphos is also studied for comparative purposes with dpp_{pent} and its ability to act as a hemilabile ligand) and therefore increase in NBA; dppe < dpp_{prop} < dppb < dpp_{pent} ~ DPEphos (Figure 4.1).

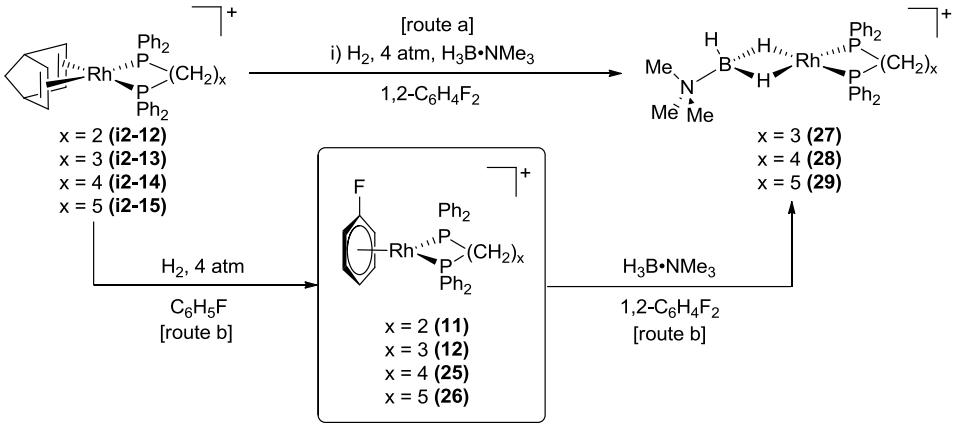
As well as a potential changes in the rate of dehydrogenation and dehydrocoupling using each of the ligands, amine-borane dehydrocoupling catalysis could show differences in product selectivity. As discussed in previous Chapters (1 and 3), the product of dehydrogenation and dehydrocoupling of $H_3B{\cdot}NMe_2H$ is exclusively $[H_2BNMe_2]_2$. However, that of $H_3B{\cdot}NMeH_2$ has previously been shown to form methylborazine or poly(*N*-methylaminoborane) depending on the catalyst and reaction conditions. The chelate backbone length, bite angle and pocket angle of the pre-catalysts discussed here may therefore effect the selective formation of these species.

4.2 Results and discussion

4.2.1 Cationic Rh(I) diphosphine $H_3B{\cdot}NMe_3$ complexes

To investigate the catalytic activity of Rh complexes containing a series of chelating diphosphines it was anticipated that in first isolating and fully characterising a series of bound $H_3B{\cdot}NMe_3$ complexes, data regarding the strength of amine-borane coordination strength could

be gathered, which would help to fine tune catalyst design. As discussed in Chapter 3, $H_3B{\cdot}NMe_3$ (TMAB) is an ideal ligand for this purpose as it mimics the proposed interaction of $H_3B{\cdot}NMe_2H$ but cannot undergo dehydrocoupling as it lacks a N-H group. Efforts to synthesise cationic Rh(I) chelating diphosphine $H_3B{\cdot}NMe_3$ complexes returned us to a similar route used for $[Rh(Ph_2P(CH_2)_3PPh_2)\{SCyp(\eta^2\text{-}C_5H_7)\}][BAr^F{}_4]$ **(14)** (Chapter 2). *In situ* hydrogenation (4 atm) of $[Rh(NBD)(Ph_2P(CH_2)_xPPh_2)][BAr^F{}_4]$ {x = 3 **(i2-13)**; 4 **(i2-14)**; 5 **(i2-15)**} and $H_3B{\cdot}NMe_3$ (1 eq., 1,2-$C_6H_4F_2$, 298 K) immediately resulted in a vivid change in colour of the solution from yellow orange to red **(27)**, or violet **(28/ 29)** (Scheme 4.1) and the formation of $[Rh(Ph_2P(CH_2)_xPPh_2)(\eta^2\text{-}H_3B{\cdot}NMe_3)][BAr^F{}_4]$ {x = 3 **(27)**; 4 **(28)**; 5 **(29)**}. No reaction was observed with under these conditions with precursor $[Rh(NBD)(Ph_2P(CH_2)_2PPh_2)][BAr^F{}_4]$ **(i2-12)**.



Scheme 4.1 Two routes for the synthesis of complexes **27-29**. $[BAr^F{}_4]^-$ anions not shown.

The ^{1}H NMR spectra for complexes **27-29** each showed a broad signal (δ ~ 1 to −2) which was assigned to the Rh-*H*$_3$B·NMe$_3$ interaction. No evidence for a hydride ligand (δ 0 to −30) was observed in the upfield region. In addition, a new singlet methyl environment shifted downfield from free $H_3B{\cdot}NMe_3$ (δ 2.63) was observed at δ 2.70, *c.f.* $[Rh(\eta^1\text{-}H_3B{\cdot}NMe_3)(\eta^2\text{-}H_3B{\cdot}NMe_3)\{PCyp_2(\eta^2\text{-}C_5H_7)\}][BAr^F{}_4]$ **(19)** δ 2.60 (s) (Chapter 3). As a result of the presence of a small excess of $H_3B{\cdot}NMe_3$ in solution, the integral and precise positioning of these broad signals at this stage was not reliable due to the rapid exchange between free and bound ligand

on the NMR timescale. As a result, the ^{11}B NMR spectra were equally uninformative. $^{31}P\{^{1}H\}$ NMR spectroscopy however showed the quantitative formation of a new Rh(I) species in each case [d, J(RhP) ~ 170 Hz]. Degassing each solution showed no change in the NMR spectra except for the disappearance of dissolved hydrogen [δ^{1}H +4.6]. Attempted isolation of these new species by recrystallisation at room temperature and 255 K were unsuccessful and resulted in oils. An improved synthetic procedure was then developed (route b, Scheme 4.1)

The C_6H_5F precursors $[Rh(\eta^6\text{-}C_6H_5F)(Ph_2P(CH_2)_xPPh_2)][BAr^F{}_4]$ {x = 2 **(11)**; 3 **(12)**; 4 **(25)**; 5 **(26)**} were prepared by hydrogenating (4 atm) complexes **i2-12-15** in C_6H_5F solvent and were isolated in excellent yield upon removal of the hydrogen atmosphere and precipitation into stirring hexanes. **11, 12, 25** and **26** were characterised by NMR spectroscopy, ESI-MS and microanalysis. Signals indicative of coordinated arene resonances appear between δ 5.7 – 5.0 and are similar to those already seen for $[Rh(\eta^6\text{-}C_6H_5F)\{PR_2(\eta^2\text{-}C_5H_7)\}][BAr^F{}_4]$ [{R = Cyp **(i-9)** δ 6.07 (m, 4H), 5.45 (m, 1H)}; {R = ^{i}Pr **(i-9a)** δ 6.09 (m, 4H), 5.46 (m, 1H)}].[1] The resonances for the coordinated arene of **11** are not unambiguously observed due to the C_6H_5F solvent peak (δ 7.31 – 6.70) reflecting a more weakly bound C_6H_5F ligand on decreasing the bite angle of the chelating diphosphine ligand. The $^{31}P\{^{1}H\}$ spectra of **11**, **12**, **25** and **26** each show a doublet (J ~ 200 Hz), as presumably the ^{19}F coupling is too small to be observed, *c.f.* **i-9** J(FP) 4 Hz; **i-9a** J(FP) 3 Hz. The formation of **11** was further substantiated by ESI-MS and NMR spectroscopy. Firstly, dissolving the isolated complex in d_6-acetone yielded a 1:1 ratio of free C_6H_5F and the $[BAr^F{}_4]^-$ anion, helping to corroborate the coordination of C_6H_5F, as well as a doublet [δ 78.9 {J(RhP) = 201 Hz}] by $^{31}P\{^{1}H\}$ NMR spectroscopy consistent with the formation of $[Rh(Ph_2P(CH_2)_2PPh_2)(acetone)_2][BAr^F{}_4]$.[11] Additionally ESI-MS of **11** showed a parent mass ion corresponding to its formation (m/z = 597.1083, calc. 597.0778). Crystals suitable for X-ray diffraction were obtained for **12**, and the structure of the cation is shown in Figure 4.2.

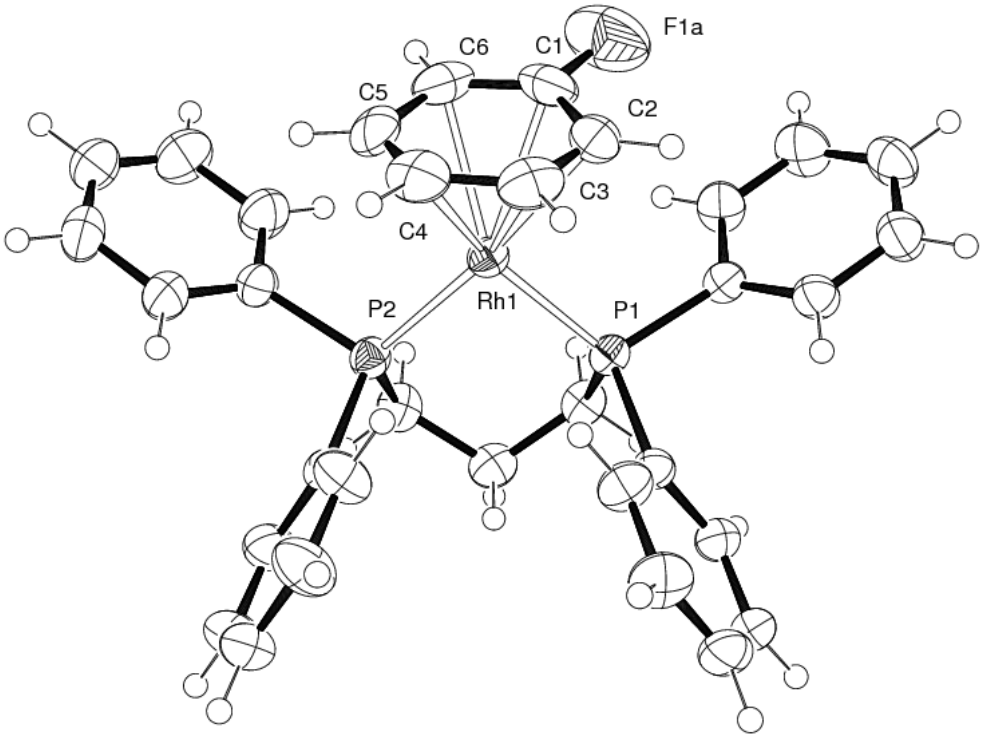


Figure 4.2 Solid-state structure of the cationic portion of **12**. Thermal ellipsoids are presented at the 50 % probability level. Selected bond lengths [Å] and angles [°]: Rh-P1 2.2266(9), Rh1-P2 2.2343(9), Rh-C_{arene} 2.292(4) – 2.377(4); P1-Rh1-P2 90.07(3).

The P1-Rh-P2 bond angle of **12** (90.07(3)°) is consistent with a *cis*-geometry of the diphosphine at the metal centre and is clearly favoured given the closeness of this angle to the NBA of dpp_{prop} (91°).[10] The η^6-capped Rh atom shares comparable Rh-C bond lengths to that seen for $[Rh(\eta^6\text{-}C_6H_5F)\{PCyp_2(\eta^2\text{-}C_5H_7)\}][BAr^F{}_4]$ **(i-9)** and $[Rh(\eta^6\text{-}C_6H_5F)(P^iBu_3)_2][BAr^F{}_4]$ **(i-166)**: [{Rh-C_{arene} 2.292(4) – 2.377(4) Å **(i-9)**}; {Rh-C_{arene} 2.299(9) – 2.411(7) Å **(i-166)**} {Rh-C_{arene} 2.244(2) – 2.337(3) Å **(12)**}].[1,12]

Stoichiometric addition of $H_3B{\cdot}NMe_3$ to complexes **12**, **25** and **26** gave **27-29** respectively in quantitative yield by NMR spectroscopy (Scheme 4.1). Recrystallisation of these species in the glove box at 238 K gave material from which full characterisation could be carried out in the absence of excess amine-borane (Table 4.1). Each complex displays a relative 3H signal assigned to the rapidly exchanging bridging and terminal H_3B hydrogen atoms as well as a

singlet (9H) assigned to the equivalent methyl groups of the $H_3B{\cdot}N\mathit{Me}_3$ ligand. Exchange of the H_3B atoms probably occurs *via* an η^2- η^1- η^2 process as has been computationally calculated by Shimoi and co-workers with $[M(CO)_5(\eta^1\text{-}H_3B{\cdot}LMe_3]$ (M = Cr/ W; L = N/ P **(i-135/1 a/b)**) complexes[13] and experimentally by Weller and co-workers in Ru[14] and Mn[15] systems with phosphine-boranes that open and close on addition of an external Lewis base. Addition of $H_3B{\cdot}NMe_3$ to **11** resulted in no reaction, presumably the limit of coordination is reached with the narrow NBA of this ligand (β = 86°). Work within our group has recently suggested an explanation for the observation that Rh(I) bis-phosphine complexes containing phosphines that force large P-Rh-P angles have stronger interactions with coordinated $H_3B{\cdot}NMe_3$.[16] A consequence of a more *trans*-like P-Rh-P fragment is to enforce a lowering in energy of the metal $1b_1$ orbital, which means it has a better interaction with the B-H bond of the amine-borane (as illustrated in a qualitative Walsh diagram, Figure 4.3). Those bis-phosphine complexes with smaller bite angles at the metal thus show a weaker interaction as this metal orbital is now much higher in energy resulting in a poorer orbital match. This argument fits well for the lack of coordination of $H_3B{\cdot}NMe_3$ with $[Rh(Ph_2P(CH_2)_2PPh_2)(\eta^6\text{-}C_6H_5F)][BAr^F{}_4]$ **(11)** as this chelating diphosphine ligand would be predicted to have the smallest P1-Rh-P2 bite angle given the NBA of the free ligand (86°).

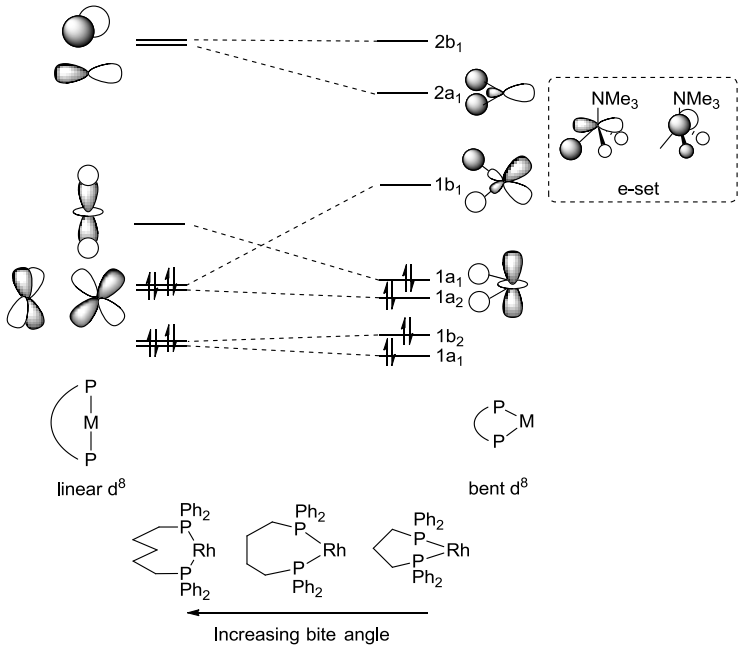


Figure 4.3 Qualitative Walsh diagram of d^8 ML_2 fragments.[16] The e-set orbitals of the $H_3B{\cdot}NMe_3$ ligand shown interact with the metal $1b_1$ and $2a_1$ orbitals which determines the strength of interaction.

The solid-state structures of **27** (Figure 4.4) and **29** (Figure 4.5) show that both have *pseudo*-square planar geometrics with $H_3B{\cdot}NMe_3$ bonding to the metal through two 3c-2e Rh-H-B bonds. The effect of the increasing length of the ligand backbone correlates with a wider P-Rh-P angle {*viz.* 98.18(3)° **(29)**} *vs.* {91.14(3)° **(27)**}. The Rh-B distances of **27** and **29** are the same within error and are comparable with bis-phosphine complexes $[Rh(PR_3)_2(\eta^2\text{-}H_3B{\cdot}NMe_3)][BAr^F{}_4]$ [{R = ^{i}Bu, 2.180(4) Å **(i-137)**}; {R = ^{i}Pr, 2.137(6) Å **(i-137a)**}; {2.198(3) Å (**27**)}; {2.199(3) Å **(29)**}],[16,20] although the Rh-B distances of **27** and **29** lie nearer the reported values for **i-137** than **i-137a**. **i-137** has a smaller P-Rh-P angle (97.35°(4)) *vs.* **i-137a** (106.8°(4)), which is consistent with a weaker interaction (longer Rh-B distance) on decreasing P-Rh-P angle matching the hypothesis for **27** and **29**.

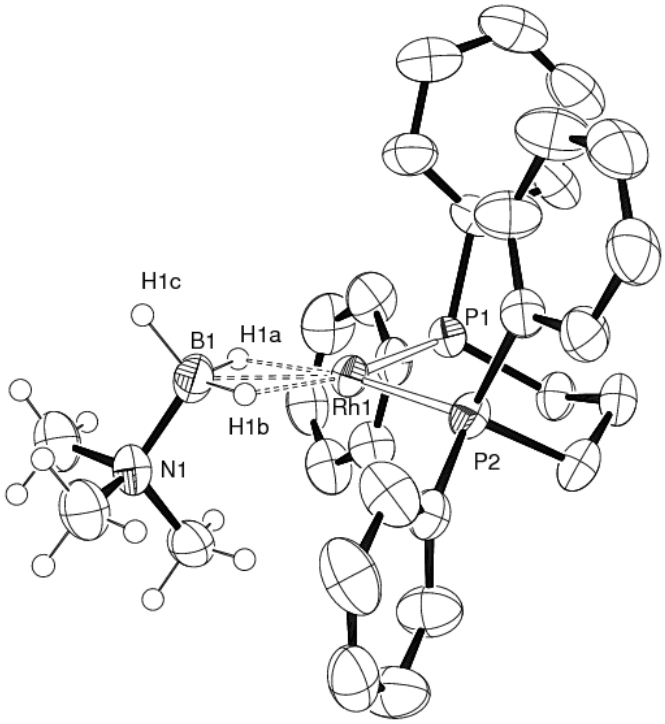


Figure 4.4 Solid-state structure of the cationic portion of **27**. Selected hydrogen atoms are omitted for clarity. Thermal ellipsoids are presented at the 50 % probability level. Selected bond lengths [Å] and angles [°]: Rh1-P2 2.1986(9), Rh1-P1 2.1998(9), Rh1-B1 2.199(4), Rh1-H1a 1.76 (avg. calc.), Rh1-H1b 1.84 (avg. calc.), B1-N1 1.592(7), B1-H1 1.167 (calc.); P2-Rh1-P1 91.14(3), Rh1-B1-N1 124.7(5).

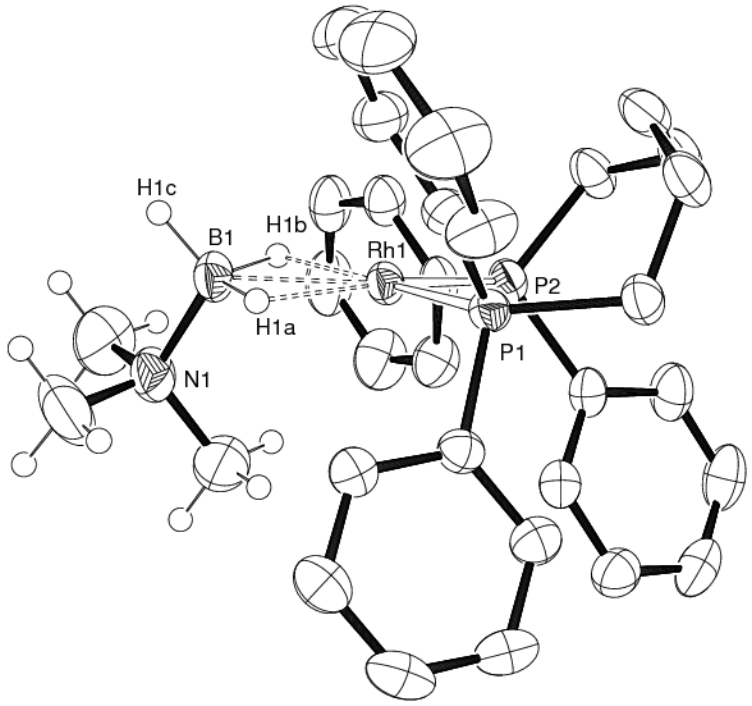
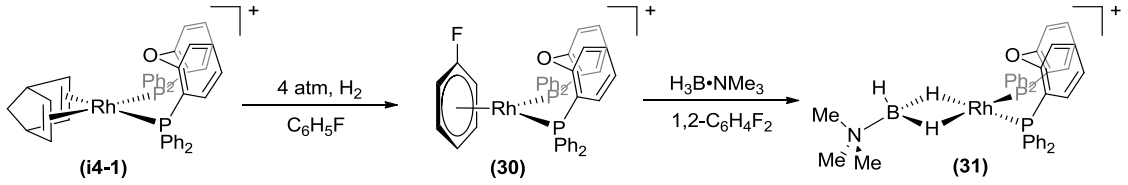


Figure 4.5 Solid-state structure of the cationic portion of **29**. Selected hydrogen atoms are omitted for clarity. Thermal ellipsoids are presented at the 50 % probability level. Selected bond lengths [Å] and angles [°]: Rh1-P2 2.2116(8), Rh1-P1 2.2166(7), Rh1-B1 2.189(3), Rh1-H1a 1.78(3), Rh1-H1b 1.81(3), B1-N1 1.585(4), B1-H1a 1.22(2), B1-H1b 1.20(2), B1-H1c 1.07(3); P2-Rh1-P1 98.18(3), Rh1-B1-N1 121.0(2).

The cationic Rh(I) DPEphos-fluoroarene complex, [Rh($\kappa^2_{(PP)}$-DPEphos)(η^6-C_6H_5F)][BAr^F_4] **(30)** could not be isolated in the same manner as **11**, **12**, **25** and **26** from its norbornadiene precursor complex [Rh(NBD)($\kappa^2_{(PP)}$-DPEphos)][BAr^F_4] **(i4-1)** (Scheme 4.2), despite repeated attempts. However it could be readily generated *in situ* as evidenced by ^{1}H and ^{31}P{^{1}H} NMR spectroscopy. The ^{1}H NMR spectrum of **30** shows three signals in a 2:2:1 ratio (δ +5.47, +5.39, +5.11 respectively) for the coordinated C_6H_5F ligand whilst by ^{31}P{^{1}H} NMR spectroscopy a doublet is observed [δ 31.8 {*J*(RhP) 220 Hz}]. ^{19}F coupling to phosphorus is again presumably too small to be observed. ESI-MS also showed a parent mass ion for {Rh(DPEphos)(C_6H_5F)}$^+$ m/z = 737.1435, (calc. 737.1040). Stoichiometric addition of $H_3B{\cdot}NMe_3$ to a crude sample of this species (oil) afforded the expected η^2-$H_3B{\cdot}NMe_3$ coordinated Rh(I) complex **(31)** from which crystals were grown and a solid-state structure was obtained (Figure 4.6).



Scheme 4.2 Synthesis of complexes **30** and **31**. $[BAr^F{}_4]^-$ anions not shown.

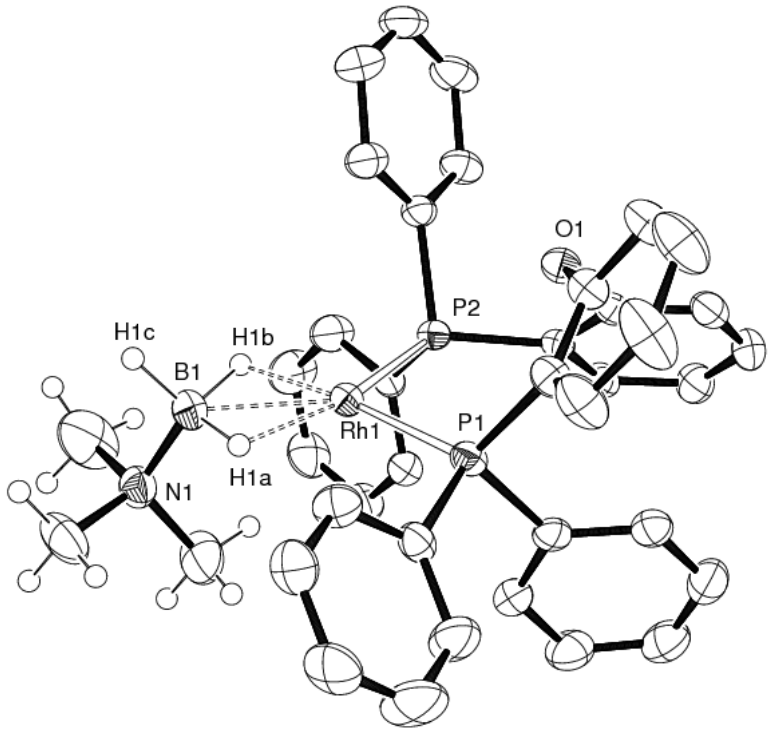


Figure 4.6 Solid-state structure of the cationic portion of **31**. Selected hydrogen atoms are omitted for clarity. Thermal ellipsoids are presented at the 50 % probability level. Selected bond lengths [Å] and angles [°]: Rh1-P2 2.2055(9), Rh1-P1 2.2334(9), Rh1-B1 2.205(4), Rh1-O1 3.547(2), Rh1-H1a 1.81(4), Rh1-H1b 1.78(3), B1-N1 1.573(5), B1-H1a 1.22(3), B1-H1b 1.22(3), B1-H1c 1.15(4); P2-Rh1-P1 96.76(3), Rh1-B1-N1 123.2(3).

The structural metrics of **31** show a similar square planar Rh(I) species with the same Rh-B bond distance within error to those for **27** and **29** (Table 4.1). Interestingly, the P1-Rh-P2 angle is smaller than that for **29** (with the dpp_{pent} ligand) despite DPEphos having a larger NBA (Table 4.1). $[Rh(\kappa^2{}_{(PP)}\text{-DPEphos})(acetone)_2][\textit{closo}\text{-}C_6B_{11}H_6Cl_6]$ **(i-42)** also shares a similar P-Rh-P angle to **31** {96.23(2) **(i-42)** *vs.* 96.76(3) **(31)**}.[17] This perhaps reflects the superior ability for the DPEphos ligand to contract into a more compact formation on coordination to the metal.

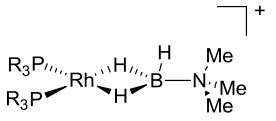
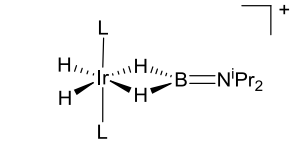
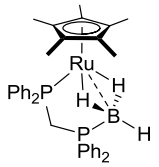
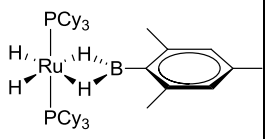
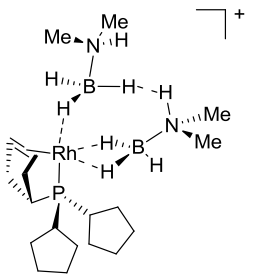
The Rh-O distance for **31** is 3.547(2) Å confirming the lack of coordination between the two atoms.

Table 4.1 Selected bond distances and NMR spectroscopy data for complexes of the generic formula [Rh(η^2-$H_3B{\cdot}NMe_3$)(diphosphine)][$BAr^F{}_4$]: [a] β = NBA, from references.[10] [b] at 298 K, in CD_2Cl_2 solution, Frequencies- ^1H (500 MHz), ^{11}B (160 MHz). [c] Free $H_3B{\cdot}NMe_3$: δ(^1H) 2.27 (s); δ(^{11}B) −7.3 [q, *J*(BH) 98].

Ligand	#	β/ ° [a]	P-Rh-P	Rh-B/ Å	Rh-P/ Å	δ(^1H)[b]	δ(^{11}B)[b]
dppe		86		not formed		-	-
dpp_{prop}	**(27)**	91	91.14(3)	2.199(3)	2.1992(9)	−1.30	+16.4 (v br)
dppb	**(28)**	96	n/a	n/a	n/a	−1.66	+18.3
dpp_{pent}	**(29)**	99	98.18(3)	2.189(3)	2.2141(8)	−1.99	+20.3
DPEphos	**(31)**	104	96.76(3)	2.205(4)	2.2194(9)	−2.00	+20.6
$H_3B{\cdot}NMe_3$		-	-	-	-	+2.27[c]	−7.3

Although the bond distances for **27**, **29** and **31** are the same within error in the solid-state, in solution the difference in Rh-H_3B interaction strength, as measured by changes in chemical shift on coordination of the $H_3B{\cdot}NMe_3$ ligand, is remarkable. Increasing the backbone chain length of the diphosphine from x = 3 [**(27)**, β = 91°] to x = 5 [**(29)**, β = 99°] gives rise to a stronger Rh-H_3B interaction as measured from the lower frequency shift of the Rh-*H*-B resonance in the ^1H NMR spectra and the high frequency shift of the broad BH_3 resonance in the ^{11}B NMR spectra (Table 4.1). This difference in chemical shift is characteristic of a change in strength of the Rh···H_3B interaction as has been illustrated previously.[14,18] A similar effect is seen for the ^1H and ^{11}B chemical shifts of the BH_2 resonance of aminoboranes upon binding to a transition metal (Table 4.2).

Table 4.2 Effect of coordination of a $H_3B{\cdot}L$ or $H_2B{\cdot}L$ fragment to a transition metal on the observed ^1H and ^{11}B chemical shifts. $[BAr^F{}_4]^-$ anions for cationic species not shown.

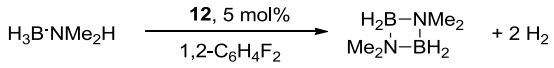
Free Ligand	δ ^{11}B	δ ^1H	Metal bound ligand	δ ^{11}B	δ ^1H	Solvent	Ref.
$H_3B{\bullet}NMe_3$	− 7.3	+ 2.27	 R = ^{i}Bu **(i-132)**; R = ^{i}Pr **(i-132a)**	**(i-137)**: + 23.1 **(i-137a)**: + 28.8	− 3.15 − 3.09	1,2-$C_6H_4F_2$	20 16
$H_2B{=}N^iPr_2$	+ 35.0	+ 4.32	 L = PCy_3 **(i4-2)** ; L = IMes **(i-182)**	**(i4-2)**: + 49 **(i-182)**: + 37.9	− 6.58 − 1.40	C_6H_5F	34 41
$H_3B{\bullet}PPh_2CH_2PPh_2$	− 40	+ 0.95	 **(i4-3)**	**(i4-3)**: + 15.6	− 3.41	CD_2Cl_2	14
$H_2B{\bullet}C_6H_2Me_3$	+ 7		 **(i-23)**	**(i-23):** + 35.8	− 5.90	C_7D_8	42
$H_3B{\bullet}NMe_2H$ $H_3B{\bullet}NMeH_2$	− 12.8 − 17.0	+ 2.13 + 2.15	 **(17/ 18)**	**(17)**: − 12.2 **(18)**: − 17.0	− 0.64 − 0.61	CD_2Cl_2	

As shown in Table 4.2, the ^{11}B signals for the related $[Rh(PR_3)_2(\eta^2\text{-}H_3B{\cdot}NMe_3)][BAr^F{}_4]$ complexes (R = ^{i}Bu **(i-137)**; ^{i}Pr **(i-137a)**) reside further to high field at δ +23.1 **(i-137)** and +28.8 **(i-137a)** than free ligand (δ − 7.3).[16,20] The ^1H signals for H_3B resonances of complexes **27-29** and **31** also lie approximately 1.5 ppm to high field compared to **i-137** and **i-137a** (*e.g.* δ −1.66 **(28)** *vs.* −3.15 **(i-137)** and −3.09 **(i-137a)**). At a first glance, the observed difference in ^1H and ^{11}B chemical shifts between **29** and **31** is perhaps not as great as expected given the value of β (NBA) for the two ligands however the P-Rh-P angles obtained from the solid-state structures

(98.18°(3) **(29)**, 96.76°(3) **(31)**) indicate that the bite angle of the two complexes is in fact similar. That both **29** and **31** show the largest P-Rh-P angles fits the trend of having the strongest Rh···H_3B interaction. Cooling complexes **27-29** to 200 K in solution did not halt the fluxional process making the H_3B signals equivalent on the NMR timescale, but did result in their substantial broadening at low temperature. For **i-137** and **i-137a** this fluxional process can be halted with the broad 3H $H_3B{\cdot}NMe_3$ resonances in their ^{1}H NMR spectra at 298 K [δ −2.12 **(i-137)**; −3.09 **(i-137a)** yielding a 2H signal [δ −5.55 **(i-137)**; −6.91 **(i-137a)**] for the Rh-*H*-B resonances and a 1H signal [δ unobserved **(i-137)**, +4.43 **(i-137a)**] for the unbound terminal B-H at 190 K.[16,20] All these factors are consistent with a stronger interaction with the amine-borane for **i-137** and **i-137a** compared to that for the chelating diphosphine complexes **27-29**.

4.2.2 Reactivity of 11, 12, 25 and 26 in the catalytic dehydrocoupling of $H_3B{\cdot}NMe_2H$

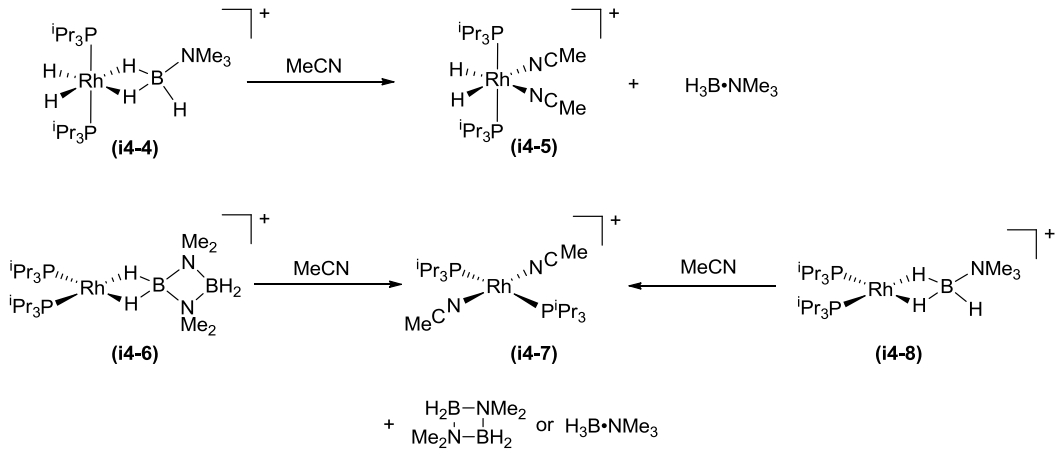
Given the apparent change in Rh···H_3B bond strength upon increasing diphosphine chain length, each of the four fluoroarene precursor complexes **11**, **12**, **25** and **26** were tested to see if these trends would extend to their catalytic activity in dehydrogenation and dehydrocoupling of $H_3B{\cdot}NMe_2H$ to $[H_2BNMe_2]_2$ (Scheme 4.3).



Scheme 4.3 Initial catalytic conditions using complex **12**.

A three-necked Schlenk flask with a stirrer bar was attached to a source of argon at constant flow and a mineral oil bubbler to provide an open system for catalysis. The pre-catalyst was added to the Schlenk flask followed by a stock solution of $H_3B{\cdot}NMe_2H$ in 1,2-$C_6H_4F_2$ (0.07 M) to start catalysis. 100 µL aliquots of the catalytic mixture were removed at timed intervals in a purged syringe, quenched in an NMR tube containing 250 µL of MeCN and frozen to 77 K in liquid nitrogen. MeCN has previously been used to halt $H_3B{\cdot}NMe_2H$ catalysis as it irreversibly coordinates to Rh preventing further interaction. Demonstration of this has already been shown with Rh(I) bis-phosphine $H_3B{\cdot}NMe_3$ complexes (*e.g.* **(i4-6)**) to form acetonitrile adducts *e.g.*

trans-[Rh(P^iPr_3)$_2$(MeCN)$_2$][BAr^F_4] **(i4-7)** and free substrate (Scheme 4.4).[16] The extent of reaction was then analysed by integration of the ^{11}B NMR spectra. Cationic Rh(I) acetonitrile complexes [Rh(diphosphine)(MeCN)$_2$][PF_6] (diphosphine = dppe, dpp_{prop}) are known.[19]



Scheme 4.4 Acetonitrile trapping resulting in the release of amine-borane ligands.[16] [BAr^F_4]$^-$ anions not shown.

At 5 mol% pre-catalyst loading using complex **12**, dehydrocoupling of $H_3B{\cdot}NMe_2H$ to $[H_2BNMe_2]_2$ was 95% complete after 60 minutes by ^{11}B NMR spectroscopy. Given this improved result in comparison with pre-catalysts [Rh(η^6-C_6H_5F)(P^iBu_3)$_2$][BAr^F_4] **(i-166)** (completion after 80 minutes at 5 mol%)[20] and [Rh(η^6-C_6H_5F)(P^iPr_3)$_2$][BAr^F_4] **(i-83)** (completion after 300 minutes at 5 mol%)[16], the catalyst loading was further reduced to 1 and 0.2 mol%, respectively, to find a limit of catalysis, the results of which are illustrated in Table 4.3 along with the data for **11**, **25** and **26** at 0.2 mol% loading.

Table 4.3 $H_3B{\cdot}NMe_2H$ catalysis at various loadings of complexes **11**, **12**, **25** and **26**. [a]Consumption of $H_3B{\cdot}NMe_2H$ measured by ^{11}B NMR spectroscopy, induction period ignored, [0.07] mol dm^3 $H_3B{\cdot}NMe_2H$, 1,2-$C_6H_4F_2$, 298 K. [b] β = NBA, from references.[10]

Complex	β(°)	Catalyst Loading (mol %)	Length of Induction Period (mins)	Time for Completion (mins)[a]	ToF/ h^{-1}, [a]
12	91	5	15	50	24
12	91	1	10	18	300
12	91	0.2	4.5	15	1250
25	96	0.2	~ 15	88	430
26	99	0.2	~ 15	162	180
11	86	0.2	n/a	n/a	n/a

Intriguingly the rate of catalysis appears to increase on *decreased* catalyst loading. Complete conversion of $H_3B{\cdot}NMe_2H$ to $[H_2BNMe_2]_2$ with **12** is observed after 65 minutes at 5 mol% loading compared to only 25 minutes at 0.2 mol % loading. Of the active pre-catalysts at 0.2 mol% loading, **12** with the smallest bite angle is the fastest (25 minutes) and **26** with the largest bite angle is the slowest taking 200 minutes which matches with the trend found for the strength of the Rh···H_3B interaction in complexes **27-29**. Consistent with the lack of reactivity of **11** with $H_3B{\cdot}NMe_3$, catalysis is not observed with complex **11** and $H_3B{\cdot}NMe_2H$, presumably as the substrate ($H_3B{\cdot}NMe_2H$) is unable to coordinate to the metal. The rates of catalysis presented by **12**, **25** and **26** are broadly consistent with those recently reported by Schneider *et al.* with $[Ru(H)(PMe_3)(PNP)]$[21] (PNP = $[(CH_2CH_2P^iPr_2)_2N]^-$, completion observed after 5 minutes at 0.1 mol% loading) given the difference in substrate concentrations (0.54 M *vs.* 0.07 M) and are superior to that stated for monodentate bis-phosphine pre-catalysts **i-166** and **i-83** by two orders of magnitude.[16] Time course plots of each of the catalytic runs in Table 4.3 are plotted in Figure 4.7.

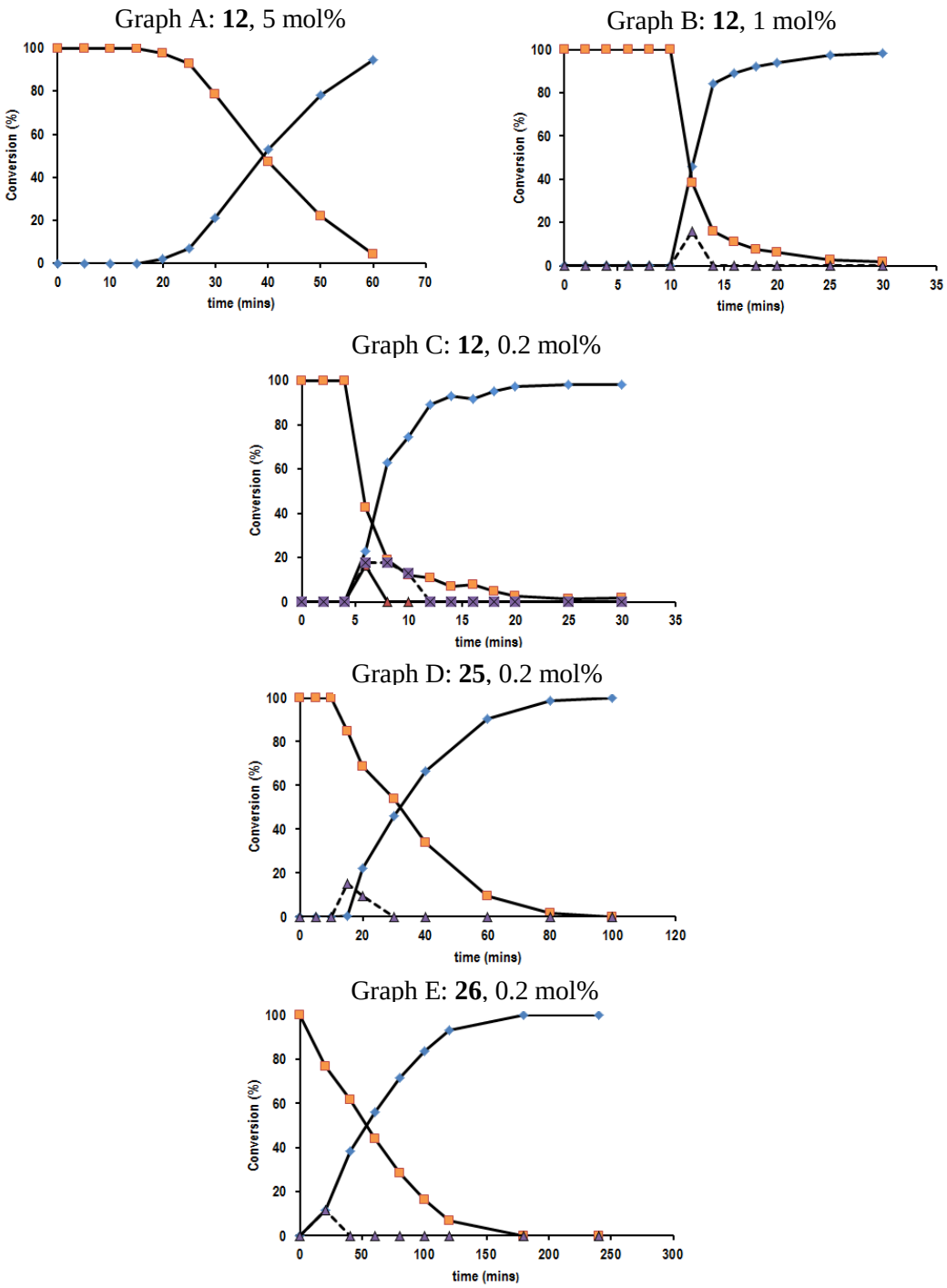
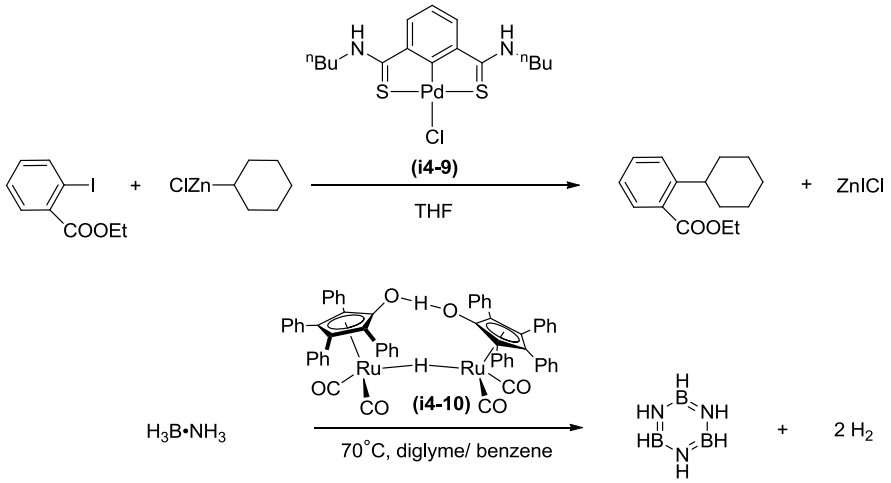


Figure 4.7 Graphs of % conversion for the dehydrocoupling of $H_3B{\cdot}NMe_2H$ to $[H_2BNMe_2]_2$ using pre-catalysts **12**, **25** and **26**. □ = $H_3B{\cdot}NMe_2H$, ☒ = Unidentified species, ◇ = $[H_2BNMe_2]_2$, Δ = $HB(NMe_2)_2$.

An induction period is observed with pre-catalysts **12**, **25** and **26**, which is notably absent in the monodentate bis-phosphine systems **i-166** and **i-83**.[16,20] The initial turnover frequencies in Table 4.3 do not include this delay before the onset of catalysis. The subsequent sigmoidal kinetic

profiles for each catalyst shown in Figure 4.7 are commonly associated with heterogeneous rather than homogeneous catalysis. Definitive homogeneous systems with an induction period have, however, recently been reported using thioimidopalladium(II) **(i4-9)** in a Negishi coupling[22] and noteably Shvo's catalyst **(i4-10)** in the dehydrocoupling of AB[23] (Scheme 4.5).



Scheme 4.5 Homogeneous systems incorporating an observed induction period. Lei's Negishi coupling using Pd(II) (top) and Williams' dehydrocoupling of AB using Shvo's catalyst (bottom).

Widegren and Finke have discussed how to determine whether a reaction is homogeneous or heterogeneous in significant detail.[24] A sigmoidal kinetic profile following an induction period is characteristic of a heterogeneous system. The initial period of inactivity in these proposed heterogeneous systems is suggested to be the time needed for cluster (colloid) nucleation after which the commencement of catalysis is rapid. In the opinion of the authors, this evidence can only act to back up further data such as, for example, the observation of metal precipitate or characterisation of such nanoclusters by Transition Emission Microscopy (TEM).[25] No metal precipitate or decolourisation of the solution (to black) associated with soluble nanoclusters was observed in our hands with any of the pre-catalysts **11**, **12**, **25** and **26**, irrespective of catalyst loading.

Poisoning tests are another tool which can shed light on the nature of the catalysis.[24,26] The addition of Hg to a catalytic mixture has long been noted to supress metal-based heterogeneous

systems.[27] Hg can coordinate to the nanocluster surface or amalgamate metal particles preventing interaction with the substrate and subsequent catalysis. However this test alone is not definitive proof of a homogeneous process - significant attenuation of activity merely lends further support for a heterogeneous catalyst. Addition of a small quantity (< 1 equivalent) of a strongly coordinating ligand has also been shown to stop heterogeneous catalysis using Rh(0) nanoclusters.[28] The idea here is that, given that a nanocluster is likely to aggregate and encapsulate a considerable number of metal atoms, only a portion will be on the surface to catalyse the reaction, so sub-stoichiometric quantities of poison can halt catalytic turnover. In our system, addition of Hg (100 µL after 31 minutes) or PPh_3 (0.3 equivalents after 31 minutes) to the catalytic mixture (**12**, 5 mol%) did not attenuate catalysis to any significant extent (Figure 4.8) suggesting a homogeneous system. Furthermore, addition of two equivalents of the free diphosphine ligand dpp_{prop} results in the immediate termination of all catalytic activity, common for homogeneous processes, presumably by forming the inactive cationic Rh(I) bis-diphosphine complex $[Rh\{Ph_2P(CH_2)_3PPh_2\}_2][BAr^F_4]$.

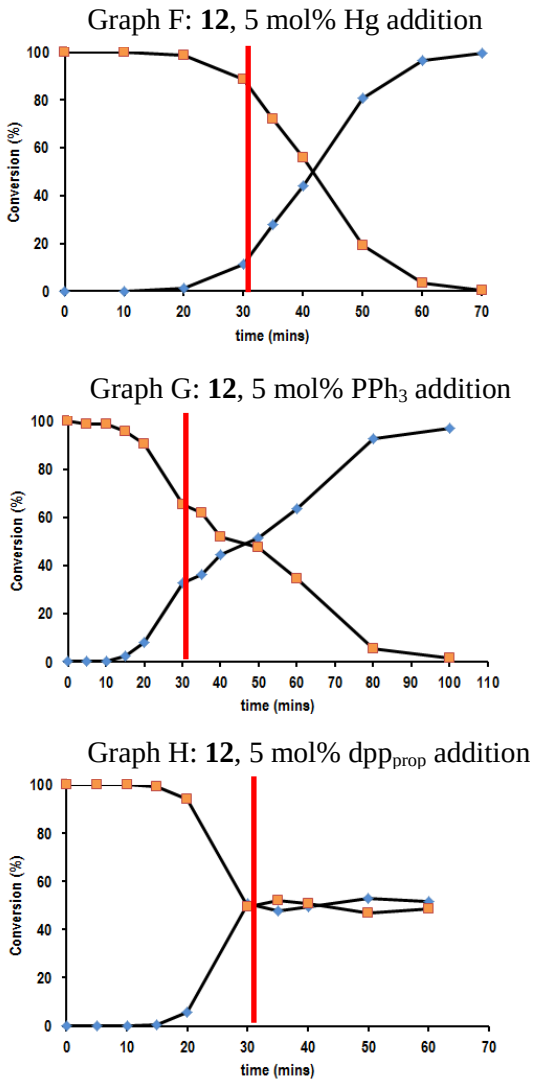
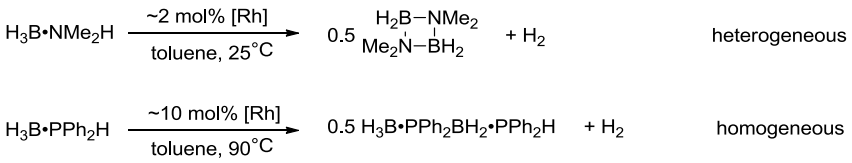


Figure 4.8 Graphs of % conversion for the dehydrocoupling of $H_3B{\cdot}NMe_2H$ to form $[H_2BNMe_2]_2$ using catalyst **12** (5 mol%, 1,2-$C_6H_4F_2$, 298 K) and known poisons; 100 µL Hg (Graph F), 0.3 eq. PPh_3 (Graph G), 2 eq. $Ph_2P(CH_2)_3PPh_2$ (Graph H). All poisons added at 31 minutes as indicated by the bold vertical line on each graph. □ = $H_3B{\cdot}NMe_2H$, ◇ = $[H_2BNMe_2]_2$.

Microfiltration experiments to differentiate between homogeneous and heterogeneous processes have also been developed by Manners and co-workers for Rh-catalysed dehydrocoupling of amine- and phosphine-boranes.[29] In combination with Hg and PPh_3 poisoning tests they were able to show that the dehydrocoupling of $H_3B{\cdot}NMe_2H$ with Rh(I) precursors was most likely to be a *heterogeneous* process as filtration of the catalytic mixture containing solid precipitate halted catalysis while that of $H_3B{\cdot}PPh_2H$ was *homogeneous* as filtration did not significantly attenuate catalysis (Scheme 4.6).



Scheme 4.6 Dehydrocoupling of amine- and phosphine-boranes with Rh(0) catalysts. [Rh] = [{Rh(1,5-COD)(μ-Cl)}$_2$], Rh/Al_2O_3, $Rh_{colloid}$/[Oct_4N]Cl, [Rh(1,5-COD)$_2$]OTf.

In a similar procedure to that of Manners, catalysis was conducted under the standard conditions used to obtain the data for Graph C, Figure 4.7. Complete conversion of $H_3B{\cdot}NMe_2H$ to $[H_2BNMe_2]_2$ was verified by ^{11}B NMR spectroscopy after 30 minutes. The catalytic solution was then extracted by syringe and filtered in the glove box using a pre-conditioned 0.2 μm cellulose filter. The filtrate was subsequently added to a new reaction flask containing a fresh batch of $H_3B{\cdot}NMe_2H$. Turnover to form $[H_2BNMe_2]_2$ was still observed (80 % $H_3B{\cdot}NMe_2H$ consumed in a further 30 minutes) again suggesting the existence of a "single-site" homogeneous process (Array A, Figure 4.9). Incomplete conversion over the 30 minutes of reactivity post filtration can be attributed to the loss of significant amount of catalyst during the filtration process in the filter housing. Manners also noted a 20 % reduction in percentage conversion in the dehydrocoupling of $H_3B{\cdot}PPh_2H$ over the same reaction timescale upon filtration of the [{Rh(1,5-COD)(μ-Cl)}$_2$] catalyst.[29] In a separate experiment, addition of a further 500 equivalents of $H_3B{\cdot}NMe_2H$ to **12** at the end of catalysis shows that the catalyst is recyclable with complete turnover to $[H_2BNMe_2]_2$ observed over 30 minutes (Array B, Figure 4.9).

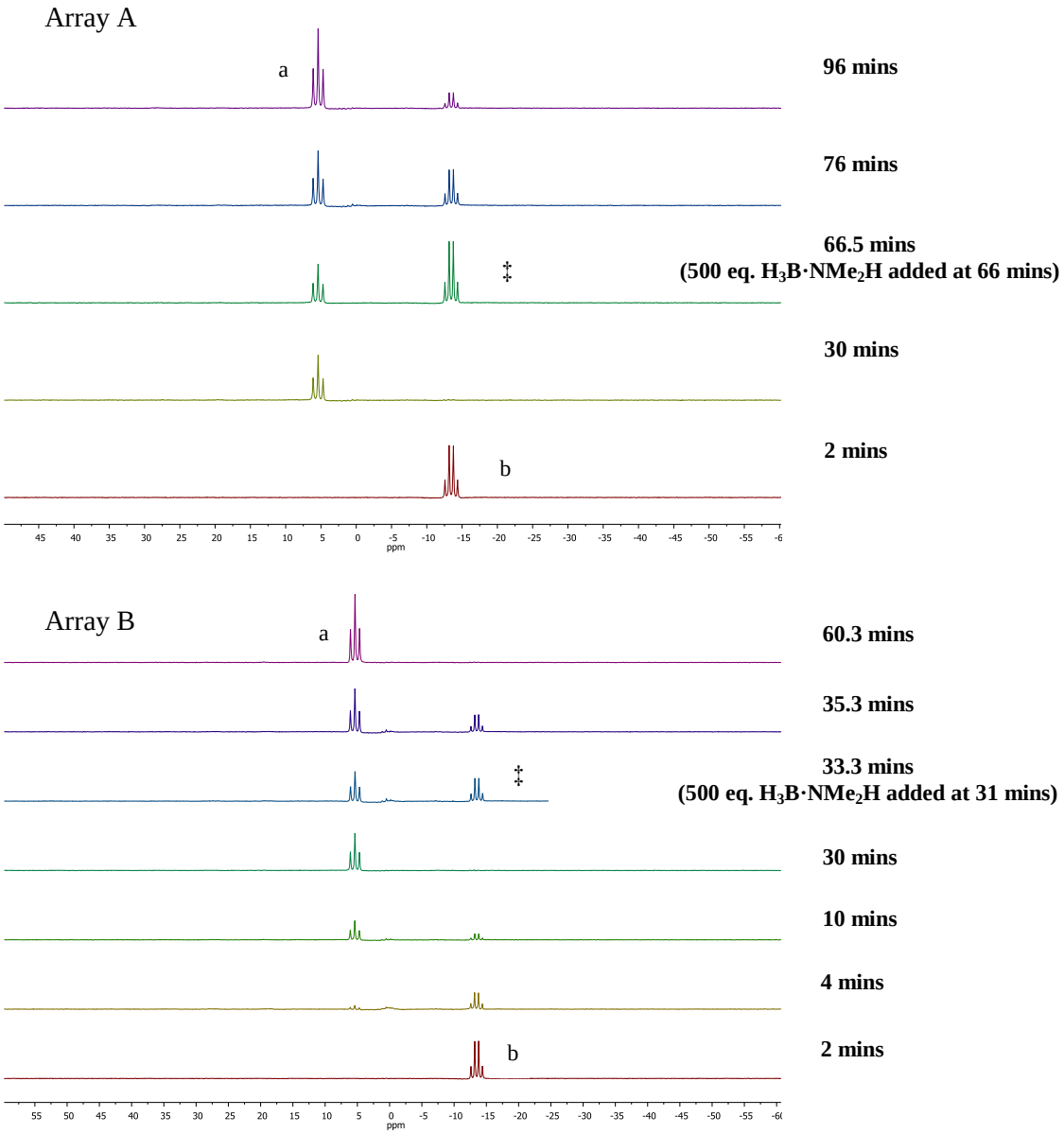


Figure 4.9 ^{11}B NMR spectra (160 MHz, 1,2-$C_6H_4F_2$) taken during the filtration (Array A) and recycling (Array B) experiments. 500 eq. $H_3B{\cdot}NMe_2H$ in 1,2-$C_6H_4F_2$ (5 mL) added to **12** at t = 0 minutes. Samples taken at times shown and quenched with MeCN prior to running. Array A -‡ A further 500 eq. $H_3B{\cdot}NMe_2H$ (based on amount of **12** remaining after 30 minutes of sampling) in 600 μL 1,2-$C_6H_4F_2$ added at 66 minutes. Array B -‡ A further 500 eq. $H_3B{\cdot}NMe_2H$ (based on amount **12** remaining after 30 minutes of sampling) in 600 μL 1,2-$C_6H_4F_2$ added at 31 minutes. a = $[H_2BNMe_2]_2$, b = $H_3B{\cdot}NMe_2H$.

Together, these tests for differentiating between homogeneous and heterogeneous catalysis suggest that this system is homogeneous with an induction period. The delay before the onset of catalysis in a homogeneous process however necessitates an explanation.

The first point of note is that the length of the induction period for **12** has an inverse relationship with catalyst loading at constant substrate concentration, *i.e.* the shortest induction period (and highest turnover frequency) is found for the lowest catalyst loading (Table 4.3). To help explain the reasons for these observations we first turned to NMR spectroscopy. Unfortunately NMR spectroscopic analysis of the reaction of $H_3B{\cdot}NMe_2H$ with **12**, **25** and **26** was inconclusive with regard to the organometallic species present in solution. This is not unexpected since such active species would be expected to be relatively short-lived. As Bergman has previously proclaimed: "if you can isolate it, it is probably not the catalyst".[30] We subsequently turned to ESI-MS to analyse the stoichiometric reaction of $H_3B{\cdot}NMe_2H$ with each of the three active catalyst systems. The ESI-MS spectrum using pre-catalyst **25** after 3 hours is shown in Figure 4.10 and is illustrative of those also found for **12** and **26**. All exhibited isotopomer patterns corresponding to $[Rh(Ph_2P(CH_2)_xPPh_2)]_2^{2+}$ **(M^+1)** and $[\{Rh(Ph_2P(CH_2)_xPPh_2)\}_2(H)(H_2BNMe_2)]^+$ **(M^+2)**. Interestingly, **(M^+1)** was by far the predominant species for **12**, the fastest pre-catalyst, while **(M^+2)** dominated in the mass spectrum of **26**, the slowest pre-catalyst (Scheme 4.7).

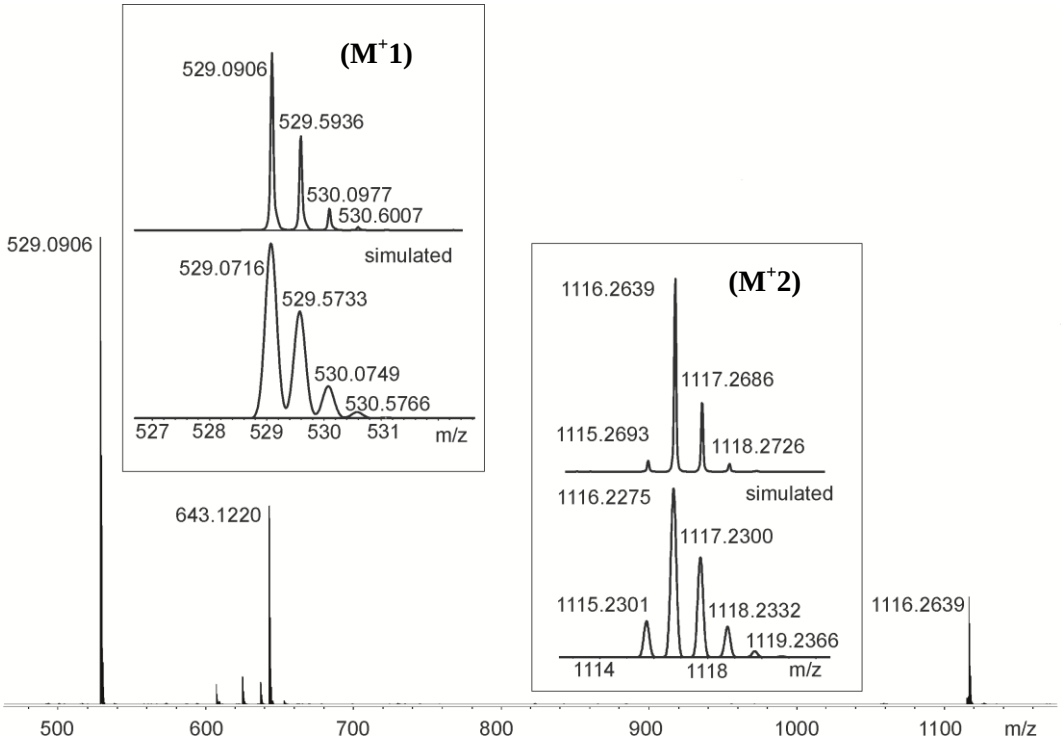
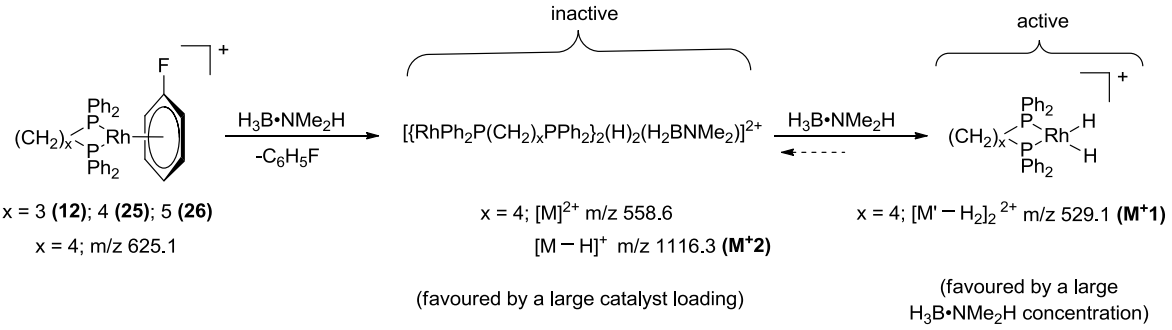
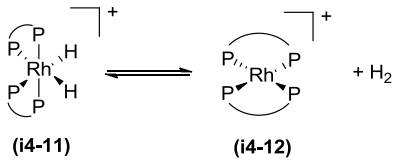


Figure 4.10 ESI-MS of the reaction of 1 equivalent of $H_3B{\cdot}NMe_2H$ with $[Rh\{Ph_2P(CH_2)_4PPh_2\}(\eta^6\text{-}C_6H_5F)][BAr^F{}_4]$ **(25)** after 3 hours. $[M]^+$ at 643.1220 = $\{Rh(C_6H_4F_2)(Ph_2P(CH_2)_4PPh_2)\}^+$



Scheme 4.7 ESI-MS of the stoichiometric addition of $H_3B{\cdot}NMe_2H$ to **12**, **25** and **26**. $[BAr^F{}_4]^-$ anions not shown.

Correlating these data with the catalytic results suggests $\mathbf{M^+1}$ fragments are associated with the active catalyst and $\mathbf{M^+2}$ with the inactive organometallic species. A plausible suggestion for the origin of the $\mathbf{M^+1}$ fragment is from highly reactive Rh(III) dihydrides, *e.g.* $\{Rh(diphosphine)(H)_2\}^+$. The stability of such dihydrides have recently been shown to be highly dependent on the nature of the diphosphine by Bercaw and co-workers who correlated the stability of $\{Rh(diphosphine)_2(H)_2\}^+$ species **(i4-11)** to dihydrogen loss with the diphosphine ligand NBA (Scheme 4.8).[31]



Scheme 4.8 Reductive elimination of H_2 from $\{Rh(diphosphine)_2(H)_2\}^+$ **(i4-11)** to form $\{Rh(diphosphine)_2\}^+$ **(i4-12)** is a thermodynamic equilibrium dependent on the NBA of the diphosphine.

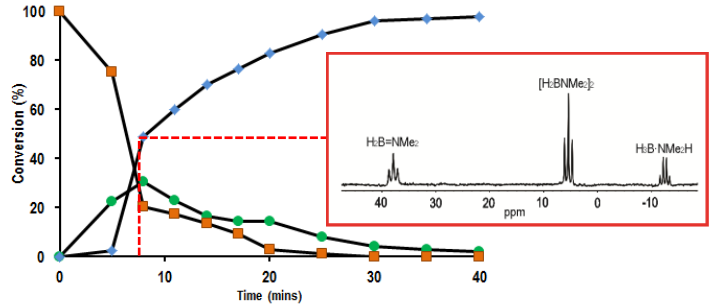
$\mathbf{M^+2}$ could originate from the initial addition of amine-borane to the pre-catalyst, lying as a dormant inactive dimeric fragment off the catalytic cycle. A related dimeric structure, $[Rh_2(P^iPr_3)_2(H)_2(\mu\text{-}H_2B{\cdot}NMe_3)_2(\mu\text{-}H_3B{\cdot}NMe_3)][BAr^F{}_4]_2$ **(i-154)**, is also a known, but slow (20 mol%, 15 hours), catalyst in the dehydrocoupling of $H_3B{\cdot}NMe_2H$.[32] Thus a delicate equilibrium between $\mathbf{M^+1}$ and $\mathbf{M^+2}$ could be responsible for the induction period in that it takes several minutes to establish a substantial concentration of an active monomeric species for catalysis to take place, a process which is significantly increased with large relative $H_3B{\cdot}NMe_2H$

concentration (*c.f.* inverse trend seen with catalyst loading for **12**). Further evidence for the formation of $\mathbf{M^{+}1}$ and $\mathbf{M^{+}2}$ in catalysis is acquired from the absence of these fragments in the ESI-MS of each of the bound $H_3B{\cdot}NMe_3$ complexes suggesting that they are a product of species forming as a result of dehydrocoupling.

4.2.3 Role of $H_2B{=}NMe_2$ in $H_3B{\cdot}NMe_2H$ dehydrocoupling

Monitoring the catalysis of $H_3B{\cdot}NMe_2H$ with complexes **12**, **25** and **26** by ^{11}B NMR spectroscopy sheds light on an important feature. Under the conditions of analysing catalysis in an open system and quenching with acetonitrile, $H_2B{=}NMe_2$ [δ +38 {t, *J*(BH) 113 Hz}] is not observed. This is contrary to several other reported Rh and Ir bis(phosphine) systems[33,34] as well as when catalysis is carried out without quenching in a sealed high pressure New Era NMR tube with this system where $H_2B{=}NMe_2$ and $B_2H_5(\mu\text{-}NMe_2)$ [δ −17 {td, *J*(BH) 133 Hz, *J*(BH) 30 Hz}] are observed during the course of the reaction. These conditions are however at a vastly different metal *vs.* amine-borane concentration to that found in the open systems. Taking aliquots of the reaction mixture containing complex **12** (0.2 mol%) without quenching in acetonitrile and instead freezing the samples at 77 K after dilution in 1,2-$C_6H_4F_2$ (250 µL) to prevent onward reactivity revealed that a significant quantity of $H_2B{=}NMe_2$ is forming on the reaction timescale which reaches a maximum of 30 % of the total boron-containing species present after 8 minutes (Figure 4.11). Clearly an effect of the acetonitrile is to rapidly accelerate the dimerisation of $H_2B{=}NMe_2$ to form $[H_2BNMe_2]_2$ which is why it is not observed in the acetonitrile-quenched ^{11}B NMR spectra. Interestingly $B_2H_5(\mu\text{-}NMe_2)$ was not observed by ^{11}B NMR spectroscopy at all in an open system suggesting that this species is favoured by either a build-up in hydrogen pressure or elevated amine-borane *vs.* metal concentrations found in catalysis conducted in a sealed NMR tube. The two open system plots with acetonitrile quenching and without are shown for comparison in Figure 4.11.

Graph I: **12**, 0.2 mol%, without MeCN quenching



Graph J: **12**, 0.2 mol%, with MeCN quenching

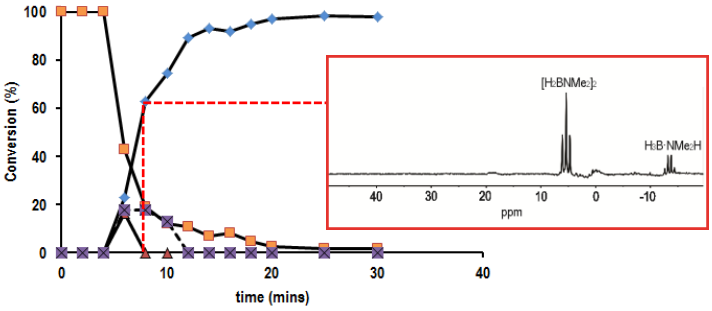
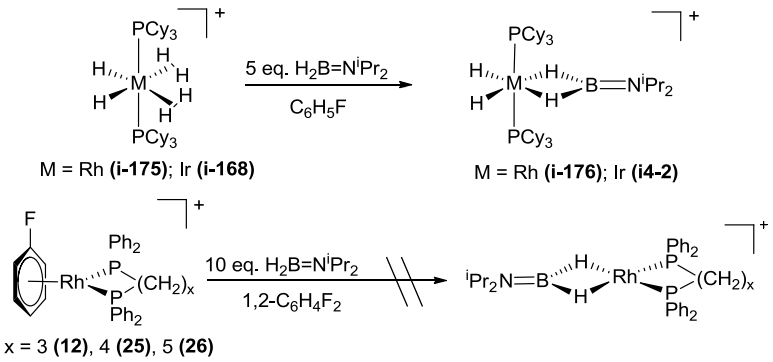


Figure 4.11 Plots of the open system catalysis of $H_3B{\cdot}NMe_2H$ with **12** at 0.2 mol% loading quenching aliquots without MeCN (Graph I) and quenching with MeCN (Graph J) as followed by ^{11}B NMR spectroscopy. ^{11}B NMR spectra (160 MHz, 1,2-$C_6H_4F_2$) after 8 minutes reaction time shown inset. □ = $H_3B{\cdot}NMe_2H$, ☒ = Unidentified species, ◇ = $[H_2BNMe_2]_2$, Δ = $HB(NMe_2)_2$, ○ = $H_2B{=}NMe_2$.

Although $H_2B{=}NMe_2$ is formed in significant quantity, ^1H and $^{31}P\{^1H\}$ NMR spectroscopy do not show conclusive evidence for the coordination of this species to the $\{Rh(diphosphine)\}^+$ fragment during catalysis with complexes **12**, **25** and **26** ($H_3B{\cdot}NMe_2H$, 5 mol% [Rh], sealed tube). This is different to the non-chelating systems whereby $[M(PR_3)_2(H)_2(\eta^2\text{-}H_2B{=}NMe_2)][BAr^F{}_4]$ (M = Rh, R = ^{i}Bu **(i-145)**; M = Ir, R= Cy **(i-170)**) are observed at the end of catalysis.[33,34] To further assess the ability of the coordination of a monomeric fragment to complexes **12**, **25** and **26**, $H_2B{=}N^iPr_2$, a stable monomer which does not undergo dimerisation,[35] was added in stoichiometric quantities to each of the pre-catalysts (Scheme 4.9). Reaction of $[M(PCy_3)_2(H)_2(\eta^2\text{-}H_2)_2][BAr^F{}_4]$ {M = Rh **(i-175)**; Ir **(i-168)**} with this aminoborane generates $[M(PCy_3)_2(H)_2(\eta^2\text{-}H_2B{=}N^iPr_2)][BAr^F{}_4]$ {M =Rh **(i-176)**; Ir **(i4-2)**} which are isolable as stable but air-sensitive solids.[36] In contrast, addition of an excess (10 equivalents) of $H_2B{=}N^iPr_2$ did not show any sign of reactivity with complexes **12**, **25** and **26** by NMR spectroscopy. This

suggests that $H_2B{=}NMe_2$ would act in similar manner with unfavourable coordination to **12**, **25** and **26** although the effect of the increased steric bulk of the isopropyl groups in hindering coordination cannot be ruled out.



Scheme 4.9 (top): Synthesis of **(i-176)** and **(i4-2)** respectively; (bottom): Addition of $H_2B{=}N^iPr_2$ to **12**, **25** and **26** does not result in coordination. $[BAr^F{}_4]^-$ anions not shown.

4.2.4 Role of $H_3B{\cdot}NMe_2BH_2{\cdot}NMe_2H$ in $H_3B{\cdot}NMe_2H$ dehydrocoupling

$H_3B{\cdot}NMe_2BH_2{\cdot}NMe_2H$ (as already discussed in Chapter 3) is a possible intermediate in the dehydrocoupling of $H_3B{\cdot}NMe_2H$. This species is only ever observed in a trace quantity at the end of catalysis with pre-catalysts **12**, **25** and **26** at 0.2 mol% loading. This observation has key implications and suggests that this system operates *via* a different mechanism compared to other Rh-based systems where $H_3B{\cdot}NMe_2BH_2{\cdot}NMe_2H$ is observed in significant quantity as an intermediate during catalysis.[16,33] Manners and co-workers have recently reported the dehydrocoupling of $H_3B{\cdot}NMe_2H$ using a catalyst photogenerated from $[FeCp(CO)_2]_2$ **(i-130)** which also does not form $H_3B{\cdot}NMe_2BH_2{\cdot}NMe_2H$.[37] With a further view to elucidating the mechanism, $H_3B{\cdot}NMe_2BH_2{\cdot}NMe_2H$ (20.8 mg, 0.180 mmol, 250 eq.) was added to **12** in 5 mL 1,2-$C_6H_4F_2$. No apparent reaction was observed after 30 minutes by ^{11}B NMR spectroscopy ($[H_2BNMe_2]_2$ not observed) or by vigorous bubbling indicative of the evolution of hydrogen.

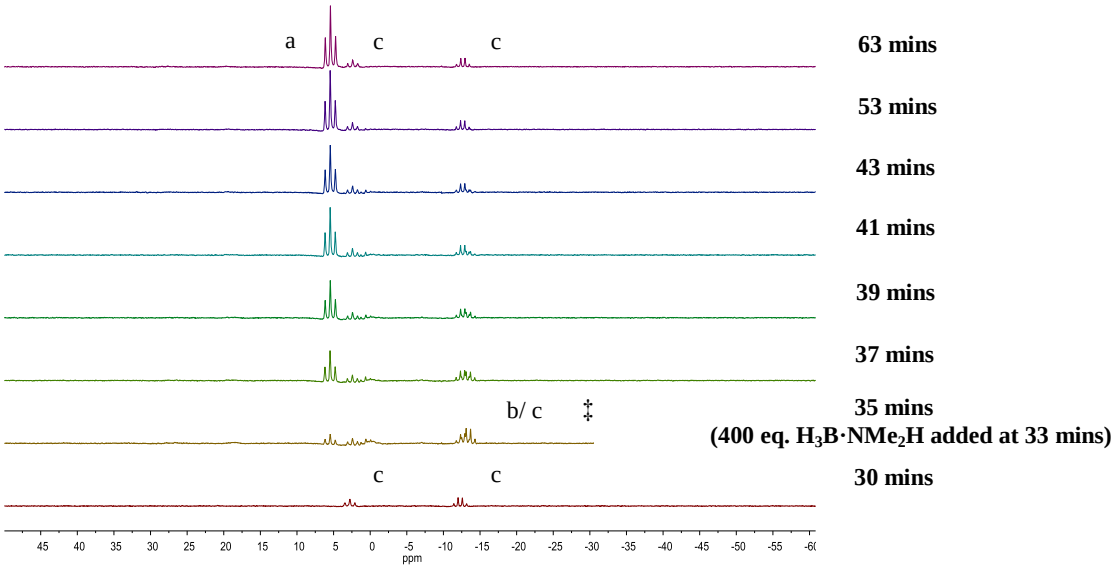
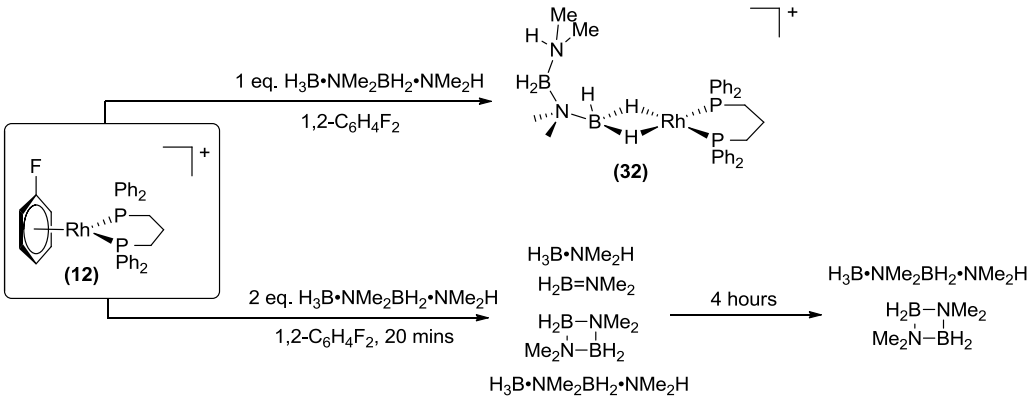


Figure 4.12 ^{11}B NMR spectra (160 MHz, 1,2-$C_6H_4F_2$) at selected time intervals of the reaction of 50 eq. $H_3B{\cdot}NMe_2BH_2{\cdot}NMe_2H$ with **12** in an open system for 30 minutes, followed by the addition of 400 eq. $H_3B{\cdot}NMe_2H$ at 33 minutes. a = $[H_2BNMe_2]_2$, b = $H_3B{\cdot}NMe_2H$, c = $H_3B{\cdot}NMe_2BH_2{\cdot}NMe_2H$. ‡ = 400 eq. $H_3B{\cdot}NMe_2H$ added to the catalyst/ $H_3B{\cdot}NMe_2BH_2{\cdot}NMe_2H$ mixture.

Repeating the reaction with the addition of $H_3B{\cdot}NMe_2H$ (16.94 mg, 0.288 mmol, 400 eq.) to the solution of pre-catalyst **12** and unreacted $H_3B{\cdot}NMe_2BH_2{\cdot}NMe_2H$ (4.16 mg, 0.036 mmol, 50 eq.) resulted in the immediate onset of catalysis (vigorous evolution of hydrogen) to form $[H_2BNMe_2]_2$. However after a further 30 minutes, $H_3B{\cdot}NMe_2BH_2{\cdot}NMe_2H$ was still present at its initial concentration (Figure 4.12). This result shows that $H_3B{\cdot}NMe_2BH_2{\cdot}NMe_2H$ does not react with **12** to form $[H_2BNMe_2]_2$ under catalytic conditions, but it also suggests that it has no reaction with free $H_2B{=}NMe_2$ formed during the reaction. $H_3B{\cdot}NMe_2BH_2{\cdot}NMe_2H$ has previously been shown to react with colloidal Rh to catalytically form $[H_2BNMe_2]_2$[38] which further supports homogeneous rather than heterogeneous catalysis with this chelating diphosphine system. The lack of induction period (judged by the immediate evolution of hydrogen) upon addition of $H_3B{\cdot}NMe_2H$ suggests that an active catalyst for the dehydrogenation of $H_3B{\cdot}NMe_2H$ is however formed on addition of $H_3B{\cdot}NMe_2BH_2{\cdot}NMe_2H$ to **12** although this complex does not act to catalyse the formation of $[H_2BNMe_2]_2$ from $H_3B{\cdot}NMe_2BH_2{\cdot}NMe_2H$.

Even though $H_3B{\cdot}NMe_2BH_2{\cdot}NMe_2H$ is not consumed in catalysis, stoichiometric addition of $H_3B{\cdot}NMe_2BH_2{\cdot}NMe_2H$ to **12** suggests that this oligomeric amine-borane is able to coordinate to the metal forming $[Rh(Ph_2P(CH_2)_3PPh_2)(\eta^2\text{-}H_3B{\cdot}NMe_2BH_2{\cdot}NMe_2H)][BAr^F{}_4]$ **(32)** (Scheme 4.10). ^{1}H NMR spectroscopy shows a characteristic broad resonance [δ −1.39 (3H)] assigned to the Rh···H_3B interaction, a broad singlet [δ +5.08 (1H)] for the N*H* and a broad signal [δ +2.38 (12H)] for the methyl groups coordinated to the nitrogens of $H_3B{\cdot}NMe_2BH_2{\cdot}NMe_2H$. No RhH resonances are observed in the low frequency portion of the spectrum (δ 0 to −30). A doublet [δ 32.0 {*J*(RhP) 163 Hz}] is observed by $^{31}P\{^1H\}$ NMR spectroscopy and two distinct boron environments (δ +17.5 and +0.7) are observed by ^{11}B NMR spectroscopy which are significantly shifted compared to free ligand [δ +2.5 {t, *B*H_2, *J*(BH) 107 Hz}, −12.8 {q, *B*H_3, *J*(BH) 94 Hz}].



Scheme 4.10 *In situ* formation of **32** and its onward reactivity in the presence of excess $H_3B{\cdot}NMe_2BH_2{\cdot}NMe_2H$. $[BAr^F{}_4]^-$ anions not shown.

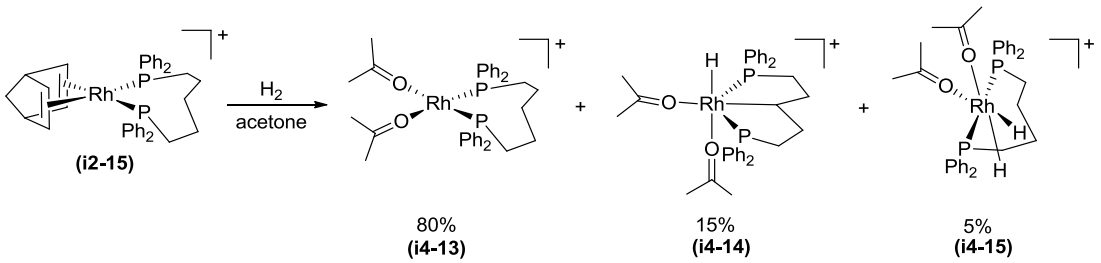
In contrast to the stoichiometric reaction of $H_3B{\cdot}NMe_2BH_2{\cdot}NMe_2H$ and **12**, addition of a slight excess (2 equivalents) of $H_3B{\cdot}NMe_2BH_2{\cdot}NMe_2H$ to **12** resulted in the observance of $H_2B{=}NMe_2$ and $H_3B{\cdot}NMe_2H$ after 20 minutes by ^{11}B NMR spectroscopy. The remaining equivalent of $H_3B{\cdot}NMe_2BH_2{\cdot}NMe_2H$ however remains in solution over 4 hours whereas $H_3B{\cdot}NMe_2H$ is consumed after an hour to form $[H_2BNMe_2]_2$. Thus it appears that the splitting of $H_3B{\cdot}NMe_2BH_2{\cdot}NMe_2H$ requires 2 equivalents of substrate and the resulting organometallic species is subsequently inactive towards further splitting of $H_3B{\cdot}NMe_2BH_2{\cdot}NMe_2H$. This result

is related to that observed for [Rh(η^1: η^2-$H_3B{\cdot}NMe_2BH_2{\cdot}NMe_2H$){$PCyp_2(\eta^2$-$C_5H_7)$}][$BAr^F_4$] **(20)** which is stable on its own but the addition of excess $H_3B{\cdot}NMe_2BH_2{\cdot}NMe_2H$ results in *catalytic* turnover to form $[H_2BNMe_2]_2$ (Chapter 3). One turnover to form $H_2B{=}NMe_2$, $[H_2BNMe_2]_2$ or $H_3B{\cdot}NMe_2H$ at 0.2 mol% catalyst loading (1 mg **12**) is below standard NMR spectroscopy detection limits consistent with the apparent observation of no reaction under catalytic conditions mentioned above. The resulting organometallic species appears to be highly active towards the dehydrogenation of $H_3B{\cdot}NMe_2H$ which is totally consumed in catalysis to leave $H_3B{\cdot}NMe_2BH_2{\cdot}NMe_2H$ remaining (Figure 4.12). This is consistent with the ESI-MS data already reported in this chapter which tentatively suggests that a dormant inactive species *e.g.* $[\{Rh(Ph_2P(CH_2)_xPPh_2)\}_2(H)_2(H_2BNMe_2)]^+$ (Scheme 4.7) can form on addition of amine-borane. Such a species could then rapidly form the suggested active catalyst *e.g.* $\{Rh(diphosphine)(H)_2\}^+$ upon the addition of $H_3B{\cdot}NMe_2H$. Recent work with [$Ir(PCy_3)_2(H)_2(\eta^2$-$H_2B{=}NMe_2)$][BAr^F_4] **(i-170)** has shown that $H_3B{\cdot}NMe_2BH_2{\cdot}NMe_2H$ is only observed as a result of an "on metal" based process from the interaction of $H_3B{\cdot}NMe_2H$ with **i-170**.[34] The observation of both free $H_2B{=}NMe_2$ and $H_3B{\cdot}NMe_2H$ together during open system catalysis with pre-catalysts **12**, **25** and **26** but without the formation of $H_3B{\cdot}NMe_2BH_2{\cdot}NMe_2H$ further supports this idea.

4.2.5 Proposed mechanism for $H_3B{\cdot}NMe_2H$ dehydrocoupling using 12, 25 and 26

This observed rapid dehydrogenation of $H_3B{\cdot}NMe_2H$ to ultimately form $[H_2BNMe_2]_2$ for complexes **12**, **25** and **26** is in contrast to other Rh and Ir systems already reported in terms of speed and the absence of observable organometallic intermediates.[16,20,33,34] The unfavourable interaction of $H_2B{=}NMe_2$ for Rh chelating diphosphine complexes (which the evidence from studies with $H_2B{=}N^iPr_2$ lends more support) prevents competition with substrate $H_3B{\cdot}NMe_2H$ for the $\{Rh(diphosphine)(H)_2\}^+$ fragment. This is possibly due to an orbital overlap effect for metal chelated diphosphine fragments not having efficient bonding orbitals of low enough energy to match with $H_2B{=}NR_2$ (R = Me, ^{i}Pr) species. In this respect stronger bonding with

aminoboranes could be speculated with phosphine ligands with larger bite angles as with amine-boranes. Rapid H_2 loss from the $\{Rh(diphosphine)(H)_2\}^+$ fragment is consistent with the absence of observable intermediate hydride complexes[31] and is in contrast to the monodentate bis-phosphine Rh and Ir systems as already discussed. Further evidence for this is the comparable catalytic activity with $H_3B{\cdot}NMe_2H$ (7.2 mg, 0.122 mmol, 20 eq.) in a sealed system with **12** (9 mg, 0.0061 mmol, 5 mol% in 400 µL 1,2-$C_6H_4F_2$) where ~ 90% conversion of $H_3B{\cdot}NMe_2H$ to $[H_2BNMe_2]_2$ is found after 35 minutes. This suggests hydrogen does not impede the dehydrogenation of $H_3B{\cdot}NMe_2H$ presumably as dihydrogen does not strongly coordinate to the complexes, which is in contrast to $[Rh(P^iBu_3)_2][BAr^F{}_4]$ **(i-125)** where catalysis is apparently inhibited by the evolution of hydrogen.[20] The slower observed catalysis **12** > **25** > **26** may therefore be as a result of an increasing bite angle (electronic effect) and the increased stability of dihydride structures which are more reluctant to reductively eliminate H_2 to regenerate a Rh(I) species. Dpp_{pent} has the largest bite angle and is reaching the limit where *trans* geometries and structures containing metal-hydrides are more favoured.[31] This has been already been shown upon the hydrogenation of $[Rh(NBD)(Ph_2P(CH_2)_5PPh_2)][BAr^F{}_4]$ **(i2-15)** in acetone to yield $[Rh(Ph_2P(CH_2)_5PPh_2)(H)_2(acetone)_2][BAr^F{}_4]$ **(i4-15)** which is observed in a 5 **(i4-15)**: 15 **(i4-14)**: 80 **(i4-13)** ratio with the monohydridic complex $[Rh(Ph_2P(CH_2)_5PPh_2)(acetone)_2(H)][BAr^F{}_4]$ **(i4-14)** and the bis-acetone adduct $[Rh(Ph_2P(CH_2)_5PPh_2)(acetone)_2][BAr^F{}_4]$ **(i4-13)** (Scheme 4.11).[11] No equivalent metal hydride species were observed with analogous dppe, dpp_{prop} or dppb complexes.



Scheme 4.11 Hydrogenation of **i2-15** acetone yields metal hydride complexes as minor reaction products. $[BAr^F{}_4]^-$ anions not shown.

The fact that amine- and aminoborane complexes $[Rh(P^iBu_3)_2(H)_2(H_3B{\cdot}NMe_2H)][BAr^F{}_4]$ **(i-143)** and $[Rh(P^iBu_3)_2(H)_2(H_2B{=}NMe_2)][BAr^F{}_4]$ **(i-145)** are present during catalysis with $\{Rh(PR_3)_2\}^+$ precursors suggests that hydrogen loss is retarded and may in turn explain their inherent slower catalysis overall. The 16-electron cationic Rh(I) bis-phosphine complexes illustrated in Figure 4.13 are stable in their own right in the absence of excess amine-borane however they do go on to catalyse the dehydrocoupling of $H_3B{\cdot}NMe_2H$ and $H_3B{\cdot}NMe_2BH_2{\cdot}NMe_2H$ to $[H_2BNMe_2]_2$ when an excess of the respective amine-borane is present.[33] This ability to coordinate such a variety of Rh(I) and Rh(III) complexes (Figure 4.13) could also be thought to slow catalysis and, in addition, provide alternate and more complex reactivity in a catalytic mixture.

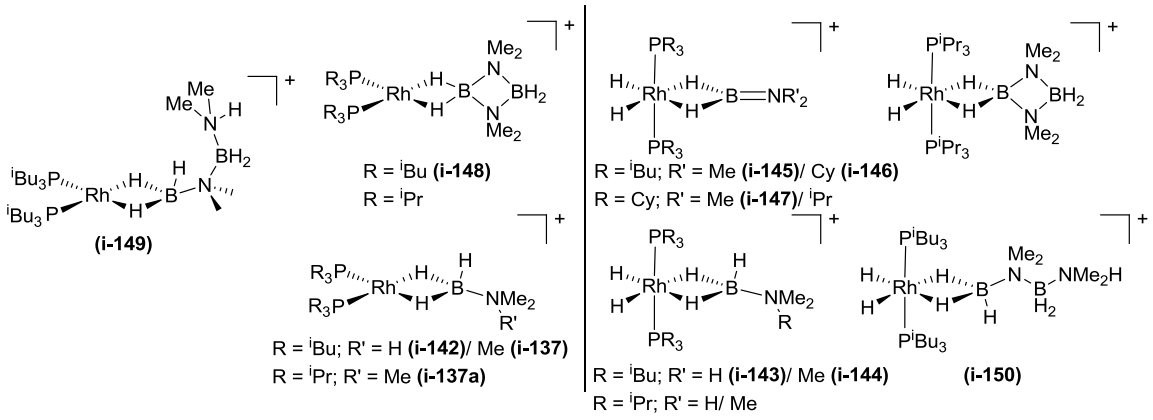
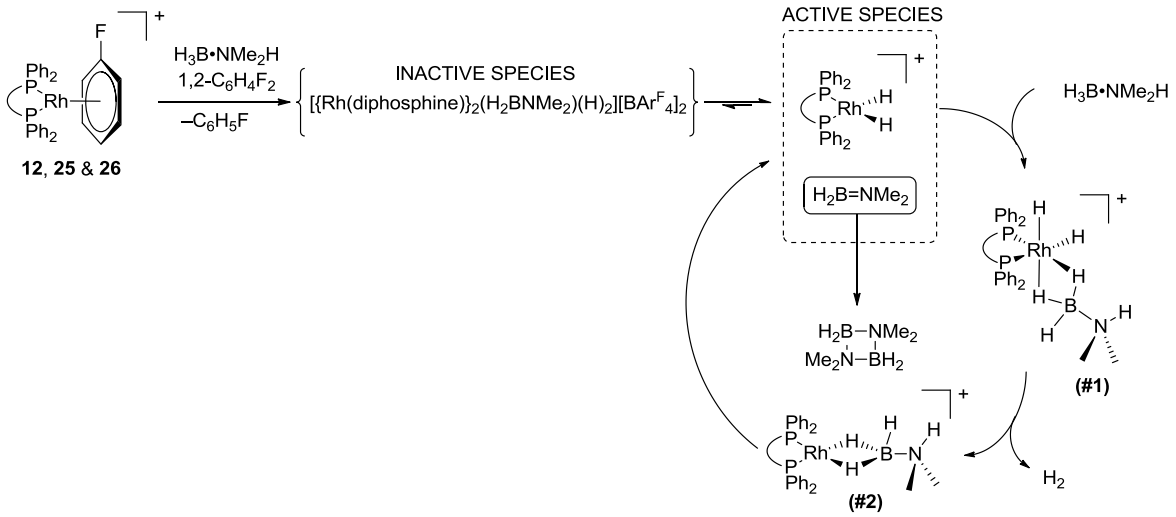


Figure 4.13 Characterised amino- and amine-borane Rh bis-phosphine complexes. $[BAr^F{}_4]^-$ anions not shown. $[Rh(P^iPr_3)_2(H)_2\{(H_2BNMe_2)_2\}][BAr^F{}_4]$ is only stable in the solid-state.

Added to this is the observation that stoichiometric addition of $[H_2BNMe_2]_2$ to **12** also shows no sign of coordination, unlike $[Rh(P^iBu_3)_2][BAr^F{}_4]$ **(i-125)** which has been shown to form $[Rh(P^iBu_3)_2\{\eta^2\text{-}(H_2BNMe_2)_2\}][BAr^F{}_4]$ **(i-148)** under the same conditions,[33] makes dehydrogenation rapid and suggests that it is the non-metal-based dimerisation of $H_2B{=}NMe_2$ to form $[H_2BNMe_2]_2$ which is the rate determining step for total conversion to $[H_2BNMe_2]_2$.

These data further support the idea that pre-catalysts **12**, **25** and **26** facilitate the dehydrogenation of $H_3B{\cdot}NMe_2H$ to $H_2B{=}NMe_2$ extremely efficiently and also suggest that $H_3B{\cdot}NMe_2BH_2{\cdot}NMe_2H$ is neither favourably produced nor consumed during this process which

is consistent with only a trace observation of $H_3B{\cdot}NMe_2BH_2{\cdot}NMe_2H$ in catalysis with $H_3B{\cdot}NMe_2H$ (0.2-5 mol% **12**, **25** and **26**) which could be forming in an off metal process or a slow parallel process. $H_3B{\cdot}NMe_2BH_2{\cdot}NMe_2H$ can coordinate to the metal centre but the fact it is not observed to undergo rapid *catalytic* dehydrocoupling implies that a different organometallic species (which is not present in the chelating system) causes its favoured formation as an intermediate and its consumption in $H_3B{\cdot}NMe_2H$ dehydrocoupling with other systems. Given the pivotal role of $H_2B{=}NMe_2$, this again leads back to the hypothesis that [Rh(diphosphine)(η^2-$H_2B{=}NMe_2$)][BAr^F_4] is not generated with these chelating diphosphines and is therefore key to the formation of $H_3B{\cdot}NMe_2BH_2{\cdot}NMe_2H$ in systems where it can coordinate, *e.g.* [$Rh(PR_3)_2(H)_2(H_2B{=}NMe_2)$][$BAr^F_4$] (R = ^{i}Bu **(i-145)**/ Cy **(i-147)**).[33,34]



Scheme 4.12 Postulated mechanism for the dehydrogenation of $H_3B{\cdot}NMe_2H$ by **12**, **25** and **26**. $[BAr^F_4]^-$ anions not shown.

The conclusions in this section suggest the mechanism shown in Scheme 4.12. This mechanism accounts for an observed induction period in the dehydrocoupling of $H_3B{\cdot}NMe_2H$ with pre-catalysts **12**, **25** and **26** with an equilibrium established between an inactive dimeric fragment and an active dihydride as elucidated by the ESI-MS data reported in Figure 4.10. This equilibrium favours the active species as a result of it immediately reacting to re-coordinate $H_3B{\cdot}NMe_2H$ presumably forming an octahedral complex **(#1)**. This complex is set up to rapidly

reductively eliminate hydrogen to form a cationic Rh(I) $H_3B{\cdot}NMe_2H$ complex **(#2)** which then undergoes dehydrogenation to eliminate $H_2B{=}NMe_2$. In this mechanism $H_2B{=}NMe_2$ does not coordinate (as suggested by the lack of reactivity with $H_2B{=}N^iPr_2$) and as a result does not promote the formation of $H_3B{\cdot}NMe_2BH_2{\cdot}NMe_2H$ and thus reforms the active Rh(III) dihydride species. The dimerisation of $H_2B{=}NMe_2$ to form $[H_2BNMe_2]_2$ subsequently takes place off metal. Assuming 30% conversion of $H_3B{\cdot}NMe_2H$ to $H_2B{=}NMe_2$ at 8 minutes (Figure 4.11, Graph I), a second order process for the dimerisation of $H_2B{=}NMe_2$ to $[H_2BNMe_2]_2$ (k = 0.08 Ms^{-1},[34] $[A_0]$ = 0.07 M) would be expected to have a half-life of approximately 10 minutes which is consistent with the observed data in Figure 4.11.

4.2.6 Reactivity of 12, 25 and 26 in the catalytic dehydrocoupling of $H_3B{\cdot}NMeH_2$

The striking rates of catalysis achieved with **12**, **25** and **26**, particularly **12**, for the dehydrocoupling of $H_3B{\cdot}NMe_2H$ prompted us to examine them in the dehydropolymerisation of the related substrate $H_3B{\cdot}NMeH_2$ (Figure 4.14). As already noted in Chapter 1, the dehydrocoupling of $H_3B{\cdot}NMeH_2$ is known to form a range of products depending on the nature of the catalyst, *e.g.* $[HBNMe]_3$ and poly(*N*-methylaminoborane), with those described in Chapter 3 resulting in the slow formation of $[HBNMe]_3$.

The reactivity of pre-catalysts **12**, **25** and **26** was tested by adding the pre-catalysts (0.2 mol% loading) to a stirred solution of $H_3B{\cdot}NMeH_2$ in 1,2-$C_6H_4F_2$ solvent (0.45 M, 5 mL) under a constant flow of argon at room temperature. The ^{11}B NMR spectra of the reaction mixtures after 2 hours all showed complete consumption of starting material [δ −17 {q, *J*(BH) 97 Hz}] with the appearance of a broad peak centred at δ −5.9 characteristic for the formation of poly(*N*-methylaminoborane).[39] The ^{1}H NMR spectrum of the polymeric material exhibits three broad signals [δ +2.85 (N*H*), +2.23 (N*Me*), +1.69 (BH_2)] which is also consistent with previous known data for poly(*N*-methylaminoborane) (Figure 4.14). Repeating this reaction with the

Schlenk flask attached to a gas burette showed that approximately 1 equivalent of hydrogen was evolved over the 2 hour period.

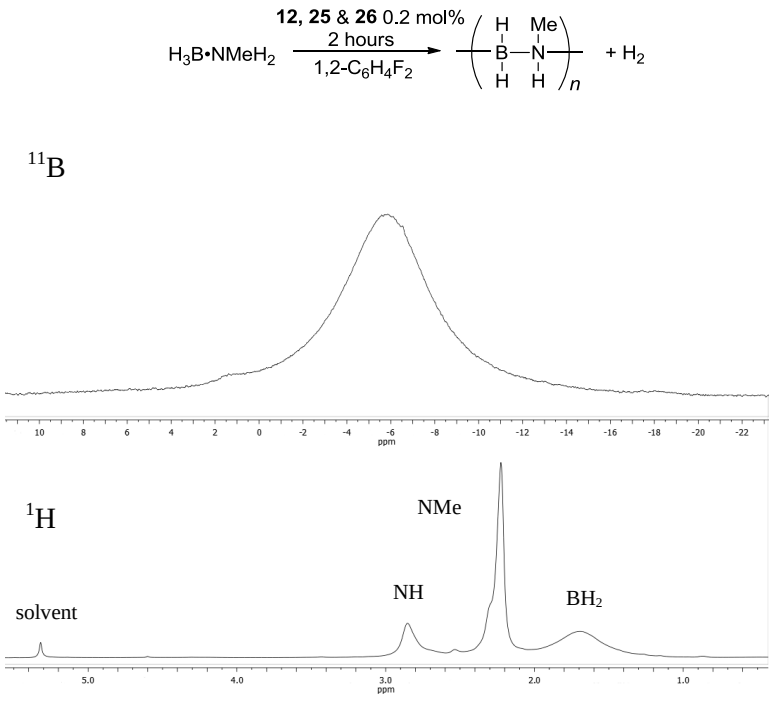


Figure 4.14 ^{11}B (160 MHz, 1,2-$C_6H_4F_2$) and ^{1}H NMR spectra (500 MHz, 1,2-$C_6H_4F_2$) of the reaction of $H_3B{\cdot}NMeH_2$ with **12** at 0.2 mol% pre-catalyst loading after 2 hours. ^{11}B NMR spectrum processed using back linear prediction.

Isolation of this material was achieved by precipitation into hexanes, redissolving in THF and a second precipitation into hexanes to yield an off-white powder. Gel Permeation Chromatography (GPC) analysis of the polymeric material was carried out by Alasdair P. M. Robertson of Prof. Ian Manners group (Bristol). A single well defined peak with a retention volume of 14.3 mL (THF solutions at 0.5 mg/ ml, containing 0.1% [$^{n}Bu_4N$]Br) confirmed the production of high molecular weight polymer with moderate polydispersity indicies (PDI) relative to polystyrene standards with each pre-catalyst (Table 4.4).

Table 4.4 Relative M_w and PDI values obtained from the dehydropolymerisation of $H_3B{\cdot}NMeH_2$ with **12**, **25** and **26** obtained from GPC and DLS data.

Pre-Catalyst	Catalyst Loading (mol%)	M_w	PDI
12	1	35000	2.7
12	0.2	171000	2.20
25	0.2	180000	1.25
26	0.2	120000	1.35

Increasing the catalyst loading (1 mol%) with **12** appeared to show a decrease in the molecular weight of the isolated polymer and an increase in the PDI. This is consistent with the existence of competing chain cleavage upon increased catalyst loading expected if the metal can also cut up the polymer chain.[40] The increased PDI for the fastest $H_3B{\cdot}NMe_2H$ dehydrogenation pre-catalyst **(12)** is also consistent with a catalyst which cuts up polymer following complete consumption of $H_3B{\cdot}NMeH_2$. Complexes **25** and **26** thus yield a polymer with a lower PDI as they presumably catalyse the dehydrogenation of $H_3B{\cdot}NMeH_2$ at a slower rate with less opportunity for the catalyst to cut up the resulting polymer, however further studies are needed to fully understand the mechanism by which these catalysts operate. Using similar conditions to the dehydrocoupling of $H_3B{\cdot}NMeH_2$, no catalytic activity was observed with $[H_2B{\cdot}NMeH]_3$ with **12** (0.2 mol% catalyst loading, 5 mL 1,2-$C_6H_4F_2$) even after two hours, further suggesting that it is not a prominent B-N intermediate in this process which is comparable to the observation that $H_3B{\cdot}NMe_2BH_2{\cdot}NMe_2H$ is also not a B-N intermediate in this system.

The proposed mechanism for the dehydrogenation of $H_3B{\cdot}NMe_2H$ also fits with the observation that in the dehydrocoupling of $H_3B{\cdot}NMeH_2$, an increase in catalyst loading results in a decrease in observed M_w of the resulting polymer. Rapid dehydrogenation of $H_3B{\cdot}NMeH_2$ to form $H_2B{=}NMeH$ would promote fast polymerisation *via* a yet unresolved mechanism. The polymer is then cut up to a greater extent with a higher catalyst loading given an increase in the concentration of metal which can interact with the polymer which is the main concept of chain-growth polymerisation.[40] That the catalyst further reacts with the growing polymer is contrary to

the observation that closely related $H_3B{\cdot}NMe_2BH_2{\cdot}NMe_2H$ has no affinity for the active catalyst. Further in depth analysis of the polymer at different catalyst loadings and different stages of the reaction would help identify whether this is indeed the case.

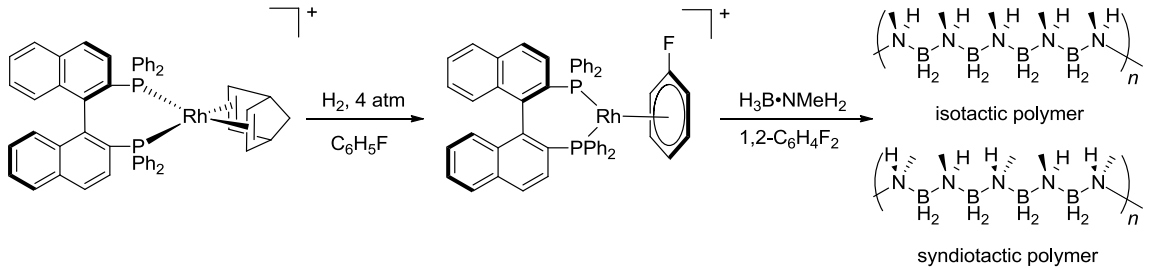
4.3 Conclusions

The catalysis of $H_3B{\cdot}NMe_2H$ with cationic Rh(I) chelating diphosphine complexes is remarkably different to that observed for cationic Rh(I) monodentate bis-phosphine and Ir(III) bis-phosphine complexes in terms of mechanism and turnover frequency. This work has demonstrated a clear structure activity relationship between isolated model cationic Rh(I) diphosphine $H_3B{\cdot}NMe_3$ complexes and catalytic activity. Increasing the bite angle of the diphosphine from dpp_{prop} to dpp_{pent} results in a stronger $Rh{\cdots}H_3B$ interaction which results in slower dehydrocoupling of $H_3B{\cdot}NMe_2H$ by the respective catalysts. Even so, rapid turnover of $H_3B{\cdot}NMe_2H$ to $[H_2BNMe_2]_2$ is achieved by these catalysts at 0.2 mol% catalyst loading. Dppe was not observed to coordinate $H_3B{\cdot}NMe_3$, consistent with the lack of reactivity of the pre-catalyst towards the dehydrocoupling of $H_3B{\cdot}NMe_2H$ thus indicating the existence of a limiting metal bite angle. Despite an observed induction period associated with each active pre-catalyst, all tests carried out indicate that this system is homogeneous. ESI-MS has led us to believe that the delay before the onset of catalysis is attributable to the formation of the active species which lies in equilibrium with a dormant species formed initially upon the addition of $H_3B{\cdot}NMe_2H$. A combination of ESI-MS and NMR spectroscopy experiments with $H_2B{=}N^iPr_2$, $H_3B{\cdot}NMe_2BH_2{\cdot}NMe_2H$ and indirectly with $H_2B{=}NMe_2$ have helped propose a likely mechanism involving rapid dehydrogenation of $H_3B{\cdot}NMe_2H$ to $H_2B{=}NMe_2$ affording an unstable $\{Rh(diphosphine)(H)_2\}^+$ fragment which readily reductively eliminates hydrogen to regenerate the active catalyst. Significantly, this mechanism *does not* involve the formation of $H_3B{\cdot}NMe_2BH_2{\cdot}NMe_2H$. Finally, using the trends found from the dehydrocoupling of

$H_3B{\cdot}NMe_2H$, we were able to design experiments to afford the rapid dehydrocoupling of $H_3B{\cdot}NMeH_2$ to afford high M_w poly(*N*-methylaminoborane) of low PDI.

4.4 Future Work

A suitable extension to this research would be to look at the possibility of forming chiral Rh-based catalysts for the polymerisation of $H_3B{\cdot}NMeH_2$. Chiral diphosphines with similar NBAs to dpp_{prop} (*e.g.* BINAP NBA = 93°) could implement the formation of syndiotactic or isotactic high molecular weight poly(*N*-methylaminoborane) as well as rapid catalysis. The ability to add control over the stereochemistry of polymer depending on the deployed catalyst would permit tuning of the properties of the polymer for use in future applications (Scheme 4.17).



Scheme 4.13 Using a chiral diphosphine catalyst could result in polymer definition with interesting properties. $[BAr^F_4]^-$ anions not shown.

Solubility of these polymers is likely to be a key issue in their formation and characterisation. Given the poor solubility of poly(*N*-methylaminoborane) in 1,2-$C_6H_4F_2$, new solvents which combine labile coordination to the $\{Rh(diphosphine)\}^+$ with the affinity to dissolve polymer are necessary and will no doubt aid the development of a mechanism for the dehydrocoupling process taking place and ultimately allow the natural extension to chiral AB polymerisation.

4.5 References

[1] Douglas, T. M.; Le Nôtre, J.; Brayshaw, S. K.; Frost, C. G.; Weller, A. S. *Chem. Commun.* **2006,** 3408-3410.

[2] Carbo, J. J.; Maseras, M.; Bo, C.; van Leeuwen, P. W. N. M. *J. Am. Chem. Soc.* **2001,** *123,* 7630-7637.

[3] Kranenburg, M.; van der Burgt, Y. E. M.; Kamer, P. C. J.; van Leeuwen, P. W. N. M. *Organometallics* **1995,** *14,* 3081-3089.

[4] Bronger, R. P. J.; Kamer, P. C. J.; van Leeuwen, P. W. N. M. *Organometallics* **2003,** *22,* 5358-5369.

[5] Marcone, J. E.; Moloy, K. G.; *J. Am. Chem. Soc.* **1998,** *120,* 8527-8528.

[6] Raebiger, J. W.; Miedaner, A.; Curtis, C. J.; Miller, S. M.; Anderson, O. P.; DuBois, D. L. *J. Am. Chem. Soc.* **2004,** *126,* 5502-5514.

[7] Mo, J.; Ruan, J.; Xu, L.; Hyder, Z.; Saidi, O.; Liu, S.; Pei W.; Xiao, J. *J. Mol. Catal. A: Chem.* **2007,** *261,* 267-275.

[8] Liron, F.; Fosse, C.; Pernolet, A.; Roulland, E. *J. Org. Chem.* **2007,** *72,* 2220-2223.

[9] Mann, G.; Baranano, D.; Hartwig, J. F.; Rheingold, A. L.; Guzei, I. A. *J. Am. Chem. Soc.* **1998,** *120,* 9205-9219.

[10] Birkholz, M.-N. Freixa, Z.; van Leeuwen, P. W. N. M. Chem. Soc. Rev. **2009,** *38,* 1099-1118.

[11] Pawley, R. J.; Moxham, G. L.; Dallanegra, R.; Chaplin, A. B.; Brayshaw, S. K.; Weller, A. S.; Willis, M. C. *Organometallics* **2010,** *29,* 1717-1728.

[12] Douglas, T. M.; Chaplin, A. B.; Weller, A. S. *Organometallics* **2008,** *27,* 2918-2921.

[13] Kawano, Y.; Kakizawa, T.; Yamaguchi, K.; Shimoi, M. *Chem. Lett.* **2006**, *35*, 568–569.

[14] Merle, N.; Koicok-Köhn, G.; Mahon, M. F.; Frost, C. G.; Ruggerio, G. D.; Weller, A. S.; Willis, M. C. *Dalton Trans.* **2004,** 3883-3892.

[15] Merle, N.; Frost, C. G.; Kociok-Köhn, G.; Willis, M. C.; Weller, A. S. *Eur. J. Inorg. Chem.* **2006,** 4068-4073.

[16] Chaplin, A. B.; Weller, A. S. *Inorg. Chem.* **2010,** *49,* 1111-1121.

[17] Moxham, G. L.; Randell-Sly, H.; Brayshaw, S. K. Weller, A. S.; Willis, M. C. *Chem. Eur. J.* **2008,** *14,* 8383-8397.

[18] Alcaraz, G.; Sabo-Etienne, S. *Coord. Chem. Rev.* **2008,** *252,* 2395-2409.

[19] Betley, T. A.; Peters, J. C. *Angew. Chem. Int. Ed.* **2003,** *42,* 2385-2389.

[20] Douglas, T. M.; Chaplin, A. B.; Weller, A. S. *J. Am. Chem. Soc.* **2008,** 130, 14432-14433.

[21] Friedrich, A.; Drees, M.; Schneider, S. *Chem. Eur. J.* **2009,** *15,* 10339-10342.

[22] Liu, W.; Wang, H.; Zhang, H.; Wu, X.; Deng, Y.; Yang, Z.; Lei, A. *Chem. Eur. J.* **2009,** *15,* 4437-4445.

[23] Conley, B. L.; Williams, T. J. *Chem. Commun.* **2010,** *46,* 4815-4817.

[24] Widegren, J. A.; Finke, R. G. *J. Mol. Catal. A: Chem.* **2003,** *198,* 317-341.

[25] Wilcoxon, J. P.; Craft, S. A.; *Nanonstruct. Mater.* **1997,** *9,* 85-88.

[26] Jaska, C. A.; Clark, T. J. Clendenning, S. B.; Grozea, D.; Turak, A.; Lu, Z.-H.; Manners, I. *J. Am. Chem. Soc.* **2005,** *127,* 5116-5124.

[27] Paal, C. Hartmann, W. *Chem. Ber.* **1918,** *51,* 711-737.

[28] Hornstein, B. J.; Aiken, J. D. III; Finke, R. G. *Inorg. Chem.* **2002,** *41,* 1625-1638.

[29] Jaska, C. A.; Manners, I. *J. Am. Chem. Soc.* **2004,** *126,* 9776-9785.

[30] Hagen, C. M.; Vieille-Petit, L.; Laurenczy, G.; Süss-Fink, G.; Finke, R. G. *Organometallics* **2005,** *24,* 1819-1831.

[31] Wilson, A. D.; Miller, A. J. M.; DuBois, D. L.; Labinger, J. A.; Bercaw, J. E. *Inorg. Chem.* **2010,** *49,* 3918-3926.

[32] Chaplin, A. B.; Weller, A. S. *Angew. Chem. Int. Ed.* **2010,** *49,* 581-584.

[33] Douglas, T. M.; Chaplin, A. B.; Weller, A. S.; Hall, M. B.; Yang, X. *J. Am. Chem. Soc.* **2009,** *131,* 15440-15456.
[34] Stevens, C. J.; Dallanegra, R.; Chaplin, A. B.; Weller, A. S.; Macgregor, S. A.; Ward, B.; McKay, D.; Alcaraz, G.; Sabo-Etienne, S. *Chem. Eur. J.* **2011,** *17,* 3011-3020.
[35] Euzenat, L.; Horhant, D.; Ribourdouille, Y.; Duriez, C.; Alcaraz, G.; Vaultier, M. *Chem. Commun.* **2003,** 2280–2281.
[36] Alcaraz, G.; Chaplin, A. B.; Stevens, C. J.; Clot, E.; Vendier, L.; Weller, A. S.; Sabo-Etienne, S. *Organometallics* **2010,** *29,* 5591–5595.
[37] Vance, J. R.; Robertson, A. P. M.; Lee, K.; Manners, I. *Chem Eur. J.* **2011,** *17,* 4099-4103.
[38] Jaska, C. A.; Temple, K.; Lough, A. J.; Manners, I. *J. Am. Chem. Soc.* **2003,** *125,* 9424-9434.
[39] Staubitz, A.; Presa Soto, A.; Manners, I. *Angew. Chem. Int. Ed.* **2008,** *47,* 6212-6215.
[40] Staubitz, A.; Sloan, M. E.; Robertson, A. P. M.; Friedrich, A.; Schneider, S.; Gates, P. J.; a. d. Günne, J. S.; Manners, I. *J. Am. Chem. Soc.* **2010,** 132, 13332-13345.
[41] Tang, C. Y.; Thompson, A. L.; Aldridge, S. *Angew. Chem. Int. Ed.* **2010,** *49,* 921-925.
[42] Alcaraz, G.; Clot, E.; Helmstedt, U.; Vendier, L.; Sabo-Etienne, S. *J. Am. Chem. Soc.* **2007,** *129,* 8704-8705.

5 EXPERIMENTAL

5.1 General

All manipulations, unless otherwise stated, were performed under an atmosphere of argon, using standard Schlenk and glove-box techniques. Glassware was oven dried at 130 °C overnight and flamed under vacuum prior to use. CH_2Cl_2, MeCN, Et_2O, THF, toluene, benzene, hexane and pentane were dried using a Grubbs type solvent purification system (MBraun SPS-800) and degassed by successive freeze-pump-thaw cycles.[1] DME was dried by bubbling argon into the solvent for 30 minutes and storing over 3 Å molecular sieves. CD_2Cl_2, C_6H_5F and 1,2-$C_6H_4F_2$ were distilled under vacuum from CaH_2 and stored over 3 Å molecular sieves. *tert*-Butylethylene was dried over sodium, vacuum distilled and stored over 3 Å molecular sieves. Microanalyses were performed by Elemental Microanalysis Ltd or London Metropolitan University. Characterisation of polymer samples from the dehydrogenation and dehydrocoupling of $H_3B{\cdot}NMeH_2$ by complexes **12**, **25** and **26** were carried out by Alasdair P. M. Robertson (University of Bristol).

5.2 Nuclear Magnetic Resonance spectroscopy

NMR spectra were recorded on Varian Unity$^+$ 500 MHz, Bruker AVII 500 MHz or Varian Venus 300 MHz spectrometers at room temperature unless otherwise stated. Residual protio solvent was used as reference for ^{1}H and ^{13}C NMR spectra in deuterated solvent samples. In 1,2-$C_6H_4F_2$ and C_6H_5F, ^{1}H NMR spectra were referenced to the centre of the high frequency solvent multiplet (δ = 7.07 and 7.11 respectively). ^{31}P and ^{11}B NMR spectra were referenced against 85% H_3PO_4 (external) and $F_3B{\cdot}OEt_2$ (external) respectively. Chemical shirts are quoted in ppm and coupling constants in Hz.

5.3 Mass spectrometry

Electrospray Ionisation Mass Spectrometry (ESI-MS) was recorded using a Bruker MicrOTOF-Q instrument directly connected to a modified Innovative Technology glove box.[2] The mass spectrometer was calibrated in positive ion mode using a 10 ng/ mL mixture of tetraalkylammonium bromides $[N(C_n\text{-}H_{2n+1})_4]Br$ (n = 2, 3, 4, 5, 6, 7, 8, 12, 16, 18) in DCM.[2] Typical acquisition parameters were; sample flow rate 4 μL/ min; nebuliser gas pressure 0.4 bar, drying gas(argon at 60 °C, flowing at 4L/ min, capillary voltage 4.5 kV, funnel voltage 200 Vpp; and the solvent CH_2Cl_2, C_6H_5F, 1,2-$C_6H_4F_2$ or $(CH_3)_2CO$. MS samples were diluted to a concentration of 1 x 10^{-6} M before running.

5.4 X-ray crystallography

Structure determinations were carried out by either Dr. Adrian B. Chaplin or Dr. Amber L. Thompson (University of Oxford). Relevant crystallographic data for complexes **1**, **2**, **4**, **9**, **10**, **12**, **14**, **17-19**, **21**, **23**, **27**, **29** and **31** can be found in Table 5.1. Data were acquired on a Nonius Kappa CCD diffractometer using graphite monochromated Mo Kα radiation (λ = 0.71073 Å) and a low-temperature device.[3] All non-hydrogen atoms were refined anisotropically. Data deposited in CCDC and can be obtained free of charge *via* www.ccdc.cam.ac.uk/data_request/cif. Graphical representations of X-ray structures were made using ORTEP3.[4]

5.5 Starting materials

$Na[BAr^F_4]$,[5] $[Rh(NBD)Cl]_2$,[6,7] Rh(NBD)$PCyp_3$Cl **(i-74)**,[8] $[Rh(\eta^6\text{-}C_6H_5F)PR_2(\eta^2\text{-}C_5H_7)][BAr^F_4]$ {R = Cyp **(i-9)**,[8] ^{i}Pr **(i-9a)**[9]}, $[Rh(Ph_2P(CH_2)_2PPh_2)Cl)]_2$,[10] [Rh(diphosphine)(NBD)]$[BAr^F_4]$ **(i2-12-15)**,[11] $H_3B{\cdot}NMeH_2$,[12] $H_3B{\cdot}NMe_2BH_2{\cdot}NMe_2H$,[13] $[H_2BNMe_2]_2$[13] and $[H_2B{\cdot}NMeH]_3$[14] were made following

literature procedures or variations thereof. $H_3B{\cdot}NMe_2H$ and $H_3B{\cdot}NMe_3$ were purchased from Aldrich and sublimed before use ($5 \sim 10^{-2}$ Torr, 298 K). $H_2B{=}N^iPr_2$ was prepared by Dr. Gilles Alcaraz (CNRS, Toulouse),[15] ligands **I-III** were synthesised by Ben Pilgrim (University of Oxford).[16] All other chemicals were used as received from Sigma-Aldrich, Acros, Fisher, Fluka, Fluorochem and Strem Chemicals.

5.6 Synthesis of new complexes

[Rh($\kappa^3_{(POP)}$-DPEphos){P(Cyp)$_2$(η^2-C$_5$H$_7$)}][BAr$^F_4$] (1)

DPEphos (16.5 mg, 0.031 mmol) was added to a solution of [Rh(η^6-C$_6$H$_5$F){PCyp$_2$(η^2-C$_5$H$_7$}][BAr$^F_4$] **(i-9)** (40 mg, 0.031 mmol) in CH_2Cl_2 (5 mL) and stirred for 2 hours. The solvent was removed *in vacuo* and the residue was washed with pentane (2 x 3 mL) and dried under reduced pressure. Diffusion of pentane into a solution of the residue in C_6H_5F gave **1** as red crystals (43 mg, 80 %).

^{1}H NMR (500 MHz, CD_2Cl_2): δ 7.73 (m, 8H, BAr$^F_4$), 7.56 (br, 4H, BAr$^F_4$) 7.50-7.25 (m, 22H, ArH), 7.18 [dd, *J*(PH) 8.5, *J*(HH) 4.4, 2H, POP bridging ArH], 7.06 (m, 4H, POP bridging ArH), 3.84 (s, 2H, HC=CH), 2.04 (bs, 1H, PC$_5$H$_7$), 1.84 [apparent t, *J*(PH) 13, 2H, PCyp CH], 1.65 – 1.30 (m, 16H, PCyp), 1.25 – 1.00 (m, 4H, PCyp).

^{31}P{^{1}H} NMR (202 MHz, CD_2Cl_2): δ 84.1 [dt, *J*(RhP) 145, *J*(PP$_{cis}$) 42], 19.0 [dd, *J*(RhP) 134, *J*(PP$_{cis}$) 42].

^{13}C{^{1}H} NMR (126 MHz, CD_2Cl_2): δ 162.2 [q, *J*(BC) 51, BAr$^F_4$], 160.1 (d, *J* = 12, C$_6$H$_4$OP), 135.4 (s, C$_6$H$_4$OP), 135.2 (s, BAr$^F_4$), 133.59 (d, *J* = 12, C$_6$H$_5$), 133.2 (d, *J* = 34, C$_6$H$_5$), 132.1 (s, C$_6$H$_4$OP), 130.8 (s, C$_6$H$_5$), 129.1 [qq, *J*(FC) 32, *J*(BC) 2.9, BAr$^F_4$], 129.0 (d, *J* = 9.5, C$_6$H$_5$), 126.7 (d, *J* = 32, C$_6$H$_4$OP), 126.4 (d, *J* = 4.8, C$_6$H$_4$OP), 125.0 [q, *J*(FC) 273, BAr$^F_4$], 120.0 (d, *J* = 4.8, C$_6$H$_4$OP), 117.9 [sept, *J*(FC) 3.8, BAr$^F_4$], 74.9 (broad s, C=C), 37.0 [dt, *J* (PC) 23, *J*(PC) 2.9, CH], 36.4 [d, *J*

(PC) 2.9, CH_2], 32.3 [d, *J* (PC) 28, CH], 31.6 (s, CH_2), 29.2 (s, CH_2), 25.9 [d, *J*(PC) 8.6, CH_2], 25.5 [d, *J*(PC) 9.5, CH_2].

ESI-MS (C_6H_5F, 373 K, 4.5 kV) positive ion: m/z, 877.2298 $[M]^+$ (100 % calc. 877.2359).

Anal. Calcd for $C_{83}H_{65}B_1F_{24}O_1P_3Rh_1$ (1741.003 $gmol^{-1}$): C, 57.26; H, 3.74. Found: C, 57.56; H, 3.16.

[Rh($\kappa^3_{(POP)}$-XANTphos){P(Cyp)$_2$(η^2-C_5H_7)}][BAr$^F_4$] (2)

XANTphos (22 mg, 0.038 mmol) was added to a solution of [Rh(η^6-C_6H_5F){PCyp$_2$(η^2-C_5H_7}][BAr$^F_4$] **(i-9)** (49.5 mg, 0.038 mmol) in CH_2Cl_2 (5 mL) and stirred for 2 hours. The solvent was removed *in vacuo* and the residue was washed with pentane (2 x 3 mL) and dried under reduced pressure. Diffusion of pentane into a solution of the residue in CH_2Cl_2 gave **2** as orange crystals (50 mg, 74 %).

^{1}H NMR (500 MHz, CD_2Cl_2): δ 7.75 (m, 8H, BAr$^F_4$), 7.57 (br, 4H BAr$^F_4$), 7.67 – 7.52 (m, 6H, ArH), 7.51 – 7.41 (m, 6H, ArH), 7.36 – 7.19 (m, 8H, ArH), 7.18 – 7.03 (m, 6H, ArH), 3.58 (s, 2H, HC=CH), 1.86 (s, 3H, CH_3), 1.85-1.17 (m, 21H, PCyp), 1.37 (s, 3H, CH_3), 1.11 – 0.89 (m, 4H, PCyp).

^{31}P{^{1}H} NMR (202 MHz, CD_2Cl_2): δ 90.7 [dt, *J*(RhP) 152, *J*(PP_{cis}) 22], 26.6 [dd, *J*(RhP) 131, *J*(PP_{cis}) 22].

^{13}C{^{1}H} NMR (126 MHz, CD_2Cl_2): δ 162.1 [q, *J*(BC) 50, BAr$^F_4$], 156.7 (t, *J* = 8.8, C_6H_3OP), 136.4 (t, *J* = 18, C_6H_5), 135.3 (t, *J* = 2.3, C_6H_3OP), 135.1 (s, BAr$^F_4$), 133.9 (s, C_6H_3OP), 133.7 (t, *J* = 11, C_6H_5), 133.0 (t, *J* = 7.3, C_6H_5), 132.5 (t, *J* = 6.1, C_6H_5), 130.5 (s, C_6H_5), 130.38 (s, C_6H_5), 129.3 (t, *J* = 4.6, C_6H_5), 129.2 [qq, *J*(FC) 31, *J*(BC) 3.1, BAr$^F_4$], 129.1 (t, *J* = 4.2, C_6H_5), 127.9 (s, C_6H_3OP), 127.3 (s, C_6H_3OP), 126.1 (dd, *J* = 17, *J* = 14, C_6H_3OP), 124.9 [q, *J*(FC) 272, BAr$^F_4$], 117.8 [sept, *J*(FC) 3.8, BAr$^F_4$], 62.2 (dd, *J* = 22, *J* = 12, C=C), 36.8 (s, qC), 36.5 [br dt, *J*(PC) 25, *J*(PC) 4.6,

CH], 35.2 [d, *J*(PC) 31, CH], 35.2 (s, CH_2), 33.0 (s, CH_3), 30.6 [d, *J*(PC) 5.3], 28.6 (s, CH_2), 25.6 [d, *J*(PC) 9.9, CH_2], 25.1 [d, *J*(PC) 11, CH_2], 22.9 (s, CH_3).

ESI-MS (C_6H_5F, 373 K, 4.5 kV) positive ion: m/z, 917.2665 $[M]^+$ (100% calc. 917.2672).

Anal. Calcd for $C_{86}H_{69}B_1O_1F_{24}P_3Rh_1$ (1781.067 $gmol^{-1}$): C, 57.99; H, 3.90. Found: C, 58.16; H, 3.72.

[Rh($\kappa^3_{(POP)}$-DPEphos)$(H)_2$($PCyp_3$)][BAr^F_4] (3) and [Rh($\kappa^2_{(PP)}$-DPEphos)$(H)_2$(η^2-H_2)($PCyp_3$)][BAr^F_4] (4)

3

A solution of **1** (25 mg, 0.0144 mmol) in C_6H_5F (2 mL) was frozen in liquid nitrogen, placed under vacuum and backfilled with H_2 and shaken for 10 minutes. Diffusion of hydrogenated pentane into the resulting solution and shaking after cooling gave **3** as colourless crystals. Complex **3** loses H_2 when removed from a H_2 atmosphere and thus microanalytical data were not obtained.

^{1}H NMR (500 MHz, CD_2Cl_2, 223 K): δ 7.80 – 7.16 (m, 21H, ArH), 7.75 (m, 8H, BAr^F_4), 7.56 (br, 4H, BAr^F_4), 7.10 (apparent triplet, *J* = 7.7, 1H, ArH), 7.00 – 6.84 (m, 3H ArH), 6.44 (apparent td, *J* = 8.2, 1.6, 2H, ArH) 5.97 (m, 2H, ArH), 1.80 – 1.20 (m, 27H, $PCyp_3$), −8.66 [apparent doublet of quintets *J*(PH_{trans}) 149, *J* = 13, 1H, T_1 = 0.52 s, RhH], −22.95 (apparent broad triplet, *J* = 26, 1H, T_1 = 0.54 s, RhH).

^{31}P{^{1}H} NMR (202 MHz, CD_2Cl_2, 248 K): δ 62.3 [ddd, *J*(PP_{trans}) 319, *J*(RhP) 114, *J*(PP_{cis}) 18], 34.0 [ddd, *J*(PP) 319, *J*(RhP) 106, *J*(PP_{cis}) 22], 27.7 [apparent dt, *J*(RhP) 104, *J*(PP_{cis}) 20].

ESI-MS (C_6H_5F, 373 K, 4.5 kV) positive ion: m/z, 879.2352 $[M\text{-}H_2]^+$ (100 %, calc. 879.2515), 881.2477 $[M]^+$ (65 %, calc. 881.2672).

4

A solution of **1** (8 mg, 0.0046 mmol) in CD_2Cl_2 (500 µL) was frozen in liquid nitrogen, placed under vacuum and backfilled with H_2 and shaken for 10 minutes. **4** was observed upon cooling this solution to 198 K at a ratio of 1:5 (**3**:**4**) and was characterised by ^{1}H NMR spectroscopy.

^{1}H NMR (500 MHz, CD_2Cl_2, 198 K): δ −1.79 (broad s, 2H, T_1 = 21 ms), −11.06 [br d, J(PH_{trans}) 149, 1H], −13.33 (br, 1H). T_1 values for the two hydride resonances are approximately 400 ms at this temperature.

[Rh(κ$^3_{(POP)}$-XANTphos)(H)$_2$(PCyp$_3$)][BAr$^F_4$] isomers (5/ 6)

A solution of **2** (8 mg, 0.0045 mmol) in CD_2Cl_2 (500 µL) was frozen in liquid nitrogen, placed under vacuum and backfilled with H_2, shaken and left to stand for 5 days. **5/ 6** were then characterised by ^{1}H and ^{31}P{^{1}H} NMR spectroscopy.

5

^{1}H NMR (500 MHz, CD_2Cl_2): δ −9.33 [br d, J(PH_{trans}) 143, 1H, T_1 = 0.25 s, RhH], −22.19 (br, 1H, T_1 = 0.22 s, RhH).

^{31}P{^{1}H} NMR (202 MHz, CD_2Cl_2): δ 50.9 [br dd, J(PP_{trans}) 319, J(RhP) 117], 35.4 [br d, J(RhP) 91], 27.3 [br d, J(RhP) 95].

ESI-MS (C_6H_5F, 373 K, 4.5 kV) positive ion: m/z, 919.2696 $[M\text{-}H_2]^+$ (100%, calc. 919.2828).

6

^{1}H NMR (500 MHz, CD_2Cl_2): δ −7.93 [apparent dqd,* J(PH_{trans}) 135, J(P_{cis}H) 13, J(RhH) 13, J(HH) 5.8, 1H, T_1 = 0.55 s, RhH], δ −20.49 [apparent multiplet,* J(P_{cis}H) 28.4, J(P_{cis}H) 12.3, J(RhH) 19.2, J(HH) 5.8, 1H, T_1 = 0.43 s, RhH]. *These complex signals were simulated using gNMR to extract the corresponding spectral parameters.

$^{31}P\{^{1}H\}$ NMR (202 MHz, CD_2Cl_2): δ 36.9 [dd, *J*(RhP) 114, *J*(PP_{cis}) 20], 20.7 [dt, *J*(RhP) 97, *J*(PP_{cis}) 20].

[Rh($\kappa^2_{(PP)}$-DPEphos)($PCyp_3$)$(H)_2$(MeCN)][BAr^F_4] (7)

A solution of **1** (8 mg, 0.0046 mmol) in C_6H_5F (500 µL) was frozen in liquid nitrogen, placed under vacuum and backfilled with H_2 and shaken for 10 minutes to give **3**. MeCN (2 µL) was added and the product was immediately characterised *in situ* by ^{1}H and $^{31}P\{^{1}H\}$ NMR spectroscopy at 298 K.

^{1}H NMR (500 MHz, CD_2Cl_2): δ 7.74 (m, 8H, BAr^F_4), 7.57 (br, 4H BAr^F_4), 7.56 – 7.37 (m, 12H, ArH), 7.34 (br t, 3H, ArH), 7.28 – 6.96 (m, 9H, ArH), 6.91 (br t, *J* = 7.3, 1H, ArH), 6.63 (br t, *J* = 7.1 1H, ArH) 6.45 – 6.27 (m, 2H, ArH), 1.75 – 1.16 (m, 30H, $PCyp_3$ and co-ordinated MeCN), −11.34 [apparent doublet of quintets,* *J*(PH_{trans}) 149, *J*($P_{cis}H$) 16.7, *J*($P_{cis}H$) 11.7, *J*(RhH) 14.4, *J*(HH) 8.5, 1H, RhH], −17.76 [apparent multiplet,* *J*($P_{cis}H$) 17.2, *J*($P_{cis}H$) 14.6, *J*($P_{cis}H$) 12.0, *J*(RhH) 10.4, *J*(HH) 8.5, 1H, RhH]. *These complex signals were simulated using gNMR to extract the corresponding spectral parameters.

$^{31}P\{^{1}H\}$ NMR (202 MHz, CD_2Cl_2): δ 50.9 [dd, *J*(PP_{trans}) 357, *J*(RhP) 110], 32.1 [dd, *J*(PP_{trans}) 358, *J*(RhP) 112], 22.9 [d, *J*(RhP) 99].

ESI-MS (C_6H_5F, 373 K, 4.5 kV) positive ion: m/z, 879.2380 $[M\text{-}MeCN\text{-}H_2]^+$ (100 % calc. 879.2515), 922.2783 $[M]^+$ (10 % calc. 922.2937). ESI-MSMS of peak 922.2783 m/z (C_6H_5F): 881.2528 $[M\text{-}MeCN]^+$ (calc. 881.2672), 879.2338 $[M\text{-}MeCN\text{-}H_2]^+$ (calc. 879.2515).

[Rh($\kappa^2_{(PP)}$-XANTphos)($PCyp_3$)(H_2)(MeCN)][BAr^F_4] (8)

A solution of **2** (8 mg, 0.0045 mmol) in CD_2Cl_2 (500 µL) was frozen in liquid nitrogen, placed under vacuum and backfilled with H_2, shaken, and left for 5 days to yield **5**/ **6**. MeCN (2 µL) was

added and the product was immediately characterised *in situ* by ^{1}H and $^{31}P\{^{1}H\}$ NMR spectroscopy at 298 K.

^{1}H NMR (500 MHz, CD_2Cl_2): δ 7.72 (m, 8H, BAr^{F}_{4}), 7.63 (ddd, *J* = 10.7, 7.7, 1.2, 2H, ArH), 7.56 (m, 4H, BAr^{F}_{4}), 7.47 - 7.36 (m, 6H, ArH), 7.33 (m, 2H, ArH), 7.28 – 6.99 (m, 14H, ArH), 6.74 (m, 1H, C_6H_3OP), 6.30 (m, 1H, C_6H_3OP), 1.92 (s, 3H, CH_3), 1.85 – 1.19 (m, 27H, $PCyp_3$), 1.38 (s, 3H, CH_3), −11.92 [apparent multiplet,* *J*($P_{trans}H$) 149, *J*($P_{cis}H$) 17.3, *J*($P_{cis}H$) 14.3, *J*(RhH) 10.8, *J*(HH) 9.2, 1H, RhH], −17.92 [apparent septet,* *J*($P_{cis}H$) 21.1, *J*($P_{cis}H$) 12.5, *J*(RhH) 10.6, *J*($P_{cis}H$), *J*(RhH) 9.2, *J*(HH) 7.3, 1H, RhH]. *These complex signals were simulated using gNMR to extract the corresponding spectral parameters.

$^{31}P\{^{1}H\}$ NMR (202 MHz, CD_2Cl_2): δ 56.6 [ddd, *J*(PP_{trans}) 365, *J*(RhP) 115, *J*(PP_{cis}) 15], 20.0 [ddd, *J*(PP_{trans}) 365, *J*(RhP) 110, *J*(PP_{cis}) 20], 15.3 [ddd, *J*(RhP) 92, *J*(PP_{cis}) 20, *J*(PP_{cis}) 15].

ESI-MS (1,2-$C_6H_4F_2$, 333 K, 4.5 kV) positive ion: m/z, 919.2881 $[M\text{-}MeCN\text{-}H_2]^+$ (100 % calc. 919.2828).

[Rh($\kappa^3_{(POP)}$-DPEphos)($PCyp_3$)][BAr^{F}_{4}] (9)

A solution of **1** (25 mg, 0.0144 mmol) in C_6H_5F (2 mL) was frozen in liquid nitrogen, placed under vacuum and backfilled with H_2 and shaken for 10 minutes to give **3**. The H_2 atmosphere was removed under vacuum by freeze/ pump/ thaw of the solution three times followed by addition of 5 μL of 3,3 dimethyl-but-1-ene. The solvent was then removed under reduced pressure and the resulting residue was washed with pentane (2 x 3 mL) and dried *in vacuo*. An orange crystal suitable for X-ray diffraction was obtained by diffusion of pentane into a solution of **9** in $C_6H_5CF_3$. Despite repeated attempts, isolation of significant solid material proved unsuccessful as the complex (although pure by NMR spectroscopy) remained an oil.

^{1}H NMR (500 MHz, CD_2Cl_2): δ 8.28 (br, 2H, ArH), 7.96 – 7.43 (m, 20H, ArH), 7.75 (m, 8H, BAr^F_4), 7.58 (br, 4H BAr^F_4), 7.29 (apparent td, *J* = 7.3, 1.6 2H, ArH, 7.16 (t, *J* = 7.6, 2H, ArH), 6.91 (br dt, *J* = 8.4, 2.0, 2H, ArH) 1.90 – 0.88 (m, 27H, $PCyp_3$).

^{31}P{^{1}H} NMR (202 MHz, CD_2Cl_2): δ 48.8 [dt, *J*(RhP) 190, *J*(PP_{cis}) 35], 33.4 [dd, *J*(RhP) 156, *J*(PP_{cis}) 35].

^{13}C{^{1}H} NMR (126 MHz, CD_2Cl_2): δ 162.3 [q, *J*(BC) 50, BAr^F_4], 158.4 (t, *J* = 6.9, C_6H_4OP), 135.9 (br m, C_6H_5), 135.4 (s, BAr^F_4), 133.7 (br m, C_6H_5), 133.4 (s, C_6H_4OP), 132.4 (s, C_6H_4OP), 132.0 (br m, C_6H_5), 129.6 (t, *J* = 5.0, C_6H_5), 129.4 [qq, *J*(FC) 31, *J*(BC) 3, BAr^F_4], 126.6 (t, *J* = 3.1, C_6H_4OP), 125.1 [q, *J*(FC) 272, BAr^F_4], 118.0 [sept, *J*(FC) 3.8, BAr^F_4], 115.6 (t, *J* = 2.3, C_6H_4OP), 41.0 [d, *J* (PC) 29, CH], 30.4 (br m, CH_2), 24.8 (br m, CH_2).

ESI-MS (C_6H_5F, 373 K, 4.5 kV) positive ion: m/z, 879.2429 $[M]^+$ (100 %, calc. 879.2515).

[Rh($\kappa^3_{(POP)}$-XANTphos)($PCyp_3$)][BAr^F_4] (10)

A solution of **2** (25 mg, 0.0144 mmol) in C_6H_5F (2 mL) was placed under 4 atm of H_2 and shaken, and left for 5 days to yield **5**/ **6**. The H_2 was removed under vacuum by freeze/ pump/ thaw of the solution. The solvent was then removed under reduced pressure and the resulting residue was washed with pentane (2 x 3 mL) and dried *in vacuo*. A crystal of **10** suitable for X-ray diffraction was obtained by diffusion of pentane into a solution of the residue in C_6H_5F. Despite repeated attempts, isolation of significant solid material proved unsuccessful as the complex (although pure by NMR spectroscopy) remained an oil.

^{1}H NMR (500 MHz, CD_2Cl_2): δ 7.98 (m, 8H, ArH), 7.74 (br, 8H, BAr^F_4), 7.58 (m, 10H, BAr^F_4 & ArH), 7.51 (m, 8H, ArH), 7.29 (m, 2H, C_6H_3OP), 7.21(t, 2H, *J* = 7.7 C_6H_3OP), 1.63 (s, 6H, CH_3), 1.61 (br m, 3H, $PCyp_3$), 1.48 (br m, 6H, $PCyp_3$), 1.31 (br m, 12H, $PCyp_3$), 0.99 (br m, 6H, $PCyp_3$).

^{31}P{^{1}H} NMR (202 MHz, CD_2Cl_2): δ 44.3 [dt, *J*(RhP) 193, *J*(PP_{cis}) 35], 33.1 [dd, *J*(RhP) 156, *J*(PP_{cis}) 35].

$^{13}C\{^1H\}$ NMR (126 MHz, CD_2Cl_2): δ 162.1 [q, *J*(BC) 50, BAr^F_4], 153.1 (t, *J* = 8.1, C_6H_3OP), 135.1 (s, BAr^F_4), 134.1 (t, *J* = 6.9, C_6H_5), 133.4 (s, C_6H_3OP), 132.44(t, *J* = 22, C_6H_5), 131.6 (s, C_6H_5), 131.4 (t, *J* = 3.1, C_6H_3OP), 131.0 (s, C_6H_3OP), 129.3 (t, *J* = 5.0, C_6H_5), 129.2 [qq, *J*(FC) 31, *J*(BC) 2.7, BAr^F_4], 126.8 (t, *J* = 2.7, C_6H_3OP), 126.5 (t, *J* = 16, C_6H_3OP), 124.9 [q, *J*(FC) 272, BAr^F_4], 117.8 [sept, *J*(FC) 3.8, BAr^F_4], 42.2 [br d, *J*(PC) 29, CH], 34.3 (s, qC), 33.6 (s, CH_3), 30.6 (s, CH_2), 25.0 [d, *J*(PC) 11, CH_2].

ESI-MS (C_6H_5F, 373 K, 4.5 kV) positive ion: m/z, 919.2708 $[M]^+$ (100% calc. 919.2828).

Preparation of $[Rh(Ph_2P(CH_2)_2PPh_2)(\eta^6\text{-}C_6H_5F)][BAr^F_4]$ (11)

A suspension of $[Rh(Ph_2P(CH_2)_2PPh_2)Cl)]_2$ (80.0 mg, 0.0745 mmol) and $Na[BAr^F_4]$ (132.1 mg, 0.149 mmol) in C_6H_5F (10 mL) was stirred at room temperature for 2 hours. Pentane (8 mL) was added to the flask to encourage the full precipitation of NaCl (which is partially soluble in C_6H_5F) and then filtered. The product was isolated by first concentrating the filtrate (~ 5 mL) and then adding the solution dropwise to pentane (30 mL) with rigorous stirring causing **11** to precipitate as a red solid. Yield 80 mg, 37 %.

^1H NMR (500 MHz, C_6H_5F): δ 8.37 (s, 8H, BAr^F_4), 7.63 (s, 4H, BAr^F_4), 1.83 (apparent d, *J* = 20, 4H, CH_2). The co-ordinated C_6H_5F signals were not unambiguously located and the phenyl signals not assigned as they were obscured by C_6H_5F solvent δ 7.31 – 6.70.

$^{31}P\{^1H\}$ NMR (121 MHz, C_6H_5F): δ 73.5 [d, *J*(RhP) 203].

ESI-MS (C_6H_5F, 60 °C, 4.5 kV) positive ion: m/z, 597.1083 $[M]^+$, (calc. 597.0778).

Anal. Calcd for $C_{64}H_{41}B_1F_{25}P_2Rh_1$ (1460.6344 $gmol^{-1}$): C, 52.63; H, 2.83. Found: C, 52.17; H, 3.25.

Preparation of $[Rh(Ph_2P(CH_2)_3PPh_2)(\eta^6\text{-}C_6H_5F)][BAr^F_4]$ (12)

$[Rh(Ph_2P(CH_2)_3PPh_2)(NBD)][BAr^F_4]$ **(i2-13)** (100 mg, 0.0680 mmol) was stirred in C_6H_5F (5 mL) in a Young's flask until fully dissolved. The flask was placed under hydrogen (4 atm) and then left

to stir at room temperature for 20 minutes. The solution was then concentrated *in vacuo* (~2 mL) and then added dropwise to pentane (30 mL) with rigorous stirring resulting in the precipitation of **12** as a red/ orange solid. Diffusion of pentane into a solution of the isolated solid of **12** in C_6H_5F (3 mL) gave **12** as red crystals. Yield: 74 mg, 74 %.

^{1}H NMR (500 MHz, C_6H_5F): δ 8.37 (s, 8H, BAr^F_4), 7.65 (s, 4H, BAr^F_4), 5.66 (m, 4H, *o&m*-C_6H_5F), 5.08 (m, 1H, *p*-C6H5F), 2.06 (m, 4H, CH_2), 1.57 (m, 2H, CH_2). The phenyl signals were not assigned as they were obscured by C_6H_5F solvent δ 7.31 – 6.70.

^{31}P{^{1}H} NMR (202 MHz, C_6H_5F): δ 25.5 [d, *J*(RhP) 196].

ESI-MS (C_6H_5F, 60 °C, 4.5 kV) positive ion: m/z, 611.1351 $[M]^+$ (calc. 611.0935).

Anal. Calcd for $C_{65}H_{43}B_1F_{25}P_2Rh_1$ (1474.6610 $gmol^{-1}$): C, 52.94; H, 2.94. Found: C, 52.85; H, 2.47.

***In situ* preparation of [Rh(Ph$_2$P(CH$_2$)$_3$PPh$_2$)(η^6-C$_6$H$_4$F$_2$)][BAr$^F_4$] (13)**

$[Rh(Ph_2P(CH_2)_3PPh_2)(NBD)][BAr^F_4]$ **(i2-13)** (9 mg, 0.0061 mmol) was dissolved in 1,2-$C_6H_4F_2$ (400 µL) in a New Era high pressure NMR tube. The NMR tube was placed under hydrogen (4 atm) and shaken at room temperature for 5 minutes. The tube was then freeze thaw degassed and backfilled with argon, NMR spectroscopic and ESI-MS data were then obtained.

^{1}H NMR (500 MHz, 1,2-$C_6H_4F_2$): δ 8.33 (m, 8H, BAr^F_4), 7.68 (m, 4H, BAr^F_4), 7.58 – 7.33 (m, 20H, Ar-H), 6.07 (m, 2H, $C_6H_4F_2$), 5.70 (m, 2H, $C_6H_4F_2$), 2.44 (m, 4H, CH_2), 1.95 (m, 2H, CH_2).

^{31}P{^{1}H} NMR (202 MHz, 1,2-$C_6H_4F_2$): δ 25.2 [d, *J*(RhP) 195].

ESI-MS (1,2-$C_6H_4F_2$, 60 °C, 4.5 kV) positive ion: m/z, 629.1168 $[M]^+$ (calc. 629.0840).

Preparation of [Rh(Ph$_2$P(CH$_2$)$_3$PPh$_2$){S(C$_5$H$_9$)(η^2-C$_5$H$_7$)}][BAr$^F_4$] (14)

732 µL of a solution of $S(C_5H_9)_2$ **(II)** in pentane (0.1019 M, 0.0746 mmol, 1.1 equivalents) and *tert*-butylethene (4 equivalents, 40 µL, 0.310 mmol) was added to an *in situ* generated solution of $[Rh(Ph_2P(CH_2)_3PPh_2)(\eta^6\text{-}C_6H_4F_2)][BAr^F_4]$ **(13)** (0.0678 mmol) in 1,2-$C_6H_4F_2$ (5 mL). The solution

was heated to 338 K for 18 hours after which the solvent was removed *in vacuo* and the resulting residue was washed with hexane (2 x 5 mL) and sonicated to yield **14** as a yellow orange solid. Diffusion of pentane into a solution of the isolated solid in 1,2-$C_6H_4F_2$ (3 mL) at 238 K gave **14** as red crystals. Yield: 77 mg, 73 %.

^{1}H NMR (500 MHz, CD_2Cl_2): δ 7.75 (m, 8H, BAr^F_4), 7.58 (br, 4H, BAr^F_4), 7.55 – 7.33 (m, 20H, Ar-H), 4.59 (v br, 2H, HC=CH), 3.22 (m, 1H, CH), 3.03 [apparent quintet, *J* (HH) 7, 1H, CH], 2.86 – 0.66 (br m, 18H, CH_2).

^{31}P{^{1}H} NMR (202 MHz, CD_2Cl_2): δ 22.3 [dd, *J*(RhP) 150, J(PP) 55], 3.4 [dd, *J*(RhP) 152, *J*(PP) 55].

Selected ^{1}H NMR (500 MHz, CD_2Cl_2, 200 K): δ 4.69 (m, 1H, HC=CH), 4.34 (m, 1H, HC=CH).

ESI-MS (1,2-$C_6H_4F_2$, 60 °C, 4.5 kV) positive ion: m/z, 683.1615 $[M]^+$ (calcd. 683.1532).

Anal. Calcd for $C_{69}H_{54}B_1F_{24}P_2Rh_1S_1$ (1546.8578 $gmol^{-1}$): C, 53.58; H, 3.52. Found: C, 53.64; H, 3.30.

***In situ* preparation of [Rh($Ph_2P(CH_2)_3PPh_2$){S(η^6-C_6H_5)(C_5H_9)}][BAr^F_4] (15)**

12.5 µL of a solution of S(C_5H_9)Ph **(III)** in pentane (0.4883 M, 0.0061 mmol) was added to an *in situ* generated solution of [Rh($Ph_2P(CH_2)_3PPh_2$)(η^6-$C_6H_4F_2$)][BAr^F_4] **(13)** (0.0061 mmol) in 1,2-$C_6H_4F_2$ (400 µL).

^{1}H NMR (500 MHz, 1,2-$C_6H_4F_2$): δ 8.33 (br, 8H, BAr^F_4), 7.68 (br, 4H, BAr^F_4), 7.55 – 7.33 (m, 20H, Ar-H), 6.47 (t, *J*(HH) 6, 1H, S-Ph), 5.70 [apparent doublet, *J*(HH) 6, 2H, S-Ph], 5.47 [t, *J*(HH) 6, 2H, S-Ph], 3.26 [quin, *J*(HH) 6, 1H, CH], 2.40 (m, 4H, dppp-CH_2), 1.90 (m, 2H, dppp-CH_2). The SPhCyp-CH_2 signals were not ambiguously assigned as they were obscured by excess free SPhCyp ligand and pentane 2.10 – 0.10.

^{31}P{^{1}H} NMR (202 MHz, 1,2-$C_6H_4F_2$): δ 25.4 [d, *J*(RhP) 196].

***In situ* preparation of [Rh(Ph$_2$P(CH$_2$)$_3$PPh$_2$){S(C$_6$H$_5$)(η^2-C$_5$H$_7$)}][BAr$^F_4$] (16)**

147 µL of a solution of S(C$_5$H$_9$)Ph **(III)** in pentane (0.4883 M, 0.0718 mmol, 1.1 equivalents) and *tert*-butylethene (40 µL, 0.310 mmol) were added to an *in situ* generated solution of [Rh(Ph$_2$P(CH$_2$)$_3$PPh$_2$)(η^6-C$_6$H$_4$F$_2$)][BAr$^F_4$] **(13)** (0.0651 mmol) in 1,2-C$_6$H$_4$F$_2$ (5 mL). The solution was heated to 378 K for 18 hours after which the solvent was removed *in vacuo* and the resulting residue was washed with hexane (3 x 5 mL) and sonicated under vacuum to yield **16** as a yellow/ brown oil.

^{1}H NMR (500 MHz, CD$_2$Cl$_2$): δ 7.75 (m, 8H, BAr$^F_4$), [7.69 – 6.65 (v br m, 20H, dppp Ar-H) {7.65, (br, 4H, BAr$^F_4$), 7.35 (m, 3H, S-Ph), 7.23 (t, *J* (HH) 8, 2H, S-Ph)}], 5.00 (br, 1H, HC=CH), 4.23 (br m, 1H HC=CH), 3.30 (m, 1H, Cyp-CH), [2.75 -1.45 (v br m, 8H, dppp-CH$_2$ and SPhCyp'-CH$_2$) {2.33 (d, *J*(HH) 16, 2H, SPhCyp'-CH$_2$)}] .

^{31}P{^{1}H} NMR (202 MHz, CD$_2$Cl$_2$): δ 23.1 [dd, *J*(RhP) 153, *J*(PP) 54], 1.8 [dd, *J*(RhP) 148, *J*(PP) 54].

Selected ^{1}H NMR (500 MHz, CD$_2$Cl$_2$, 200 K): δ 7.30 (m, 3H, S-Ph), 7.17 (t, *J* (HH) 8, 2H, S-Ph), 6.91 (m, 3H, dppp Ar-H), 6.81 (m, 2H, dppp Ar-H), 4.94 (m, 1H, HC=CH), 4.05 (m, 1H, HC=CH), 2.85 - 2.44 (m, 4H, dppp-CH$_2$), 2.33 [d, *J*(HH) 16, SPhCyp'-CH], 2.26 (d, *J*(HH) 16, SPhCyp'-CH), 2.22 – 2.11 (m, 1H, dppp-CH), 2.06 [d, *J*(HH) 16, 1H, SPhCyp'-CH], 1.70 (m, 1H, dppp-CH), 1.57 [d, *J*(HH) 16, 1H, SPhCyp'-CH].

ESI-MS (1,2-C$_6$H$_4$F$_2$, 60 °C, 4.5 kV) positive ion: m/z, 691.1204 [M]$^+$ (calcd. 691.1219).

Preparation of complexes [Rh{P(C$_5$H$_9$)$_2$(η^2-C$_5$H$_7$)}(H$_3$B·NRR'Me)$_2$][BAr$^F_4$] (17 – 19)

Reaction of [Rh(η^6-C$_6$H$_5$F){P(C$_5$H$_9$)$_2$(η^2-C$_5$H$_7$)}][BAr$^F_4$] **(i-9)** with 2 equivalents of amine borane in 1,2-C$_6$H$_4$F$_2$ solution gave the corresponding bis-amine borane complexes **17 – 19** immediately in quantitative yield by NMR spectroscopy. Similar yields were observed in C$_6$H$_5$F solution for

$H_3B{\cdot}NMeH_2$ and $H_3B{\cdot}NMe_2H$, however with $H_3B{\cdot}NMe_3$, the bis-σ-amine borane complex **19** was formed in only low yield (~ 20%) by NMR spectroscopy. At room temperature in these solvents, **17** and **18** proceed to dehydrocouple in solution over 6 hours. Complexes **17 – 19** have only limited stability in CD_2Cl_2. The bis-σ-amine borane complexes were isolated as pale yellow air and temperature sensitive crystals by recrystallisation from C_6H_5F/ pentane or 1,2-$C_6H_4F_2$/ pentane and stored at −35 ºC:

Representative procedure for the preparation of [Rh{P(C_5H_9)$_2$(η^2-C_5H_7)}($H_3B{\cdot}NMe_2H$)$_2$][BAr^F_4] (17)

$H_3B{\cdot}NMe_2H$ (2.3 mg, 0.039 mmol, 2 eq.) was added to a solution of [Rh(η^6-C_6H_5F){P(C_5H_9)$_2$(η^2-C_5H_7)}][BAr^F_4] **(i-9)** (25.0 mg, 0.019 mmol) in 1,2-$C_6H_4F_2$ (3 mL). Diffusion of pentane into the solution at −35 °C gave 4 as pale yellow crystals. Yield 13.9 mg, 59 %.

[Rh{P(C_5H_9)$_2$(η^2-C_5H_7)}($H_3B{\cdot}NMe_2H$)$_2$][BAr^F_4] (17)

^{1}H NMR (500 MHz, 1,2-$C_6H_4F_2$): δ 8.33 (s, 8H, BAr^F_4), 7.69 (s, 4H, BAr^F_4), 4.08 (br, 2H, 2×NH), 3.64 (s, 2H, HC=CH), 2.60 [d, *J*(HH) 6, 12H, 2×N-CH_3], 2.14 – 1.02 (m, 23H, $PCyp_2Cyp$'), −0.64 (br, 6H, 2×BH_3).

^{31}P{^{1}H} NMR (202 MHz, 1,2-$C_6H_4F_2$): δ 107.4 [d, *J*(RhP) 168].

^{11}B NMR (160 MHz, 1,2-$C_6H_4F_2$): δ −12.2 (br).

^{1}H NMR (500 MHz, CD_2Cl_2): δ 7.73 (s, 8H, BAr^F_4), 7.58 (s, 4H, BAr^F_4), 3.99 (br, 2H, 2×NH), 3.60 (s, 2H, HC=CH), 2.58 [d, *J*(HH) 6, 12H, 2×N-CH_3], 2.25 – 1.15 (m, 23H, $PCyp_2Cyp$'), −0.76 (br, 6H, 2×BH_3).

^{1}H{^{11}B} NMR (selected data, 500 MHz, CD_2Cl_2): δ −0.74 (br, 6H, 2×BH_3).

^{1}H NMR (500 MHz, CD_2Cl_2, 200 K): δ 7.74 (s, 8H, BAr^F_4), 7.56 (s, 4H, BAr^F_4), 4.33 (br, 1H, NH), 3.52 (br, 1H, NH), 3.45 (s, 2H, HC=CH), 2.52 [d, *J*(HH) 5, 12H, 2×N-CH_3], 2.20 – 1.05 (m, 23H, $PCyp_2Cyp$'), −1.57 (br, 5H, BH_2 + BH_3). The remaining 1H B*H*$_3$ signal was not unambiguously assigned. A ^{1}H-^{1}H-COSY shows correlation of two N-H peaks (δ 4.33 and 3.52) with CH_3 groups (δ 2.52).

^{1}H{^{11}B} NMR (selected data, 500 MHz, CD_2Cl_2, 200 K): δ −1.49 (br, 3H, BH_3), −1.63 (br, 2H, BH_3).

^{31}P{^{1}H} NMR (202 MHz, CD_2Cl_2): δ 106.4 [d, *J*(RhP) 167].

^{31}P{^{1}H} NMR (202 MHz, CD_2Cl_2, 200 K): δ 105.3 [d, *J*(RhP) 165].

^{11}B NMR (160 MHz, CD_2Cl_2): δ −12.8 (br).

^{11}B NMR (160 MHz, CD_2Cl_2, 200 K): δ −20.3 (br).

ESI-MS (1,2-$C_6H_4F_2$, 60 °C, 4.5 kV) positive ion: m/z, 457.2647 $[M]^+$ (100%, calc. 457.2563).

[Rh{$P(C_5H_9)_2(\eta^2\text{-}C_5H_7)$}$(H_3B{\cdot}NMeH_2)_2$][$BAr^F_4$] (18)

^{1}H NMR (500 MHz, 1,2-$C_6H_4F_2$): δ 8.34 (s, 8H, BAr^F_4), 7.68 (s, 4H, BAr^F_4), 3.72 (br, 4H, 2×NH_2), 3.63 (s, 2H, HC=CH), 2.60 [br t, *J*(HH) 5, 6H, 2×N-CH_3], 2.10 – 1.03 (m, 23H, $PCyp_2Cyp$'), −0.61 (br, 6H, 2×BH_3).

^{31}P{^{1}H} NMR (202 MHz, 1,2-$C_6H_4F_2$): δ 104.7 [d, *J*(RhP) 168].

^{11}B NMR (160 MHz, 1,2-$C_6H_4F_2$): δ −16.9 (br).

^{1}H NMR (500 MHz, CD_2Cl_2): δ 7.74 (s, 8H, BAr^F_4), 7.58 (s, 4H, BAr^F_4), 3.76 (br, 4H, 2×NH_2), 3.57 (s, 2H, HC=CH), 2.59 [t, *J*(HH) 6, 6H, 2×N-CH_3], 2.32 – 1.15 (m, 23H, $PCyp_2Cyp$'), −0.74 (br, 6H, 2×BH_3).

^{1}H{^{11}B} NMR (selected data, 500 MHz, CD_2Cl_2): δ −0.74 (br, 6H, 2×BH_3).

^{1}H NMR (500 MHz, CD_2Cl_2, 200 K): δ 7.73 (s, 8H, BAr^F_4), 7.56 (s, 4H, BAr^F_4), 4.00 (br, 2H, NH_2), 3.51 (br, 2H, NH_2), 3.43 (s, 2H, HC=CH), 2.54 (br m, 6H, 2×N-CH_3), 2.25 – 1.05 (m, 23H,

$PCyp_2Cyp$'), −1.45 (br, 5H, BH_2 + BH_3). The remaining 1H BH_3 signal was not observed, presumably as it was broad and/or obscured by the aliphatic signals.

$^1H\{^{11}B\}$ NMR (selected data, 500 MHz, CD_2Cl_2, 200 K): δ −1.46 (br, 5H, BH_2 + BH_3).

$^{31}P\{^1H\}$ NMR (202 MHz, CD_2Cl_2): δ 107.3 [br d, *J*(RhP) 169].

$^{31}P\{^1H\}$ NMR (202 MHz, CD_2Cl_2, 200 K): δ 105.6 [d, *J*(RhP) 164].

^{11}B NMR (160 MHz, CD_2Cl_2): δ −16.8 (br).

^{11}B NMR (160 MHz, CD_2Cl_2, 200 K): δ −24.0 (br).

ESI-MS (1,2-$C_6H_4F_2$, 60 °C, 4.5 kV) positive ion: m/z, 384.1757 $[M\text{-}H_3B{\cdot}NMeH_2]^+$ (27%, calc. 384.1496), 415.2194 $[M\text{-}BH_3]^+$ (52%, calc. 415.1918), 435.1408 $[M\text{-}2(H_3B{\cdot}NMeH_2)+C_6H_5F]^+$ (44%, calc. 435.1119), 453.1313 $[M\text{-}2(H_3B{\cdot}NMeH_2)+C_6H_4F_2]^+$ (100%, calc. 453.1024).

$[Rh\{P(C_5H_9)_2(\eta^2\text{-}C_5H_7)\}(H_3B{\cdot}NMe_3)_2][BAr^F{}_4]$ (19)

^1H NMR (500 MHz, 1,2-$C_6H_4F_2$): δ 8.33 (s, 8H, $BAr^F{}_4$), 7.69 (s, 4H, $BAr^F{}_4$), 4.02 (s, 2H, HC=CH), 2.69 (s, 18H, 2×N-CH_3), 2.19 – 1.01 (m, 23H, $PCyp_2Cyp$'), 0.86 (br, 6H, 2×BH_3).

$^{31}P\{^1H\}$ NMR (202 MHz, 1,2-$C_6H_4F_2$): δ 108.6 [d, *J*(RhP) 174].

^{11}B NMR (160 MHz, 1,2-$C_6H_4F_2$): δ −6.3 (br).

^1H NMR (500 MHz, CD_2Cl_2): δ 7.74 (s, 8H, $BAr^F{}_4$), 7.58 (s, 4H, $BAr^F{}_4$), 3.92 (s, 2H, HC=CH), 2.67 (s, 18H, 2×N-CH_3), 2.32 – 1.06 (m, 23H, $PCyp_2Cyp$'), 0.08 (br, 6H, 2 x BH_3).

$^1H\{^{11}B\}$ NMR (selected data, 500 MHz, CD_2Cl_2): δ 0.07 (br, 6H, 2 x BH_3).

^1H NMR (500 MHz, CD_2Cl_2, 200 K): δ 7.74 (s, 8H, $BAr^F{}_4$), 7.56 (s, 4H, $BAr^F{}_4$), 3.78 (s, 2H, HC=CH), 2.63 (s,18H, 2×N-CH_3), 2.22 – 1.01 (m, 23H, $PCyp_2Cyp$'), −0.02 (v br,* 2H, BH_3), −1.54 (v br,* 3H, BH_3). The remaining 1H BH_3 signal was not observed, presumably as it was broad and/or obscured by the aliphatic signals. *Precise integration of these peaks was difficult as they were very broad (and ^{11}B decoupling does not sharpen them appreciably).

$^{31}P\{^{1}H\}$ NMR (202 MHz, CD_2Cl_2): δ 109.5 [br d, *J*(RhP) 178].

$^{31}P\{^{1}H\}$ NMR (202 MHz, CD_2Cl_2, 200 K): δ 107.5 [d, *J*(RhP) 171].

^{11}B NMR (160 MHz, CD_2Cl_2): δ −6.2 (br).

^{11}B NMR (160 MHz, CD_2Cl_2, 200 K): δ −8.9 (br).

ESI-MS (1,2-$C_6H_4F_2$, 60 °C, 4.5 kV) positive ion: m/z, 412.2041 $[M\text{-}H_3B{\cdot}NMe_3]^+$ (50%, calc. 412.1812), 453.1275 $[M\text{-}2(H_3B{\cdot}NMe_3)+C_6H_4F_2]^+$ (100%, calc. 453.1024).

Preparation of $[Rh\{P(C_5H_9)_2(\eta^2\text{-}C_5H_7)\}(\eta^2\text{:}\eta^1\text{-}H_3B{\cdot}NMe_2BH_2{\cdot}NMe_2H)][BAr^F{}_4]$ (20)

$H_3B{\cdot}NMe_2BH_2{\cdot}NMe_2H$ (2.1 mg, 0.018 mmol, 1 eq.) was added to a solution of $[Rh)(\eta^6\text{-}C_6H_5F)\{P(C_5H_9)_2(\eta^2\text{-}C_5H_7)\}][BAr^F{}_4]$ **(i-9)** (24.0 mg, 0.018 mmol) in 1,2-$C_6H_4F_2$ (3 mL). Diffusion of pentane into the solution at – 35 °C gave **20** as pale yellow crystals which were stored at −35 °C. Yield 12.5 mg, 51 %. At temperatures higher than 0 °C solid **20** melts thus a satisfactory microanalysis could not be obtained.

^{1}H NMR (500 MHz, 1,2-$C_6H_4F_2$): δ 8.34 (s, 8H, $BAr^F{}_4$), 7.69 (s, 4H, $BAr^F{}_4$), 4.19 (bs, 1H, NH), 3.79 (s, 2H, HC=CH), 2.75 [d, 6H, *J*(HH) 5, NH-CH_3], 2.67 (s, 6H, N-CH_3), 2.08 – 1.44 (m, 21H, $PCyp_2Cyp'$), 1.23 [br dd, 2H, *J*(PH) 47, *J*(HH) 14, PCyp'-CH_2], 0.10 [br, 3H, *J*(BH) 111, BH_3], −1.94 [br, 2H, *J*(BH) 117, BH_2].

$^{1}H\{^{11}B\}$ NMR (500 MHz, 1,2-$C_6H_4F_2$): δ 0.10 [d, 3H, *J*(RhH) 21, BH_3], −1.94 (br, 2H, BH_2).

$^{31}P\{^{1}H\}$ NMR (202 MHz, 1,2-$C_6H_4F_2$): δ 114.6 [d, *J*(RhP) 170].

^{11}B NMR (160 MHz, 1,2-$C_6H_4F_2$): δ −4.3 (br).

ESI-MS (1,2-$C_6H_4F_2$, 60 °C, 4.5 kV) positive ion: m/z, 455.2420 $[M]^+$ (calcd. 455.2406).

^{1}H NMR (500 MHz, CD_2Cl_2): δ 7.74 (s, 8H, $BAr^F{}_4$), 7.58 (s, 4H, $BAr^F{}_4$), 4.10 (bs, 1H, NH), 3.80 (s, 2H, HC=CH), 2.63 [d, 6H, *J*(HH) 5, NH-CH_3], 2.58 (s, 6H, N-CH_3), 2.23 – 1.50 (m, 21H,

$PCyp_2Cyp$'), 1.34 [br dd, 2H, *J*(PH) 47, *J*(HH) 14, PCyp'-CH_2], −0.05 [br, 3H, *J*(BH) 111, BH_3], −2.10 [br, 2H, *J*(BH) 117, BH_2].

$^1H\{^{11}B\}$ NMR (500 MHz, CD_2Cl_2): δ −0.06 [d, 3H, *J*(RhH) 21, BH_3], −2.10 (br, 2H, BH_2).

$^{31}P\{^1H\}$ NMR (202 MHz, CD_2Cl_2): δ 114.6 [d, *J*(RhP) 169].

^{11}B NMR (160 MHz, CD_2Cl_2): δ −4.3 (br).

^1H NMR (500 MHz, CD_2Cl_2, 200 K): δ 7.74 (s, 8H, BAr^F_4), 7.57 (s, 4H, BAr^F_4), 4.20 (bs, 1H, NH), 3.68 (s, 2H, HC=CH), 2.56 [d, 6H, *J*(HH) 5, NH-CH_3], 2.54 (s, 6H, N-CH_3), 2.18 – 1.37 (m, 21H, $PCyp_2Cyp$'), 1.26 [br dd, 2H, *J*(PH) 47, *J*(HH) 14, PCyp'-CH_2], −1.30 (br, 2H, BH_3), −2.32 (br, 2H, BH_2). The remaining B-H signal was not observed, presumably it was broad and/or obscured by the aliphatic signals.

$^1H\{^{11}B\}$ NMR (500 MHz, CD_2Cl_2, 200 K): δ −1.35 (v br, 2H, RhH_2BH), −2.32 (br, 2H, BH_2)

$^{31}P\{^1H\}$ NMR (202 MHz, CD_2Cl_2, 200 K): δ 113.1 [d, *J*(RhP) 169].

^{11}B NMR (160 MHz, CD_2Cl_2, 200 K): δ very broad, no clear signals observed.

Preparation of [Rh{$P^iPr_2(\eta^2\text{-}C_5H_7)$}($\eta^2$:$\eta^1$-$H_3B{\cdot}NMe_2BH_2{\cdot}NMe_2H$)][$BAr^F_4$] (21)

$H_3B{\cdot}NMe_2BH_2{\cdot}NMe_2H$ (2.2 mg, 0.019 mmol, 1 eq.) was added to a solution of [Rh(η^6-C_6H_5F){$P^iPr_2(\eta^2\text{-}C_5H_7)$}][$BAr^F_4$] **(i-9a)** (24.0 mg, 0.019 mmol) in 1,2-$C_6H_4F_2$ (0.5 mL). Quantitative conversion to **21** was observed by NMR spectroscopy. Crystalline material was difficult to obtain however a single pale yellow crystal suitable for X-ray diffraction was obtained from the diffusion of pentane into a 1,2-$C_6H_4F_2$ (3 mL) solution at −35 °C.

^1H NMR (500 MHz, 1,2-$C_6H_4F_2$): δ 8.33 (s, 8H, BAr^F_4), 7.68 (s, 4H, BAr^F_4), 4.35 (bs, 1H, NH), 3.81 (s, 2H, HC=CH), 2.72 [d, 6H, *J*(HH) 5, NH-CH_3], 2.66 (s, 6H, N-CH_3), 1.93 (m, 2H, P^{iP}r-CH), 1.83 [dd, 2H, *J*(HH) 14, *J*(PH) 13, PCyp'-CH_2], 1.78 (m, 1H, PCyp'-CH), 1.32 [apparent ddt, 2H,

J(PH) 46, *J*(HH) 14, *J*(HH) 3, PCyp'-CH_2], 1.11 [dd, 6H, *J*(PH) 15, *J*(HH) 7, P^iPr-CH_3], 1.07 [dd, 6H, *J*(PH) 15, *J*(HH) 7, P^iPr-CH_3], 0.12 [br, 3H, *J*(BH) 110, BH_3], −2.14 [br, 2H, *J*(BH) 119, BH_2].

$^1H\{^{11}B\}$ NMR (500 MHz, 1,2-$C_6H_4F_2$): δ 0.12 [d, 3H, *J*(RhH) 19, BH_3], −2.12 (br, 2H, BH_2).

$^{31}P\{^1H\}$ NMR (202 MHz, 1,2-$C_6H_4F_2$): δ 123.0 [d, *J*(RhP) 176].

^{11}B NMR (160 MHz, 1,2-$C_6H_4F_2$): δ −4.3 (br).

ESI-MS (1,2-$C_6H_4F_2$, 60 °C, 4.5 kV) positive ion: m/z, 403.2066 $[M]^+$ (Calcd. 403.2092).

^1H NMR (500 MHz, CD_2Cl_2): δ 7.74 (s, 8H, BAr^F_4), 7.58 (s, 4H, BAr^F_4), 4.13 (bs, 1H, NH), 3.82 (s, 2H, HC=CH), 2.62 [d, 6H, *J*(HH) 6, NH-CH_3], 2.59 (br s, 6H, N-CH_3), 2.08 (m, 2H, P^iPr-CH), 1.95 (br m, 1H, PCyp'-CH), 1.94 [dd, 2H, *J*(HH) 13, *J*(PH) 12, PCyp'-CH_2], 1.44 [apparent ddt, 2H, *J*(PH) 46, *J*(HH) 14, *J*(HH) 3, PCyp'-CH_2], 1.24 [dd, 6H, *J*(PH) 14, *J*(HH) 7, P^iPr-CH_3], 1.18 [dd, 6H, *J*(PH) 14, *J*(HH) 7, P^iPr-CH_3], −0.02 [br, 3H, *J*(BH) 110, BH_3], −2.26 [br, 2H, *J*(BH) 119, BH_2].

$^1H\{^{11}B\}$ NMR (500 MHz, CD_2Cl_2): −0.03 [d, 3H, *J*(RhH) 21, BH_3], −2.25 (br, 2H, BH_2).

$^{31}P\{^1H\}$ NMR (202 MHz, CD_2Cl_2): δ 123.4 [d, *J*(RhP) 176].

^{11}B NMR (160 MHz, CD_2Cl_2): δ −4.3 (br).

^1H NMR (500 MHz, CD_2Cl_2, 200 K): δ 7.74 (s, 8H, BAr^F_4), 7.56 (s, 4H, BAr^F_4), 4.25 (bs, 1H, NH), 3.70 (s, 2H, HC=CH), 2.58 – 2.53 (m, 12H, NH-CH_3 , N-CH_3), 1.99 (m, 2H, P^iPr-CH), 1.88 (br m, 1H, PCyp CH), 1.82 [dd, 2H, *J*(HH) 13, *J*(PH) 12, PCyp'-CH_2], 1.37 [br dd, 2H, *J*(PH) 46, *J*(HH) 13, PCyp'-CH_2], 1.14 [dd, 6H, *J*(PH) 14, *J*(HH) 7, P^iPr-CH_3], 1.09 [dd, 6H, *J*(PH) 14, *J*(HH) 7, P^iPr-CH_3], −1.34 (br, 2H, BH_3), −2.48 (br, 2H, BH_2). The remaining B-H signal was not observed, presumably it was broad and/or obscured by the aliphatic signals.

$^1H\{^{11}B\}$ NMR (500 MHz, CD_2Cl_2, 200K): −1.35 (v br, 2H, RhH_2BH), −2.49 (br, 2H, BH_2).

$^{31}P\{^1H\}$ NMR (202 MHz, CD_2Cl_2, 200K): δ 121.6 [d, *J*(RhP) 172].

^{11}B NMR (160 MHz, CD_2Cl_2, 200K): δ very broad, no clear signals observed.

Preparation of [Rh{P(C_5H_9)$_2$(η^2-C_5H_7)}{η^1:η^1:η^1-(H_2B·NMeH)$_3$}][BAr^F_4] (22)

[H_2B·NMeH]$_3$ (3.5 mg, 0.027 mmol, 1.5 eq.) was added to a solution of [Rh(η^6-C_6H_5F){P(C_5H_9)$_2$(η^2-C_5H_7)}][BAr^F_4] **(i-9)** (24.0 mg, 0.018 mmol) in 1,2-$C_6H_4F_2$ (3 mL). The solution was stirred for 24 hours. Diffusion of pentane into the solution at 20 °C gave **22** as pale yellow crystals. Yield 10.5 mg, 43 %.

^{1}H NMR (500 MHz, 1,2-$C_6H_4F_2$): δ 8.34 (s, 8H, BAr^F_4), 7.69 (s, 4H, BAr^F_4), 3.81 (s, 2H, HC=CH), 3.26 (br s, 3H, NH), 2.73 [d, *J*(HH) 5, 9H, N-CH_3], 2.17 – 1.44 (m, 21H, PCyp$_2$Cyp'), 1.16 [apparent ddt, 2H, *J*(PH) 49, *J*(HH) 14, *J*(HH) 3, PCyp'-CH_2], −3.16 (br, 3H, Rh<u>H</u>BH). The RhHB<u>H</u> signal was not unequivocally identified, presumably it was broad and/or obscured by the aliphatic signals.

^{1}H{^{11}B} NMR (500 MHz, 1,2-$C_6H_4F_2$): δ 2.63 (br d, 3H, *J* = 9, RhHB<u>H</u>), −3.17 (br, 3H, Rh*H*BH).

^{31}P{^{1}H} NMR (202 MHz, 1,2-$C_6H_4F_2$): δ 113.1 [d, *J*(RhP) 161].

^{11}B NMR (160 MHz, 1,2-$C_6H_4F_2$): δ −5.3 (br).

ESI-MS (1,2-$C_6H_4F_2$, 60 °C, 4.5 kV) positive ion: m/z, 468.2497 $[M]^+$ (calcd. 468.2533).

^{1}H NMR (500 MHz, CD_2Cl_2): δ 7.74 (s, 8H, BAr^F_4), 7.58 (s, 4H, BAr^F_4), 3.81 (s, 2H, HC=CH), 3.10 (bs, 3H, NH), 2.62 [d, *J*(HH) 5, 9H, N-CH_3], 2.37 – 1.42 (m, 21H, PCyp$_2$Cyp'), 1.15 [apparent ddt, 2H, *J*(PH) 49, *J*(HH) 14, *J*(HH) 3, PCyp'-CH_2], −3.30 (br, 3H, Rh<u>H</u>BH). The RhHB<u>H</u> signal was not unequivocally identified, presumably it was broad and/or obscured by the aliphatic signals.

^{1}H{^{11}B} NMR (500 MHz, CD_2Cl_2): δ 2.40 (br d, 3H, *J* = 10, RhHB<u>H</u>), −3.30 (br, 3H, Rh<u>H</u>BH).

^{31}P{^{1}H} NMR (202 MHz, CD_2Cl_2): δ 112.6 [d, *J*(RhP) 161].

^{11}B NMR (160 MHz, CD_2Cl_2): δ −5.6 [br dd, *J*(BH) 117, 83].

^{1}H NMR (500 MHz, CD_2Cl_2, 200 K): δ 7.73 (s, 8H, BAr^F_4), 7.55 (s, 4H, BAr^F_4), 3.69 (s, 2H, HC=CH), 3.19 (bs, 3H, NH), 2.57 (v br, 9H, N-CH_3), 2.24 – 1.30 (m, 21H, PCyp$_2$Cyp'), 1.09 [br dd, 2H, *J*(PH) 49, *J*(HH) 14, PCyp'-CH_2], −1.08 (br, 2H, Rh<u>H</u>BH), −8.31 (br, 1H, Rh<u>H</u>BH). The

remaining RhHBH signals were not unequivocally identified, presumably they are broad and/or obscured by the aliphatic signals.

^{1}H{^{11}B} NMR (500 MHz, CD_2Cl_2, 200 K): δ −1.08 (br, 2H, RhHBH), −8.31 (br, 1H, RhHBH).

^{31}P{^{1}H} NMR (202 MHz, CD_2Cl_2, 200 K): δ 111.3 [d, *J*(RhP) 159].

^{11}B NMR (160 MHz, CD_2Cl_2, 200 K): δ very broad, no clear signal observed.

Anal. Calcd for $C_{50}H_{55}B_4F_{24}N_3P_1Rh_1.C_6H_4F^2$ (1445.170 $gmol^{-1}$): C, 46.54; H, 4.11; N, 2.91. Found: C, 46.16; H, 4.05; N, 2.81.

Preparation of [Rh{P^{i}Pr$_2$(η^2-C$_5$H$_7$)}{η^1:η^1:η^1-(H$_2$B·NMeH)$_3$}][BAr$^F_4$] (23)

$[H_2B{\cdot}NMeH]_3$ (3.5 mg, 0.027 mmol, 1.5 eq.) was added to a solution of [Rh(η^6-C_6H_5F){P^{i}Pr$_2$(η^2-C_5H_7)}][BAr$^F_4$] **(i-9a)** (24.0 mg, 0.019 mmol) in 1,2-$C_6H_4F_2$ (3 mL). The solution was stirred for 24 hours. Quantitative conversion to **23** was observed by NMR spectroscopy from *in situ* generated samples. Crystalline material was difficult to obtain however a single pale yellow crystal suitable for X-ray diffraction was obtained from the diffusion of pentane into a 1,2-$C_6H_4F_2$ (3 mL) solution at −35 °C.

^{1}H NMR (500 MHz, 1,2-$C_6H_4F_2$): δ 8.33 (s, 8H, BAr$^F_4$), 7.68 (s, 4H, BAr$^F_4$), 3.81 (s, 2H, HC=CH), 3.31 (br s, 3H, NH), 2.71 [d, *J*(HH) 6, 9H, N-CH_3], 1.98 (m, 2H, P^{i}Pr-CH), 1.81 (br m, 1H, PCyp'-CH), 1.76 [virtual triplet, 2H, *J*(HH) ~ *J*(PH) 13, PCyp'-CH_2], 1.34 – 1.15 (m, 12H, P^{i}Pr-CH_3) 1.26 – 1.05 (partially obscured multiplet, 2H, PCyp'-CH_2), −3.32 [collapsed quartet, 3H, *J*(BH) 87, RhHBH]. The remaining RhHBH signal was not unequivocally identified, presumably it is broad and/or obscured by the aliphatic signals.

^{1}H{^{11}B} NMR (500 MHz, 1,2-$C_6H_4F_2$): δ 2.62 (br d, 3H, *J* = 10, RhHBH), −3.32 (br, 3H, RhHBH).

^{31}P{^{1}H} NMR (202 MHz, 1,2-$C_6H_4F_2$): δ 120.7 [d, *J*(RhP) 165].

^{11}B NMR (160 MHz, 1,2-$C_6H_4F_2$): δ −5.2 [br dd, *J*(BH) 118, 87].

ESI-MS (1,2-$C_6H_4F_2$, 60 °C, 4.5kV) positive ion: m/z, 416.2230 $[M]^+$ (calcd. 416.2218).

^{1}H NMR (500 MHz, CD_2Cl_2): δ 7.73 (s, 8H, $BAr^F{}_4$), 7.58 (s, 4H, $BAr^F{}_4$), 3.85 (s, 2H, HC=CH), 3.18 (bs, 3H, NH), 2.62 [d, *J*(HH) 5, 9H, N-CH_3], 2.08 (m, 2H, P^{i}Pr-CH), 1.97 (br m, 1H, PCyp'-CH), 1.82 [virtual triplet, 2H, *J*(HH) ~ *J*(PH) 13, PCyp'-CH_2], 1.34 - 1.19 (m, 12H, P^{i}Pr-CH_3), 1.28 – 1.08 (partially obscured multiplet, 2H, PCyp'-CH_2), −3.44 [collapsed quartet, 3H, *J*(BH) 87, Rh<u>H</u>BH]. The remaining RhHB<u>H</u> signal was not unequivocally identified, presumably it is broad and/or obscured by the aliphatic signals.

^{1}H{^{11}B} NMR (500 MHz, CD_2Cl_2): δ 2.40 (br d, 3H, *J* = 9, RhHB<u>H</u>), −3.43 (br, 3H, Rh<u>H</u>BH).

^{31}P{^{1}H} NMR (202 MHz, CD_2Cl_2): δ 120.7 [d, *J*(RhP) 163].

^{11}B NMR (160 MHz, CD_2Cl_2): δ −5.5 [dd, *J*(BH) 118, 87].

^{1}H NMR (500 MHz, CD_2Cl_2, 200 K): δ 7.73 (s, 8H, $BAr^F{}_4$), 7.55 (s, 4H, $BAr^F{}_4$), 3.73 (s, 2H, HC=CH), 3.20 (bs, 3H, NH), 2.56 (v br, 9H, N-CH_3), 2.00 (m, 2H, P^{i}Pr-CH), 1.90 (br m, 1H, PCyp'-CH), 1.70 [virtual triplet, 2H, *J*(HH) ~ *J*(PH) 13, PCyp'-CH_2], 1.16 [dd, 12H, *J*(HH) 7, *J*(PH) 14, P^{i}Pr-CH_3] 1.23 – 0.97 (partially obscured multiplet, 2H, PCyp'-CH_2), −1.11 (br, 2H, Rh<u>H</u>BH), −8.80 (v br, 1H, Rh<u>H</u>BH). The remaining RhHB<u>H</u> signals were not unequivocally identified, presumably they are broad and/or obscured by the aliphatic signals.

^{1}H{^{11}B} NMR (500 MHz, CD_2Cl_2, 200 K): δ −1.11 (br, 2H, Rh<u>H</u>BH), −8.85 (br, 1H, Rh<u>H</u>BH).

^{31}P{^{1}H} NMR (202 MHz, CD_2Cl_2, 200 K): δ 119.3 [d, *J*(RhP) 162].

^{11}B NMR (160 MHz, CD_2Cl_2, 200 K): δ very broad, no clear signal observed.

Preparation of [Rh{η^1:η^1:η^1-(H_2B·NMeH)$_3$}$(H)_2$PCyp$_3$][$BAr^F{}_4$] (24)

24 is observed as an organometallic species present during $[H_2B·NMeH]_3$ catalysis with **22** (20 mol %, 1,2-$C_6H_4F_2$, 298 K) and was characterised *in situ* by NMR spectroscopy and ESI-MS.

^{1}H NMR (500 MHz, 1,2-$C_6H_4F_2$, selected data): δ −3.16 (br, 3H, Rh<u>H</u>BH), −18.74 (br t, 2H, *J* = 20).

$^{31}P\{^{1}H\}$ NMR (202 MHz, 1,2-$C_6H_4F_2$): δ 83.5 [d, *J*(RhP) 147].

^{11}B NMR (160 MHz, 1,2-$C_6H_4F_2$): δ very broad, no clear signal observed.

ESI-MS (1,2-$C_6H_4F_2$, 60 °C, 4.5 kV) positive ion: m/z, 472.2752 $[M]^+$ (calcd. 472.2752).

Preparation of $[Rh(Ph_2P(CH_2)_xPPh_2)(\eta^6\text{-}C_6H_5F)][BAr^F{}_4]$ x = 4 (25); 5 (26).

In a typical experiment, $[Rh(Ph_2P(CH_2)_xPPh_2)(NBD)][BAr^F{}_4]$ (x = 4 **(i2-14)**; x = 5 **(i2-15)**) (100 mg) was stirred in C_6H_5F (5 mL) in a Young's flask until fully dissolved. The flask was placed under hydrogen (4 atm) and then left to stir at room temperature for 20 minutes. The solution was then concentrated *in vacuo* (~2 mL) and then added dropwise to pentane (30 mL) with rigorous stirring resulting in the precipitation of **25**/ **26** as a red/orange solid. Yield: 72 mg, 72 % **(25)**, 78 mg, 78 % **(26)**.

25

^{1}H NMR (500 MHz, C_6H_5F): δ 8.37 (s, 8H, $BAr^F{}_4$), 7.65 (s, 4H, $BAr^F{}_4$), 5.50 (m, 2H, *o/m*-C_6H_5F), 5.44 (m, 2H, *o/m*-C_6H_5F), 5.10 (m, 1H, *p*-C_6H_5F), 1.99 (m, 4H, CH_2), 1.24 (m, 4H, CH_2). The phenyl signals were not assigned as they were obscured by C_6H_5F solvent δ 7.31 – 6.70.

$^{31}P\{^{1}H\}$ NMR (121 MHz, C_6H_5F): δ 38.4 [d, *J*(RhP) 199].

ESI-MS (C_6H_5F, 60 °C, 4.5 kV) positive ion: m/z, 625.1256 $[M]^+$ (calc. 625.1091).

Anal. Calcd for $C_{66}H_{45}B_1F_{25}P_2Rh_1$ (1488.6876 $gmol^{-1}$): C, 53.25; H, 3.05. Found: C, 53.28; H, 3.38.

26

^{1}H NMR (500 MHz, C_6H_5F): δ 8.37 (s, 8H, $BAr^F{}_4$), 7.65 (s, 4H, $BAr^F{}_4$), 5.54 (m, 2H, *o/m*- C_6H_5F), 5.49 (m, 2H, *o/m*-C_6H_5F) 5.26 (m, 1H, *p*-C_6H_5F), 2.11 (m, 2H, CH_2), 1.95 (m, 4H, CH_2), 1.59 (m, 4H, CH_2). The phenyl signals were not assigned as they were obscured by C_6H_5F solvent δ 7.31 – 6.70.

$^{31}P\{^{1}H\}$ NMR (202 MHz, C_6H_5F): δ 27.0 [d, *J*(RhP) 207].

ESI-MS (C_6H_5F, 60 °C, 4.5 kV) positive ion: m/z, 639.1730 $[M]^+$ (calc. 639.1248).

Anal. Calcd for $C_{67}H_{47}B_1F_{25}P_2Rh_1$ (1502.7142 $gmol^{-1}$): C, 53.55; H, 3.15. Found: C, 53.56; H, 3.37.

Preparation of $[Rh(Ph_2P(CH_2)_3PPh_2)(\eta^2\text{-}H_3B{\cdot}NMe_3)][BAr^F_4]$ (27)

$H_3B{\cdot}NMe_3$ (1.2 mg, 0.016 mmol) was added to a solution of **12** (24 mg, 0.016 mmol) in 1,2-$C_6H_4F_2$ (3 mL). Diffusion of pentane at −35 °C yielded **27** as red crystals. Yield: 14 mg, 59 %.

^{1}H NMR (500 MHz, CD_2Cl_2): δ 7.74 (m, 8H, BAr^F_4), 7.68 – 7.60 (m, 8H, Ph), 7.49 – 7.35 (m, 12H, Ph), 2.59 (s, 9H, NMe), 2.40 (m, 4H, CH_2), 2.01 (m, 2H, CH_2), −1.30 (br, 3H, BH_3).

$^{31}P\{^{1}H\}$ NMR (202 MHz, 1,2-$C_6H_4F_2$): δ 34.0 [d, *J*(RhP) 167].

^{11}B NMR (160 MHz, CD_2Cl_2): δ 16.4 (v br).

ESI-MS (1,2-$C_6H_4F_2$, 60 °C, 4.5 kV) positive ion: m/z, 629.1168 $[M\text{-}H_3B{\cdot}NMe_3{+}C_6H_4F_2]^+$ (100 %, calc. 629.0840), 515.0861 $[M\text{-}H_3B{\cdot}NMe_3]^+$ (40 %, calc. 515.0559).

Preparation of $[Rh(Ph_2P(CH_2)_4PPh_2)(\eta^2\text{-}H_3B{\cdot}NMe_3)][BAr^F_4]$ (28)

$H_3B{\cdot}NMe_3$ (1.2 mg, 0.016 mmol) was added to a solution of **25** (24 mg, 0.016 mmol) in 1,2-$C_6H_4F_2$ (3 mL). Diffusion of pentane at −35 °C yielded **28** as purple crystals. Yield: 19 mg, 80 %.

^{1}H NMR (500 MHz, CD_2Cl_2): δ 7.74 (m, 8H, BAr^F_4), 7.69 – 7.61 (m, 8H, Ph), 7.54 – 7.41 (m, 12H, Ph), 2.51 (s, 9H, NMe), 2.47 (m, 4H, CH_2), 1.84 (m, 4H, CH_2), −1.66 (br, 3H, BH_3).

$^{31}P\{^{1}H\}$ NMR (202 MHz, 1,2-$C_6H_4F_2$): δ 47.1 [d, *J*(RhP) 170].

^{11}B NMR (160 MHz, CD_2Cl_2): δ 18.3 (br).

ESI-MS (1,2-$C_6H_4F_2$, 60 °C, 4.5 kV) positive ion: m/z, 643.1342 $[M\text{-}H_3B{\cdot}NMe_3{+}C_6H_4F_2]^+$ (100 %, calc. 643.0997), 602.2105 $[M]^+$ (10 %, calc. 602.1784).

Preparation of [Rh($Ph_2P(CH_2)_5PPh_2$)(η^2-$H_3B{\cdot}NMe_3$)][BAr^F_4] (29)

$H_3B{\cdot}NMe_3$ (1.2 mg, 0.016 mmol) was added to a solution of **26** (24 mg, 0.016 mmol) in 1,2-$C_6H_4F_2$ (3 mL). Diffusion of pentane at −35 °C yielded **29** as purple crystals. Yield: 21 mg, 89 %.

^{1}H NMR (500 MHz, CD_2Cl_2): δ 7.74 (m, 8H, BAr^F_4), 7.57 (m, 8H, Ph), 7.55 – 7.30 (m, 12H, Ph), 2.55 (s, 9H, NMe), 2.66 (m, 2H, CH_2), 2.39 (m, 4H, CH_2), 1.75 (m, 4H, CH_2), −1.99 (br, 3H, BH_3).

^{31}P{^{1}H} NMR (202 MHz, 1,2-$C_6H_4F_2$): δ 34.9 [d, *J*(RhP) 176].

^{11}B NMR (160 MHz, CD_2Cl_2): 20.3 (br).

ESI-MS (1,2-$C_6H_4F_2$, 60 °C, 4.5kV) positive ion: m/z, 657.0915 [M-$H_3B{\cdot}NMe_3$+$C_6H_4F_2$]$^+$ (100 %, calc. 657.1153), 616.1779 [M]$^+$ (75 % calc. 616.1941).

***In situ* preparation of [Rh($\kappa^2_{(PP)}$-DPEphos)(η^6-C_6H_5F)][BAr^F_4] (30)**

[Rh($\kappa^2_{(PP)}$-DPEphos)(NBD)][BAr^F_4] **(i4-1)** (9 mg) was dissolved in C_6H_5F (400 µL) in a New Era high pressure NMR tube. The NMR tube was placed under hydrogen (4 atm) and shaken for 5 minutes. The tube was then freeze thaw degassed and backfilled with argon, NMR spectroscopy and ESI-MS data were then obtained.

^{1}H NMR (500 MHz, C_6H_5F): δ 8.37 (s, 8H, BAr^F_4), 7.64 (s, 4H, BAr^F_4), 7.35 (m, 6H, Ar-H), 6.65 (apparent triplet, 2H, *J* = 7, Ar-H), 6.50 (m, 2H, Ar-H), 5.47 (m, 2H, *o/m*-C_6H_5F), 5.39 (m, 2H, *o/m*-C_6H_5F,) 5.11 (m, 1H, *p*-C_6H_5F). The remaining DPEphos Ar-H signals are obscured by C_6H_5F solvent δ 7.31 – 6.70.

^{31}P{^{1}H} NMR (202 MHz, C_6H_5F): δ 31.8 [d, *J*(RhP) 220].

ESI-MS (C_6H_5F, 60 °C, 4.5 kV) positive ion: m/z, 737.1435 [M]$^+$, (calc. 737.1040).

Preparation of [Rh($\kappa^2_{(PP)}$-DPEphos)(η^2-$H_3B{\cdot}NMe_3$)][BAr^F_4] (31)

$H_3B{\cdot}NMe_3$ (1.2 mg, 0.016 mmol) was added to a solution of **30** (24 mg, 0.016 mmol) in 1,2-$C_6H_4F_2$ (3 mL). Diffusion of pentane at −35 °C yielded **31** as purple crystals. Yield: 21 mg, 89 %.

^{1}H NMR (500 MHz, 1,2-$C_6H_4F_2$): δ 8.34 (s, 8H, BAr^F_4), 7.68 (s, 4H, BAr^F_4), 2.64 (s, 9H, NMe), −1.74 (br, 3H, BH_3). The DPEphos Ar-H signals were not unambiguously assigned as they were obscured by 1,2-$C_6H_4F_2$ solvent δ 7.30 – 6.70.

^{31}P{^{1}H} NMR (202 MHz, 1,2-$C_6H_4F_2$): δ 42.6 [d, *J*(RhH) 188].

^{11}B NMR (160 MHz, 1,2-$C_6H_4F_2$): δ 20.7 (br).

ESI-MS (1,2-$C_6H_4F_2$, 60 °C, 4.5 kV) positive ion: m/z, 714.2412 $[M]^+$, 714.1734 (calc.).

***In situ* preparation of [Rh($Ph_2P(CH_2)_3PPh_2$)(η^2-$H_3B{\cdot}NMe_2BH_2{\cdot}NMe_2H$)][$BAr^F_4$] (32)**

$H_3B{\cdot}NMe_2BH_2{\cdot}NMe_2H$ (1 mg, 0.0061 mmol, 1 eq.) was added to **12** (13 mg, 0.0061 mmol, 1 eq.) in 1,2-$C_6H_4F_2$ (400 μL) in an NMR tube and the resulting complex **(32)** was immediately characterised by NMR spectroscopy.

^{1}H NMR (500 MHz, 1,2-$C_6H_4F_2$, selected data): δ 5.08 (br s, 1H, N*H*), 2.38 (br, 12H, N*Me*) −1.39 (br, 3H, BH_3). The BH_2 resonance was not observed, presumably it was broad and/or obscured by the aliphatic signals.

^{31}P{^{1}H} NMR (202 MHz, 1,2-$C_6H_4F_2$): δ 32.0 [d, *J*(RhP) 163].

^{11}B NMR (160 MHz, 1,2-$C_6H_4F_2$): δ +17.5 (br), +0.7 (br).

5.7 Dehydrocoupling methodology

5.7.1 $H_3B{\cdot}NMe_2H$ dehydrocoupling experiments for dehydrocoupling plots (Chapter 4)

A stock solution of $H_3B{\cdot}NMe_2H$ in 1,2-$C_6H_4F_2$ (0.07 M) was added to a Schlenk flask under argon containing the catalyst (**11/ 12/ 25/ 26**) which was itself attached to an external mineral oil bubbler. 100 μL aliquots were taken over time; these were quenched immediately in an NMR tube by addition of MeCN (250 μL) and frozen at 77 K until analysis by ^{11}B NMR spectroscopy. ^{11}B NMR

spectra were processed using back linear prediction. Peaks which never reach > 10 % total integration value were not included in the analysis but are detailed in the footnotes of each plot.

5.7.2 $H_3B{\cdot}NMeH_2$ polymerisation (Chapter 4)

To a Schlenk flask charged with catalyst (**12/ 25/ 26**) and $H_3B{\cdot}NMeH_2$ (100 mg, 2.2 mmol) was added 1,2-$C_6H_4F_2$ (5 mL) and the resulting solution stirred open to argon for 2 hours. The reaction was subsequently quenched by addition of hexane (30 mL). After the precipitation of the polymer (*ca.* 10 minutes), the solvent was removed by decantation and the resulting solid redissolved in THF (3 mL). This solution was filtered into a new Schlenk containing hexane (30 mL). After decanting all solvent the resulting solid was dried overnight *in vacuo*. These polymerisations were essentially quantitative by ^{11}B NMR spectroscopy, even though isolated yields are lower. GPC data were obtained in THF solutions at 0.5 mg/ml, containing 0.1 % [nBu_4]NBr and use polystyrene standards for column calibration. Both the instrumentation and method are described in detail elsewhere.[17]

Isolated poly(*N*-methylaminoborane) yields following $H_3B{\cdot}NMeH_2$ catalysis with complexes **12**, **25** and **26**:

0.2 mol % **12** (1,2-$C_6H_4F_2$): 57 mg, 60 %

0.2 mol % **25 (**1,2-$C_6H_4F_2$): 48 mg, 50 %

0.2 mol % **26 (**1,2-$C_6H_4F_2$): 14 mg, 15 %

1 mol % **12 (**1,2-$C_6H_4F_2$): 72 mg, 75 %

5.8 References

[1] Pangborn, A. B.; Giardello, M. A.; Grubbs, R. H.; Rosen, R. K.; Timmers, F. J. *Organometallics* **1996,** *15,* 1518-1520.

[2] Lubben, A. T.; McIndoe, J. S.; Weller, A. S. *Organometallics* **2008,** *27,* 3303-3306.

[3] Cosier, J.; Glazer, A. M. *J. Appl. Cryst.* **1986,** *19,* 105-107.

[4] Farrugia, L. J. *J. Appl. Cryst.* **1997,** *30,* 565.

[5] Buschmann, W. E.; Miller, J. S.; *Inorganic Syntheses, 2002, Vol. 33, p. 83-91.*

[6] Abel, E. W.; Bennett, M. A.; Wilkinson, G. *J. Chem. Soc.* **1959,** 3178-3182.

[7] Schrock, R. R.; Osborn, J. A. *J. Am. Chem. Soc.* **1971,** *93,* 2397-2407.

[8] Douglas, T. M.; Le Nôtre, J.; Brayshaw, S. K.; Frost, C. G.; Weller, A. S. *Chem. Commun.* **2006,** 3408-3410.

[9] Dallanegra, R.; Chaplin, A. B.; Tsim, J.; Weller, A. S. *Chem. Commun.* **2010,** 3092-3094.

[10] Uehara, A.; Bailar, J. C. *J. Organomet. Chem.* **1982,** *239,* 11–15.

[11] Pawley, R. J.; Moxham, G. L.; Dallanegra, R.; Chaplin, A. B.; Brayshaw, S. K. Weller, A. S. Willis, M. C. *Organometallics* **2010,** *29,* 1717-1728.

[12] Aldridge, S.; Downs, A. J.; Tang, C. Y.; Parsons, S.; Clarke, M. C.; Johnstone, R. D. L.; Robertson, H. E.; Rankin, D. W. H.; Wann, D. A. *J. Am. Chem. Soc.* **2009,** *131,* 2231-2243.

[13] Jaska, C. A.; Manners, I. *J. Am. Chem. Soc.* **2004,** *126,* 9776-9785.

[14] Narula, C. K.; Janik, J. F.; Duesler, E. N.; Paine, R. T.; Schaeffer, R. *Inorg. Chem.* **1986,** *25,* 3346-3349.

[15] Euzenat, L.; Horhant, D.; Ribourdouille, Y.; Duriez, C.; Alcaraz, G.; Vaultier, M.; *Chem. Commun.* **2003,** 2280-2281.

[16] Dallanegra, R.; Pilgrim, B.; Chaplin, A. B.; Donohoe, T. J.; Weller, A. S. *Dalton Trans.* **2011,** *Submitted* and references therein.

[17] Staubitz, A.; Sloan, M. E.; Robertson, A. P. M.; Friedrich, A.; Schneider, S.; Gates, P. J.; a. d. Günne, J. S.; Manners, I. *J. Am. Chem. Soc.*, **2010,** *132,* 13332-13345.

5.9 Crystallographic data

Complex	**1**	**2**	**4**
CCDC Number	-	-	-
Formula	$C_{83}H_{65}BF_{24}OP_3Rh$	$C_{86}H_{69}BF_{24}OP_3Rh$	$C_{89}H_{74}BF_{25}OP_3Rh$
M	1740.98	1781.04	1841.11
Crystal System	Triclinic	Triclinic	Triclinic
Space group	*P*-1	*P*-1	*P*-1
a [Å]	13.42380(10)	12.81190(10)	13.3042(3)
b [Å]	14.29540(10)	16.2707(2)	17.7665(3)
c [Å]	20.7081(2)	20.9044(2)	20.6626(5)
α[deg]	73.4829(4)	84.2396(4)	111.7567(9)
β [deg]	84.0057(4)	72.9026(4)	97.3499(8)
γ [deg]	83.9868(4)	85.5884(4)	94.8652(11)
V [Å^3]	3777.28(5)	4138.93(7)	4452.23(16)
Z	2	2	2
θ range [deg]	$5.097 \leq \theta \leq 27.485$	$5.097 \leq \theta \leq 27.485$	$0.998 \leq \theta \leq 27.485$
Reflns collected	24027	25833	23438
R_{int}	0.0219	0.0243	0.0337
Completeness	99.0%	98.9%	94.9%
No. of data/restr/ param	13197/ 507/ 1136	14469/ 382/ 1089	14947/ 764/ 1161
R_1 [$I > 2\sigma(I)$]	0.0329	0.0420	0.0510
wR_2 [all data]	0.0794	0.1190	0.01435
GoF	1.030	1.073	1.055
Largest diff. pk and hole [eÅ^{-3}]	0.611, -0.473	0.706, -0.399	0.685, -0.0646

Complex	**9**	**10**	**12**
CCDC Number	-	-	801544
Formula	$C_{83}H_{67}BF_{24}OP_3Rh$	$C_{86}H_{71}BF_{24}OP_3Rh$	$C_{65}H_{43}BF_{25}P_2Rh$
M	1743.00	1783.06	1474.65
Crystal System	Monoclinic	Triclinic	Triclinic
Space group	$P2_1/c$	*P*-1	*P*-1
a [Å]	13.99560(10)	12.85900(10)	12.5134(2)
b [Å]	33.5274(3)	17.13950(10)	13.5513(2)
c [Å]	17.8616(2)	21.8146(2)	19.5061(4)
α[deg]	90.00	99.1448(4)	105.8393(7)
β [deg]	108.1544(4)	106.8047(4)	94.3128(7)
γ [deg]	90.00	100.7042(4)	94.6952(9)
V [Å^3]	7964.09(13)	4405.40(6)	3154.98(9)
Z	4	2	2
θ range [deg]	$5.097 \leq \theta \leq 27.485$	$5.097 \leq \theta \leq 29.575$	$5.14 \leq \theta \leq 26.37$
Reflns collected	25718	27541	19313
R_{int}	0.0419	0.0217	0.0246
Completeness	98.8%	98.9%	96.0 %
No. of data/restr/ param	13918/ 1081/ 1129	15395/ 3812/ 1365	12382 / 654 / 1005
R_1 [$I > 2\sigma(I)$]	0.0572	0.0991	0.0458
wR_2 [all data]	0.1396	0.2549	0.1145
GoF	1.042	1.115	1.020
Largest diff. pk and hole [eÅ^{-3}]	0.730, -0.688	1.466, -1.161	0.622, -0.545

	14	**17**	**18**
CCDC Number	818288	735078	735077
Formula	$C_{69}H_{54}BF_{24}P_2RhS$	$C_{55}H_{58}B_3F_{25}N_2PRh$	$C_{51}H_{57}B_3F_{24}N_2PRh$
M	1546.84	1388.34	1320.30
Crystal System	Orthorhombic	Triclinic	Triclinic
Space group	Pna2(1)	*P*-1	*P*-1
a [Å]	22.6994(2)	14.7071(2)	12.6080(2)
b [Å]	17.48010(10)	14.8581(2)	13.6943(2)
c [Å]	18.62650(10)	16.3258(2)	16.9699(3)
α[deg]	90.00	67.6439(7)	104.7624(6)
β [deg]	90.00	66.3534(6)	90.8926(6)
γ [deg]	90.00	82.1548(8)	96.0267(6)
V [Å^3]	7390.77(9)	3021.80(7)	2814.88(8)
Z	4	2	2
θ range [deg]	$5.097 \leq \theta \leq 27.485$	$5.10 \leq \theta \leq 26.37$	$5.09 \leq \theta \leq 26.37$
Reflns collected	14554	20676	20087
R_{int}	0.082	0.0187	0.0213
Completeness	99.0%	98.9%	99.2%
No. of data/restr/ param	14554/ 1093/ 1095	12248 / 2138 / 1249	11416 / 727 / 933
R_1 [$I > 2\sigma(I)$]	0.0421	0.0510	0.0328
wR_2 [all data]	0.1160	0.1415	0.0774
GoF	1.037	1.027	1.049
Largest diff. pk and hole [eÅ^{-3}]	0.591, -0.363	0.857, -0.940	0.741, -0.467

	19	**21**	**23**
CCDC Number	735079	767949	767950
Formula	$C_{59}H_{65}B_3F_{26}N_2PRh$	$C_{47}H_{51}B_3F_{24}N_2PRh$	$C_{46}H_{51}B_4F_{24}N_3PRh{\cdot}½(C_5H_{12})$
M	1462.44	1266.21	1315.09
Crystal System	Monoclinic	Triclinic	Monoclinic
Space group	$P2_1/c$	*P*-1	$P2_1/c$
a [Å]	19.28810(10)	13.11340(10)	13.22060(10)
b [Å]	13.44730(10)	15.09320(10)	18.33470(10)
c [Å]	50.3375(4)	15.6507(2)	24.0722(2)
α[deg]	90.00	84.6142(4)	90.00
β [deg]	90.9527(2)	78.4318(4)	98.7365(4)
γ [deg]	90.00	86.9282(4)	90.00
V [Å^3]	13054.4(2)	3019.40(5)	5767.30(7)
Z	8 (*Z*' = 2)	2	4
θ range [deg]	$5.10 \leq \theta \leq 26.37$	$5.10 \leq \theta \leq 26.37$	$5.14 \leq \theta \leq 26.37$
Reflns collected	41740	23676	22949
R_{int}	0.0311	0.0154	0.0231
Completeness	96.4%	99.2 %	99.2 %
No. of data/restr/ param	25743 / 4719 / 2600	12244 / 982 / 962	11699 / 590 / 930
R_1 [$I > 2\sigma(I)$]	0.0617	0.0466	0.0415
wR_2 [all data]	0.1700	0.1364	0.1143
GoF	1.019	1.082	1.041
Largest diff. pk and hole [eÅ^{-3}]	1.000, -0.741	0.744, -0.855	0.699, -0.619

	27	**29**	31
CCDC Number	801541	801542	-
Formula	$C_{69.5}H_{55}B_2F_{26.5}NP_2Rh$	$C_{69}H_{66}B_2F_{24}NP_2Rh$	$C_{71}H_{52}B_2F_{24}NOP_2Rh$
M	1594.11	1551.70	1577.61
Crystal System	Triclinic	Monoclinic	Monoclinic
Space group	*P*-1	$P2_1/c$	$P2_1/n$
a [Å]	12.9731(2)	14.94180(10)	13.02740(10)
b [Å]	17.4492(2)	19.2670(2)	19.4003(2)
c [Å]	18.3033(3)	25.1468(2)	31.6717(3)
α[deg]	110.1373(6)	90.00	90.00
β [deg]	95.3780(7)	91.2143(3)	96.1826(3)
γ [deg]	99.4374(7)	90.00	90.00
V [Å^3]	3786.61(9)	7237.73(11)	7958.00(13)
Z	2	4	4
θ range [deg]	$5.50 \leq \theta \leq 26.37$	$5.11 \leq \theta \leq 26.37$	$5.09 \leq \theta \leq 27.485$
Reflns collected	26357	28480	25411
R_{int}	0.0216	0.0224	0.0236
Completeness	98.3 %	99.2 %	98.1%
No. of data/restr/ param	15201 / 1688 / 1196	14685 / 542 / 1018	13803 / 344/ 987
R_1 [$I > 2\sigma(I)$]	0.0529	0.0427	0.0456
wR_2 [all data]	0.1541	0.1072	0.1401
GoF	1.046	1.025	1.100
Largest diff. pk and hole [eÅ^{-3}]	0.840, -0.604	0.663, -0.405	0.713, -1.087

5.10 Publications

9) Dallanegra, R.; Chaplin, A. B.; Douglas, T. M.; Weller. A. S. Rhodium phosphine-alkene complexes of DPEphos and XANTphos. *Paper in preparation.*

8) Dallanegra, R.; Pilgrim, B.; Chaplin, A. B.; Donohoe, T. J.; Weller, A. S. *Dalton Trans.* **2011,** *Accepted*.

7) Dallanegra, R. Robertson, A. P. M.; Chaplin, A. B.; Manners, I. Weller A. S. *Chem. Commun.* **2011,** *47*, 3763-3765.

6) Stevens, C. J.; Dallanegra, R.; Chaplin, A. B.; Weller, A. S.; Macgregor, S. A.; Ward, B.; McKay, D.; Alcaraz, G.; Sabo-Etienne, S. *Chem. Eur. J.* **2011,** *17*, 3011-3020.

5) Dallanegra, R.; Chaplin, A. B.; Tsim, J.; Weller, A. S. *Chem. Commun.* **2010,** 3092-3094.

4) Pawley, R. J.; Moxham, G. L.; Dallanegra, R.; Chaplin, A. B.; Brayshaw, S. K. Weller, A. S. Willis, M. C. *Organometallics* **2010,** *29*, 1717-1728.

3) Moret, S.; Dallanegra, R.; Chaplin, A. B.; Douglas, T. M.; Hiney, R. M. Weller, A. S. *Inorg. Chim. Acta.* **2010,** 574-580.

2) Dallanegra, R.; Chaplin, A. B.; Weller, A. S. *Angew. Chem. Int. Ed.* **2009,** *48*, 6875-6878.

1) Douglas, T. M.; Brayshaw, S. K.; Dallanegra, R.; Kociok-Köhn, G.; Macgregor, S. A.; Moxham, G. L.; Weller, A. S.; Wondimagegn, T.; Vadivelu, P. *Chem. Eur. J.*, **2008**, *14*, 1004-1022.